DOE/MC/30171 -- 5298
(DE97002038)
Volume II

Recycle Of Contaminated Scrap Metal, Volume II

Semi-Annual Report
September 1993 - January 1996

July 1996

Work Performed Under Contract No.: DE-AC21-93MC30171

For
U.S. Department of Energy
Office of Environmental Management
Office of Technology Development
Washington, DC

U.S. Department of Energy
Office of Fossil Energy
Morgantown Energy Technology Center
Morgantown, West Virginia

By
Molten Metal Technology, Inc.
Waltham, Massachussetts 02154

DISCLAIMER

Disclaimer

DOE/MC/30171 -- 5298
(DE97002038)
Volume II

Recycle Of Contaminated Scrap Metal, Volume II

Semi-Annual Report
September 1993 - January 1996

Work Performed Under Contract No.: DE-AC21-93MC30171

For

U.S. Department of Energy
Office of Environmental Management
Office of Technology Development
1000 Independence Avenue
Washington, DC 20585

U.S. Department of Energy
Office of Fossil Energy
Morgantown Energy Technology Center
P.O. Box 880
Morgantown, West Virginia 26507-0880

By
Molten Metal Technology, Inc.
400-2 Totten Pond Road
Waltham, Massachussetts 02154

July 1996

lten Metal Technology

Molten Metal Technology, Inc. • 400-2 Totten Pond Road • Waltham, MA 02154 U.S.A. • Tel: 617-487-9700 • Fax: 617-487-7870 • http: //www.mmt.com

July 24, 1996

U.S. Department of Energy
Morgantown Energy Technology Center
Attn: Contractor Reports Receipt Coordinator
M/S F07
PO Box 880
3610 Collins Ferry Road
Morgantown, WV 26507-0880

Subject: Contract Number DE-AC21-93MC30171

Please find enclosed the following deliverable under the subject contract:

- Six (6) hard copies of the Interim Report entitled "Recycle of Contaminated Scrap Metal."

Due to software incompatibilities, it was agreed to with Bill Huber that MMT would deliver this report in paper format rather than on CD-ROM. This deliverable is in releasable form in accordance with the terms and conditions of the subject contract.

If you require any additional information, feel free to contact me at (617)768-4521.

Sincerely,
MOLTEN METAL TECHNOLOGY, INC.

KMBeane

Kathleen M. Beane
Senior Contracts Administrator
Government Sector

cc: V. Gatto
L. Ghoniem
B. Payea
J. Zimmerman

PRDA INTERIM REPORT
TABLE OF CONTENTS

List of Figures

List of Tables

List of Frequently Used Acronyms

ALARA	As Low As Reasonably Achievable
APU	Advanced Processing Unit
BDAT	Best Demonstrated Available Technology
C/M/R	Ceramic/Metal/Refractory
CAA	Clean Air Act
CAS	Calcium Aluminosilicates
CEP	Catalytic Extraction Processing
CET	Compensated Embedded Thermocouple
CFCC	Continuous Fiber-reinforced Ceramic Composite
CPU	Catalytic Processing Unit
CSTRs	Continuously Stirred Tank Reactor
CWA	Clean Water Act
DEP	Department of Environmental Protection
DF	Decontamination Factors
ΔG_i	Change in Gibbs Free Energy
DOE	Department of Energy
DRE	Destruction Removal Efficiency
EDX	Energy Dispersive X-Ray
EDXS	Energy Dispersive X-Ray Spectrometer
EPA	Environmental Protection Agency
GC	Gas Chromatography
GHT	Gas Handling Train

GLR	Glass-Liquid-Refractory
HEPA	High Efficiency Particulate
HLW	High Level Waste
HVAC	Heating, Ventilation, and Air Conditioning
ICP	Inductively-Coupled Plasma
ICTF	Integrated Containment Test Facility
IR	Infrared
LADR	Leaching and Dissolution Resistance
LCD	Liquid Crystal Display
LDL	Lower Detection Limit
MLLW	Mixed Low Level Waste
MMT	Molten Metal Technology
MOCP	Molten Oxide Ceramic Phase
MS	Mass Spectrometer
NAA	Neutron Activation Analysis
ODEs	Ordinary Differential Equations
OFT	Optical Fiber Thermometry
OSHA	Occupational Safety and Health Administration
PCB	Polychlorinated Biphenyl
PCT	Product Consistency Test
PDEs	Partial Differential Equations
PFR	Plug Flow Reactor
PICs	Products of Incomplete Combustion
PID	Proportional Integral Derivative

PLC	Programmable Logic Controller
POHCs	Primary Organic Hazardous Constituents
PSR	Perfectly Stirred Reactor
PVC	Polyvinyl Chloride
Q-CEP	Quantum Catalytic Extraction Process
RCRA	Resource Conservation and Recovery Act
RTD	Residence Time Distribution
SEM	Scanning Electron Microscopy
SPC	Statistical Process Control
TCLP	Toxicity Characteristic Leaching Procedure
THC	Total Hydrocarbons
TOX	Total Organic Halides
TRU	Transuranic Waste
TSD	Treatment, Storage, and Disposal
VHMs	Volatile Heavy Metals
VOC	Volatile Organic Constituent
VPR	Variable Pressure Reactor
WAC	Waste Acceptance Criteria
WETF	West End Treatment Facility
XRD	X-Ray Diffraction
XRF	X-Ray Fluorescence

5. Task 1.4 - Optimization of the Vitreous Phase for Stabilization of Radioactive Species

MMT has performed extensive theoretical and experimental studies to develop an operable, highly stable, non-leachable ceramic phase product that maximizes the amount of waste loading and minimizes the amount of interaction with the containment system. This section also includes the results of experimental studies directed at the optimization of the CEP containment system to provide robust performance with wide variations in feed composition and to extend refractory operating life.

5.1. Ceramic Phase Development and Quality

Ceramic phase waste loading experiments were performed using actual radionuclides at CEP facilities located in Oak Ridge, TN. While these experiments were not performed under this contract, a summary of their results has been in this report as they are known to be of interest to DOE. These experiments validated previous ceramic phase studies performed with surrogate radionuclides. Studies were also performed to evaluate electrochemical reactions that occur preferentially at the ceramic/metal/refractory interface which can result in localized degradation of the refractory material. Ceramic phase stability was evaluated using Toxicity Characteristic Leaching Procedure (TCLP), Product Consistency Test (PCT), and in-house test protocols for various ceramic phase compositions. These experiments have conclusively demonstrated that CEP ceramic phase product consistently meets or exceeds final product form stability requirements. Finally, methods to perform on-line determination of the viscosity of the ceramic phase were investigated to ensure the operability of the ceramic phase product prior to commencing product removal operations.

5.1.1. Ceramic Phase Waste Loading

Ceramic phase waste loading experiments using actual radionuclides were performed to evaluate CEP partitioning of radionuclides and the performance of various ceramic systems as a final product form. Experiments were performed using uranium and cerium, uranium hexafluoride (UF_6), and mixed-waste water treatment solids from the West End Treatment Facility at Oak Ridge, TN.

5.1.1.1. Distribution of Uranium in Iron-Glass Systems and Uranium-Cerium Glass Syntheses: Experimental Methods and Results

5.1.1.1.1. Experiments

Experiments were conducted to verify the results of the ceramic phase studies performed with surrogate radionuclides. The radionuclide contaminant oxide or metal was included in the iron charge at the bottom of the crucible. Carbon

dioxide was injected to provide the potential for oxidation of the contaminant, which was partitioned into a calcium aluminosilicate or lithium boron calcium aluminosilicate phase. The initial carbon level in the iron was consistent in the range around 3.2 wt%, and the process temperature was 1500-1575°C. Glass synthesis experiments were also performed in which oxide mixtures containing different amounts of uranium and cerium were melted in graphite crucibles. This ensured that the glasses were synthesized under heavily reducing conditions. The crucibles from the glass syntheses were pulled out of the reactor at very high temperatures (> 1000°C) in order to obtain a fast cooling rate and a glassy product and minimize crystallization. In a few instances, the alumina crucibles containing the iron and glass were removed from the reactor at high temperatures for the same reason.

A summary of the different experiments is presented in Table 5.1. The first experiments were done to prepare glass and metal samples containing different amounts of uranium. These were used to prepare calibration standards for α,β and γ analysis. The next experiments investigated the removal of uranium from the metal phase with subsequent capture in the ceramic phase. Both uranium metal and oxide were used in these experiments in conjunction with two different glasses. Partitioning of both uranium and cerium was evaluated. The final experiment was a glass synthesis experiment in which three different glasses containing known amounts of CeO_2 and UO_2 were prepared. The primary purpose of this synthesis was to investigate high levels of waste loading and incorporation of these elements into glasses.

Table 5.1
Description of Experiments

Description	Comment
Synthesis of UO_2-Ca-Al-Si glass calibration standards	Standard for $\alpha\beta$ counting
Synthesis of metal calibration standard	Standard for γ spectroscopy
Partitioning: UO_2 into Ca-Al-Si glass	0.9 wt% UO_2[a]
Partitioning: UO_2 into Li-B-Ca-Al-Si glass	0.9 wt% UO_2[a]
Partitioning: U into Li-B-Ca-Al-Si glass	One metal strip
Partitioning: U into Li-B-Ca-Al-Si glass	Heavy loading, 2 metal strips
Partitioning: UO_2 and CeO_2 into Li-B-Ca-Al-Si glass	5.0 wt% UO_2, 1.0 wt% CeO_2[a]
Synthesis of UO_2-CeO_2-Li-B-Ca-Al-Si glasses	Investigate waste loading
[a]Calculated glass loading. Assumes complete capture in the glass.	

In the partitioning experiments, the crucibles were loaded with iron, uranium and the glass mixture. The crucibles were heated to the desired temperature and an alumina lance was lowered into the melt for gas injection. A similar procedure was followed in the metal calibration preparation except that only iron and uranium were loaded into the alumina crucible and inert gas was injected (as opposed to the inert/carbon dioxide mixure). In the glass synthesis/glass calibration standard preparation, the glass/contaminant mixtures were loaded into graphite crucibles and inert gas was simply used to blanket the reactor (no injection). This combination ensured that the glasses were synthesized under very reducing conditions. In both experiments, these crucibles were pulled out of the reactor at a temperature near 1000 °C to obtain a rapid cooling rate.

The actual quantities of each material used in the experiments are presented in Table 5.2. Two different glasses were used. The Ca-Al-Si glass was chosen because it was expected to be a very fluid glass compatible with the high alumina crucible. It should also be a very leach resistant material. In actual use, the glass appeared to have an acceptably low viscosity and minimal chemical interaction with the crucible. The final appearance was of a very dense material, with a glassy phase present in the interior only.

Table 5.2
Summary of Experimental Parameters.

Iron (g)	Glass (g)	Composition[a]	Contaminant (g), Type
	99.97	Ca-Al-Si	1.0401, UO_2
	100.06	Ca-Al-Si	0.4802, UO_2
	100.02	Ca-Al-Si	0.1295, UO_2
7000.14		None	3.6082, U
4200.42	499.76	Ca-Al-Si	4.50, UO_2
4202.18	508.93	Li-B-Ca-Al-Si	4.48, UO_2
4201.04	508.78	Li-B-Ca-Al-Si	4.70, U
4201.71	509.10	Li-B-Ca-Al-Si	9.50, U
4205.81	509.64	Li-B-Ca-Al-Si	25.26, UO_2; 5.04, CeO_2
	101.84	Li-B-Ca-Al-Si	5.00, UO_2; 1.01, CeO_2
	101.49	Li-B-Ca-Al-Si	10.00, UO_2; 4.88, CeO_2
	49.91	Li-B-Ca-Al-Si	0.50, UO_2; 0.56, CeO_2

[a]Glass composition. Ca-Al-Si: 38CaO-027 Al_2O_3-35SiO_2; Li-B-Ca-Al-Si: 2.4Li_2O-06.1B_2O_3-29.1CaO-12.1Al_2O_3-50.3SiO_2 (mol%)

The Li-B-Ca-Al-Si composition is higher in silica, but modified with small amounts of lithium and boron. These additives were included to increase waste loading and decrease viscosity. This composition resulted in foaming, and in several instances the glass level reached the top of the crucible. Chemical interaction with the crucible was again minimal and the final material was also very dense. Overall, the samples did appear to have glassy material in the center of the layer (after cooling). In both of the synthesis experiments, all samples, regardless of chemical composition and contaminant type and concentration, visually appeared glassy. This was further examined by electron microscopy.

5.1.1.1.2. General Sample Preparation and Data Analysis

Metal, glass, crucible, and glass wool samples were collected. These were analyzed by various means as described below. As part of the reactor assembly procedure, the insulation pieces placed above the top of the crucible and the glass wool used inside the cold trap were weighed. This was done as a contingency for later calculational purposes in case any activity was detected after the experiment in these materials.

Four different types of analyses were performed. Trace concentrations of uranium and cerium in metal and glass samples were determined by Neutron Activation Analysis.

Analysis was done on-site using two different techniques. Gamma spectroscopy was the only energy sensitive technique available and can be used to determine radionuclide distribution, concentration and total sample Curie content. Since uranium is not a gamma emitter, it is detected in this system by looking at its daughter products.

A Tennelec (Oxford) $\alpha\beta$ counting system (Model LB5100) was used to analyze glass samples. This low background counting system is typically used for smear (swipe) analysis and yields discrete alpha, beta and gamma activity levels, but does not give energy discrimination (radionuclide identification). All of the activity measured from this instrument was therefore attributed to uranium (α activity associated with uranium, β and γ activity from uranium daughter products). Based on comparison with the gamma spectroscopy data, this was a reasonable, although not always *completely* justified assumption. For example, some contamination from other sources did appear in several samples. Based upon previous experience obtained from optimizing sample geometry and counting times, initial analysis of the glasses was done using the low level $\alpha\beta$ counter.

For gross initial measurement, a frisker (Geiger counter) was used (Ludlum, Model 177-61). Measurements were made by placing the detector at the top of each crucible or near a sample. Since this yields neither radiation type (it detects β and γ radiation combined) nor energy, the measurement was used simply as a quick method for detecting the presence or absence of relatively large concentrations of uranium (daughters).

5.1.1.1.3. Analysis of Glass Samples: αβ counting

Samples from each of the three glasses synthesized in experiment 040 were obtained. The glass calibration samples were prepared for analysis by crushing and sieving through a 1-2 mm^2 screen, and labelled as 040-CS1, -CS2 and -CS3. Several one gram samples of each glass sample powder were spread in a very thin layer on the sticky side of 1 1/2" diameter paper (Mohawk). These Mohawks were placed into standard aluminum dishes and sample holders, which fit into the αβ counter. Sample weights were held roughly constant as this was a variable which could potentially affect the calibration. The effect may be a function of the coverage of the detector surface area. A single low mass sample was also used for comparison. The weights and identifications of each crushed glass sample are shown in Table 5.3.

Table 5.3
Weights Of Glass Calibration Standard Samples (RPU2-94-040)

Sample #	CS1 (g)	Sample #	CS2 (g)	Sample #	CS3 (g)
1	1.0020	5	1.2052	9	1.1335
2	1.0174	6	1.0234	10	1.0321
3	1.1205	7	0.9847	11	1.1052
4	1.0034	8	1.0536	12	0.9463
13	0.4725				

Figure 5.1 shows the measured alpha activity (in disintegrations/minute) in each sample as a function of sample mass. The labels on the plot are the uranium loading in the glasses. The data for each of the three glasses are roughly grouped together when samples of nearly equal mass are taken.

These data were used to calculate activity/gram of sample and activity/gram of uranium in sample. These results are shown in Figure 5.2 and Figure 5.3. The plot of activity per gram of sample shows that there is little variation within a set of duplicate samples (11.1% was the highest standard error). The data for the glass with the highest uranium content had the lowest standard error. The one data point taken from a 1/2 gram glass sample (as opposed to the other 1 gram samples) shows that the activity/mass level is significantly above the expected level (1863.6 vs. 1542.6 + 93.8). This plot is important because of the method in which the sample is prepared and analyzed. Ideally, there is a uniformly thin

layer of glass spread over the entire sample paper surface, and correspondingly the detector surface area utilized is maximized.

Figure 5.3 shows the amount of uranium in the sample plotted as a function of the measured alpha activity. The uranium content is calculated based upon the initial loading and assuming a uniform concentration. A linear fit describes the data very well (R^2 = 0.983). This includes the 1/2 gram, high uranium concentration sample.

Figure 5.1
Alpha Activity In Crushed Glass Samples

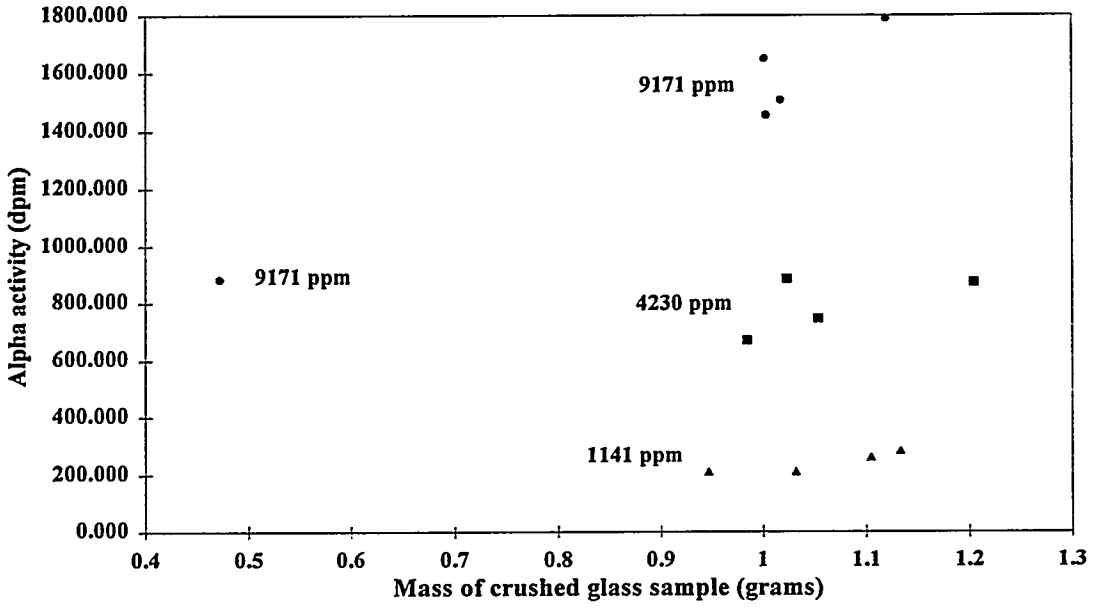

Figure 5.2
Alpha Activity Per Gram Of Sample

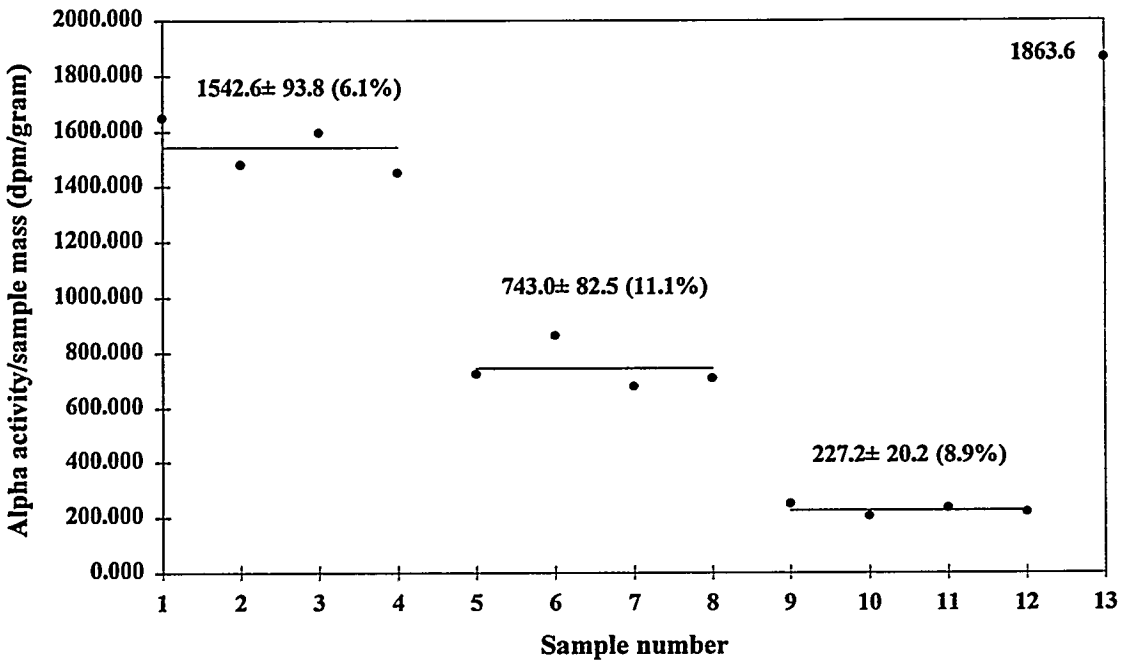

Figure 5.3
Alpha Activity Versus Uranium Content

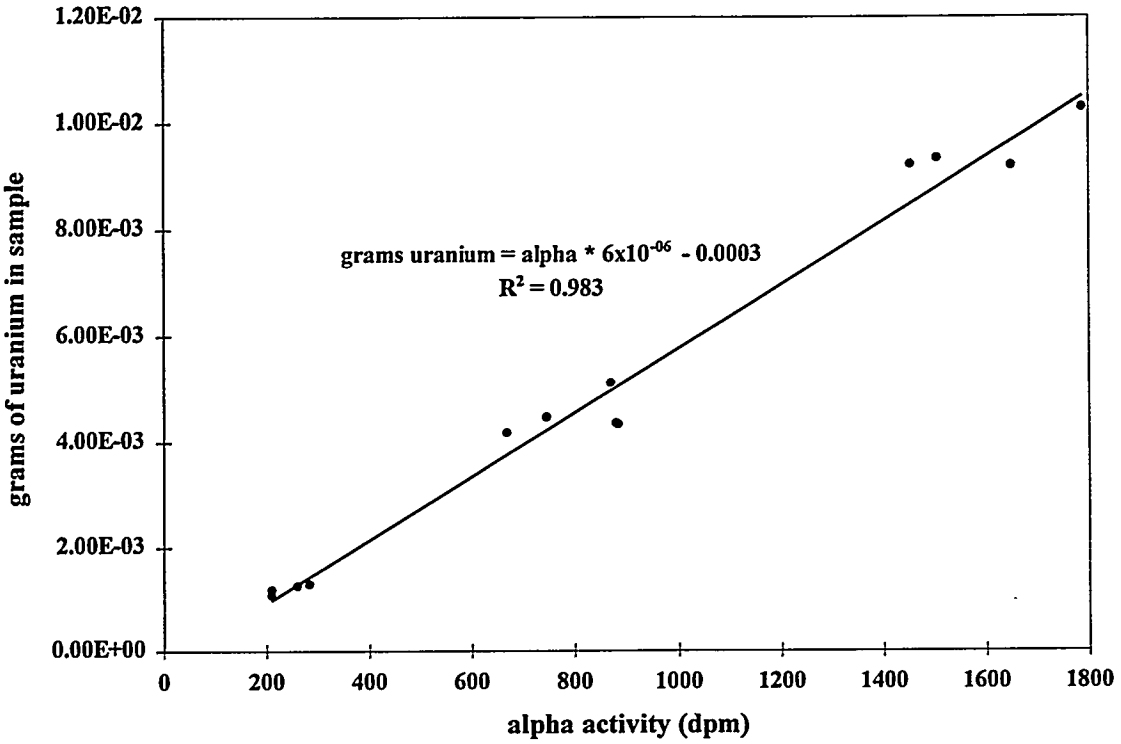

The measured beta activity per sample mass and beta activity versus uranium level are plotted in Figure 5.4 and Figure 5.5. There is less variation within a given set as compared to the alpha measurements. The largest standard error within a set is 5.8% and the linear fit to the data is also slightly improved, with $R^2 = 0.993$.

Figure 5.4
Beta Activity Per Gram Of Sample

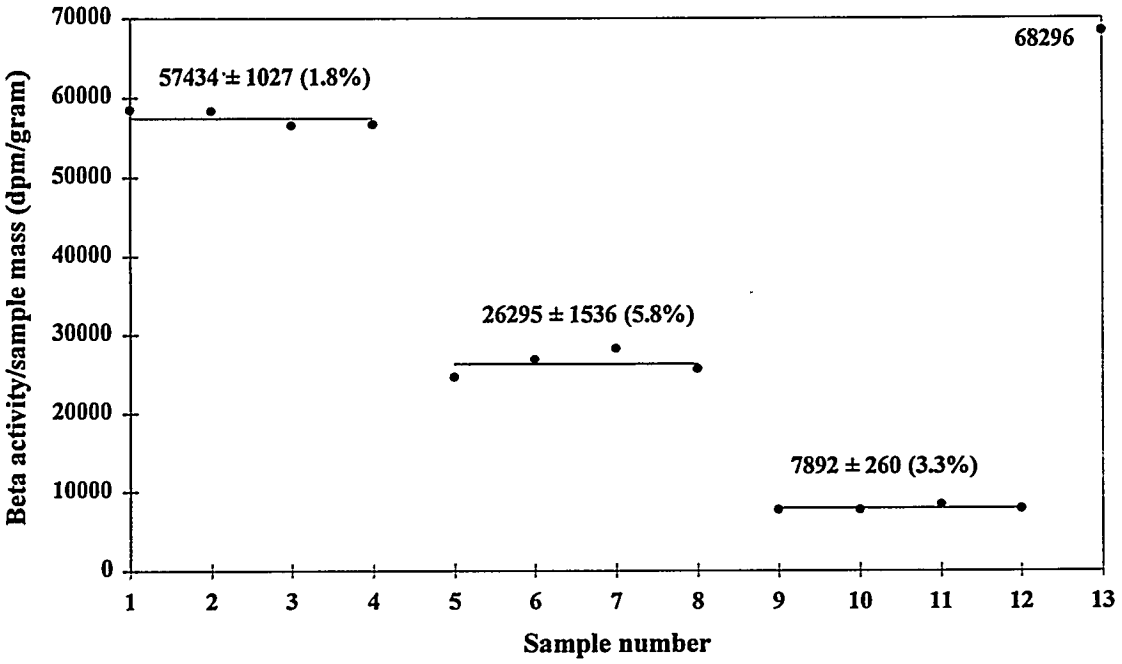

Figure 5.5
Beta Activity Versus Uranium Content

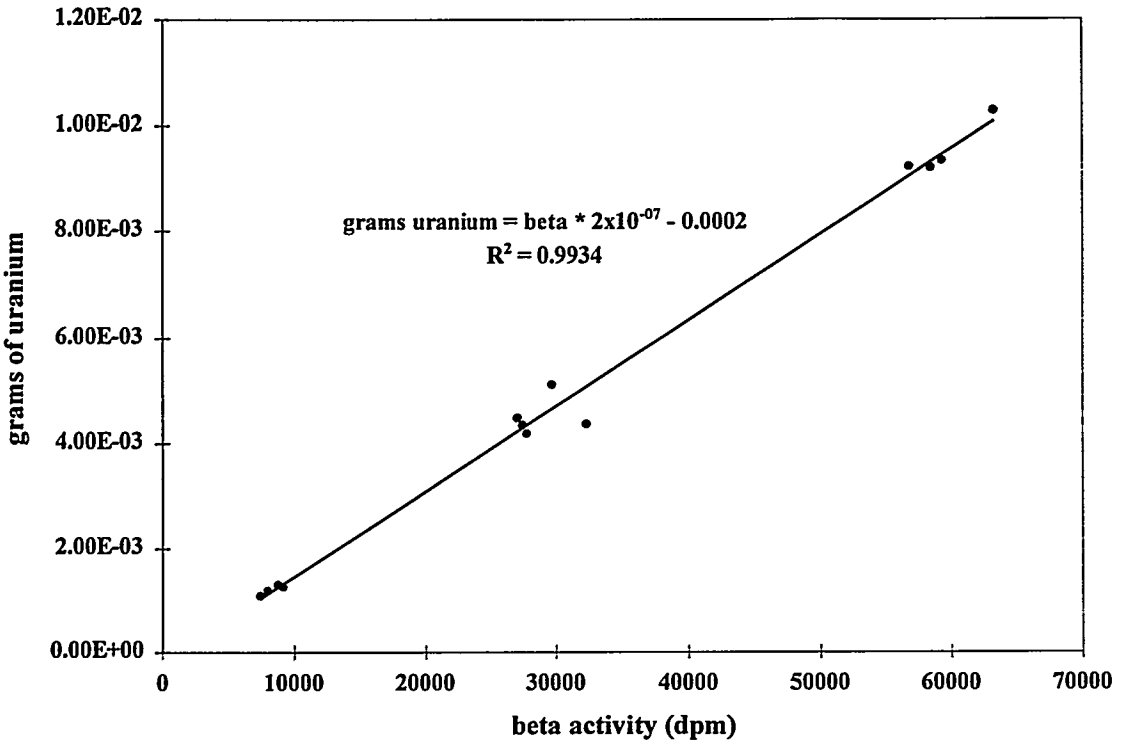

Figure 5.6 and Figure 5.7 show that the standard error and coefficient of variation are further improved with the measurement of gamma activity. For all three measurements, sample 13 (the low mass standard) was always an outlier. This demonstrates the necessity for consistency in sample preparation techniques using the derived calibration curves.

Figure 5.8 groups all data on one plot. This figure is simply presented to demonstrate the overall good correlation in the data and to show the slightly different concentration dependencies for the measured activity levels.

The results presented above show that the sample preparation and analysis method was adequate for measurement of alpha, beta and gamma activity levels. Very good correlation was found between the amount of uranium in a glass sample and the measured activity. The quantity of glass used in the analysis is important as the low mass sample showed significantly different results. This difference may either be due to how the glass was spread onto the sample paper or to the mass of the sample.

In subsequent experiments, glass samples were prepared and analyzed according to the procedure described above. Uranium concentrations in the glasses were calculated from the measured α, β and γ activities according to the simple linear equations presented in Figure 5.3, Figure 5.5 and Figure 5.7.

Figure 5.6
Gamma Activity Per Gram Of Sample

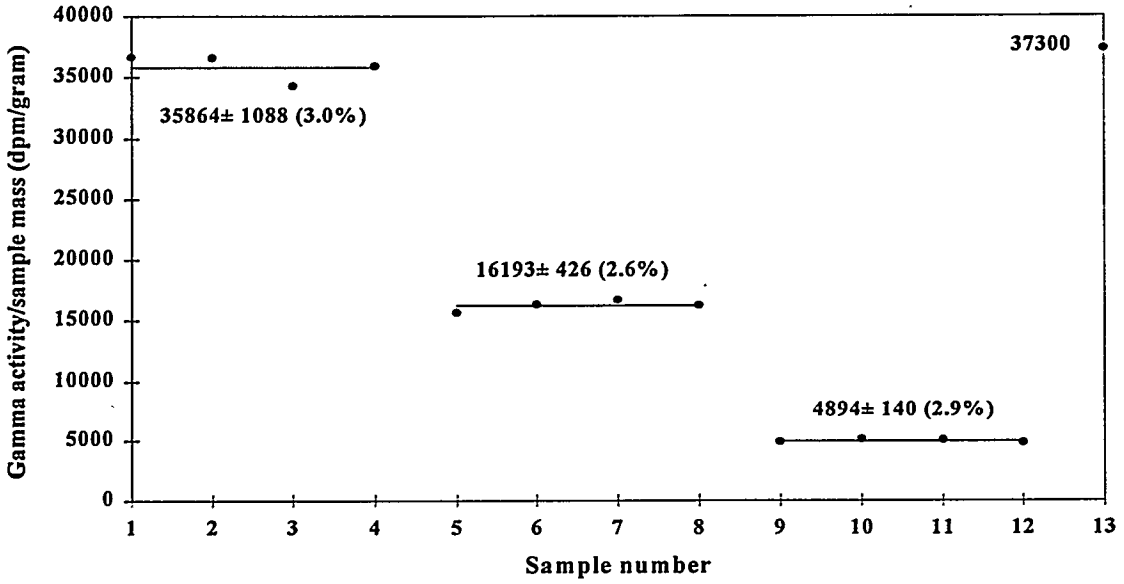

Figure 5.7
Gamma Activity Versus Uranium Content

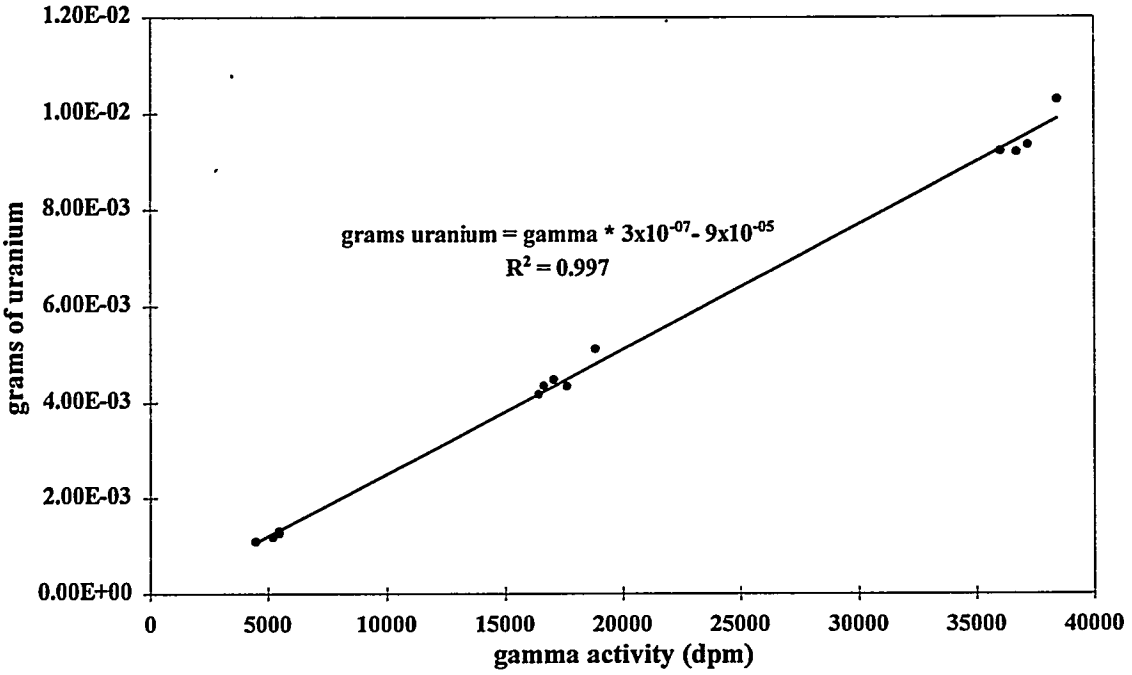

Figure 5.8
Comparison Of Alpha, Beta And Gamma Activities As A Function Of Uranium Content In Crushed Glass Samples

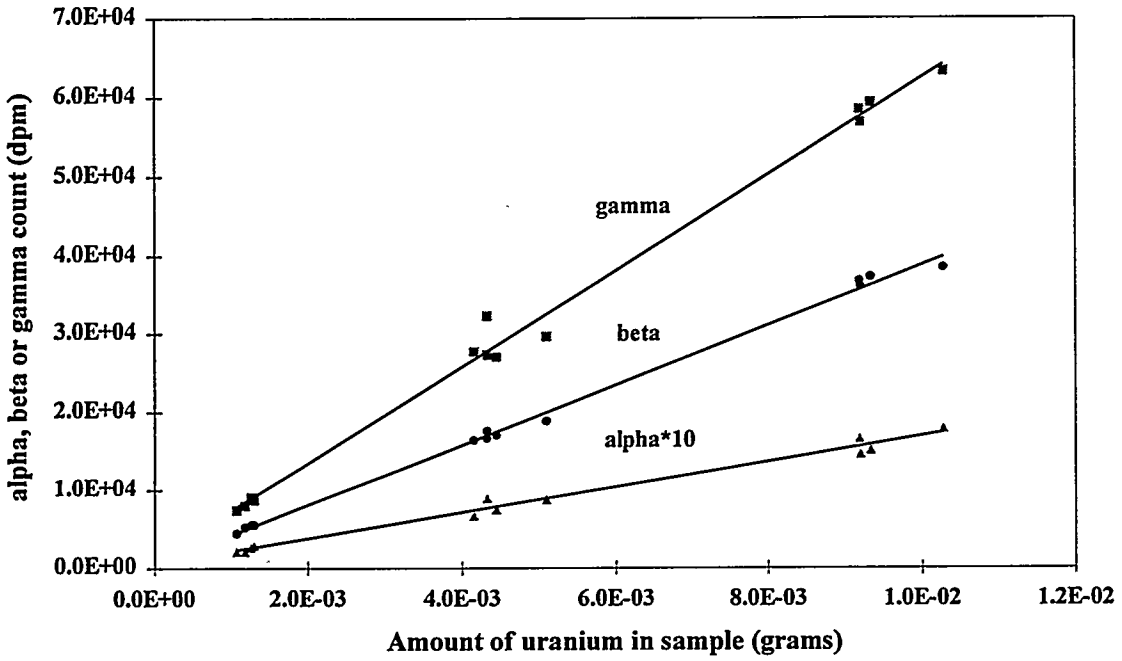

5.1.1.1.4. Analysis of Metal Samples: γ Spectroscopy

A 1/2" drill bit and small magnet were used to drill and collect filings from the metal pieces. Samples were sent to the lab for analysis by gamma spectroscopy. The initial series of samples were simply counted as sent in planchet dishes. Later in this set of experiments, some samples were dissolved and counted in Marinelli beakers. Gamma spectroscopy was tried for this analysis because uranium daughters are gamma emitters (also anticipating that self shielding in the metal samples would be significant).

5.1.1.1.5. Analysis of Glass Samples: Electron Microscopy

Samples were analyzed using SEM and EDX. The instrument used was a JEOL JXA 840 scanning microanalyzer, with EDX capability for elemental analysis and a Kevex Quantum detector. Both secondary electron imaging and backscattered electron imaging were done.

Results:

Results from each of the different experiments are discussed in this section.

5.1.1.1.6. Sample No. 040: Ca-Al-Si Glass Synthesis

The glass synthesis and determination of αβ counting calibration standards has been described at length above. Additional analysis was done on sample RPU2-94-040-S1 by electron microscopy. Figure 5.6 shows a low magnification (12X) SEM photo of glass sample RPU2-94-040-S1, which contains greater than 9000 ppm uranium. This piece was taken from the bottom of the crucible. The curved lines seen in the photo are a result of the morphology of the base of the crucible, due to the tool used to machine the graphite stock. The sample appeared (at both low and high magnification) to be homogeneous. The conclusion is that homogeneous glass containing uranium was synthesized under reducing conditions.

5.1.1.1.7. Sample No. 042: Partitioning of UO_2: Ca-Al-Si Glass

Several samples were taken from different positions in the glass layer. Four crushed glass samples were prepared from Experiment No. S3 for immediate analysis. Weights and measured activities are shown in Table 5.4. Uranium concentrations are calculated from the calibration curves derived in Experiment No. 040.

Table 5.4
Analysis Of Sample No. 042-S3

Weight (g)	α (dpm)[1]	β (dpm)[1]	γ (dpm)[1]	α: U(g)[2]	β: U(g)[2]	γ: U(g)[2]	α wt% U[3]	β wt% U[3]	γ wt% U[3]
0.8172	855.061	32949.87	21525.47	0.0048	0.0064	0.0064	0.591	0.782	0.779
0.5579	702.834	25922.37	15438.51	0.0039	0.0050	0.0045	0.702	0.893	0.814
0.4637	563.563	22733.15	13927.95	0.0031	0.0043	0.0041	0.665	0.937	0.882
0.3566	498.785	18989.76	10698.14	0.0027	0.0036	0.0031	0.755	1.009	0.875
wt% in glass	α	β	γ	all					
Average	0.678	0.905	0.837	**0.807**					
Std Dev	0.069	0.095	0.049	**0.120**					
Std Error (%)	10.2	10.5	5.9	**14.8**					

[1]Analytical result.
[2]Calculated from one of the following equations:
grams of uranium = $\alpha(dpm)*6x10^{-6} - 3x10^{-4}$.
grams of uranium = $\beta(dpm)*2x10^{-7} - 2x10^{-4}$.
grams of uranium = $\gamma(dpm)*3x10^{-7} - 9x10^{-5}$.
[3]Weight percent of uranium in the glass.

The average uranium concentration in the glass is calculated individually from the three data sets. An overall average is also calculated using every data point. This shows that the average uranium concentration in the glass was 0.807 ± 0.120 wt% (14.8% error). If all of the uranium loaded into the crucible went into the glass, then the predicted uranium concentration would be approximately

$$4.50 \text{ g } UO_2 * [238/(238+32)]/499.41 \text{ grams of glass} * 100 = 0.794 \text{ wt\%}.$$

This shows that within error, all uranium was recovered in the glass. There is no obvious basis for choosing the alpha, beta or gamma data as the most accurate. Therefore, the average over all data points is used.

Table 5.5
Uranium Concentration In The Metal

Sample	uranium concentration (ppm)	decontamination (%)
M7	0.28	99.97
M8	0.62	99.93
M9	0.69	99.93

The calculated initial uranium concentration in the metal was 944.35 ppm (=4.50 g UO_2 * [238/(238+32)]/4200.42*1x10^6. The final uranium concentrations were less than 1 ppm. These all indicate a metal decontamination greater than 99% ((initial-final)/initial*100). These results are consistent with the data for the glass samples, as both indicate >99% removal from the metal and partitioning to the glass.

5.1.1.1.8. Experiment No. 043: Partitioning of UO_2: Li-B-Ca-Al-Si Glass

The glass was very viscous and foamy. Compatibility with the alumina crucible was excellent. The glass consisted of two phases. It was primarily a greenish white material with a dark green glassy phase in the center. Separate samples were taken from these two phases for the different types of analysis. Eighteen different samples were taken from nine locations on the surface and interior of the metal.

Glass samples weights and measured α, β and γ activities are shown in Table 5.6. Results are presented for heterogeneous sample S3 and homogeneous sample S5.

Averages, standard deviations and standard errors are shown for S3 and S5 individual data and for all samples. The average measured uranium concentration in S3 was 0.843 ± 0.148 wt% (17.6% error), while the average for S5 was 0.785 ± 0.200 wt% (25.5% error). The average for the measurements on all samples was 0.818 ± 0.170 wt% (20.8% error). The predicted uranium concentration, assuming complete partitioning to the ceramic phase, is 0.777 wt%. Within the error of the data, this is in very good agreement with the overall measured average value (0.818/0.777*100 = 105%).

Table 5.6
αβγ Counting Results For Experiment No. 043

xperiment No. 043-S3

	α (dpm)[1]	β (dpm)[1]	γ (dpm)[1]	α: U(g)[2]	β: U(g)[2]	γ: U(g)[2]	α wt% U[3]	β wt% U[3]	γ wt% U[3]
	612.146	25087.87	14896.89	0.0034	0.0048	0.0044	0.649	0.927	0.842
	440.486	17626.95	9883.23	0.0023	0.0033	0.0029	0.695	0.987	0.853
	398.381	18830.19	11458.39	0.0021	0.0036	0.0033	0.584	0.996	0.935
	514.98	21184.91	12109.32	0.0028	0.0040	0.0035	0.712	1.031	0.904

xperiment No. 043-S5

	α (dpm)[1]	β (dpm)[1]	γ (dpm)[1]	α: U(g)[2]	β: U(g)[2]	γ: U(g)[2]	α wt% U[3]	β wt% U[3]	γ wt% U[3]
	297.976	11869.54	7453.42	0.0015	0.0022	0.0021	0.627	0.916	0.904
	197.571	7317.52	4273.29	0.0009	0.0013	0.0012	0.669	0.955	0.901
	106.883	5363.88	3140.37	0.0003	0.0009	0.0009	0.346	0.884	0.863
	S3[4]					**S5[4]**			
wt% in glass	α	β	γ	all		α	β	γ	all
Average	0.660	0.985	0.884	0.843		0.547	0.918	0.889	0.785
Std Dev	0.057	0.043	0.044	0.148		0.176	0.035	0.023	0.200
Std Error (%)	8.7	4.4	4.9	17.6		32.1	3.9	2.5	25.5
wt% in glass	**All[5]**								
Average	**0.818**								
Std Dev	**0.170**								
Std Error (%)	**20.8**								

Analytical result.
Calculated from one of the following equations:
rams of uranium = $\alpha(dpm)*6x10^{-6} - 3x10^{-4}$.
rams of uranium = $\beta(dpm)*2x10^{-7} - 2x10^{-4}$.
rams of uranium = $\gamma(dpm)*3x10^{-7} - 9x10^{-5}$.
Weight percent of uranium in the glass.
Results for samples RPU2-94-043-S3 and RPU2-94-043-S5.
Results for all samples.

Four metal samples were analyzed using NAA. These samples were taken from the interior, along one side of the metal (from top to bottom, from three separate locations). Results (Table 5.7) indicate that the highest residual uranium concentration was about 5 ppm. Assuming a uniform uranium concentration throughout the metal, this corresponds to a metal decontamination of 99.46% (= (initial-final)/initial*100 = (939.76 ppm-5.07 ppm)/939.76ppm*100). These results also show that there was not a (top to bottom) uranium concentration gradient in the metal.

Table 5.7
NAA Results For Uranium Concentration In Metal Samples (Experiment No. 043)

Sample	Uranium Concentration (ppm)	Decontamination (%)
M19	2.31	99.75
M20	5.07	99.46
M21	0.86	99.91
M22	0.58	99.94

5.1.1.2. Retention Of Sodium, Lithium And Boron In Radioactive Waste Glasses Under High Temperature Reducing Conditions

5.1.1.2.1. Background and Objectives:

Most of the base glass compositions used in CEP experiments are simple calcium aluminosilicates (CAS). They have been chosen in part because of the high operating temperatures and reducing conditions of the reactor. For use as waste glasses, CAS compositions are known to be superior in terms of their durability and stability.[1] However, the limits on waste loading of these glasses can be restrictive compared to (for example) lower temperature borosilicate glasses.[2] The loading is also a function of the oxygen fugacity of the reactor environment. For example, uranium is more soluble in glasses under oxidizing conditions as U^{+6}, with decreased incorporation into glasses as U^{+4} under reducing conditions.[3] In some instances it may be desirable to modify the glass structure as necessary for increased waste loading. This can be done by addition of network modifiers such as alkalis or boron. Addition of these elements to glasses can result in decreased melt viscosity and increased waste loading. This dual purpose may be utilized in one scenario where elements containing these compounds are added to the reactor immediately prior to tapping.

Considering the elements and their simple oxides only, there are a few different reactions paths which may be followed. The starting materials in the glass batches were usually oxides or carbonates. After carbon dioxide loss from the carbonate, the following reaction pathways are possible:

$$Cs_2O \rightarrow 2Cs + 1/2O_2(g) \rightarrow 2Cs(g) + 1/2O_2(g)$$
$$Na_2O \rightarrow Na_2O(g) \rightarrow 2Na(g) + 1/2O_2(g).$$

These are identified as pathways as they are not intended to show the complete chemical reactions, which would involve reductants such as carbon or iron. The first reaction shows the reduction of Cs^+ to Cs^0, with liberation of oxygen. This is followed by volatilization of the elemental cesium, which has a boiling point near 700 °C. The second reaction pathway shows sublimation of sodium monoxide (at 1275 °C), followed by reduction to gaseous elemental sodium. Both series of reactions are possible, with the actual path dependent upon the specific element and reaction conditions. It is important to note that these reactions can occur not only during "normal" processing conditions, but also during the heating period prior to melting of the entire metal and oxide charge. The proposed reactions do not include the more complicated considerations of bonding within a material such as sodium tetraborate or within the (entire) molten oxide.

Figure 5.9
Volatility Of Alkali Metals And Oxides As A Function Of Temperature. Boiling Points Are Indicated.[6]

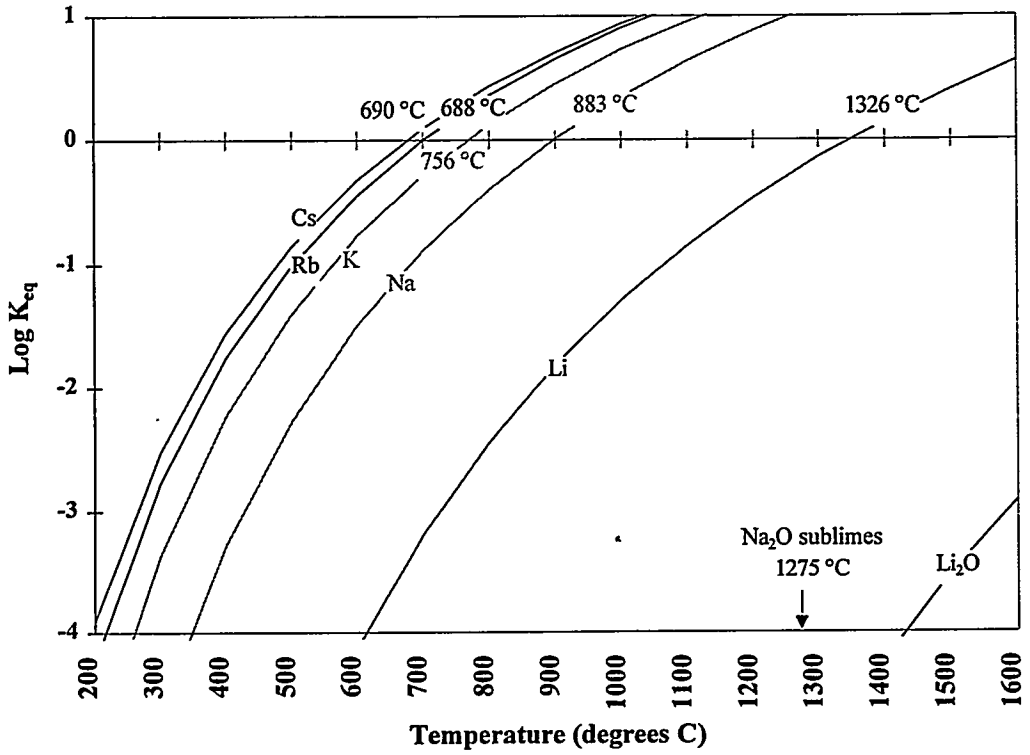

The individual parts of these reactions for the different elements can be shown as the vapor pressure of the element and oxide and the free energy of reduction of the oxide (shown in more typical form below as the oxidation reaction). Figure 5.9 shows the potential for volatilization, expressed as the equilibrium constants for formation of gaseous alkali metals and oxides from the corresponding condensed phase.[4] This figure shows that on the basis of both elemental and oxide volatility, lithium is the best choice as an alkali additive. The other alkalis volatilize at temperatures far below normal operating temperatures (data were not available for francium but the trend is apparent).[5] Sodium is the second choice, but is obviously inferior. Lithium forms the only stable high temperature simple oxide as Na_2O sublimes and the remaining alkali oxides decompose at temperatures near 400°C. Boron is non-volatile at reactor temperatures (log $K_{eq} \approx$ -8 at 1600°C).

The other important factor is if the additive will be reduced to the metal phase. Comparison of the free energy of oxidation to other bath components (Figure 5.10) indicates that sodium, cesium, potassium and rubidium should be reduced, while lithium will remain as the oxide.[4] Boron may also be reduced (similar to the potential reduction of silicon). Coupling this with the non-volatility, the

primary method of boron removal from the glass will be via reduction. These conclusions neglect the formation of other volatile oxide compounds. The kinetics of the reduction process for all elements is another factor not considered here that but may be important under the scenario of using various additive materials prior to tapping.

Figure 5.10
Free Energy Of Formation Of Oxides Of Alkalis, Primary Glass Forming Elements And Carbon

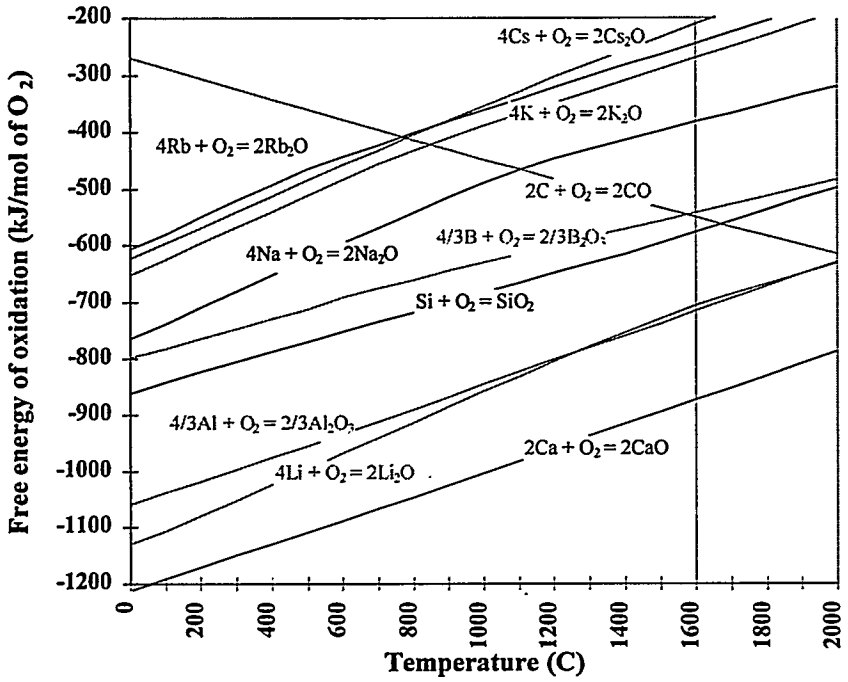

In order to evaluate the loss of these materials (via either pathway), elemental analysis for boron, sodium and lithium was done on glass samples following bench scale experiments. These three elements were combined in the initial batch (present throughout the duration of the experiment), and were added as either sodium or lithium carbonates, boron oxide, or sodium tetraborate. All elements were not present in every experiment. Post-run samples were analyzed by ICP.[7] These results are presented below.

The MMT Leaching and Dissolution Resistance test method was used to evaluate the leachability and stability of several waste glasses.[8] This testing was done on glasses prepared as part of surrogate partitioning studies (in the same reactor used here). Test results showed that the glass leachability was extremely low, even with additions of the network modifiers. Leach testing was also done on other glasses synthesized in simple crucible melts at high temperatures under

typical reducing conditions. Several of these glasses contained network modifiers, RCRA metals and uranium. All glasses passed both the TCLP and the Product Consistency Test (PCT), which is used to evaluate high level waste glasses.[9]

5.1.1.2.2. Summary of experiments and results:

Experiments were done in both on bench scale CEP systems. Two different types of crucibles were used: an alumina crucible and a Zircon crucible. Crucibles were loaded with the iron charge containing the surrogate material (HfO_2), with the glass components added above. All five experiments used different glasses.

Details on the amounts of material and crucible used in each experiment are given in Table 5.8. Iron was always the bath metal, with an initial carbon level of 3.16 wt%, except for 05-94-013 (3.97 wt%). The initial hafnia concentration was approximately 1000 ppm in the metal, with the calculated HfO_2/glass ratio and glass/metal ratio remaining nearly constant.

Table 5.8
Summary Of Charge Preparation

Run#	Metal	Initial C (wt%)	HfO_2/ Glass (%)	Glass/ metal (%)	Crucible
05-94-010	Fe	3.16	0.97	10.4	Alumina
05-94-013	Fe	3.97	1.01	10.0	Zircon
05-94-029	Fe	3.16	1.02	10.0	Alumina
10-94-004	Fe	3.16	1.01	9.8	Alumina
10-94-005	Fe	3.16	0.99	9.9	Alumina

The mixture was heated until molten, and a four hole lance was lowered into the crucible to a position near the bottom. A mixture of carbon dioxide and argon was subsequently injected for a specified period of time. This ensured vigorous mixing and provided an oxidant. Upon completion of the gas injection, the lance was removed, the reactor turned off, and the melt allowed to slowly cool to room temperature. Post-run samples were sent for major component analysis by ICP (all glass components and hafnium). Other metal and glass samples were analyzed for hafnium content by NAA.

Table 5.9 shows the process conditions for the experiments. This includes the reactor temperature measured at the susceptor, which is about 25-75°C greater than the actual process temperature.[10] The total time the bath was molten and

time of gas injection are included, as are the gas injection rates and measured offgas flow rates (which include purge gases).

Table 5.9
Summary of Process Conditions

Run#	Temp (°C)	Molten (min)	Gas inject (min)	Ar (SLPM)	CO_2 (SLPM)	Offgas (SLPM)
05-94-010	1525	90	67	0.18-0.5	0.024	1.52
05-94-013	1375	76	66	0.18	0.025	1.52
05-94-029	1500	54	48	0.15	0.021	1.52
10-94-004	1550	94	87	0.89	0.099	3.07
10-94-005	1550	103	95	0.89	0.099	3.23

5.1.1.2.3. Results and Discussion:

Results for oxide recovery in the ceramic phase for each experiment are presented in Table 5.9. The recovery of hafnium is inconsistent. Such results are typical for bench scale partitioning experiments, in which as opposed to the other glass formers, the hafnium was initially loaded at the bottom of the crucible into the metal. Analysis of metal samples for hafnium content indicate typical final concentrations on the order of 1 ppm. The hafnium not recovered in the glass may therefore be associated with the oxide crucible. While mass balance closure on the bench scale is not conclusive, nearly 97% recovery in the ceramic phase of tuyere injected hafnium has been demonstrated on the pilot scale.[12]

Table 5.10
ICP Results And Data Analysis For Glass Sample From 10-94-004.

Oxides	004-C4	scaled	HfO_2 rec	Initial HfO_2	% recovered	
Al2O3	25.14	25.48				
CaO	23.21	23.52				
FeO	0.31					
SiO2	43.99	44.59				
Na2O	0.97	0.98				
B2O3	3.96	4.01				
Li2O	0.47	0.48				
HfO2	1.00		4.28	4.04	106.05	
ZrO2	0.00	0.00				
	99.06	99.06				
	97.75					

Excellent retention is observed for calcium, aluminum and silicon. Results for sodium show consistently high levels recovered in the glass. This may not be expected based upon the sublimation, reduction and volatilization reactions and is the subject of further experimentation. The experiment involving lithium had nearly 90% recovery in the ceramic phase. A high retention level is in agreement with simple thermodynamic arguments. The boron data consistently demonstrated the lowest recovery. This is attributed to reduction into the metal.

Figure 5.11
Elemental Recovery In The Ceramic Phase For Each Experiment

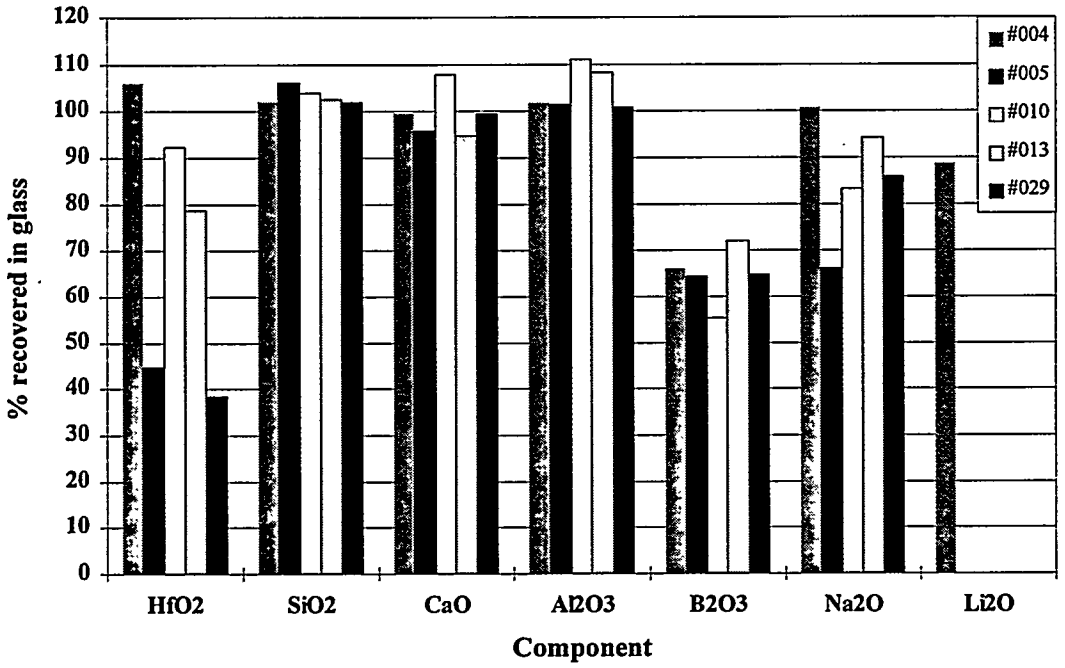

Figure 5.12
Average Recovery In The Ceramic Phase. Error Bars Represent One Standard Deviation. (Lithium Was Only Used In A Single Experiment)

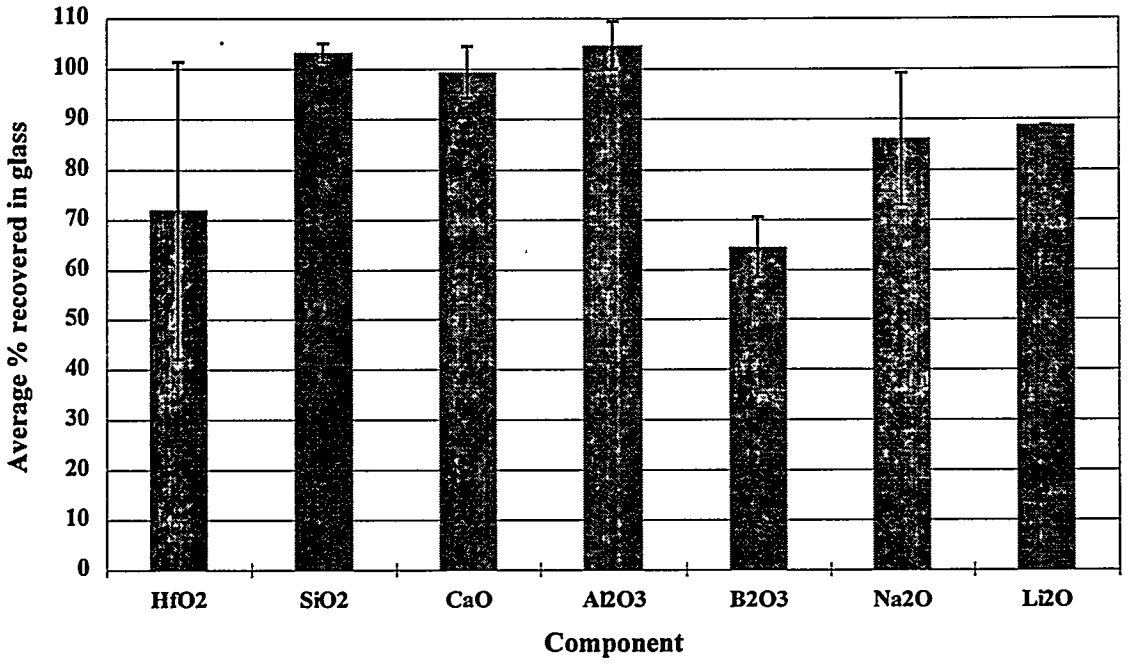

Figure 5.12 presents a summary of the data, including the average recovery of each component. The error bars on this plot represent one standard deviation. Within error, nearly all of the Hf, Si, Ca, Al, Na and Li are accounted for in the glass. Only boron shows a significant deviation from 100% recovery.

Comparisons were made between data for each experiment and processing conditions such as total time molten, time of gas injection and gas flow rate. These data are shown in Figure 5.13 and Figure 5.14. Figure 5.13 shows that there is a correlation between process temperature and material recovery in the glass for sodium and boron.

The line in Figure 5.13 is simply drawn as a guide and not meant to imply a linear temperature dependence. The temperature dependence may be related to several factors including the free energy of reduction and the vapor pressure. All process temperatures were greater than 1275°C, so sodium oxide sublimation is expected to occur, accompanied by the gas phase reduction of Na_2O to Na. Temperature dependencies of the equilibrium constants of these reactions are quite different with this limited amount of data.

Figure 5.13
Temperature Dependence Of Ceramic Phase Recovery For B_2O_3 And Na_2O

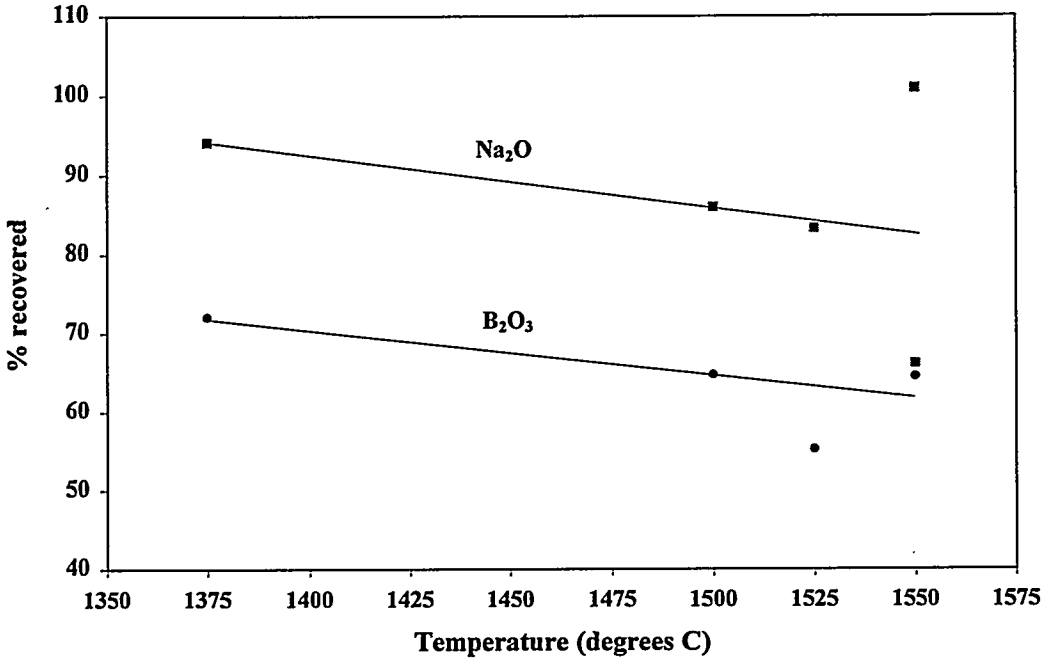

Figure 5.14
Time Dependence Of Boron And Sodium Recovery In The Glass

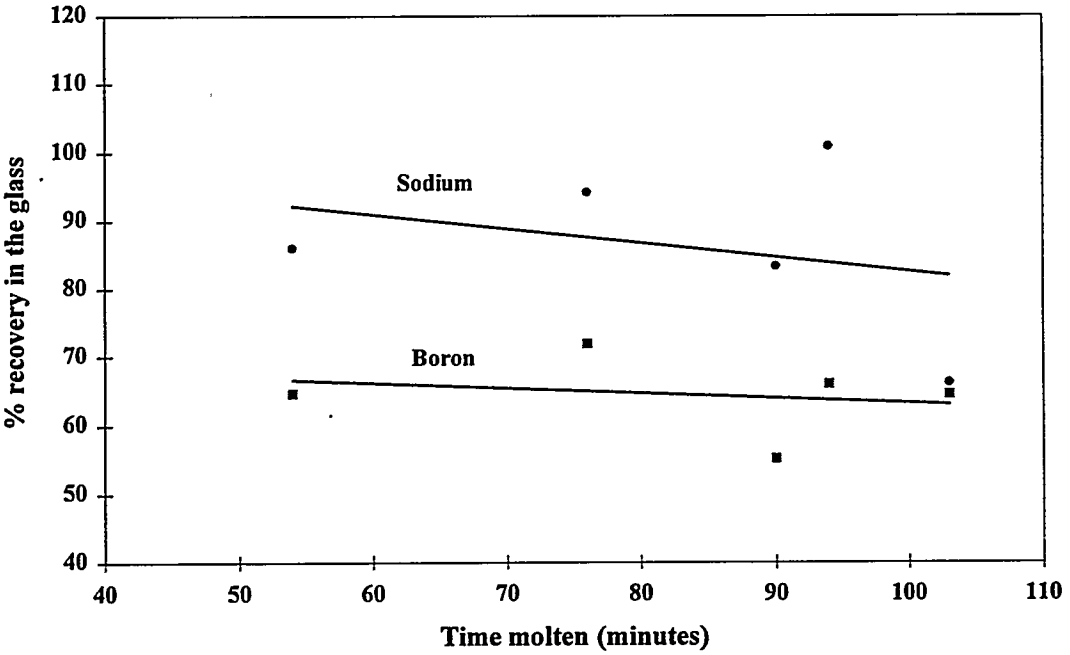

The reaction for the reduction of boron, $B_2O_3 + 3C = 2B + 3CO(g)$, becomes increasingly thermodynamically favorable at higher temperatures, with $\Delta G > 0$ until $T > 1575°C$. This does not mean that the reaction will not occur at lower temperatures. It does indicate that the temperature trend observed in Figure 5.13 is in the correct direction. The actual temperature dependence should be much more significant, as from 1375°C to 1550 °C the equilibrium constant for the above reaction varies from about 1×10^{-3} to 5×10^{-1}.[4] This assumes that this is a strictly thermodynamic result in which ideal solution behavior is observed.

A variable of interest is the starting form of the material. The first three experiments used a combination of sodium carbonate and boron oxide, while the last two experiments used sodium tetraborate. Somewhat similarly, glass frit is used in many applications. For instance, it may be used to minimize foaming. Table 5.11 presents statistics on the sodium and boron oxide recoveries as a function of the starting materials. Within one standard deviation, the results are the same. However, the experiments involving the Na_2CO_3/B_2O_3 mixture had lower average recoveries and higher standard errors. This process variable that may be explored in the future.

Table 5.11
Dependence Of Boron And Sodium Recovery On Starting Material

	Na_2CO_3 / B_2O_3[1]			$Na_2B_4O_7$[1]		
	Average (%)	Std Dev[2]	% Error[3]	Average (%)	Std Dev[2]	% Error[3]
B_2O_3 recovery	62	5.9	9.5	68	5.1	7.5
Na_2O recovery	83	17.4	20.8	90	5.8	6.4

[1]Initial form of sodium and boron.
[2]One standard deviation.
[3]Standard error.

Conclusions:

The loss of alkalis and boron from the glass by either volatilization or reduction was investigated by comparison between the initial batch glass mixture and final analysis of the glass after removal from the reactor. Data were adjusted to account for crucible dissolution. The following conclusions can be made.

- Mass balance closure in the ceramic phase for the major component oxides CaO (99 ± 5 wt%), Al_2O_3 (105 ± 5 wt%) and SiO_2 (103 ± 2 wt%) is excellent.
- Recovery of hafnium was 72 ± 30 wt%. This is excellent closure considering the small scale of these experiments.

- The one experiment involving lithium shows high retention (89%) in the ceramic phase.
- Sodium retention in the glass is surprisingly high (86 ± 13 wt%).
- Boron recovery was the poorest of any element. This was consistent for all five experiments (65 ± 6 wt%), with a standard error of only 9%.
- On average, the amount of crucible material dissolved into the ceramic phase is 7.1 ± 3.4 wt% of the initial glass weight.
- Ceramic phase recovery of sodium and boron decreases as temperature is increased. In the absence of stricter process controls, quantitative modelling is preliminary at this point.

References:

[1]C.M. Jantzen, "Systems Approach to Nuclear Waste Glass Development," J. Non-Cryst. Solids **84**, 215 (1986).

[2]For a comparison of the properties of different types of radioactive waste glasses see reference 1 and "Radioactive Waste Forms for the Future," W. Lutze and R.C. Ewing, eds., North-Holland, Amsterdam (1988).

[3]H.D. Schreiber, "The Chemistry of Uranium in Glass-Forming Aluminosilicate Melts," J. Non-Cryst. Solids **91**, 129 (1983); H.D. Schreiber, G.B. Balazs and B.J. Williams, "Chemistry of Uranium in Aluminophosphate Glasses," J. Amer. Ceram. Soc. **65**, 449 (1982); H.D. Schreiber and G.B. Balazs, "The chemistry of uranium in borosilicate glasses. Part 1. Simple base compositions relevant to the immobilisation of nuclear waste," Phys. Chem. Glasses **23**, 139 (1982).

[4]Calculations done using HSC Chemistry, version 2.0, Outokumpu Research Oy, Finland.

[5]Data from "CRC Handbook of Chemistry and Physics," 74th edition, D.R. Lide ed., CRC Press, Boca Raton (1993).

[6]F.A. Cotton and G. Wilkinson, "Advanced Inorganic Chemistry," 5th edition, Wiley Interscience, New York (1988).

[7]Analyses were done by Commercial Testing and Engineering Company (Denver, CO).

[8]J.M. Jewell, "Leaching and Dissolution Resistance (LADR) Testing of PRDA Samples," IPR-94-036 (December 1994).

[9]S.-B. Xing, I.S. Muller and I.L. Pegg, "Development of Glass Compositions for Molten Metal Slag Wastes," Final report for Molten Metal Technology, Inc. from GTS Duratek and Vitreous State Laboratory at The Catholic University of America (1994).

[10]Run summary 10-94-003 from CTP-94-009, "Optimization of the Vitreous Phase for Stabilization of Radioactive Species."

[11]C. Herbst and E. Hinkle, "Hafnium and Cerium Partitioning Experiments: NAA and XRF Results and Data Analysis," IPR submitted.

[12]Mahesh Desai, "Addendum to Interim Progress Report (IPR-94-017) of Chlorine Injection Study: Iron System," (December 2, 1994).

5.1.1.3. UF_6 Conversion Program

5.1.1.3.1. Introduction

The thermodynamic feasibility of a molten metal process based on Catalytic Extraction Processing (CEP) technology has been established for the economical conversion of uranium hexafluoride (UF_6) to uranium oxide (UO_x) and anhydrous hydrogen fluoride (HF). Based on the advantages of this technology over traditional commercial uranium chemistry, an experimental program is underway separate from this contract, to demonstrate a CEP-based process for conversion of depleted UF_6 tails and is described here to inform the reader.

As part of the initial phase of this program, a CEP reactor system has been installed in Oak Ridge, TN to perform engineering-scale UF_6 conversion studies. The primary goals of the program include verification of the process chemistry associated with the proposed CEP process. Initial experimental results have demonstrated safe, reliable processing as predicted by feasibility studies.

5.1.1.3.2. Background

Uranium hexafluoride is one of the most widely used chemical compounds of uranium. Over one billion pounds of UF_6 have been produced over the past fifty years in support of the U.S. uranium isotope enrichment enterprise. There is a growing concern regarding the long-term environmental risks associated with continued storage of large UF_6 inventories. The Department of Energy (DOE) currently stores approximately 610,000 metric tons of UF_6, with an additional 22,000 metric tons stored by USEC. Safety concerns, combined with pending legal impacts of EPA hazardous waste rulemaking on the industry, have increased interest in economical conversion of depleted UF_6 to a more stable uranium compound. This uranium would be recycled in other applications elsewhere in the DOE complex or nuclear industry, while the valuable fluorine would be recycled to the commercial chemical market as anhydrous HF.

Current UF_6 conversion processes use various methods to produce ceramic grade uranium oxide (UO_2) for fabrication of nuclear reactor fuel. The two basic methods employed include wet processes based on precipitation from aqueous solutions and dry processes involving hydrolysis and reduction in fluidized beds, rotating kilns, or flame reactors. Wet processes have the disadvantages of complexity and production of large quantities of secondary waste. Problems with dry processes include non-uniform ceramic product properties and production of radioactive aerosols which must be trapped.

In view of the practical limitations of existing commercial uranium recovery processes, CEP has been proposed as an efficient and economical method of UF_6 recycling. Production of both a uniform UO_x ceramic product and anhydrous HF has been

thermodynamically predicted for CEP reaction conditions. Based on the favorable expected results, an experimental plan was developed to demonstrate CEP conversion of UF_6.

5.1.1.3.3. Method of Approach

5.1.1.3.3.1. Processing Scenarios

Three process flowsheets have been considered for uranium recovery. The baseline flowsheet employs a traditional approach to UF_6 conversion, hydrolysis with steam and reduction with hydrogen. The baseline also features quantitative recovery of the latent fluorine value as anhydrous hydrogen fluoride (HF). In this case, the complex and interrelated chemical reactions involving numerous uranium intermediates and complexes can be described by the overall equation:

$$UF_6 + 2H_2O + H_2 \rightarrow UO_2 + 6HF.$$

An important advantage of this conversion is that the two end products are separated with uranium as a stable solid and the fluoride as anhydrous HF vapor.

The second flowsheet alternative is based on reaction of UF_6 with lime (CaO) with conversion of the fluorine to fluorspar, CaF_2. This mineral is one of the most insoluble and chemically and thermally stable fluorides. It is the preferred chemical feedstock for the industrial production of HF and has direct use as a metallurgical flux. Other metal oxides such as Al_2O_3 and MgO can also be utilized. With CaO, the process can be represented by the overall equation:

$$UF_6 + 3CaO + CH_4 \rightarrow UO_2 + 3CaF_2 + CO + 2H_2.$$

A third process scenario has been proposed for the production of uranium metal instead of oxide. For example, it is possible to produce a U-Fe alloy for AVLIS feed or a very dense product for fabrication or casting of radiation shielding. In addition to the alloy, this chemistry will result in the production of a secondary metal fluoride of industrial significance:

$$UF_6 + 2Al + 2Fe \rightarrow UFe_2 + 2AlF_3.$$

5.1.1.3.3.2. Demonstration Program Objectives

The primary objectives of the UF_6 demonstration program are the following:

- Determine the most effective and economical conversion process. This includes demonstration of the necessary technical feasibility with the concurrent understanding and development of scale-up relationships to commercial-sized units. The overall process optimization will also include evaluation of energy

balance, reagent uses and costs, recycling opportunities and potential development of alternative reactor geometries.

- Demonstrate recycling of feed materials. The production of usable uranium by-products or a uranium material suitable for environmental disposal and valuable fluoride by-products such as HF, AlF_3, CaF_2, and/or MgF_2 will be shown.

- Demonstrate co-processing of alternative waste materials. Contaminated scrap metals (e.g., aluminum, iron, nickel, copper) will be used as bath materials and to concurrently demonstrate metal decontamination capabilities. For example, iron and nickel decontamination has been accomplished previously with CEP to greater than 99% contaminant removal. Aluminum will be used as a co-feed to reduce UF_6. Other potential co-feeds include contaminated waste water, waste water treatment sludge (CaO source), waste oils, and spent activated carbon.

- Determine optimal method for uranium product removal. Efficient removal of UO_2 without fluxing agents will be investigated. Fluxing options and glass compositions will be developed as necessary. In view of the commercial application, low cost flux materials will be emphasized. The density of the UO_x product will be maximized to reduce disposal costs if re-use options are not favorable. The final form, stability and valence state of the uranium oxide will be verified for the disposal option.

- Evaluate refractory materials and longevity. Both crucible and lance/tuyere materials will be evaluated in each of the different processing schemes and with different bath materials.

- Optimize feed system design for enhanced conversion. Lance and tuyere configurations and operating conditions will be evaluated, including recessed lance designs and utilization of different superficial gas injection velocities prevent lance plugging and promote reactant mixing. Additionally, the behavior of uranium intermediate complexes will be studied.

5.1.1.3.3.3. Experimental Testing Objectives

The following specific test objectives will be achieved in the scope of the first experimental campaign, which encompasses initial testing on all three baseline flowsheets to establish the technical feasibility of UF_6 processing. The primary test objectives include:

- Quantify conversion in the different reaction scenarios. The partitioning of elements between off-gas and condensed phase products according to thermodynamic predictions will be demonstrated. This will be done by varying the feed to co-feed ratios and following the product distributions with the mass spectrometer.

- Demonstrate the conversion of fluorine to predictable products. For the baseline flowsheet, production of HF and the absence of UF_6 in the off-gas to the detection limit of the mass spectrometer (≤ 100 ppm) will be demonstrated. Analysis of the chemical traps will also be used to determine the presence of UF_6 in the process off-gas. For the second and third flowsheets, the quantitative production of metal fluorides will be shown.

- Demonstrate uranium containment in a recoverable condensed phase. Methods for uranium removal and the necessity for added fluxes will be evaluated, including development and testing of initial flux compositions. In the case of uranium recovery in the metal, the chemical composition of the uranium-iron alloy will be determined.

- Evaluate compatibility of lance and crucible materials with feed and typical ceramic compositions. The baseline materials used in these first experiments are graphite and alumina. The capabilities and limitations of these materials will be evaluated, including an evaluation of the necessity for using coatings and alternative materials.

- Evaluate the use of copper as the metal catalyst. Thermodynamic calculations indicate the favorability of using this metal. However, the reaction kinetics with a copper-based system relative to iron have not been fully quantified.

5.1.1.3.3.4. Experimental Facility Overview

The experimental facility incorporates the general capability to feed gaseous UF_6 and various co-feeds to a Catalytic Processing Unit (CPU) in a variety of process flowsheet scenarios

5.1.1.3.3.4.1. Feed System

The feed system consists of an electrically-heated environmental enclosure for generating a UF_6 vapor feed, gas manifolds for various gaseous components, a steam generator, and a solid feeder. The UF_6 feeder accommodates a standard 5A/B UF_6 feed cylinder (with nominal 25 kg UF_6 capacity) and is equipped with flow and temperature controls as well as leak detection instruments. The feed system is designed to deliver up to a nominal 1 kg/hr of UF_6 vapor at a pressure of up to 25 psig. Gaseous co-feeds as well as purge and blanket gases (N_2 and Ar) are received in standard industrial high pressure cylinders and manifolded to the CPU with integral pressure and flow controls. Solid co-feeds (e.g., CaO and CaF_2) are batch-charged to the CPU (along with the initial metal charge) as well as lance-fed to the CPU in a continuous mode from a feed hopper.

The CPU is a crucible-based reactor modified by MMT specifically for UF_6 service. The unit will operate with a variety of molten metals, including iron, nickel, and copper. The nominal temperature range is 1000°C to 1700°C. The crucible design will

accommodate a nominal 45 kg of metal and will allow the collection of sufficient ceramic product to support a 6 hour experimental campaign. Multiple tests may be performed for each experimental campaign. The CPU can be operated under a broad range of processing conditions to enable parametric mapping of process performance for the assumed reaction scenarios. The CPU operates at essentially atmospheric pressure. Metal and ceramic phase tapping is not provided although the design allows metal and ceramic phase sampling.

5.1.1.3.3.4.2. Off-Gas System

The off-gas system consists of a ceramic process filter to remove entrained metal and ceramic particulates from the CPU, chemical traps to quantitatively react the CPU-generated HF and residual UF_6, and HEPA filters for final particulate removal. The ceramic filter operates in the 100°C to 200°C temperature range to preclude the adsorption of HF and UF_6. The chemical traps are designed to accommodate a variety of chemical sorbents and operated over a sufficiently broad temperature range to allow optimization of trapping kinetics. The baseline sorbent is alumina (Al_2O_3) operating at a temperature of 300°C.

5.1.1.3.3.4.3. Purge System

The purge system consists of a cold trap, chemical traps, and HEPA filter to remove bulk process gas from the experimental system after completion of an experimental campaign. Valving is provided to allow process gas evacuation and inert gas purging (with N_2 or Ar) of the UF_6 feed cylinder pigtail, feed lines, and reactor before removing the CPU for post-run examination. Analytical instruments also vent to the Purge System for uranium recovery and HF fixation. The design also provides a surge drum to collect bulk process gas released from the feed system or CPU under a significant pressure surge event.

5.1.1.3.3.4.4. Analytical and Control System

The analytical and control system includes instruments for the quantitative off-gas analysis for process control and performance determination. Reactor control is based primarily on off-gas analysis. The progression of a typical experiment will be tracked by the evolving concentrations of HF, CO, and H_2 in the CPU off-gas. Process gas sampling capability utilizing a mass spectrometer is provided before and after the chemical trap. Off-line analytical equipment is provided for compositional analysis of the ceramic and metal phases. After completion of an experimental campaign, the crucible will be removed from the CPU and bisected for quantitative analysis. X-ray fluorescence or energy dispersive x-ray diffraction will be used to provide quantitative elemental distributions in the crucible, metal, and ceramic (as well as any interface). Scanning electron microscopy (SEM) will be utilized to identify any distinct phase regions of interest in the crucible, metal, ceramic, and any interfaces. Electron probe

microanalysis will be used to determine the chemical identity of the distinct phases identified by the SEM.

5.1.1.3.3.4.5. Containment System

The containment system provides multiple physical barriers to ensure double- and triple-containment of radioactive gases and solids, as well as flammable and toxic process components, in the event of a primary process breach. The feed system, CPU, off-gas system, and purge system are located in separate, independently-ventilated, secondary-containment structures. The CPU is readily removable from the containment structure for post-run examination. A hooded work area is also provided for disassembly of the CPU crucible after a test. All components of the facility are located in a third containment structure for ultimate environmental isolation and protection of workers. HF, H_2 and CO monitors with alarm circuits are provided in the various containment structures to alert the operator to process leaks.

5.1.1.3.4. Procedures

5.1.1.3.4.1. Experimental Procedure

Determination of the test conditions for a specific run begins with selection of a flowsheet scenario. The overall chemical reaction equation is used to specify co-feeds required for stoichiometric conversion of UF6. Thermodynamic predictions are used to guide the specification of the type of metal catalyst and operating conditions to achieve the desired elemental partitioning.

Reactor operating parameters are based on constraints defined by the given flowsheet scenario. The reactor feed rate is limited by the maximum allowable off-gas flow, minimizing entrainment of metal and ceramic products in the off-gas. Well-mixed conditions in the CPU ensure that the residence time required for conversion is well below that set by the feed rate. Constant temperature is maintained throughout the run with induction coil power input. The CPU temperature and feed rates are controlled for steady-state operation.

Analysis of CPU gaseous product flow rates and compositions is achieved on-line with rapid sensing instrumentation. UF_6 conversion is monitored continuously to the analytical limits of detection equipment. After a run, the metal and ceramic products are emptied from the CPU for analysis. These results are combined with feed and off-gas data to define the material balance for the reactor system. Alpha and gamma spectroscopy field measurements will be made on the condensed phase as an immediate indication of the presence and distribution of uranium. This testing will identify any undesirable uranium phases such as UO_2F_2 and UF_4 that represent incomplete conversion of UF_6.

5.1.1.3.4.2. UF_6 Processing Health and Safety Issues

The CEP conversion process involves radiological, chemical, and flammable gas hazards. The experimental system is designed to be inherently safe with process safety based primarily on engineered controls and fail-safe features rather than reliance on administrative limits and actions. The following discussion of specific hazards focuses on system and operational considerations to ensure process safety and protection of the operations staff during the experimental campaigns.

5.1.1.3.4.3. General Radiation Management Plan

Radiation exposures of the work force, the public, and the environment will be maintained well below applicable regulatory limits and generally accepted radiochemical management guidelines, consistent with the As-Low-As-Reasonably-Achievable (ALARA) principal. Implicit in the ALARA philosophy is the cautious assumption that no threshold or dose exists below which there is no detriment. Any radiation exposure, however small, carries with it some element of risk. Under the linear no-threshold hypothesis, the risk associated with radiation is proportional to dose. Consequently, no radiation exposure will occur from waste processing operations and related waste management activities without a positive net technological, economic, and societal benefit. Wherever there is a potential for radiation exposure, both a health physics program and an ALARA program will be implemented. Each employee involved in radiological work will demonstrate responsibility and accountability through an informed, disciplined, and cautious attitude toward radiation and radioactivity. Performance of the radiation control program will be based on actual radiation exposures compared to regulatory limits.

5.1.1.3.5. Experimental Results

Reliable processing of UF_6 to form UO_x and HF via the baseline flowsheet scenario has been demonstrated. In these initial tests, UF_6 was injected into a molten copper bath at 1250°C through a Ni-Al_2O_3-C lance. No ceramic flux additives were used in these trials. The metal bath was contained within a graphite crucible. Two different reaction pathways were investigated by varying the co-feed material. In the first trial, carbon dioxide and hydrogen were fed to convert UF_6 via a UF_4 intermediate. Hydrogen and superheated steam were co-fed in the second trial to convert UF_6 through the UO_2F_2 pathway. In both tests, no residual UF_6 was detected in either the process off-gas or the chemical traps to a Lower Detection Limit (LDL) of 100 ppm.

Other experimental results confirmed the design of the bench-scale facility. No damage to the graphite crucible was observed after the run. Feed injection studies have led to a better understanding of lance configurations and materials for use in UF_6 applications. Uranium oxide collection as a particulate product was demonstrated, as was the high-temperature uranium reaction chemistry predicted by thermodynamic feasibility studies. The flexibility of the facility was also shown to provide a functional mechanism

for studying uranium conversion reactions in several different chemical pathways and reactor configurations.

Safety programs for UF_6 processing have been demonstrated, confirming the functionality of the inherently safe facility design. The safety parameters that were verified include safe handling of UF_6 and HF, effective chemical trapping of HF product, containment of CO and H_2, environmental monitoring, and on-line instrumentation.

5.1.1.4. Processing of Mixed-Waste Water Treatment Solids

The efforts described in this section were not conducted under this contract, but are included to inform the reader of results of experiments which may be of interest.

5.1.1.4.1. Feed Description

The mixed-waste sludge used in these experiments is a byproduct of industrial wastewater treatment. The bulk composition is shown in Table 5.12. The major constituents present in the sludge are shown in Table 5.13.

Table 5.12
Bulk Composition of Mixed-Waste Sludge

Constituent	Concentration
Water	63-68 wt%
Carbonate ($CO_3^=$) (estimated)	40-74 wt%
Calcium (Ca)	10-27 wt%
Aluminum (Al)	2-8 wt%
Sodium (Na)	1 wt%
Iron (Fe)	1-3 wt%

Table 5.13
Major Sludge Constituents (Dry Basis)

Constituent	Concentration*
Ca	41 wt%
Al	2 wt%
Na	2 wt%
Fe	5 wt%
Mg	<1% wt%
U_3O_8	<1% wt%
SiO_2	<1%
$CO_3^=$ (Estimated)	20%
OH^- (Estimated)	27%

Based on X-Ray Fluorescence Results and Carbon Balance (XRF Analysis Performed by Southwest Research Institute)

The sludge is also contaminated with residual organics, chlorine, phosphorus, RCRA metals, and nickel. The combined chlorine and fluorine level is 0.5 wt%, and the phosphorous level is roughly 1 wt% on a dry weight basis.

The major radionuclides in the mixed-waste sludge are U, Tc, and Cs with respective average activities of 1.2×10^{-3} μCi/g, 8.7×10^{-4} μCi/g and 1.8×10^{-6} μCi/g.

5.1.1.4.2. Ceramic Phase Optimization

The goals of the ceramic-phase optimization strategy for Q-CEP processing of mixed-waste sludge, consistent with those for CEP processing of any feed with a significant concentration of ceramic-phase formers, are operability, functionality and final-form stability. In the case of operability, the ceramic phase composition must be engineered to form a liquid with a workable viscosity and a minimum corrosivity toward refractory containment. Functionality goals include engineering the composition such that the ceramic phase accommodates major ceramic-forming components and captures minor hazardous and/or radioactive components in a non-leachable form. Finally, the ceramic phase must have stability with respect to recycling application requirements or expected exposure during long-term storage. In Q-CEP applications, there is an additional goal of maximizing volume reduction.

5.1.1.4.2.1. Ceramic Durability Background

5.1.1.4.2.1.1. Mechanisms

The chemical durability of a glass is a function of both its kinetic rate of approach to equilibrium and its final thermodynamic equilibrium state in an aqueous environment. The thermodynamic stability relates to chemical composition and the type of bonding of the glass. The kinetic stability, while influenced by structural features in the glass, is strongly influenced by the sample geometry and testing conditions. The kinetic processes are predominantly diffusion-controlled and a function of the exposed surface area of the sample, temperature, and nature of the leachant solution.

In order to understand or predict the leachability of the ceramic phase it is important to identify the mechanism(s) by which the material is leaching or dissolving. The leaching or dissolution of a glass can be evaluated in terms of the types of reactions of the glass with an aqueous environment. These types of reactions have traditionally been discussed in terms of major processes observed for glass leaching and dissolution. The major processes identified for glass leaching and dissolution are:

- Preferential leaching of mobile ions (modifying ions: Na^{+}, Ca^{++}, Pb^{++}, etc.)
- Preferential dissolution of network formers
- Total or uniform dissolution
- Precipitation from solution
- Development of surface charge

The effect of reactant concentration, time, and temperature help identify the mechanisms of glass dissolution.

5.1.1.4.2.1.2. Engineering a Non-leachable Ceramic Phase

The first step in engineering a non-leachable ceramic phase is understanding the mechanisms by which ceramic phase systems leach or dissolve. Once the mechanism(s) of dissolution is known, adjustments can be made in the chemistry or final form of the ceramic phase to minimize the reactivity of the material. Efforts to enhance the non-leachability of the ceramic phase during CEP operations include 1) optimization of target ceramic phase chemistry, 2) chemical additives to the system prior to tapping to enhance the resistance to leaching, 3) post-treatment of the tapped material, which may include re-melting or a thermal treatment to enhance a crystalline phase, and/or 4) changing the quench rate of the tapped material (slow cool vs. rapid quench will influence the final form of the material). In general, increasing the quench rate of the liquid increases the likelihood of forming a glassy or vitreous material.

5.1.1.4.2.1.3. Development of Ceramic Phase Chemistry

The following approach for ceramic phase chemistry development can be taken to maximize non-leaching characteristics:

- Formation of a three-dimensional network with a high degree of connectivity of the glass structure to provide a solid base network;
- Incorporation of specific components into the glass network to enhance the thermodynamic stability of the leachable components in the structure. This includes ion substitution, formation of complexes, and trapping of ions in the interstitial or void space of the network;
- Minimization of diffusion pathways for mobile ions to enhance the kinetic stability of leachable components in the structure. This is accomplished by decreasing the void or interstitial space of the glass network.

This approach is focused on the development of a glass structure that maximizes both the kinetic and thermodynamic stability of the glass. In general, this is achieved by developing a glass structure with a high degree of connectivity (minimize non-bridging oxygen) while minimizing diffusion pathways for mobile ions.

5.1.1.4.2.1.4. Final Form of the Ceramic Phase

The final microscopic and macroscopic forms of the ceramic phase also play a major role in the leaching characteristics of the material. The resultant microstructure of the ceramic phase is a function of the ceramic phase chemistry and the quench rate of the melt (i.e., mode of tapping). The microstructure is also related to the glass forming ability (glass vs. polycrystalline), liquid/liquid phase separation, and precipitation of a crystalline phase(s).

The macrostructure of the ceramic phase is primarily determined by the mode of ceramic phase tapping, crushing, and grinding. In general, increasing the quench rate increases the likelihood of obtaining a 'glassy' material. The crushing and grinding of the ceramic phase will be determined by end user specification of the ceramic phase product. However, regulatory tests will define the exposed surface area for leachability testing.

The following approach can be taken to maximize the non-leachable characteristics of the ceramic phase:

- Minimize precipitation of soluble phases.
- Avoid liquid/liquid phase separation.

- Minimize exposed surface area.

5.1.1.4.2.2. $CaO-SiO_2-Al_2O_3$ and $CaO-B_2O_3-Al_2O_3$ Comparison

Two different ceramic-phase systems, $CaO-SiO_2-Al_2O_3$ (CAS) and $CaO-B_2O_3-Al_2O_3$ (CABAL), were selected for study in West End Treatment Facility (WETF) sludge processing. These systems were selected based on expected compatibility with the WETF components (particularly $CaCO_3$), previous experience in the case of CAS, and potential volume reduction in the case of CABAL.

5.1.1.4.2.3. WETF Ceramic Phase Optimization Strategy

In addition to non-leachability, the WETF ceramic phase compositions are optimized by considering ceramic phase partitioning, viscosity and liquidus limits, containment interaction, effects of waste stream incorporation on properties, and final form stability.

5.1.1.4.2.3.1. Phase Partitioning

The WETF feed has several major and minor components which will partition to the ceramic phase, including Ca, Al, Mg, Si, Na, K, Li, S, Cl, and U. Of these components, Ca and Al are the major species which influence ceramic optimization strategies.

5.1.1.4.2.3.2. Viscosity and Liquidus

Operable Q-CEP ceramic-phase compositions are defined by the viscosity and liquidus temperatures. In the selected composition windows for both the CAS and CABAL systems, viscosity and liquidus temperature of the ceramic-phase are affected mostly by variations in the CaO content. Specifically, viscosity at the operating temperature will decrease as the loading of CaO from the WETF feed increases. These same increases in CaO content result in increases in the liquidus temperature. As a result, these opposing effects of CaO must be balanced through adjustment of the ceramic composition.

5.1.1.4.2.3.3. Containment

To maximize volume reduction for Q-CEP processing of WETF sludge, it is desirable to maximize the loading of CaO in the ceramic-phase. This has important implications on containment performance. A highly basic (high CaO-content) ceramic-phase composition is incompatible with acidic (SiO_2- based) containment. A basic (MgO or CaO -based) or amphoteric (Al_2O_3 - based) containment system is preferable for containment of basic ceramic-phase liquids. In the case of alumina-based containment, it is preferable to maximize the Al_2O_3 content of the ceramic phase (within the compatible composition range) which will minimize the thermodynamic driving force for corrosion. However, efforts to decrease the corrosion potential by increasing the Al_2O_3 content must be balanced against increases in liquidus temperatures caused by increasing alumina content.

5.1.1.4.2.3.4. UO_2 Effects

Uranium incorporation has minor effects on the optimization strategies for the ceramic phase. At low loading concentrations, U^{4+} is incorporated into the ceramic phase in oxygen-coordinations which are independent of ceramic-phase composition. This incorporation of uranium at levels below its solubility limit lowers both the viscosity at operating temperatures and liquidus temperatures of the ceramic-phase. Because these effects are minor as compared to the effects of major components, optimization strategies for Q-CEP ceramic phase need to consider uranium incorporation in terms of second-order effects.

5.1.1.4.2.3.5. Experimental Program Objectives

The overall goal of the experimental program was to demonstrate the successful capture of hazardous and radioactive materials into targeted phases, generating a stable ceramic phase which has potential to be recycled into useful products, yet also meets the requirements for land disposal as low-level mixed waste.

The experimental program was divided into two stages: bench-scale and pilot-scale. The bench-scale runs were carried out in Q-CEP experimental units and focused on ceramic phase development and process chemistry optimization. The pilot tests focused on the scalability and operability demonstrations. These runs were performed on the RPU-3 reactor system, the former APU-1 that was operated in MMT's Fall River facility modified for operation in a radioactive environment.

Specific objectives of the bench-scale demonstration were:

- demonstration of radionuclide capture in the ceramic and metal phase;
- quantification of radionuclide capture through partitioning and mass balance determinations;
- analysis of ceramic and metal quality to meet Waste Acceptance Criteria;
- analysis of ceramic quality to meet market specifications of the identified products; and
- generation of ceramic product required for final form waste acceptance analysis.

Specific objectives of the pilot scale demonstration included:

- baseline mixed-waste sludge processing;
- feed injection system optimization;
- ceramic/metal tapping system optimization; and

- off-gas quality evaluation for potential recycle.

5.1.1.4.2.3.6. Anticipated Partitioning

The RCRA metals contained in the mixed-waste sludge stream are Pb, Ba, Cr, Cd, Ag, Hg, and As. The predicted partitioning of these elements is summarized in Table 5.14, as determined by both thermodynamics and physical properties (e.g., boiling point). The Phase I experiments confirmed the partitioning of the RCRA metals, as shown in Table 5.15.

Table 5.14
RCRA Metals Partitioning

Elements	Partitioning Phase	Predicted Partitioning Basis
Ba	Ceramic Phase	Gibbs Free Energy of Oxidation
Cr Ag	Metal Phase	Gibbs Free Energy of Oxidation
Cd Hg As Pb	Gas Phase	Volatility Volatility Volatility Vapor Pressure

Table 5.15
Recycling Analysis of Q-CEP Processing of Sludge

Product Phase	Wt % of Feed (wet)	Partitioning of Radioactivity[a]	Partitioning of RCRA Metals[b]
Water[c]	57%	0%	0%
Synthesis Gas	20%	0%	0%
Ceramic	21%	>99%	20%
Metal	2%	<1%	53%
Volatiles[d]	<1%	<1%	28%
Total	100.0%	100.0%	100.0%

[a]Normalized using pCi/g feed.
[b]Normalized using wt% of all hazardous metals.
[c]Recovered prior to Q-CEP™, and not a factor in recycle determination.
[d]Volatile metals include As, Cd, Hg, and Pb.

The third column of Table 5.15 summarizes the partitioning results experienced with the radionuclides. The dried sludge consists of about 1 wt% uranium, representing nearly 50% of the activity (~2000 pCi/g). Previous partitioning studies indicated that U could be captured in a CAS glass up to 10 wt%. Based on this and thermodynamic data, the uranium was expected to partition to the ceramic phase. Th and Pa, which represent the bulk of the remaining activity, were also expected to partition to the ceramic phase, but were not specifically analyzed for that purpose. Cs, representing less than 0.01% of the total activity, partitioned to the gas phase.

5.1.1.4.2.3.7. Ceramic Product Applications

Q-CEP processing includes the ability to tailor both the chemical and physical composition of the ceramic product to achieve desirable physical and chemical characteristics; and product removal equipment (for granulation, casting, separation, spinning, or further chemical reaction), augmented with cooling rate control equipment, can be installed to enhance the physical properties of the material and transform it into the requisite commercial form.

The various applications for Q-CEP's ceramic product may be divided into two categories: specialty inorganic markets and traditional markets for ceramic products evolved from steelmaking. Q-CEP ceramic products can be engineered to satisfy either market because Q-CEP ceramics are differentiated from steelmaking by-products in the following ways:

- Q-CEP is operated with greater control over the chemical and physical qualities of the ceramic phase, and
- Q-CEP can be operated to include or exclude a wide spectrum of elements in order to enhance ceramic performance.

Multiple uses of ceramic products derived from mixed waste have been identified, including local applications which could potentially be viewed as closed-loop recycling. These can be divided into three categories of applications: chemical reagents and feedstocks, construction materials, and support and utility materials. Three specific uses have been identified as viable applications, each of which is described below. Other uses of the ceramic product which are being pursued include fiberglass container fabrication, use as an aggregate for concrete applications within the DOE complex, and use as a flux material for other Q-CEP™ facilities. These uses are not as well-developed at this time but are being pursued as viable options for the ceramic product.

5.1.1.4.2.4. Substitute for Hydrated Lime

The ceramic product produced from Q-CEP™ will be suited for use as a substitute for hydrated lime as a neutralizing agent in wastewater treatment facilities. Hydrated lime is typically produced by the slow addition of water to crushed or ground quicklime. It

is used in wastewater treatment processes for neutralization and to precipitate phosphates and various heavy metals. Lime also assists the clarification process in wastewater treatment by coagulating a high percentage of solid and dissolved organic compounds.

The ceramic product from sludge processing will be in the form of quicklime; however, the ceramic material can be hydrated to produce a substitute product that will have essentially the same properties as hydrated lime. These include the available calcium oxide and the basicity factor (BF), which is an indicator of neutralization ability. Generally, high-calcium hydrated lime has greater than 90 percent available calcium oxide and a BF of 0.71-0.73.

5.1.1.4.2.5. Cementitious Component for Use in Cement and Concrete

The ceramic produced from Q-CEP™ may be well suited for use as a cementitious product for cement and concrete applications. "Synthetic" materials such as steelmaking ceramics have traditionally proven excellent substitutes for hydraulic cement, exhibiting lower unit weight and simultaneous higher strength in concrete compared to portland cement. These cements are generally more resistant to attack by sulfates, show greater fire repellence, and are more durable overall. Q-CEP ceramic materials are expected to perform as equal or superior to traditional synthetic materials for cementitious applications. Potential applications of the Q-CEP ceramic as a cementitious component include radioactive and mixed waste solidification, general building material, structural support and shielding for radioactive waste repositories, structural support for treatment, storage, and disposal (TSD) facilities, ceramic shielding containers, and waste container linings.

Per ASTM, hydraulic cement is a cement that sets and hardens by chemical interaction with water, and is capable of doing so under water. The hydration product that is formed upon reaction of steelmaking ceramic, generally ground granulated blast furnace slag (GGBFS), is essentially the same as the principal hydration product of portland cement, calcium silicate hydrate. Steelmaking ceramic demonstrates excellent hydraulic activity, and can be used alone or interground with traditional clinker.

Steelmaking ceramic has been used in the production of blended cements since 1905 in the United States, added at the concrete mixer as a separate cementitious substance. Blended cements, in which ground granulated steelmaking ceramic is combined with portland cement, are covered by ASTM C595. Three types of cement are addressed, varying in ceramic content, which can exceed 70 wt%. Blended cement is commonly used in ready-mixed concrete, where the steelmaking ceramic generally exceeds 50 wt% of the total cementitious component. This blend has convenient setting characteristics and usually yields the greatest strength and most favorable costs.

Solidification or stabilization of liquid wastes containing heavy metals by cement fixation is ongoing at several hazardous waste facilities. Typical cement fixation processes permanently dispose of low-level hazardous waste by mixing it with a combination of portland cement and blast furnace slag (GGBFS), and/or flyash. Tests are currently underway to demonstrate that the ceramic product from processing mixed-waste sludge is an effective substitute for either the GGBFS or portland cement in these operations.

5.1.1.4.2.6. Abrasive Blasting Media

Abrasive blast cleaning is a process for cleaning or finishing by means of abrasive particles directed at high velocity against the workpiece. These particles may be dry or suspended in a liquid. Abrasive blast cleaning decontaminates and prepares surfaces for subsequent finishing. Typical uses are removal of rust, scale, dry soils, mold, sand, or paint; roughening surfaces in preparation for bonding, painting, or other coating; removing burrs; developing a matte surface finish; and carving in glass or porcelain. Hardness, density, size, and shape are important considerations in choosing an abrasive for a specific application.

5.1.1.4.2.6.1. Experimental Systems

5.1.1.4.2.7. Bench-Scale Experimental Setup

The bench-scale experiments were carried out utilizing the containment system originally used for ion exchange radioactive feed experiments. Figure 5.15 illustrates the experimental setup of the bench-scale runs. Three layers of independent containment barriers surround the crucible holding the molten metal bath. The iron charge, sludge, and any solid co-feeds were batch-loaded into the crucible and heated within the reactor.

Figure 5.15
Schematic of Bench-Scale Experimental Setup

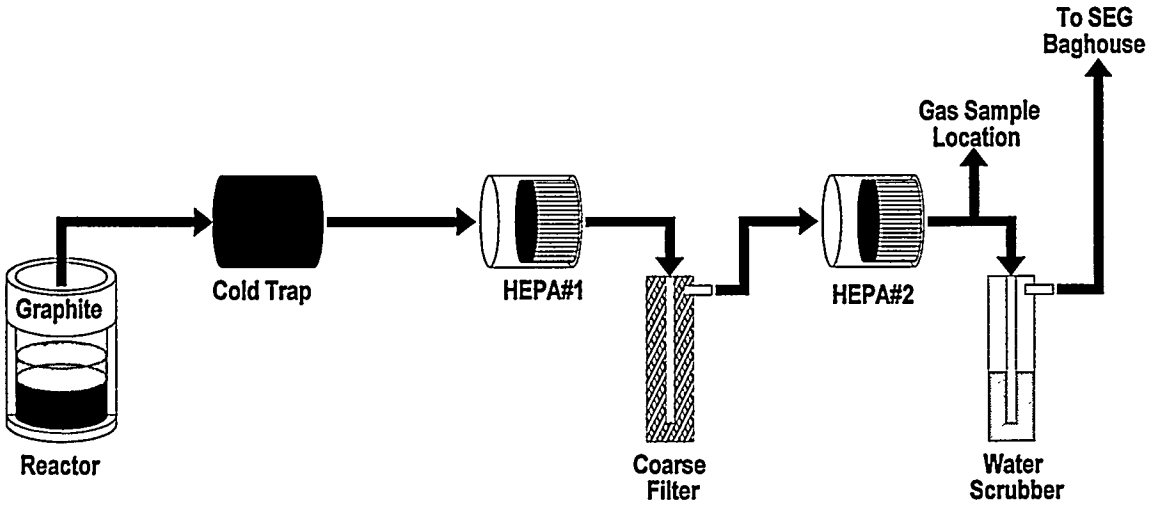

5.1.1.4.2.8. Pilot-Scale Experimental Setup

Pilot-scale experiments were performed on the RPU-3 reactor system. illustrates the reactor configuration. Off-gas piping and reactor pressure relief stations are installed at the top of the reactor as well as a port used alternately for lance feed or bulk feed addition.

5.1.1.4.2.9. Experimental Analysis

The following analytical tests were performed to meet the objectives of the experimental plan:

<u>To demonstrate Q-CEP™ ceramic phase met the Envirocare requirements</u>

- Waste Acceptance Criteria (WAC)
- Gamma Spectroscopy (Natural and Man-made Isotopes)
- Uranium & Thorium Isotopic Analysis
- TCLP (8 metals/32 organics)
- Total metals and organics
- TOX (Total Organic Halides)
- Hydrogen Sulfide
- Hydrogen Cyanide

- Soil pH/paint filter liquids test

To demonstrate Q-CEP™ ceramic phase met the identified market specifications

- Hydrated Lime
- Basicity test (ASTM-C911-94 standard specification for quicklime, hydrated lime, and limestone for chemical uses)
- Neutralization (WETF simulation) tests (designed by customer)
- Uranium capture in the decant liquid (requested by customer)
- Cementitious Component
- Chemical analysis (SiO_2, Al_2O_3, Fe_2O_3, MgO, SO_3)
- Recipe development (Ceramic/Cement/Flyash combination)
- Compressive strength (ASTM C-109)
- Time of Setting (ASTM C-266)
- Abrasive Blasting Media/Aggregate
- Mohs hardness
- Unconfined compressive strength
- Bulk specific gravity (ASTM C-127 and ASTM C-128)
- Surface moisture content/moisture content (ASTM D-2166)

To demonstrate the operability of the system

- Elemental composition (ICP, XRF)
- Tc-99 analysis
- Mass spectrometer off-gas analysis
- LECO carbon, sulfur analysis

To date, the status of the Phase I proof-of-process demonstration studies is as follows:

- Performed 15 bench-scale ceramic tests;
- Performed a 27 hour pilot-scale run;

- Performed a series of potential-driven neutralization tests;
- Performed a series of recipe development tests for cement product development; and
- Continued pilot-scale operability testing, bench-scale product development, and slurry injection system development.

The major findings from Phase I studies include:

- Meeting Envirocare WAC requirements with all ceramic products passing TCLP;
- Achieving overall mass balance closure of 100±5%;
- Demonstrating uranium capture in the ceramic phase;
- Demonstrating reliable operation for scale-up in future demonstrations;
- Meeting market specifications of targeted products for DOE on-site reuses (ceramic product development)

5.1.1.4.2.9.1. Leachability and Land Disposal Acceptance

Mixed-waste sludge contains RCRA metals arsenic, barium, cadmium, chromium, silver, mercury, and lead. The results shown in Table 5.16 demonstrate that the ceramic product passed TCLP for all the metals of concern. As predicted, no evidence of arsenic, cadmium, mercury or lead was found in the ceramic phase. Chromium partitioned primarily to the metal phase and was undetected in the ceramic leachate. Barium, as predicted, was present in the ceramic phase. These results were consistent with historic Q-CEP ceramic TCLP results.

Table 5.16
TCLP Results for Q-CEP Ceramic Phase

	As	Ba	Cd	Cr	Pb	Hg	Se	Ag
Regulatory Limit (mg/l)	5.0	7.6	0.19	0.86	0.37	0.025	0.16	0.30
LDL/(mg/l)	0.027	0.0026	0.0034	0.0096	0.0294	0.0001	0.0748	0.0055
Feed	0.0661	0.208	ND	1.09	ND	ND	ND	0.012
Run #044	ND	2.3	ND	ND	ND	ND	ND	ND
Run #050	ND	1.9	ND	ND	ND	ND	ND	ND
Run #051	ND	2.44	ND	ND	ND	ND	ND	ND
Run #054	ND	0.148	ND	ND	ND	ND	ND	ND

Q-CEP ceramic products have also passed Waste Acceptance Criteria for low-level mixed-waste disposal facilities. This process includes the submittal of specific analytical results as performed by a certified laboratory, followed by shipment of representative samples for fingerprint analyses. Table 5.17 summarizes the analytical results achieved. Based on these results, the ceramic phase has been demonstrated to meet the WAC for disposal.

Table 5.17
Q-CEP Ceramics Pass Waste Acceptance Criteria

Characteristic	Evaluation Method	Q-CEP Results
Radiological evaluation	Major Radionuclides	U-238, Tc-99, Pa-234
Hazardous Waste Characteristic	Marked Applicable Components	Nickel, Sulfides, Beryllium, Thallium, Chromium, Barium
Land Disposal Restriction	TCLP	Passed TCLP for both RCRA metals and organics
Corrosivity	Soil pH	9.6
Free Water Content	Paint Filter Liquids Test	Passed
Toxicity	Cyanide released	<50 mg/kg
	Sulfide released	<25 mg/kg
	TOX	ND
	Total organics	ND
Ignitability	Flash Point	N/A

5.1.1.4.2.9.2. Mass Balance

An overall mass balance was determined by measuring the inputs and outputs of the system. Inputs included the sludge feed, flux-forming co-feeds, and an estimated loss of the graphite crucible from CO generation. Outputs included predominantly the ceramic product, carbon monoxide from feed oxygen, and hydrogen from feed hydroxides. Table 5.18 summarizes the results from representative bench-scale testings. An overall mass balance closure of 100±5% was achieved.

Table 5.18
Mass Balance Closure for Bench-Scale Sludge Processing

	Run #042	Run #044	Run #046	Run #054
Inputs (g)				
Sludge*	466	382	459	500
Al2O3*	0	0	29	87.5
SiO2*	0	118	12.2	238
B2O3*	0	0	0	0
Carbon consumed from the crucible(1)	72	60	72	78
Total Input (g)	**538**	**560**	**572.2**	**903.5**
Outputs (g)				
Ceramic*	304	353	310	630
water vaporized prior to processing(2)	23	19	23	25
release of CO from carbonate(3)	41	34	41	44
Hydrogen(4)	7.4	6	7.3	7.9
Carbon Monoxide(5)	168	139	167	181
Total Outputs (g)	**543.4**	**551**	**548.3**	**887.9**
Closure (%)	**101.0**	**98.4**	**95.8**	**98.3**

* Actual Measurement
(1) Determined based on the consumption of excess oxygen
(2) Water vapor observedduring the startup
(3) Carbonate was decomposed during heat-up (batch process)
(4) Hydrogen released from hydroxides in sludge
(5) Generated from excess oxygen in the system

5.1.1.4.2.9.3. Radionuclide Partitioning

The specific radionuclides of interest included U, Tc, and Cs. Uranium was demonstrated to partition predominantly to the ceramic phase. Previous experiments

on uranium oxide had demonstrated a uranium loading up to 10 wt% in the ceramic phase with a curie balance closure 100±10%. Th and Pa, which are daughter isotopes of U, were expected to behave similarly as uranium. Cs was expected to be recovered in the gas phase. Empirical measurement was limited by analytical equipment due to the small quantity of Cs in the feed (<0.01% of the activity). Previous experiments had demonstrated cesium capture in the Q-CEP™ gas handling train with a curie balance closure of 100±10%. Tc-99 was expected to partition to the metal phase; limited analytical tests were performed, and further analyses may be required to confirm the validity of the results. Until DOE establishes release limits for volumetrically-contaminated materials, both the ceramic and metal phase will be handled as radioactive products to be reused within the DOE complex. A steady profile of activity distribution was achieved during sludge processing, which was consistent with the expected partitioning of radionuclides.

5.1.1.4.2.9.4. Ceramic Operability and Recyclability

5.1.1.4.2.10. Operability Demonstration

Q-CEP operability was demonstrated in the Phase I proof-of-process tests by steady-state operations with successful feed injection, product generation and removal. During the pilot-scale study, the mixed-waste sludge was top-charged into the system. Steady operation was demonstrated through consistent off-gas composition and predictable ceramic product generation. The ceramic phase was partially tapped through the tapping valve into the ceramic mold cart. A minor design modification to the tapping system has been completed, and further experiments will be carried out to optimize the tapping mechanism.

5.1.1.4.2.11. Ceramic Product Specifications

5.1.1.4.2.11.1. Substitute for Hydrated Lime

The basicity factor test was identified as a key indicator for the evaluation of the application of hydrated lime for various chemical uses (ASTM C911). The basicity factor test is an indicator of the relative effectiveness of the neutralization agent. This test is based on pure CaO having a basicity factor of 1. A neutralization ability test was also carried out. For the test, neutralization was defined as the amount of material required to raise 50 ml of 1.0 N HNO_3 to a pH of 9.5±0.2.

A series of experiments were carried out on the Q-CEP™ ceramic phase. These tests were used to determine the basicity and neutralization capability of various compositions of Q-CEP™ ceramic product for comparison with reagent-grade CaO and $Ca(OH)_2$, and the commercial-grade hydrated lime currently used in water treatment facilities. Major findings from these tests included:

- The neutralization ability of Q-CEP™ ceramic phase was comparable with commercial-grade material.
- A linear relationship between calcium content and the basicity factor was demonstrated.
- Uranium was not detected in the decant liquid from a simulated wastewater process, confirming that U is effectively captured in the alumina-silica matrix and that it remains in the precipitate after neutralization.

5.1.1.4.2.11.2. Cementitious Component for Use in Concrete

Q-CEP™ ceramic samples were sent to a third-party laboratory (International Technology Corporation) to carry out a recipe development program based on standard compressive strength tests (ASTM C-109). The resultant screening test results for unconfined compressive strength (UCS) at 7 days for Q-CEP™ ceramics were in the range of 320-580 psi. The UCS after 28 days would be expected to be considerably higher and well above the level of 60 psi at 28 days as recommended by the Nuclear Regulatory Commission (NRC) guidance on waste forms. Additional analyses are pending to complete the specifications profile of Q-CEP™ ceramics.

5.1.1.4.2.11.3. Abrasive Blasting Media

Q-CEP™ ceramic was analyzed for suitability in abrasive blasting applications. Samples were sent to an outside laboratory to test the following properties: bulk specific gravity, Mohs hardness, and moisture content. Results are shown in Table 5.19.

Table 5.19
Comparison of Ceramic Product Test Results to Abrasive Blasting Media Specifications

Specification	Limit	Result
Bulk specific gravity	min 2.5	2.46 - 2.86
Hardness (Mohs scale)	min 6	6.5
Moisture content, %	max 0.5	0.1 - 0.3

These results indicate that an abrasive material meeting typical specifications is achievable from the mixed-waste ceramic product.

5.1.2. Ceramic Phase Interaction With Containment System

5.1.2.1. Electrochemical Reaction Study of the Ceramic/Metal/Refractory Interface

The present experimental study indicates that electrochemical reactions take place preferentially at the ceramic/metal/refractory interface, which causes the most severe degradation of the refractory, at least on a bench scale CEP unit. Using the HP Castable alumina electrodes, in the presence of a silica-lime-alumina ceramic phase on top of iron bath, reduction of Al, Ca from ceramic phase to metal was dominant at cathode. That led to enrichment of Al and Ca in the cathode region of metal phase.

It was observed that refractory anode corroded faster than refractory cathode. This electrochemical process degraded the anode at the C/M/R interface initially and weakened the anode. In an extreme case, an anode might have been cut off at the C/M/R interface and the remains of the anode went to the ceramic phase. Anode reaction included ceramic/metal near anode and ceramic/metal/refractory reactions. The possible anode reactions in which refractory anode was involved directly are:

$$3C + Al_2O_{3\ (\text{refractory anode})} = 2Al^{3+}{}_{(\text{ceramic})} + 3\,CO + 6\,e \text{ and}$$

$$Al_2O_{3\ (\text{refractory})} = 2Al^{3+}{}_{(\text{ceramic})} + 3\,[O] + 6\,e \quad \text{followed by}$$

$$[O] + [M] = MO$$

where [O] diffused to the bulk metal phase and reacted with [C], [Al], [Ca] and [Si], where C, Al, Ca and Si was not directly involved in the electrode reaction. Consumption of [O] in the anode area kept the anode reaction on the right hand side favorable. These two reaction are partially responsible for the fast corrosion of anode.

Three kind of electrodes (graphite, corundum and HP Castable alumina) were tested to study the electrochemical reaction at the ceramic/metal /refractory interface. The high alumina refractory (commercially available) showed a more controllable behavior than others.

A potential application of this technique to real CEP reactor is suggested.

5.1.2.1.1. Secondary Goals

- Evaluate the performance of the electrodes that are fabricated from graphite and commercial refractory cast (high alumina).
- Evaluate performance of electric circuit of the system as a whole.
- Measure the internal potential difference caused by electrochemical reactions.
- Measure the conductivity of the refractory electrodes at high temperature

- Evaluate material deposition of any material along the metal/ceramic interface ("Flux Line") of crucibles.
- Determine the extent of erosion/corrosion of materials along the flux line of crucibles.
- Study effect of polarization of both graphite refractory electrodes on controlling interfacial reactions.

5.1.2.1.2. Ionic Conduction of Refractory Oxides at High Temperature

5.1.2.1.2.1. Principles Of Ionic Conduction In Ceramics

When considering point defects and atomic mobility, a distinguishing feature of ionic crystals is the effective charge that an ionic species may have within the crystal lattice. Mass transport in a ceramic or refractory is typically caused by transport of one charged specie coupled with the transport of an ion or defect of the opposite charge. This observation has been proved for ceramic materials at high temperature [1] (above 1/3 of melting point). Therefore, electrochemical potential should be considered as a motivating force for mass transport as well as the chemical potential or concentration gradient. The electrochemical potential of the ith species η_i, is the sum of the chemical potential μ_i and the electrical potential ϕ acting on it:

$$\eta_i = \mu_i + Z_i F \phi$$

where Z_i is the effective charge and F is the Faraday constant. The flux due to an electrochemical potential gradient is thus given by

$$J_i = c_i v_i = -c_i B_i \frac{\partial \eta_i}{\partial x_i} = -c_i B_i \left[\frac{\partial \mu_i}{\partial x} + Z_i F \frac{\partial \phi}{\partial x} \right]$$

The first term on the right hand side of the equation refers to the contribution from a chemical potential gradient, while the second term refers to the electrical potential gradient. Even though one may control the overall external voltage as a constant or even 0, an electrical potential gradient exists always due to irreversible electrode kinetics and local charge migration. Examination of the two gradient terms in this equation shows the importance of the ionic nature of ceramics. For example, a concentration gradient (chemical-potential gradient) in one direction may be offset by an electrical-field gradient that motivates the ion in the opposite direction.

5.1.2.1.2.2. Applications Of Ionic Conduction In Solid State Materials

Ionic conduction property in ceramics (or materials) has found many applications. Some oxides, such as CaO stabilized ZrO_2 and β-aluminas, can be used as solid electrolytes, high temperature oxygen sensors, and high temperature membrane.

In this project, an investigation was begun into a new application of the ionic conduction behavior of ceramics. The ionic conduction property of refractory ceramics was used to limit electrochemical reactions taking place at the "sacrificial" electrode while protecting the refractory crucible materials. For instance, two refractory rods inserted in the molten bath across ceramic/metal interface and connected externally with an Ammeter, show an electric current passing the meter. That current corresponds to the transport of electrons caused by the electrochemical reactions at the ceramic/electrode/metal interface. By applying an external potential across the two electrodes, the direction of current can be controlled, and consequently, electrode reactions can be controlled by the external potential. The principles are the same as alumina smelting but with opposite process [4].

5.1.2.1.3. Double Crucible Tests With Graphite Electrodes

5.1.2.1.3.1. Setup

An open end graphite susceptor was used for heating. The set point temperature was controlled using an imbedded thermocouple.

Two crucibles were used for this experiment, a large crucible and a small crucible. The small one was cemented to the inside bottom of the large one. The small crucible was centered at the bottom of the large which was centered in the furnace hearth. Two rods (an electrode and a lance) were placed in the small crucible; this region was designated as Melt Two. Three rods (electrode, lance, thermocouple) were placed in contact with the bottom of the large crucible, but not touching the small crucible; this region was designated as Melt One.

A modified furnace cover was fabricated to accommodate the electrode setup. Two electrode rods were inserted into the furnace cover, bottom up, prior to covering the furnace. The electrodes were inserted in such a way so that one electrode was in Melt One and the other in Melt Two. The electrodes were kept above the melt in the beginning and lowed after the bath was molten. Also, one thermocouple was inserted into each crucible and kept above the materials. Argon was injected to the bath through a lance. The Additional graphite was added to saturate the bath with C in order to protect the C electrodes and Al added to the bath to promote Al-Al_2O_3 related electrode reaction.

In this experiment, the bottom of the smaller crucible was cemented to the larger crucible, and both crucibles contained iron and molten oxides. One electrode (Molybdenum or platinum/graphite bonded with zirconia cement) was inserted into each crucible, and by applying a voltage across the electrodes, it was possible to perform two experiments simultaneously to determine the biasing polarity. This setup allowed reinforcement of the reaction to take place on either surface of the inner crucible by changing the polarity of the external basing voltage. A scheme is illustrated in Figure 5.16. In principle, by applying an external electrical potential across the inner crucible, one side corrodes faster than the other. If the inside of the small crucible corrodes more quickly, anode reaction is the dominant corrosion process; if the outside of the small crucible corrodes more quickly, cathode reaction is the dominant corrosion.

Figure 5.16
(Left) Double Experimental Setup;
(Right) Illustration of the Initial Graphite Electrode

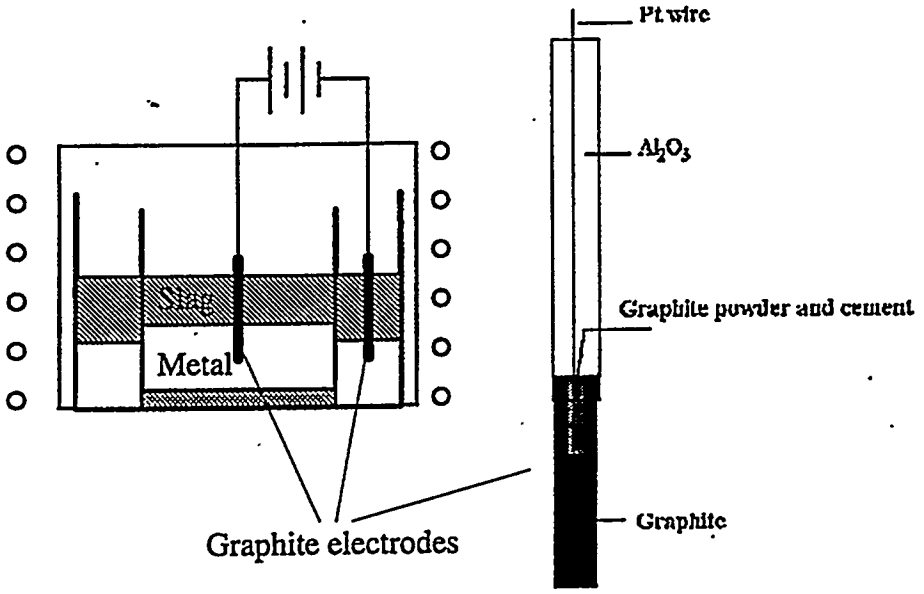

The electrical conductivity of the refractory crucible was below 10^{-10} $(ohm\ cm)^{-1}$ for temperatures below 500°C. Electric current (> 10nA) going through the circuit was observed for temperature exceeding 500°C. This measurement indicates ionic species (principally impurities in the refractory) were activated as charge carriers.

During the heating process above 500°C, there were potential differences (1.5 V AC and 1 V DC) between these two electrodes after removing external biasing voltage, and this potential decayed to 10 to 100mV in about one hour. This electrode potential was caused by the internal electrochemical reactions. The internal potential was against the applied external potential. The mechanism of this internal potential cannot be

determined by this double crucible experiments with graphite electrodes due to the strong polarization of graphite electrodes.

The AC component was measured using an LCD oscilloscope; the signal had the same frequency as the induction coil, and disappeared when the induction power supply was turned off. DC EMF existed as a function of temperature. The DC component corresponds to electrode reactions taking place at metal/refractory, ceramic/metal/refractory (C/M/R) and electrode/ceramics interfaces. The reactions correspond to electron transfer through the circuit. Consequently, electrochemical reactions occur at the C/M/R interface at high temperatures even without external biasing voltages. This observation is consistent with the accelerated corrosion/erosion at the C/M/R interface (flux line corrosion) with or without external biasing voltages.

In addition to the electrochemical reaction, other factors also contribute to the electrode current. Only one induction heating source was used, the temperature difference (about 20°C) between the inner and outer crucibles produced additional chemical potential difference; activity differences of species in both baths caused the concentration difference of charge carriers, a net electric field was established across the inner crucible. These three parts may be the explanation for the EMF observed across the inner crucible.

5.1.2.1.3.2. Polarization and Other Concerns

Since an external potential was applied to suppress or accelerate the internal ceramic/metal/refractory (C/M/R) reaction, electrode polarization was inevitable. Figure 5.17 shows typical polarization curves observed using graphite electrodes and the simplified circuit is illustrated in Figure 5.18 This circuit was actually open (because of its extremely high resistivity) by the inner crucible at room temperature. The ionic conduction of the alumina crucible increases exponentially with increasing temperature. The chemical compositions of the crucibles are similar to the refractory electrodes discussed in next section, along with the ionic conduction properties.

Electric current I was measured directly at constant temperature (1500°C); $I=(V_o - \varepsilon(T, t)/(R_x(T)+ R)$, where V_o is the total external voltage applied; $\varepsilon(T, t)$ is the overall overpotential across the two graphite electrodes (polarization potential + electrochemical potential) and can be calculated from this equation and data on the curve, $R_x(T)$ is the resistance across the inner crucible is a function of temperature only, R is a standard resistor. This polarization curve indicates graphite is not a good selection for the experimental.

From the experiments conducted, graphite electrodes showed severe polarization in comparison to the refractory electrodes. One of the reasons was that CO bubbles formed on the surface of the graphite electrodes; the CO bubbles reduced current efficiency substantially as shown in Figure 5.17. Because the metal bath was stirred

using an argon flow, concentration polarization was only a small part of the overall process in comparison to the gas bubbles on the surface of the electrode.

Figure 5.17
Polarization curve (Run R013-94-43) obtained for double crucible tests with graphite electrodes using the circuit illustrated in Figure 5.18

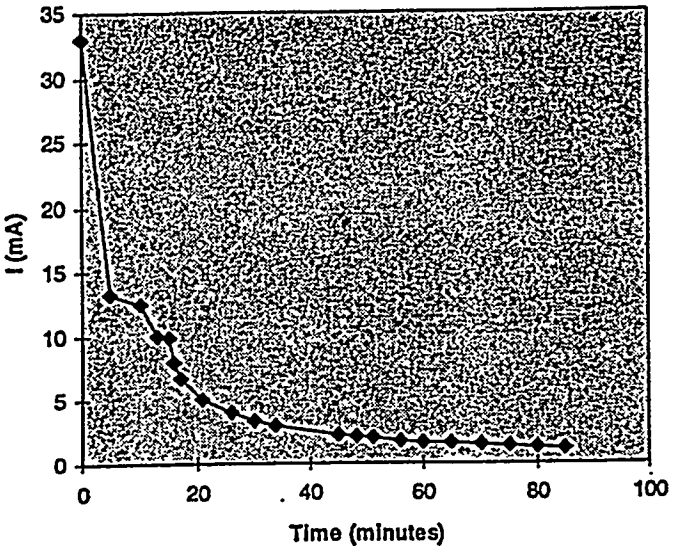

Figure 5.18
Schematic of Circuit used for polarization measurements

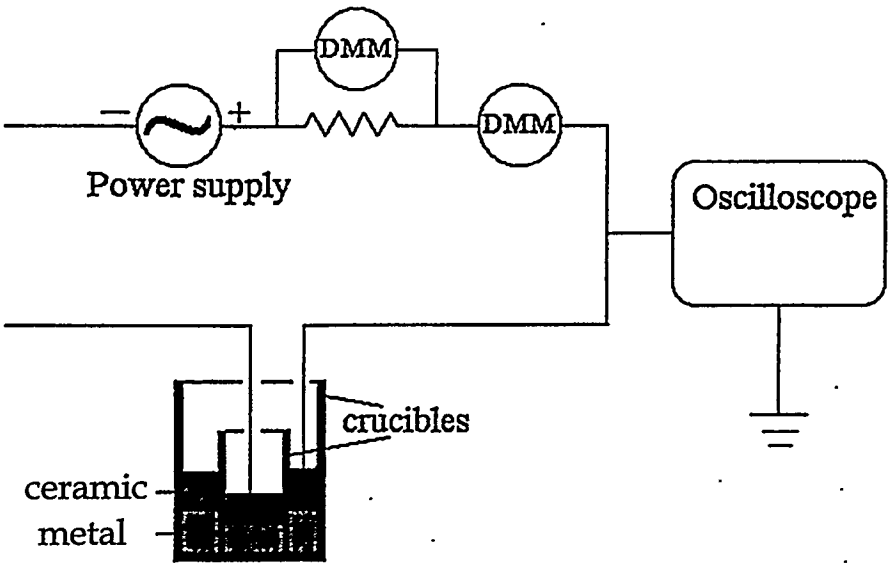

After the induction heating power was turned off, both molten baths (melt 1 and melt 2)

maintained a temperature above 800°C for at least another 10 hours. Therefore, interfacial reactions continued taking place for a much longer time than the experimental period itself. The final corrosion/erosion phenomena shown in Figure 5.19 through Figure 5.21 involves the effect of internal reaction (without external voltage) and the forced reaction (with external voltage).

Figure 5.19 shows the cross section of a sample which was used as a baseline run without external DC biasing voltage. The electric resistance was measured from 200 to 2000 ohms at 1540°C across the wall of the inner crucible. The large uncertainty range of resistance measurements may be attributed to the spontaneous polarization of the graphite electrodes. In the absence of an external potential, a net electric current was observed because the whole setup formed an electrochemical cell. The corrosion/erosion along the flux line (around ceramic/metal/refractory interface) was observed to be more severe than other areas of this sample. A voltage drop (about 10 to 100mV) was observed between the two electrodes without an applied external voltage. This voltage drop implies that spontaneous electrochemical reactions are taking place even in the absence of the external potential. This test is an analog to aqueous electrolyte cells.

Figure 5.20 illustrates the cross section of another sample. The above polarization curve (Figure 5.17) of graphite electrodes were measured from this experiment. During this run, it was observed that the connection between the graphite and alumina tube was deflected while the electrodes were being inserted to molten bath. The inside surface of the inner crucible (anode) degraded about 3 times faster than the outside surface (cathode) in physical dimension by observation. It could have been caused by the anode reactions at the Fe/inner surface/ceramic interface. It was also noticed that the inside of the inner crucible had a more severe corrosion than the baseline run in comparison to the photo shown in Figure.

One may argue that, in addition to the electrochemistry process, the volume difference of ceramic phase in melt 1 and melt 2 could have caused a different containment dissolution rate. Both melts contained equal proportions of lime, silica and alumina, but melt 1 contained 203.8g these oxides, while melt 2 contained 113.9g. The baseline test (Figure 5.19), however, did not show the flux-line degradation as in Figure 5.19, it is believed that the electrochemical process played a more important role than the dissolution for the compositions of the alumina-bearing ceramic phase.

Figure 5.21 shows the cross section of sample R013-94-044. Modified electrodes were used for this run and both electrodes were in good condition after the run. A polarization curve similar to Figure 5.17 was also observed qualitatively. It was noticed that the inside of the inner crucible had more severe corrosion than the baseline run as shown in Figure 5.19. The overall observation was similar to test R013-94-043. The possible explanation is that the dominant anode reaction is $3C + Al_{Al2O3}$ (ceramic or refractory) = $2Al^{3+}$ (ceramic) + 3CO + 6e. Once the polarization reached such a level

(after about one hour as shown in Figure 5.17) that the applied external potential was not high enough to drive the reaction forward, both sides of the crucible started to degrade.

Figure 5.19
Photograph of the cross section of sample R013-94-043

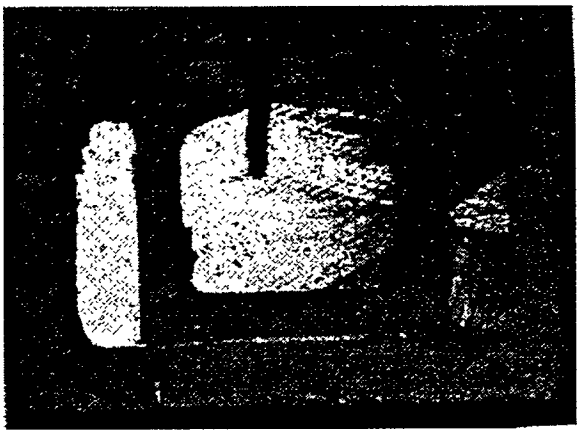

Figure 5.20
Photograph of the cross section of sample R013-94-043

Figure 5.21
Cross section of sample R013-94-044

The external electric potential was applied across the inner crucible after the bath was molten. That potential produced gradients of charged particles across the wall of the inner crucible. The inner crucible behaved like a battery or a charged capacitor as shown in Figure 5.23, a voltage existed across the wall of the inner crucible. Therefore, the electrochemical corrosion could continue after removal of the external potential applied. This potential is caused by the bipolar migration of opposite charged ions, it decays parabolically with time by ionic diffusion. The duration of this process may be expressed approximately as $t=l^2/(\pi^2 D)$, where l is the average distance that ions move and D is the chemical diffusion coefficient. This diffusion process can last for hours.

Chemical analysis of Al, Si, Ca and C in the near electrodes show that Al and Ca were reduced to metal in the cathode bath (outer crucible). Thermodynamics favor the reduction of Si from ceramic phase to metal by graphite, i.e., $SiO_2 + 2C\ (gr) = [Si]_{(1\%)} + 2CO$, but not the reduction of Al and Ca in this study. The Silica reduction by graphite depends on temperature, CO partial pressure in the gas phase and C activity in the molten iron phase. Figure 5.22 shows computed results of free enthalpy (Gibbs free energy) with respect to temperature and CO partial pressure when 1 wt.% Si was reduced. The top graph was calculated with pure graphite (a_C=1) for varying CO values. The bottom one is close to our experimental conditions, P_{CO} =0.05 atm, a_{SiO2}=0.43, and C content changed from 3 wt.% to saturation during operation. The bottom graph also indicates that 3% C in an iron bath can reduce Si from the ceramic phase to the molten iron both at temperatures above 1535°C, and a graphite-saturated bath can reduce Si above 1515°C. Both Fe baths were eventually saturated with graphite, the reduction of Si was controlled by thermodynamics, and consequently Si content of both the anode and cathode regions are close.

Originally 1 wt% aluminum was added to the bath. At 1540C, the activity product of $a^2_{[Al\ 1wt.\%]}P^3_{CO}$=0.023, where, the activity coefficient of Al is f_{Al}=2.8, the maximum Al content in iron bath under C-saturation conditions is 0.05 wt%. This is very close to the

Al composition in the anode. The Al content in the cathode region, however, was even higher than 1 wt%. Similar conclusions can be made for Ca. Therefore, the cathode reactions were dominated by the reduction of Ca and Al. The anode reaction was a little more complicated and will be discussed in Section 5.1.2.1.4.

The advantage of the double crucible experiments was to separate the anode and cathode regions completely , therefore, chemical and electrochemical information in the two electrode regions could be studied. In addition, these double crucible experiments showed that an external electrical potential can accelerate refractory corrosion locally. In order to reach a more complete conclusion about the feasibility of using this electrochemical method to increase the life time of CEP reactor, the graphite electrodes were replaced with refractory electrodes.

Figure 5.22

(Top): Theoretical calculation of Si reduction from ceramic phase by pure graphite with respect to temperature and partial pressure of CO. (Bottom): P_{CO} =0.05 atm, a_{SiO2}=0.43, and C content changed from 3 wt.% to saturation during operation[1].

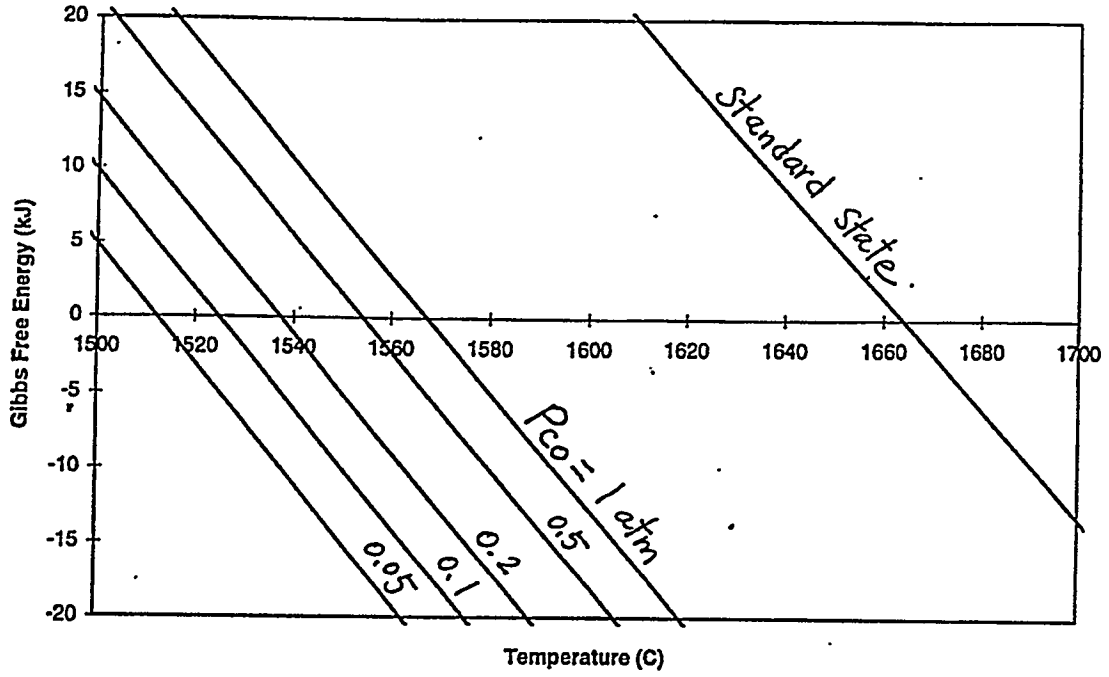

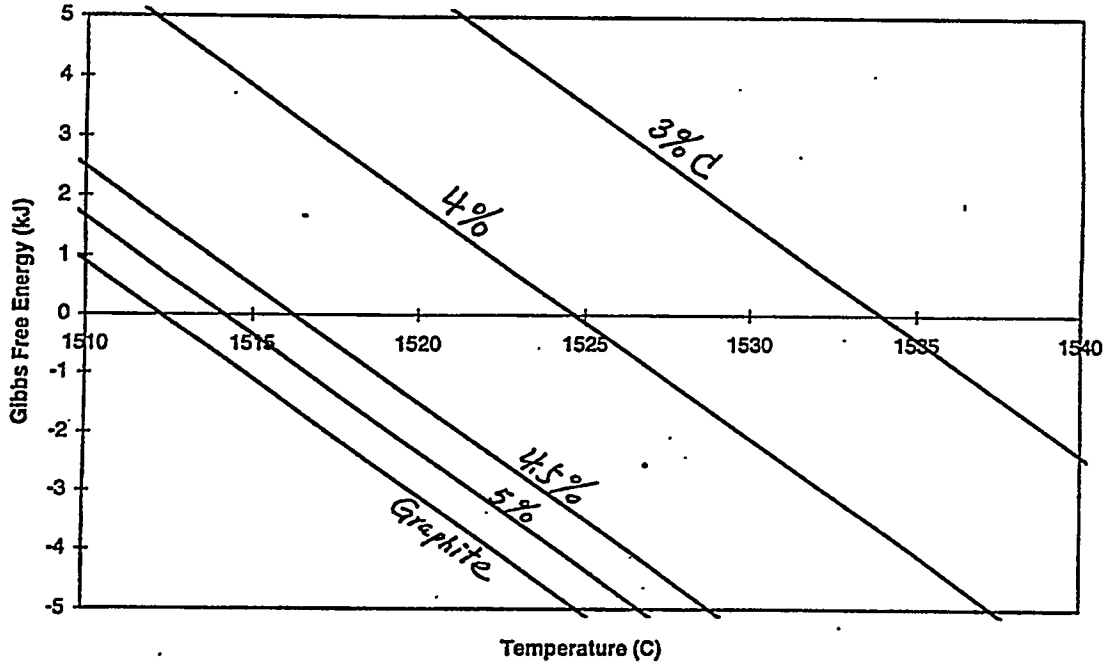

1 These data have been experimentally proved for iron and steel making process[14].

Figure 5.23
Schematic illustration of charge distribution within a ceramic block or refractory brick at high temperature

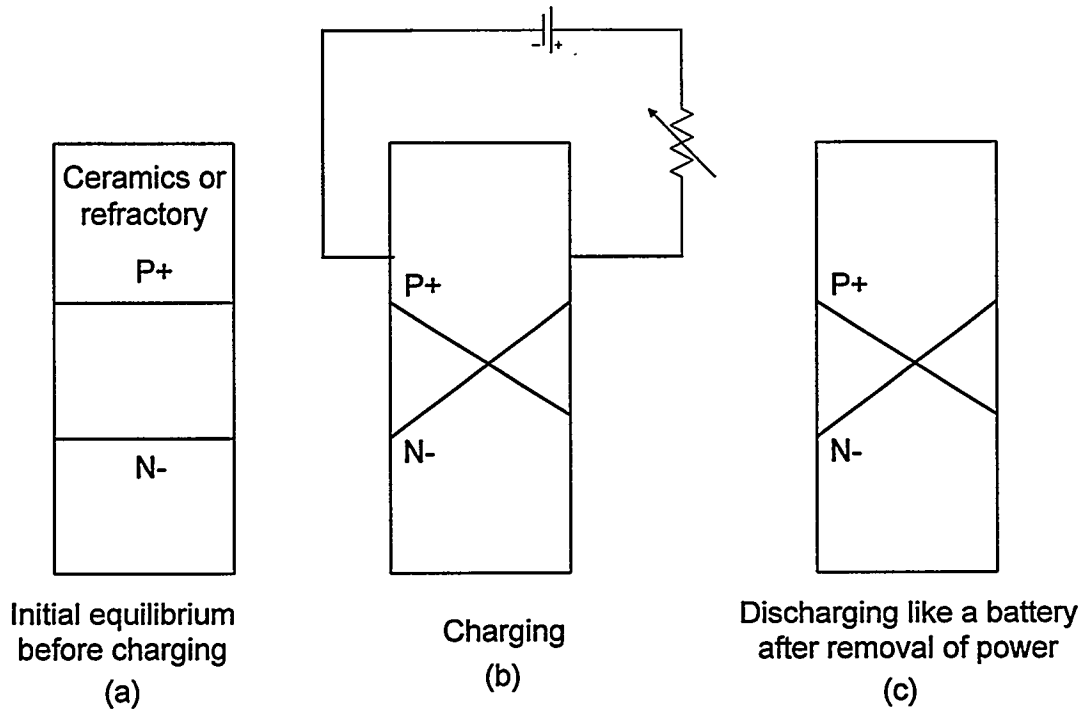

5.1.2.1.4. Single crucible tests with refractory electrodes

5.1.2.1.4.1. Setup

A graphite susceptor was used for this set of tests. A single large crucible was used for these experiments Two refractory electrodes were placed inside the crucible as shown in the following illustrations (Figure 5.24, Figure 5.25).

Before the furnace cover was placed over the furnace, two rods (Pt/alumina or Mo/alumina electrodes) were inserted through the furnace cover, bottom up. In order to make certain that the two electrodes would touch the bottom of the crucible, the alumina rods were marked (shield tubes for the electric wires) before loading. The electrodes were kept above the melt before the external power was supplied and lowered down to the bath after melting. Also, one thermocouple was inserted into the crucible and kept above the loading materials to monitor the bath temperature. The lance was inserted into the last swagelock and Ar gas was injected to the molten metal. The biasing voltage was directly applied when heating starts.

5.1.2.1.4.2. Materials:

The typical loading materials were 3.2%C-Fe with a lime - silica - alumina ceramic phase layer. Aluminum scraps were added to the bath to promote Al-Al_2O_3 related electrode reaction (anode reaction). As discussed in the double-crucible experiments, the final Al content in anode region was controlled by thermodynamics while the reduction of Al, Ca to metal was dominant at the cathode region. These single-crucible experiments had only one metal bath, therefore, chemical species migrate between anode and cathode regions. HP-CAST ULTRA 96% alumina was used to manufacture electrodes.

Figure 5.24 is a schematic diagram of the single-crucible experimental setup for direct testing of refractory bricks as electrodes. Figure 5.25 shows the configuration of refractory electrodes used for the single crucible experiments; the drawing was to scale. These electrodes had much less polarization than the graphite electrodes, but the cathode and anode regions were not separated, which made the final chemical analysis difficult to interpret. Both platinum and molybdenum wires were chosen as the electrode lead wires and both worked satisfactorily.

Figure 5.24
A schematic illustration of the single crucible experimental setup for direct testing of refractory bricks as electrodes.

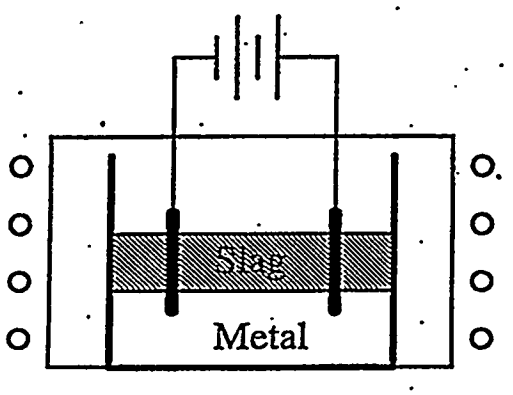

Figure 5.25
Configuration of refractory electrodes used for the single crucible experiments drawing is to scale.

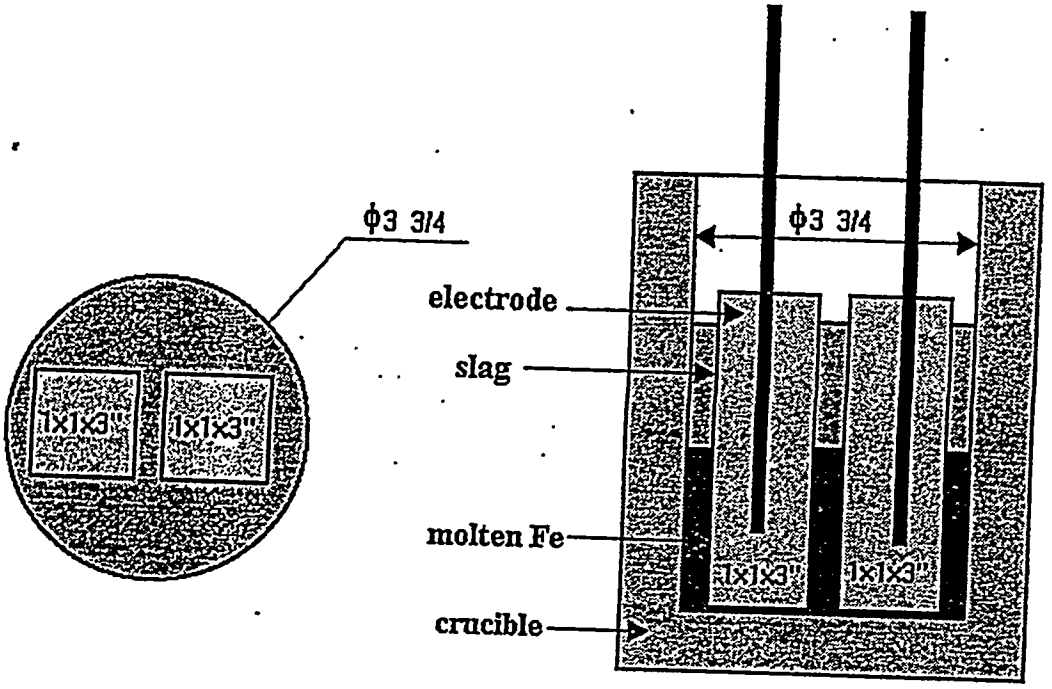

5.1.2.1.4.3. Experimental Results

The voltage drop across a standard resistor in series to the two electrodes was nominal as illustrated in Figure 5.26. The schematic shows the circuit used for studying the C/M/R interface reactions in terms of electrochemical potential. An oscilloscope was used for monitoring the AC component of the current which had the same frequency as the induction power as measured for the double crucible experiments. The AC component disappeared when the induction power supply was switched off. DC EMF existed as a function of temperature. The DC component corresponded to electrode reactions taking place at ceramic/metal/refractory (C/M/R) interface and the ionic conduction of the ceramic phase. At room temperature, the resistance of the refractory electrodes was larger than 10^{+12} ohms. The resistance of the refractory electrodes (HP-Cast-Ultra, 96% alumina, ultra high purity corundum) decreased exponentially with increasing temperature due to activation of mobile point defects such as impurities, vacancies and interstitials in or among the crystal lattices, and these point defects cause ionic conduction in the refractory electrodes. A maxima in the electrical conductance of HP-Cast-Ultra, 96% alumina was observed between 250°C and 400°C. This maxima is a typical phenomena of β-alumina effect. The ionic conduction in β-alumina is caused by the mobil Na^+ and K^+ cations intercalated in alumina lattice. This maxima is attributed to ionic conduction of Na^+ and K^+ impurity cations in the castable refractories.

Figure 5.26
Schematic of the circuit used for studying the C/M/R interface reactions in terms of electrochemical potential

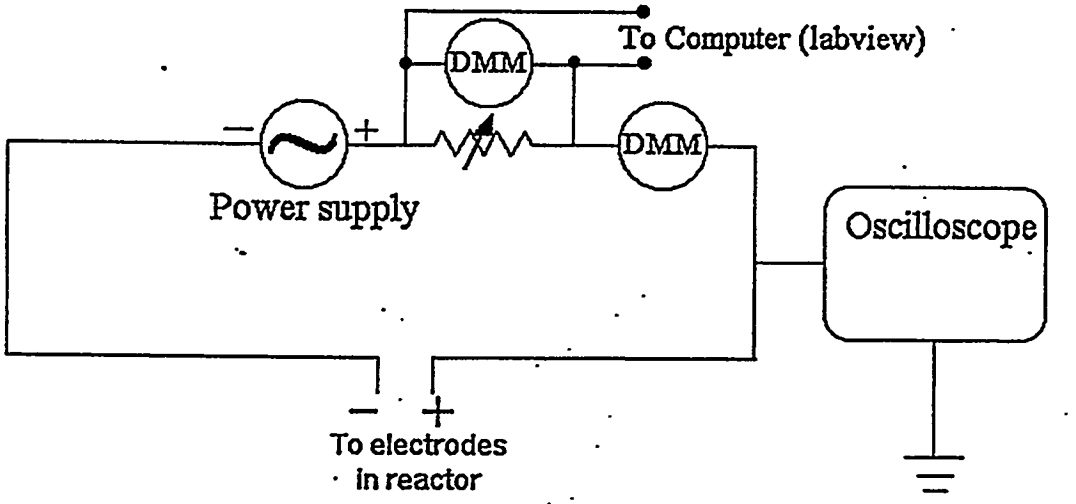

5.1.2.1.5. Electrical resistance and internal potential of high alumina electrodes

The resistance between the two refractory electrodes shows a reversible dynamic property. Therefore the resistance is a function of temperature only. The internal potential measurements reflect the electrode kinetics behavior during the heating and cooling process; it is a function of temperature, temperature gradient and time (history of the electrode).

A simplified relationship can be derived as follows: $V_0-V=\varepsilon(T, t, I) + I R_x(T)$, where V_0 is the total applied voltage, V is the measured voltage drop across the standard resistor, $I=V/R$ or directly measured, ε is the internal potential between the two electrodes, R_x is the resistance between the electrodes. Figure 5.27 shows the measurements of the above relation over five minutes. Other similar results at different temperatures are given in Table 5.20. The resistance between the two HP Ultra High alumina electrodes may be described as

$$R_x \approx 0.09 \exp(132kJ/RT) \text{ ohm}$$

or the resistivity of the HP Ultra High alumina is

$$\rho \approx 0.45 \exp(132kJ/RT) \text{ ohm cm}$$

This equation explains the exponential increase of conductivity of the HP alumina with temperature. This equation was valid for temperature above 600C. This result is consistent with the ionic conduction mechanism in ceramic materials.

Figure 5.27
The relationship between the voltage across the electrodes and electrode current

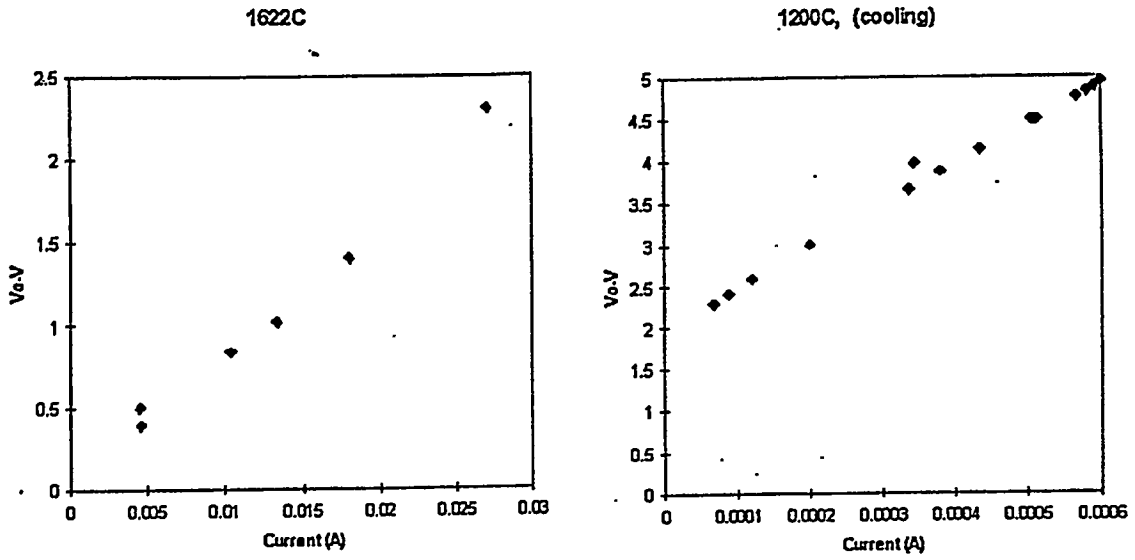

Table 5.20
Measurements between the two electrodes for high alumina refractory electrodes

Temperature	Internal potential (ε)	Resistance (Ω)
950°C (heating) (from Fig. 13)	0.3V	434000
1400°C (heating) (from Fig. 13)	0.5	1600
1620°C (Stable)	0.02 V	81
1200°C (cooling)	2.0 V	4956
640 °C (cooling)	1.6 V	2297000
630 °C (cooling)	1.7 V	2480000
620 °C (cooling)	1.8 V	2780000
25°C	N/A	>5 x 10^{12} ohms

5.1.2.1.5.1. Temperature and Potential Profiles

Figure 5.28 presents a temperature profile of test R013-94-068 and the corresponding measurement with time potential drop (and with temperature) is shown in Figure 5.29. A thermocouple was placed directly above the bath during heating period A and cooling period C, and it was immersed in the molten metal bath during period B. Shoulders D and E represent the melting and solidification processes of the metal phase.

The solid line in Figure 5.28 is experimental results, the dashed-line is the real bath temperature.

The results in Figure 5.29 are closely related to the temperature profile in Figure 5.28. A maxima (point M) of conductivity was observed at about 300°C during the heating period, and can be attributed to Na^+ and K^+ cations (0.2%Na_2O +K_2O) in the refractory electrodes. The voltage across the reference resistor was measured directly. Each part of this profile is displayed separately in Figure 5.30. By referring to the temperature profile, the voltage drop over the standard resistor increases with rising temperature; this was attributed to the increasing conductivity of the refractory electrodes with rising temperature. The cause of peak N is thought to have resulted from mechanical breakdown at that moment and formation of an air capacitor followed by capacitor the charging process. The external voltage applied was 5V and the reference resistors were 10^7 Ω, 10^5 Ω and 10^3 Ω, respectively in different temperature ranges. Selection and switching of these standard resistors can be determined by the equation $R_x \approx 0.09 \exp(132kJ/RT)$ ohm. This equation also explains the shape of the three segments in Figure 5.29. At the bottom of each segment, the resistance of the refractory electrodes was dominant; at the top of each segment, the standard resistor was dominant.

In practice it is desirable to have a considerable current density through two electrodes[2]. In order to increase the efficiency of the applied power, most therefore necessary of the external potential must be applied across the two electrodes and it is to select electrode materials which have high ionic conductivity with rising temperature, and to set the standard resistor to less than half of the electrodes' resistance, i.e., to divide more voltage on the electrodes.

2 In Al smelting process, the amount of Al produced is proportional to the effective current density applied to the electrochemical cell.

Figure 5.28
(R013-94-068): Temperature profile of test R013-94-068

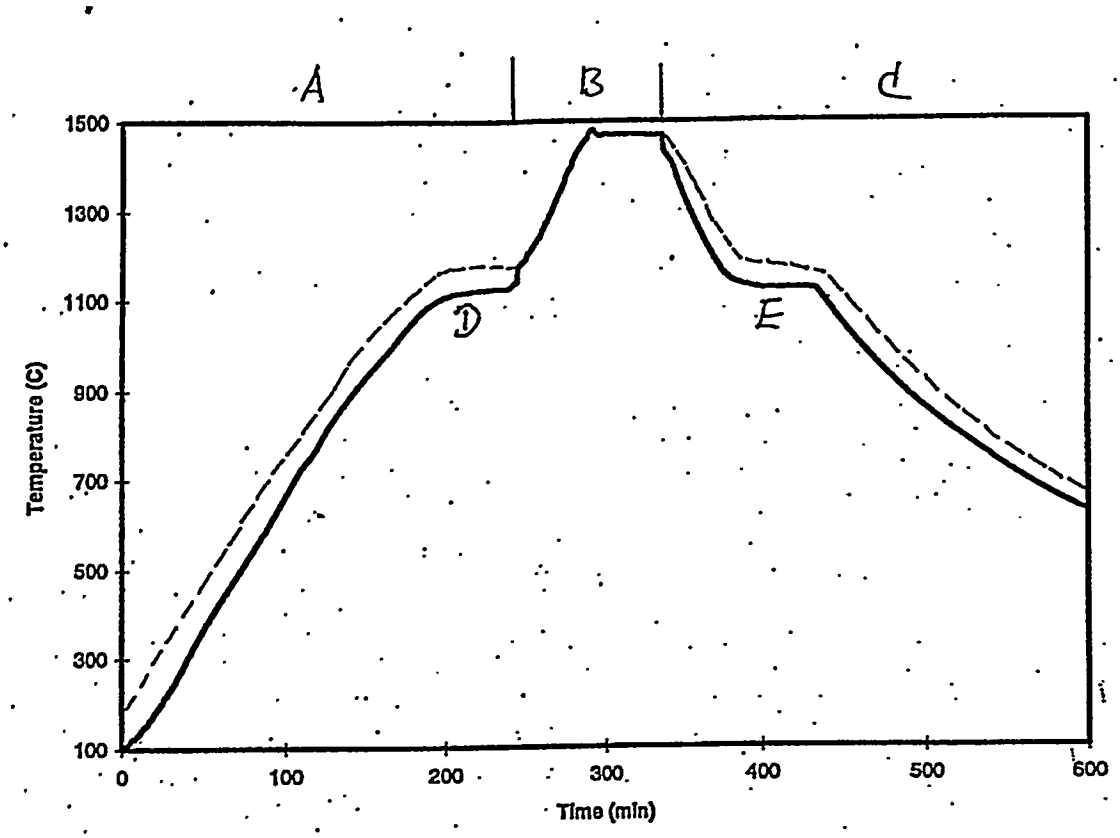

Figure 5.29
Electrode potential measurements for test R013-94-068

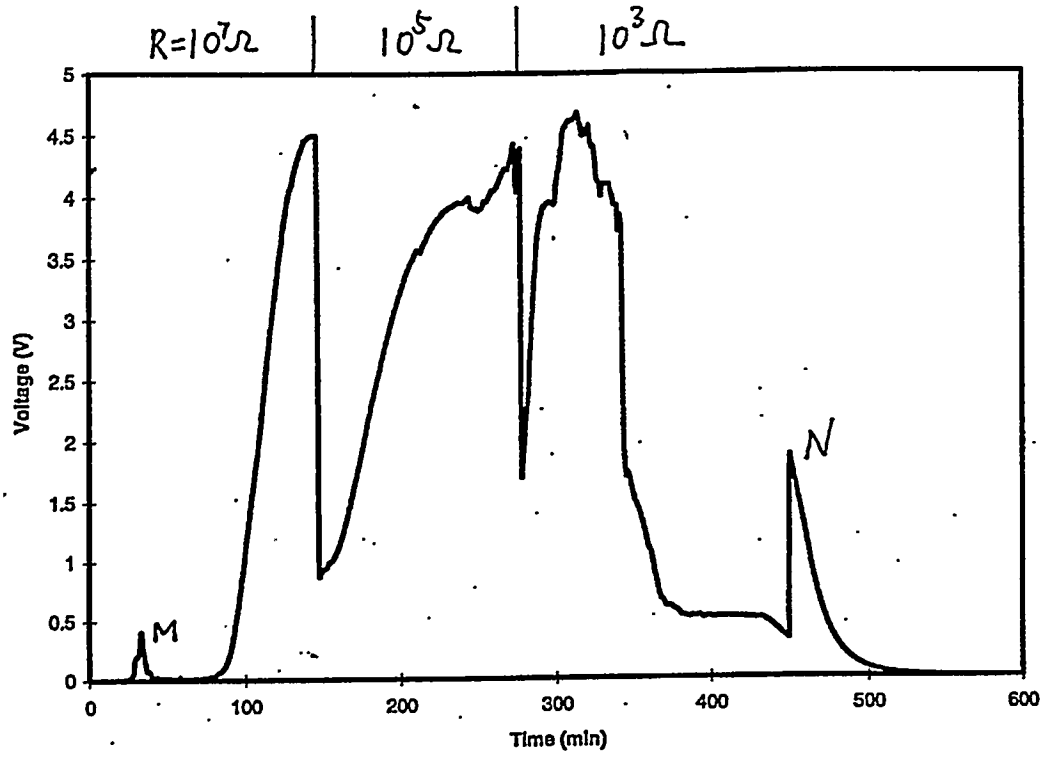

Figure 5.30
Resistance and electrode potential measurements for test R013-94-068

A: $R=10^7\Omega$

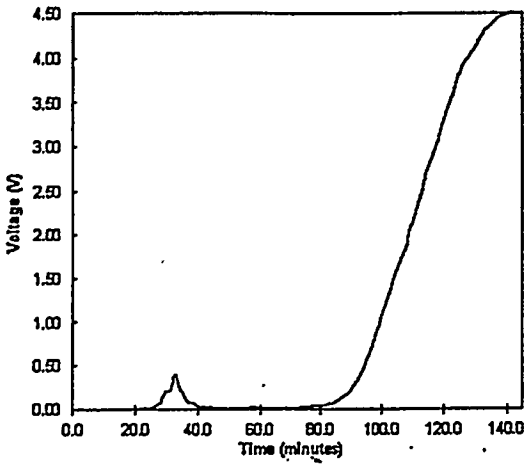

B: $R=10^5\Omega$

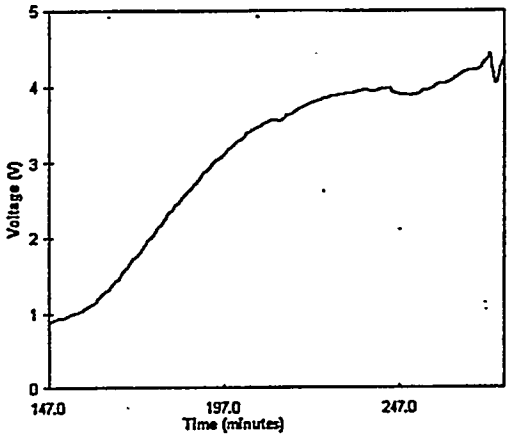

C: $R=10^3\Omega$

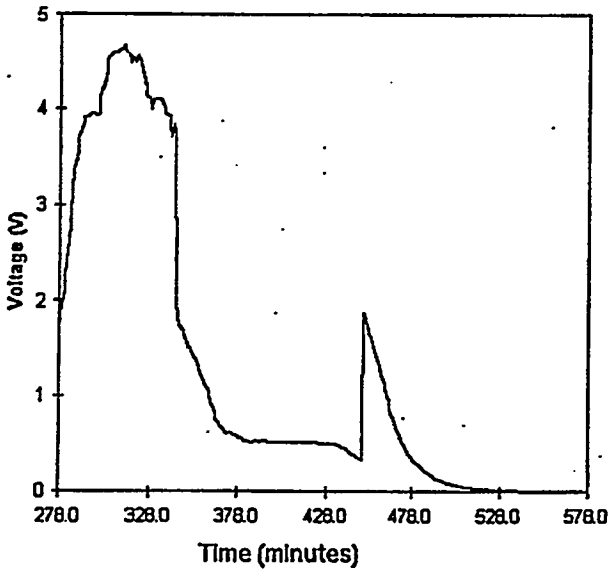

5.1.2.1.6. Post-Run Study and Electrode Reactions

Most of the experiments indicated that the anode has a faster reaction rate than the cathode. In one typical test, the anode disappeared from metal completely (R013-94-060) which is shown in Figure 5.31. Based on analysis, electrochemical reaction is only partially responsible for the consumption of the anode. The electrochemical process degraded the anode at the C/M/R interface initially, and weakened the anode, finally the anode may have been cut off at the C/M/R interface and the remains of the anode went to the ceramic phase.

The faster degradation of the HP Castable alumina anode suggests that the refractory anode was directly involved in the anode reactions, while the cathode was more like an "inert" electrode which supplied electrons to the electrode process. Some of the possible electrode reactions are discussed in next section.

Based on results obtained from the double crucible tests, reduction of Al and Ca from ceramic phase were the dominant cathode reaction. In the present single crucible tests, this phenomenon was not as clear as in the double crucible tests, but the cathode reactions are believed to be the same.

Metallic cations commonly present in molten ceramic are Mg^{2+}, Ca^{2+}, Fe^{2+} and Al^{3+} (Al may exist in the form of ionic complex). If these cations participate in the cathode reaction, reduction of the corresponding metals will occur. During electroslag refining process when a consumable iron electrode is cathodic under DC condition, it has been observed that aluminum is reduced from Al_2O_3 bearing ceramics (ESR ceramic) [24, 25] and the aluminum content increases in the refined iron ingot. In the present experiments, the electrochemical principles used in aluminum smelting and in electroceramic remelting process are the same, but the processes is just the opposite.

A possible overall sequence of electrode reaction includes:

Anode reactions (oxidation):

1 $M = M^{n+}$ (ceramic) + n e
2 O^{2-} (ceramic) = [O] + 2 e
3 M_2O_n (ceramic or refractory)= M^{n+} (ceramic)+ 2 [O] + n e or
4 $nC+M_2O_n$ (ceramic or refractory)= $2M^{n+}$ (ceramic) + n CO + 2n e

Where M represents Al, Fe, Si, Ca, etc.

1. **$M = M^{n+}$ (ceramic) + n e,** This anode reaction implies that metals like Al can be oxidized and moved to the ceramic phase. The reaction is possible but not dominant. Originally, there was 1% Al in the metal phase. Thermodynamically, some part of the initial Al in the bath could be oxidized. This anode reaction does

not explain the fact of the accelerated fast corrosion rate of the anode. Consequently, the anode reaction is not dominant.

2. **O^{2-} (ceramic) = [O] + 2 e,** This anode reaction was possible, but not consistent with the fact that the anode corroded faster than, the cathode. The Oxygen anion can lose two electrons and become elemental oxygen, dissolving in the metal phase. This is a common reaction in steel making processes between slag and metal; the anode reaction could take place at the ceramic/metal interface. Initially, the metal bath contained 3.2-3.4 wt.% C, the equilibrium oxygen content [O] was less than 0.002 wt.% (20ppm) based on thermodynamic calculation. The [O] will react with [C] and form CO. Five to ten percent CO was observed in the gas phase during the operation.[3]

3(a) **M_2O_n (ceramic)= M^{n+} (ceramic)+ 2 [O] + n e,** This reaction occurred when metal oxide in the ceramic phase was involved in the electrode reaction, oxygen anions were oxidized to elemental [O] and dissolved into the metal phase while metal cations were left in the ceramics. It is similar to reaction 2 and it also produced CO.

3(b) **M_2O_n (refractory electrode)= M^{n+} (ceramic)+ 2 [O] + n e,** This is a possible anode reaction. This reaction could take place at the ceramic/metal/refractory interfaces simultaneously. This reaction could explain the fast corrosion of the refractory anode. Subsequently, the reduced [O] in metal phase could react directly with Al, C and other metals in metal phase away from the electrodes to form CO and metal oxides, i.e., the above electrode reaction followed by oxidation reactions such as:

$$2[Al]_{in\ Fe} + 3[O]_{in\ Fe} = Al_2O_3 \text{ in ceramic}$$

$$[Ca]_{in\ Fe} + [O]_{in\ Fe} = Ca \text{ in ceramic}$$

$$[C]_{in\ Fe} + [O]_{in\ Fe} = CO$$

4. **nC+M_2O_n (ceramic or refractory)= 2M^{n+} (ceramic) + n CO + 2n e,** Principally, this reaction is similar to reaction 3, but here, carbon is directly involved in the anode reactions. This reaction could also partially explain the fact of accelerated corrosion of the anode. Final chemical analysis (LECO analysis)[4] indicated the final C content in bulk metal varied from 2.2% to 2.6%, about 0.5 to 1% carbon

---

3 Another source of CO was from the residual oxygen reaction with the graphite susceptor we used. The future experiments similar to this should use iron as the heating element directly.

4 The raw cast iron contained 3.2 to 3.4 wt.% graphite, which was not dissolved into the Fe phase. XRD analysis showed that α-Fe and graphite co-exist in the Udeholm cast iron. In fact, only 0.1 wt.% C can dissolve into the bulk metal Fe at room temperature and most C exists as graphite flakes or spheroidals (formed by chemical segregation during solidification). Therefore, the LECO analysis gives the average C content in the Fe-C mixture, not the C dissolved into the metal phase for Fe-C systems.

depleted in the iron bath[5], i.e., about 6.5 to 13 grams carbon was oxidized. That amount of carbon can reduce 18g to 36g (4.7cm^3 to 9.4cm^3) alumina. By physical dimension measurement, the opening cut on the refractory anode was about 1cm at the C/M/R interface (the width of the flux line), the total alumina volume at the flux line region is 6.3cm^3 while the whole anode was 32cm^3 It appears that the depleted carbon can account for the depletion of alumina on the anode at the flex line. The alumina particles in ceramic phase near anode suggests the remains of the anode went to the ceramic phase following the flux line corrosion. In total, this electrode reaction and reactions in 3(b) are responsible for the anode depletion at the flux line area.

Cathode reactions (reduction):

5 M^{n+} (ceramic)+ n e =M or

6 M_2O_n (ceramic or refractory) + 2 n e = 2 M + n O^{2-} (ceramic)

7 [O] + 2 e = O^{2-} (ceramic)

During the present experiments, external biasing power (5 V) was continuously applied to the refractory electrodes. This condition kept the inherent electrochemical reaction going in one direction. The cross-section view of the crucible (Figure 5.31) showed that cathode had very little corrosion. This observation was consistent with the double crucible experiments. According to the results from the double crucible experiments, cathode reaction 5 represents the dominant cathode process. The following explains the possibility of each cathode reactions:

5. **M^{n+}(ceramic)+ n e =M,** This reaction implies that metallic anions in ceramic phase were reduced to metal (like Al, Si, Ca) by receiving electrons at the cathode surface (C/M/R). If this process was dominant, then the cathode was in good condition, and metals like Al, Ca and Si were enriched. The present test showed the fairly good condition of cathode, and the double crucible test showed Al and Ca enrichment in the cathode region. Recalling reactions 3(b) and (4) above, the ceramic phase (with 14% alumina dissolved) played an important role as an ionic electrolyte to transfer metallic cations from anode to cathode.

6(a). **M_2O_n (ceramic) + 2 n e = 2 M + n O^{2-} (ceramic),** this reaction is similar to reaction 5. Oxygen anions are left in the ceramic phase and transport to anode region through the ceramic phase.

---

5 C depletion is a normal phenomenon observed during melting of metals for most of our tests at MMT. If the reactor chamber was purged using high purity argon at 1.5 scfm for over five hours (on 10 lb unit), the C depletion can be minimized. Normally, the C depletion should be less than 0.2 wt. % C for 1.5 kg Udeholm cast iron. The residue oxides in metals are another source of oxygen to deplete C.

6(b) M_2O_n **(refractory) + 2 n e = 2 M + n** O^{2-} **(ceramic),** this cathode reaction has a totally different physical insight from reaction 6(a). It means that cations in the refractory cathode received electrons from the cathode itself and reduced to metal, while oxygen anions moved to the ceramic phase. If this were the case, then the cathode would have corroded. It was against the observation. Therefore reaction 6(b) was not dominant.

7. **[O] + 2 e =** O^{2-} **(ceramic),** This reaction is a spontaneous cathode process in steel making process[14]. In the present experiments, this reaction is possible but not dominant. The metal bath contains about 3.2 wt. % C initially, oxygen solubility was calculated to be less than 20 ppm (activity of oxygen and its interaction with C was considered in this calculation). This level of oxygen did not dominate a cathode process.

Comparison of the initial composition of the ceramic phase with its final composition indicated that the total alumina content had increased; therefore, most of the refractory anode ended up in the ceramic phase.

In summary, reactions 5 and 7 are consistent with the fact that cathode was nearly in the originally shape. The high C content in the bath implies a low oxygen content (less than 20 ppm), therefore, reaction 7 is not dominant. Reaction 6 might occur to a small degree, but is not the dominant reaction based on the post run analysis. Therefore, reaction 5 is the most probable cathode reaction, with Al^{3+} (ceramic)+ 3 e =Al proposed as the dominant cathode reaction.

The overall electrode reaction can be expressed as:

8. $3C+Al_2O_{3\,(\text{refractory anode})} = 2[Al]_{(\text{cathode})} + 3\,CO$ with $E^0 = -0.43V$ or

9. $Al_2O_{3\,(\text{refractory anode})} = 2[Al]_{(\text{cathode})} + 3\,[O]_{(\text{anode})}$ with $E^0 = -0.91V$

followed by oxidation reactions

$$2[Al]_{\text{in Fe}} + 3[O]_{\text{in Fe}} = Al_2O_{3\ \text{in ceramic}}$$

$$[Ca]_{\text{in Fe}} + [O]_{\text{in Fe}} = CaO_{\text{in ceramic}}$$

$$[C]_{\text{in Fe}} + [O]_{\text{in Fe}} = CO$$

Reactions 8 and 9 are not spontaneous reactions ($\Delta G^0 = -6FE^0 > 0$, F is Faraday constant), but can take place under external electrical field as in the Al smelting process. The reduced Al reacts with CO or dissolved [O] to form aluminum oxide, and enters the ceramic phase.

Whether other electrochemical reactions occur will depend on their positions in the electrochemical series (electrode potential) and on their kinetics in relation to the

postulated main electrode reactions above. The latter will largely determine the form of the current-voltage at the two electrodes. The electrode kinetics is related to many factors, such as, the overpotentials across two electrodes, voltage drop across electrode/molten bath interface and across ceramic/metal interface, and electrochemical potential of a specific reaction. The first three factors can only be determined using more sophisticated experiments and instruments like differential pulse polarography and chronopotentiometry. The electrochemical potential can be computed from thermochemical data (see Table 5.21). For instance, 1.66V or more external potential is needed to drive $Al^{3+} + 3e^- = Al$ forward, or it would be reversed spontaneously. Considering the other voltage drops and polarization, a minimum of 5 Volts was required to drive this reaction at the cathode/bath interface by using HP Castable alumina electrodes.

Table 5.21

Possible electrochemical reactions within the melt, E (volt)= -ΔG°/nF, where n is the number of electrons transferred in a reaction, F=96500 Faraday

Reaction	ΔG° at 1600 °C(Joules)	E (Volts)
$Al=Al^{3+} + 3e^-$ (Al may exist in ionic complex in ceramic phase)	-480,500	1.660
$Fe=Fe^{2+} + 2e^-$	-84,900	0.440
$Fe=Fe^{3+} + 3e^-$	-10,400	0.036
$Fe^{3+} + e^-=Fe^{2+}$	-74,400	0.771
$C(s) + 1/2O_2=CO(g)$	-275,000	1.43
$C(s) + O_2=CO_2$	-395,700	1.03
$CO_2(g) + C(s)=2CO(g)$	-156,100	0.81
$2Al(l) + 3/2O_2(g)=Al_2O_3$	-1,077,000	1.86
$Fe(l) + 1/2O_2=FeO(l)$	-147,800	0.77
$3C+Al_2O_3$ (refractory) $= 2Al$ (metal) + 3 CO	+252000 > 0	-0.43V

Figure 5.31
Top view and cross section of sample R013-94-060

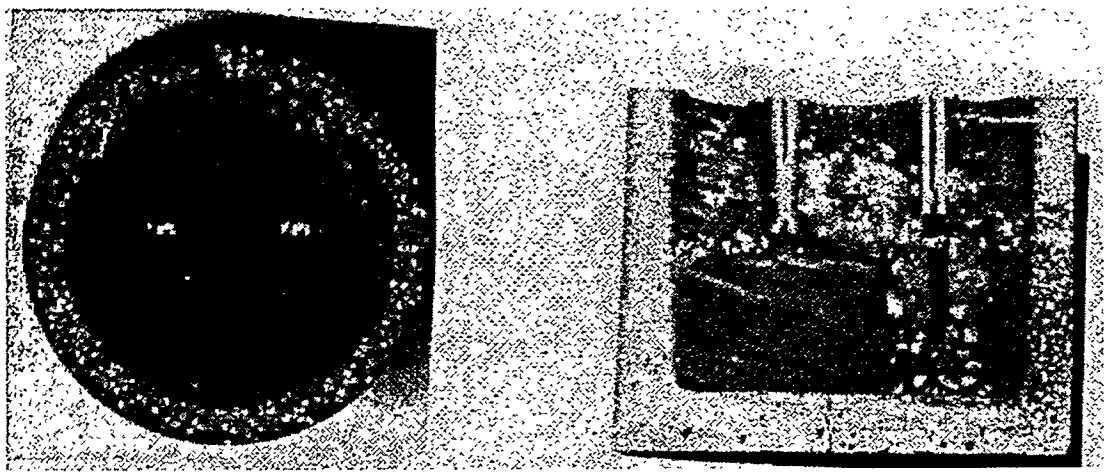

5.1.2.1.7. Test Without Ceramic Phase (HP Castable Alumina)

Under experimental conditions similar to above, test was conducted without ceramic phase. No significant corrosion was observed. Both refractory anode and cathode were in good condition. It appears that ceramic phase as an electrolyte plays an important role for the electrochemical process at the C/M/R interface.

5.1.2.1.8. Conclusions

Presently, one of the most important criteria for determining the optimal refractory material is the degradation rate in the melt system. Local degradation of refractory at the ceramic/metal/refractory interface is well known in many chemical reactors and metallurgical furnaces. This so called "flux-line" degradation may be attributed to different factors[6]. We believe the electrochemical corrosion is an important factor responsible for the degradation of refractory oxide containment at flux line. This subject has not yet studied in literature due to its experimental complexity at high temperature. This report focused on the electrochemical issues of the ceramic/metal/refractory reactions.

Literature review has produced a hypothesis that the flux-line degradation of the refractory materials is electrochemical in nature. Our recent experiments further confirmed that phenomenon by directly measuring the electric current generated from two refractory electrodes at CEP operation temperature. Thus, it is believed that the degradation rate of the refractory lining at the ceramic/metal/refractory interface can be controlled partially by applying a bias voltage across the refractory brick.

6 Some people considered the Marangoni interfacial flow can cause physical degradation of refractory. There are many publication about this subjects, readers of interest may refer to references [16-23] at the end of this report.

In the present experiments, an external electrical field was applied across an alumina crucible or two alumina electrodes in a given molten steel and molten ceramic environment. It was observed that by using a sacrificial anode, it was possible to reduce the degradation rate of the refractory cathode at the ceramic/metal/cathode interface and to increase the lifetime of the cathode materials. We may design our CEP reactor in such a way that the whole containment is used as a cathode. This concept may lower the overall operating costs of the CEP systems.

The present experiments employed HP Castable high purity alumina (96%) electrodes to study the electrochemical corrosion of refractory materials and indicated that electrochemical reactions took place preferentially at the ceramic/metal/refractory interface, which causes the most severe degradation of the refractory, at least on a bench scale CEP unit.

For the double crucible tests, we found the enrichment of Al and Ca in a separated cathode compartment of molten iron, but Si showed enrichment in both cathode and anode regions. Al^{3+} (part of it) and Ca^{2+} are mobile cations[7] and reduction of Al and Ca from ceramic phase are believed to the dominant cathode reactions, i.e., $Al^{3+}_{(ceramic)} + 3\ e = [Al]_{(metal)}$. Si did not exist in a simple cation in ceramic phase but formed more complex ionic structures. Si Reduction to metal phase (in both anode and cathode compartment) from ceramic phase was controlled by thermodynamics.

The faster degradation of HP Castable alumina anode indicated that the refractory anode was directly involved in the anode reactions, while the cathode was more like an "inert" electrode which supplied electrons to the electrode process. In terms of electrochemistry and experimental observation, the following anode reaction

$$3C + Al_2O_{3\ (refractory)} = 2Al^{3+}_{(ceramic)} + 3\ CO + 6\ e$$

is the most possible reaction responsible for the fast degradation of anode, but the amount of C depleted in the iron bath was not enough to consume the whole anode. Other mechanisms shown below must exist in addition to the anode reaction above.

$$Al_2O_{3\ (refractory)} = 2Al^{3+}_{(ceramic)} + 3\ [O] + 6\ e \text{ followed by reaction}$$

[O] + [M] =MO in the bulk metal, where M stands for Al, Ca, C, etc.

[O] diffused to the bulk metal phase and reacted with [C], [Al], [Ca] and [Si], where C, Al, Ca and Si was not directly involved in the electrode reaction. Consumption of [O] in the anode area kept the anode reaction forward to right hand side. Neither of the two anode reactions are spontaneous, but they can take place in the presence of a biasing voltage.

---

7 Al^{3+} showed neutrality, i.e., it has a property between acidic and basic cations in metallurgical slag. Al^{3+} can exist both in free cation form and in a complex form.

These two reactions can also partially explain the fact of fast corrosion of anode. Final chemical analysis indicated the total C depleted in bulk metal can account for the depletion of alumina on the anode at the flux line area only (1 cm wide). There must be other mechanisms responsible for the disappearing anode in addition to the electrochemical corrosion. The alumina particles in ceramic phase near anode suggests the remains of the anode ended up in the ceramic phase following the flux line corrosion. In total, the anode reactions started to corrode the anode at the C/M/R interface (flux line) and cut off at the C/M/R interface, the remains of the anode went to the ceramic phase.

5.1.2.1.8.1. References

1. Per Kofstad, High Temperature Oxidation of Metals, (1963).
2. W. D. Kingery, H. K. Bowen and D. R. Uhlmann, Introduction to Ceramics, (1976).
3. Per Kofstad, High Temperature Corrosion, (1988).
4. N. Jarrett, W. B. Frank and R. Keller, Advances in the Smelting of Aluminum, Alcoa lab.
5. E. T. Turkdogan, Physicochemical Properties of Molten Slags and Glass, The Metal Society, London, 1983.
6. J. F. Elliot, M. Proc. 4th International Conference on Molten Slags and Fluxes, The Iron and Steel Institute of Japan, 1992
7. S. B. Hammond, Electrical Engineering, McGraw-Hill Book Company, Inc.
8. M. P. Peover, Electroslag Remelting: A Review of Electrical and Electrochemical Aspects, in Journal of the Institute of Metals, v100, (1972) p.97.
9. D. R. Crow, Principles and Applications of Electrochemistry, 2nd ed., (19790, Chapman and Hall.
10. Stanley Wolf, Guide to Electronic measurements and Laboratory Practice, 2nd ed., Prentice-Hall, Englewood Cliffs, New Jersey, 1983.
11. P. W. Nicholson, Nuclear Electronics, John Wiley & Sons, 1974.
12. A. J. Diefenderfer, Principles of Electronic Instrumentation, 2nd ed., W. B. Saunders Company, 1979.
13. 4th Intern. Conf. on Molten Slags and Fluxes, Sendai, Japan, 1992.
14. J. F. Elliot, Notes for Course 3.50 "Physicochemistry of metallurgical Process"
15. J. Thomson, Philos. Mag., 10(1855)330
16. C. Marangoni, Ann. Phys. Chem., 143(1871)337
17. J. T. Davies and E. K. Rideal: "Interfacial Phenomena", 1963, New York, Academic Press.
18. J. T. Davies, "Turbulence Phenomena", 1972, New York, Academic Press.
19. J. K. Bromacombe and F. D. Richardson, Inst. Min. Metall. Trans. Section C, 82(1973)63
20. V. Stanek and J. Szekely, Chem. Eng. Sci., **25**(1970)699
21. P. Kozakevitch, G. Urbain and M. Sage, Review Metall., **52**(1955)161
22. J. K. Bromacombe and F. Weinberg, Metall. Trans. **3**(1972)2298
23. R. G. Barton and J. K. Bromacombe, Metall. Trans., **B8**(1977)417

24. Boris E. Paton, et al, "Method of Obtaining metal Hollow Ingots by the Electroslag Remelting", US patent 3,721,286, 1971
25. Mitchell, J. Szekely and J. F. Elloitt, in Electroslag Refining, The Iron and Steel Institute, 1973, pp3-15

5.1.2.2. Chemical Skulling

5.1.2.2.1. Introduction

The longevity of the containment system can be increased through the formation of a chemical skull, or chemical barrier layer, , at the refractory/ceramic interface which decreases the reactivity between the two materials. When processing a chlorinated waste stream, a precipitation reaction between chlorine and a CaO-Al_2O_3-SiO_2 system provides the basis for formation of a chemical skull. Initial experiments were conducted to characterize the melt behavior as chloride (in the form of $CaCl_2$) is introduced to a CaO-Al_2O_3-SiO_2 system. Samples were analyzed using optical microscopy, scanning electron microscopy with semi-quantitative analysis (SEM/EDS), and x-ray diffraction (XRD). Data obtained from the first series of experiments formed the basis for a second series of experiments that investigated two chemical skulling methods on various CaO-Al_2O_3-SiO_2 ceramic phase compositions in a crucible. Both chemical skulling methods were found to be effective in forming a chemical barrier between the molten ceramic phase and the containment system, thereby reducing the reactivity between the two and increasing the longevity of the containment system.

5.1.2.2.2. Initial Testing

The objective of the initial test program was to characterize the melt behavior as chloride (in the form of $CaCl_2$) was introduced to a specified CaO-Al_2O_3-SiO_2 system. It is important to note that these experiments were performed expressly to investigate the methods for purposely generating a chemical skull, not for the overall optimization of the ceramic phase product. A series of melts were made that systematically added $CaCl_2$ to the batch materials of a CaO-Al_2O_3-SiO_2 base glass composition. The melts were removed from the furnace and quenched by dipping the bottom of the crucible into water. Analysis of the quenched samples and melt observations (prior to quench) were used to characterize the melt behavior as a function of chloride content.

The chloride content of the samples ranged from 0 to 2.82 wt% Cl; the chloride content is representative of the bulk sample. Samples containing chloride contents up to 0.63 wt% Cl were fluid melts at 1600°C, and quenched into transparent glassy samples. Sample AU03-94-4, containing 0.86 wt% Cl, was a fluid melt at 1600°C, and displayed some crystallization upon cooling. The crystallization appeared to be surface nucleated, with the crystallization front growing into the bulk sample.

5.1.2.2.3. Analytical Results

The samples were analyzed using optical microscopy, scanning electron microscopy with semi-quantitative elemental analysis (SEM/EDS), and X-ray diffraction (XRD). Samples were characterized in terms of the formation of a second, crystalline phase as a function of the chloride content of the sample.

5.1.2.2.3.1.1. Optical Microscopy

Samples 1, 2 and 3 were glassy, with no second phase (crystallization) observed. Sample 7 had two distinct phase regions; 1) glassy region and 2) large crystallized regions which had a jagged crystal front growing into the glassy region. Figure 5.32 shows a micrograph of the crystallized region for sample 7, with dendritic crystal growth running throughout the region.

Figure 5.33 and Figure 5.34 show optical micrographs of sample 5; the photos show the presence of a second phase distributed throughout the sample. Figure 5.33 represents regions of the sample that have lower crystal density (translucent appearance). The crystal size varies throughout the sample and displays a dendritic crystal growth pattern.

Figure 5.35 and Figure 5.36 show the low and high density crystallization regions of sample 6, respectively. Crystal growth in sample 6 was more extensive than that observed for sample 5, with many of the crystals becoming interconnected (See Figure 5.36).

Figure 5.32
Optical micrograph of a large crystallized region of sample 4 (magnification = 1000x).

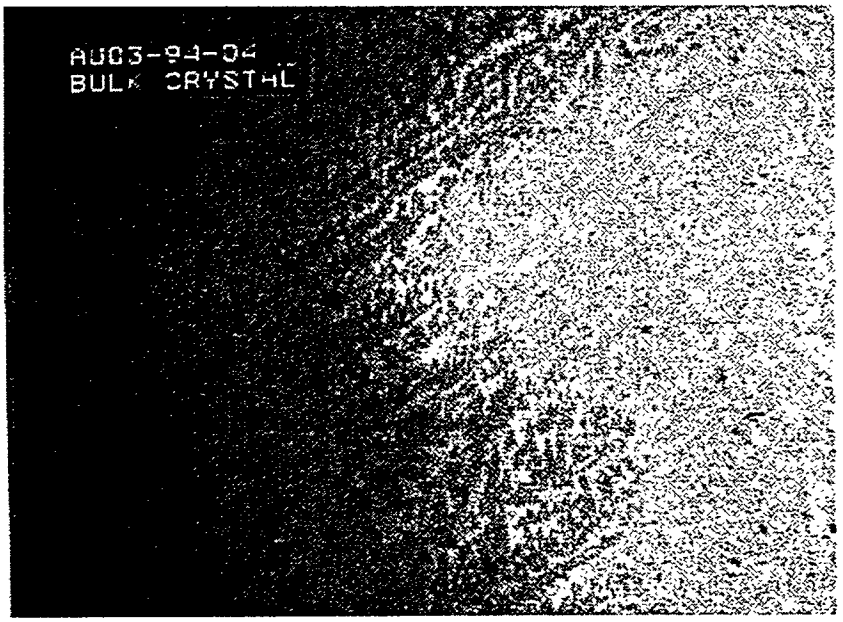

The crystal volume percent of samples 5 and 6 was estimated using a rid intersection technique. The average crystal volume percent was determined using over 600 points and is provided in Table 5.22. While the volume percent crystallization varies throughout each sample, sample 6 has a higher average volume percent crystallization.

The increase in volume percent crystallization correlates with increasing chloride content of the sample.

Table 5.22
Estimated Crystallized Volume Percent

Sample	Ave. Crystal Volume (%)
5	46
6	59

Figure 5.33
Optical micrographs of bulk crystallization of sample 5; low density crystallization region (magnification = 1000x)

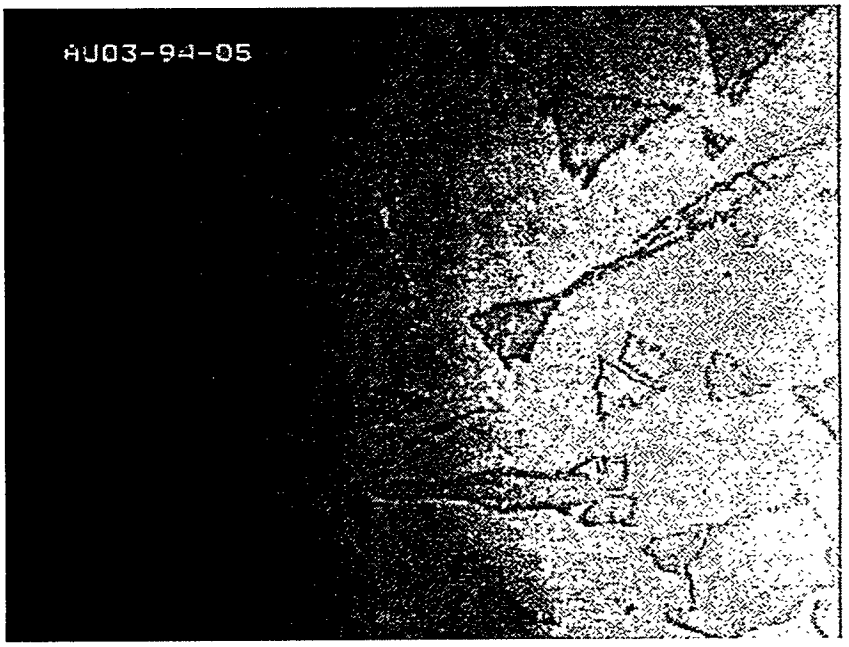

Figure 5.34
Optical micrographs of bulk crystallization of sample 5; high density crystallization region (magnification = 1000x)

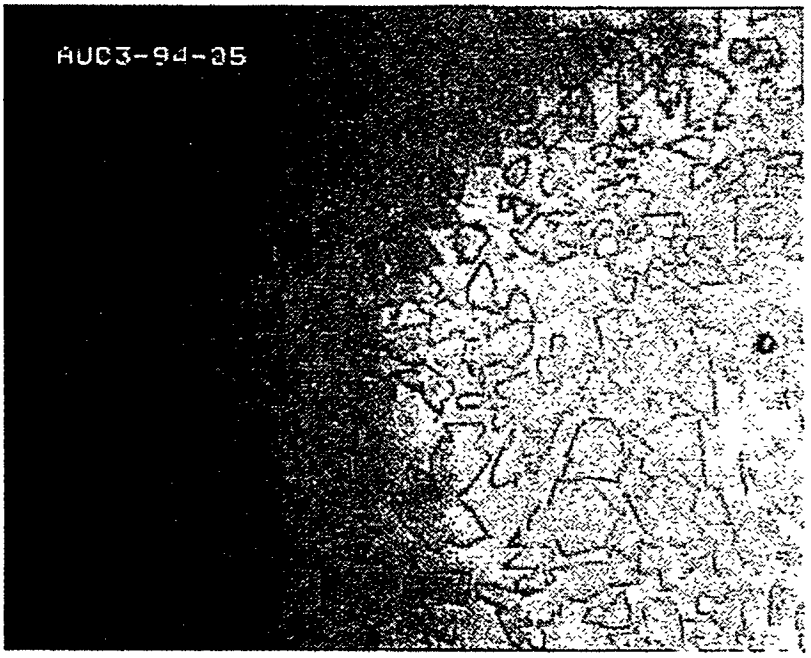

Figure 5.35
Microscopic photo of bulk crystallization of sample 6; low density crystallization region (magnification = 1000x)

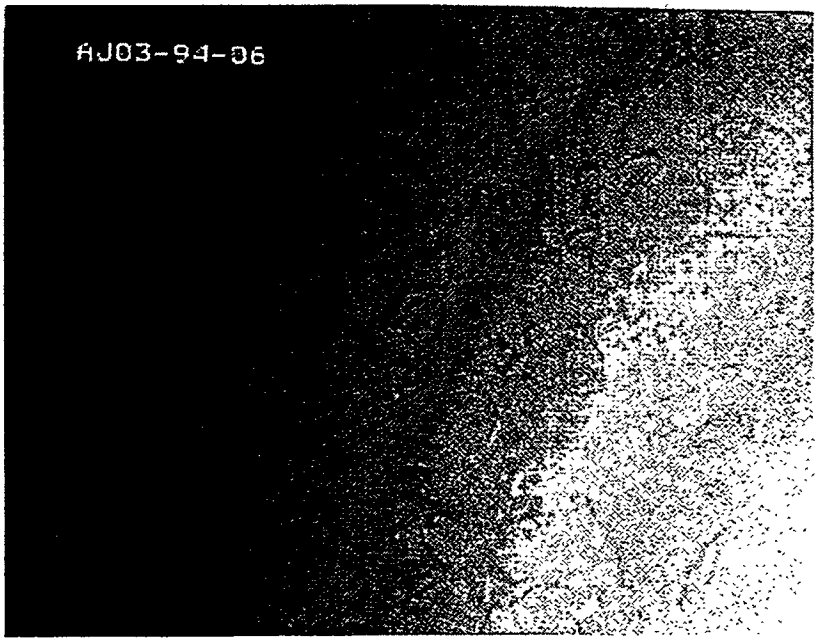

Figure 5.36
Microscopic photo of bulk crystallization of sample 6; high density crystallization region (magnification = 1000x)

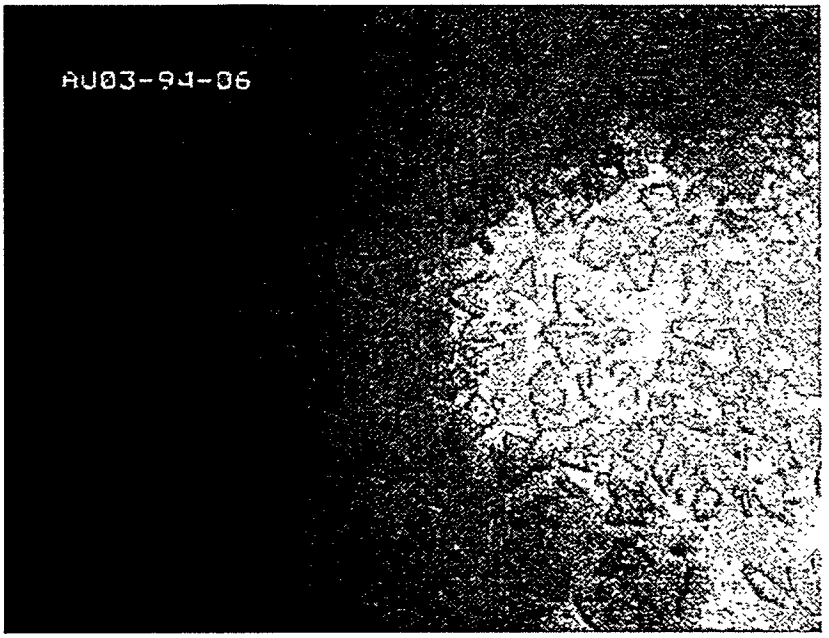

5.1.2.2.3.1.2. SEM/EDS Microanalysis

SEM/EDS microanalysis of selected samples was used to investigate the morphology, and identify the elemental make-up of the various phases. In general, samples that contained bulk crystallization (i.e. samples 5 and 6) contained three distinct phase regions as shown in Figure 5.36 and Figure 5.37: 1) glassy matrix phase, 2) bulk crystalline phase, and 3) a boundary crystalline phase between the glass and crystal phases. Semi-quantitative elemental analysis (EDS(of the phase regions was obtained for samples 5 and 6, with similar results collected for the two samples. Figure 5.38 through Figure 5.41 show the SEM/EDS analysis for sample 5. Figure 5.38 shows a SEM micrograph of the sample (10,000x) with the various phases labeled, while Figure 5.39 through Figure 5.41 show the EDS spectra for these phase regions.

Figure 5.37
SEM Micrograph of Sample 5, 2000x Magnification

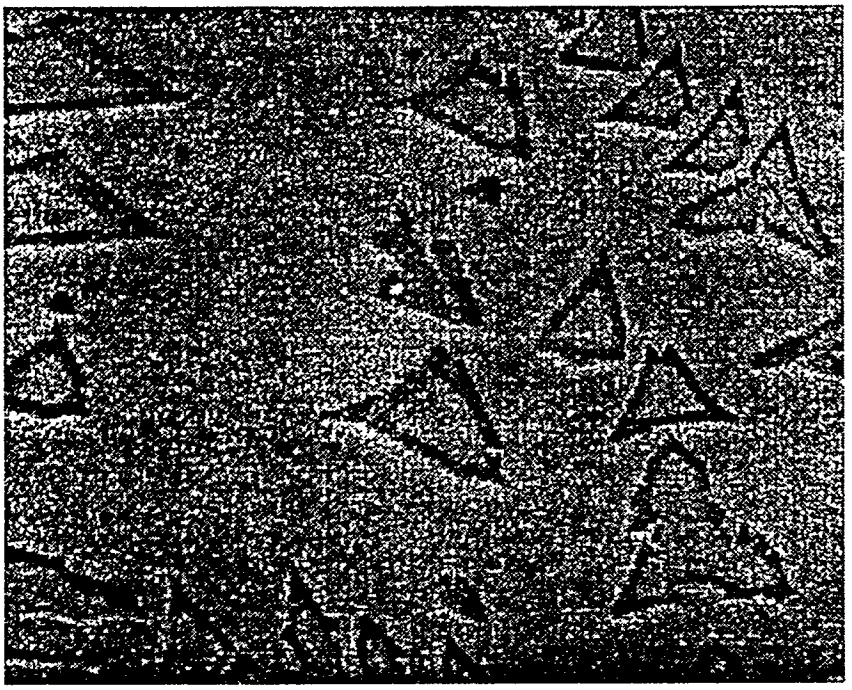

CAM-UML 2μm 20KeV X2000

Figure 5.38
SEM micrograph of sample 5, 10,000x magnification. Region IV shows the glassy matrix phase, region III shows the bulk crystallization phase, and region II shows the boundary phase between the glass and crystal phases.

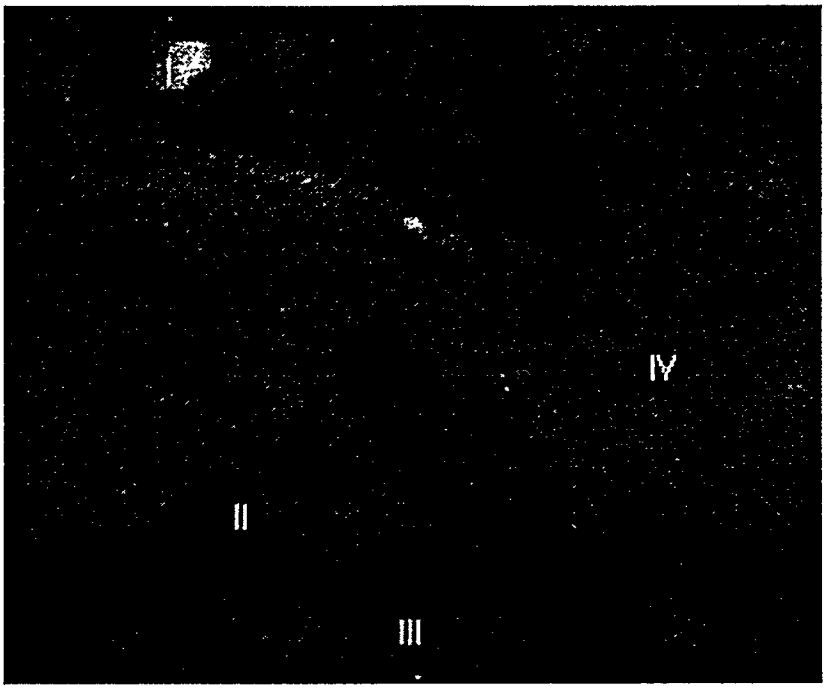

CAM-UML 2μm 20KeV X2000

Figure 5.39
SEM/EDS Analysis Of Region IV, The Glassy Matrix Phase

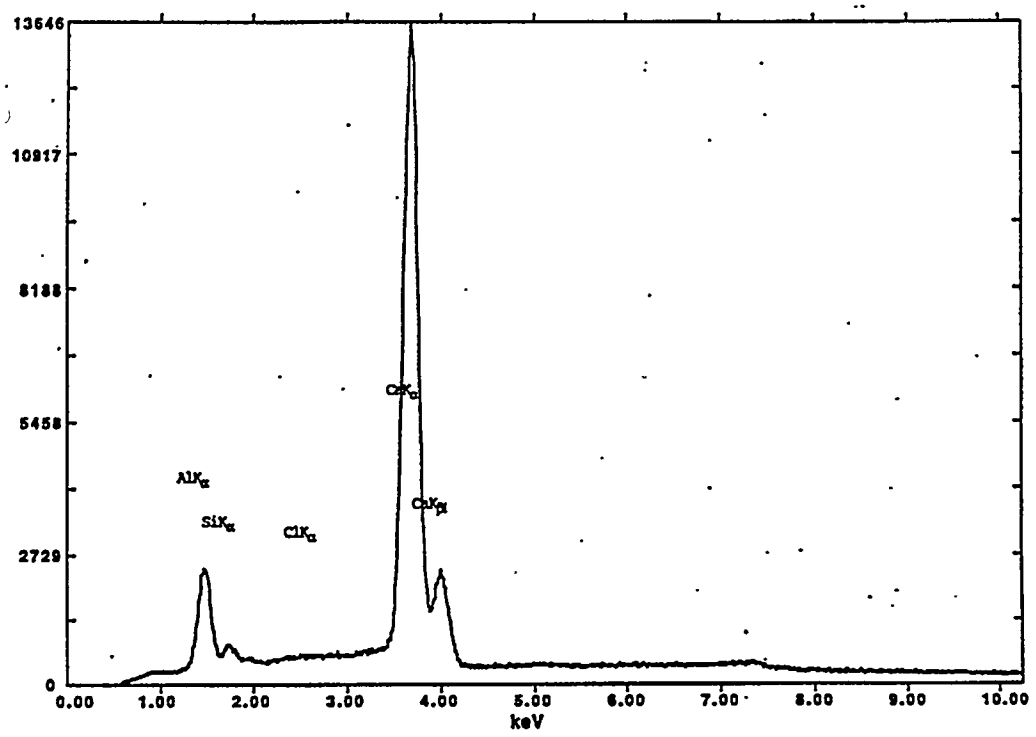

Figure 5.40
SEM/EDS Analysis Of Region III, The Bulk Crystalline Phase

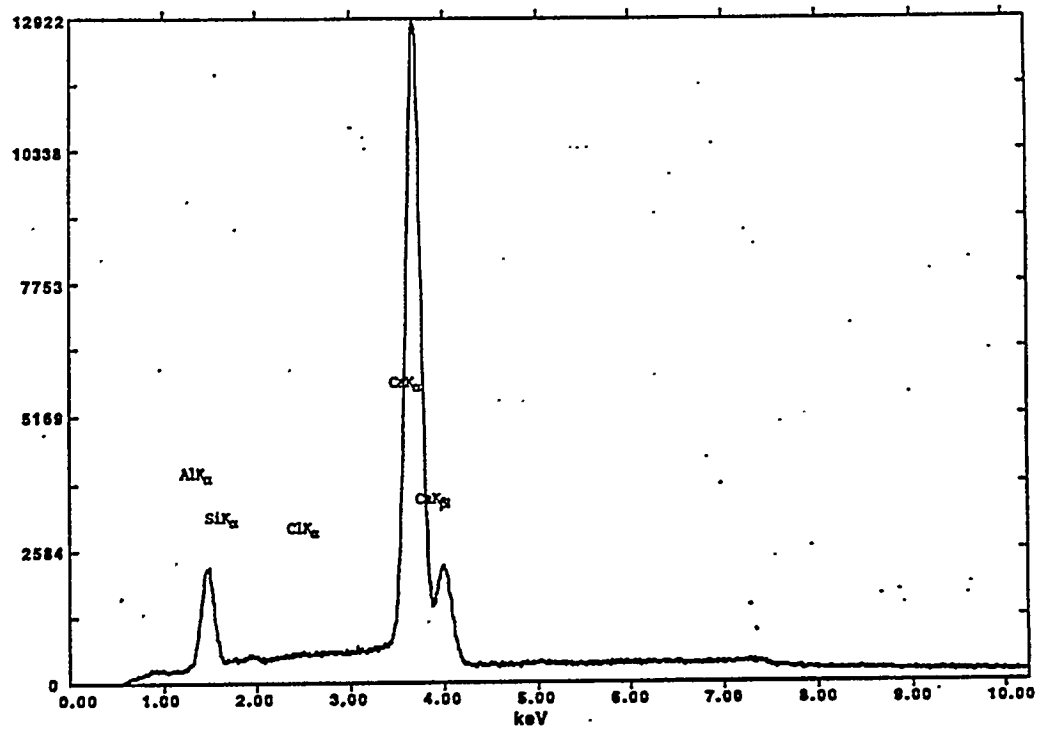

Figure 5.41
SEM/EDS Analysis of Region II, the Boundary Phase Between the Glass and Crystal Phases

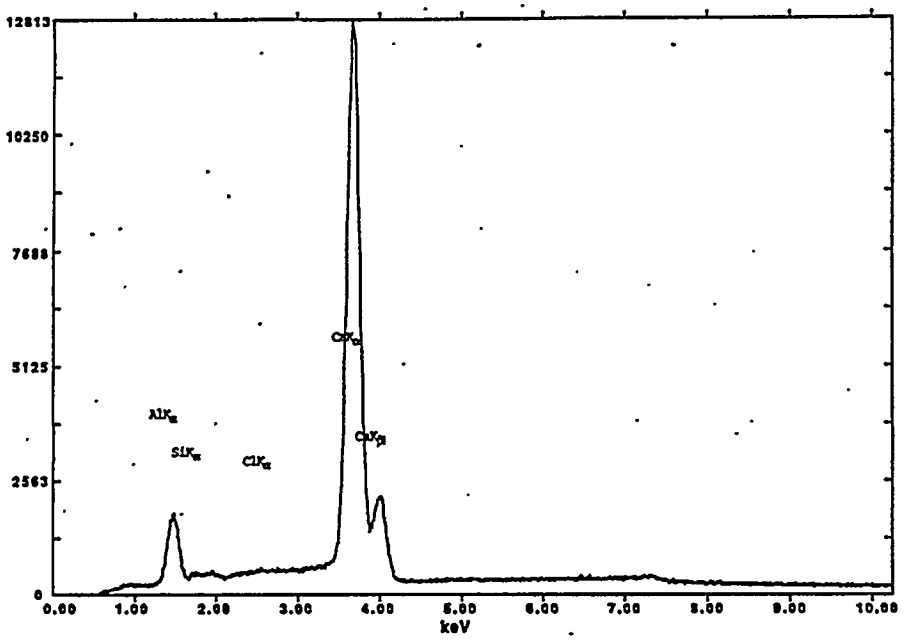

Elemental analysis of the various phases provided important insight into the variation in chloride content between the bulk crystalline, boundary, and glassy matrix phases. The role of chloride in the formation of the skull was determined, as was the threshold chloride concentration for crystallization and the relationship between chloride content and volume of crystallization.

5.1.2.2.3.1.3. X-ray Diffraction

The presence of a crystalline phase, and phase identification was investigated using XRD analysis of selected samples. XRD patterns of powdered samples were obtained using a Rigaku diffractometer (10-90 degree 2-theta scans). Figure 5.42 shows an XRD pattern for sample 7 (0.63% Cl); similar patterns were obtained for samples 1 and 3. The single broad peak, positioned at approximately 31 degrees 2-theta, is characteristic of a glassy sample; this peak is often referred to as an amorphous hump and is a result of the non-periodic nature of a glassy structure. Figure 5.43 through Figure 5.45 show the XRD patterns for samples 4, 5, and 7, respectively. As the chloride content increases, XRD reveals the emergence and growth of a crystalline phase at the expense of the glassy phase. Figure 5.43 shows the presence of a distinct crystalline pattern riding on top of the amorphous hump. As the chloride content increases further in 5.13 and Figure 5.45 respectively, the intensity of the crystalline pattern increases while the amorphous hump decreases in intensity.

Figure 5.42
CRD Patter for Sample 7, Showing a Characteristic Amorphous Hump at 31 degrees 2-theta

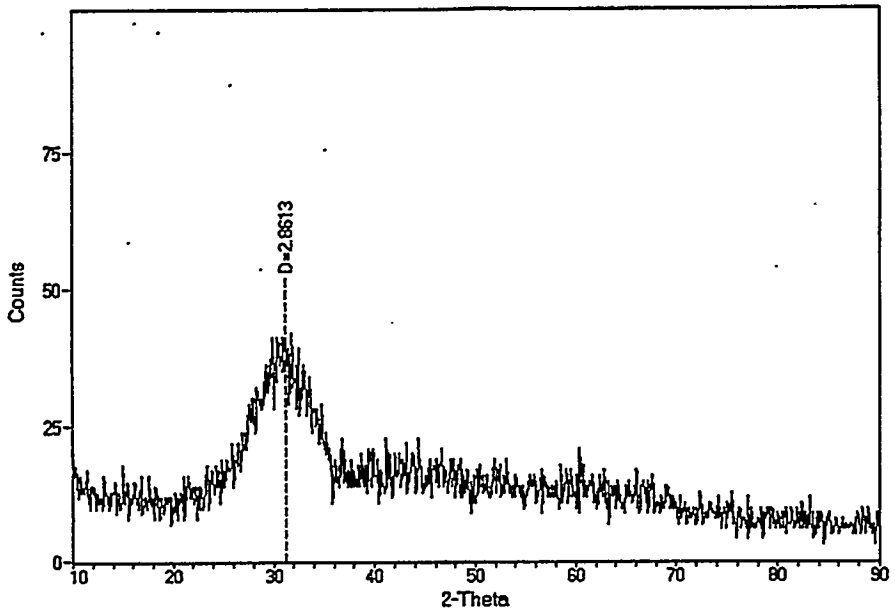

Figure 5.43
CRD Pattern for Sample 4

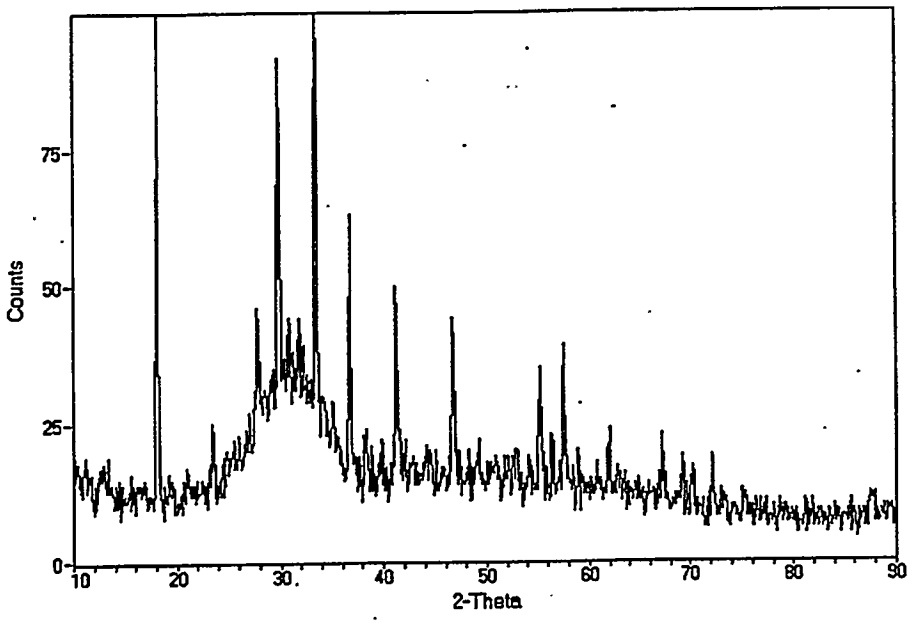

Figure 5.44
XRD Pattern for Sample 5

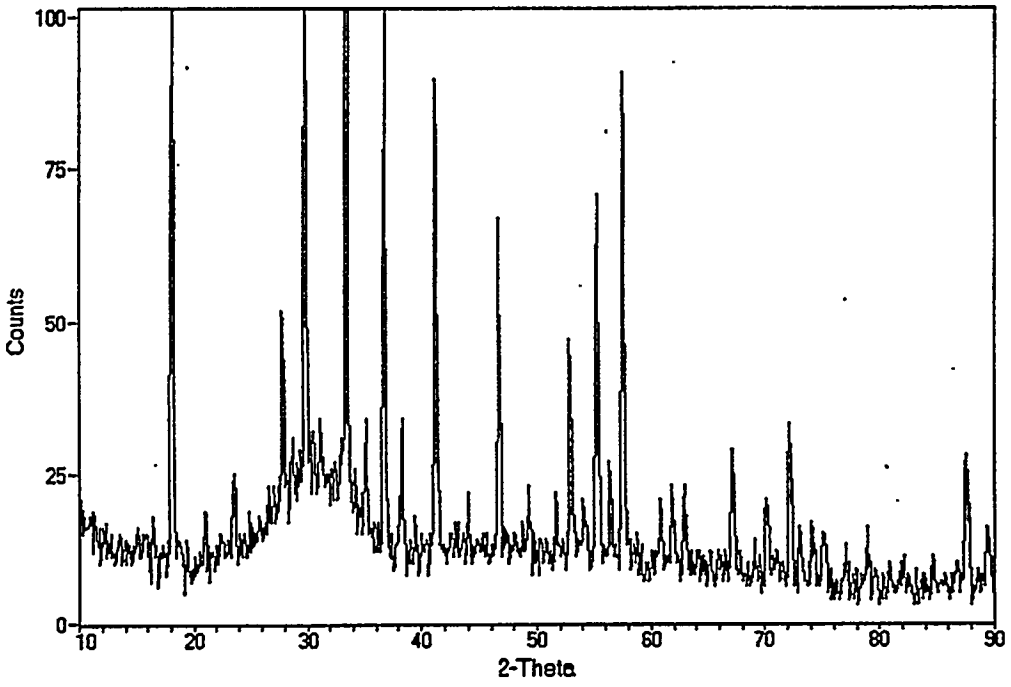

Figure 5.45
XRD Pattern for Sample 7

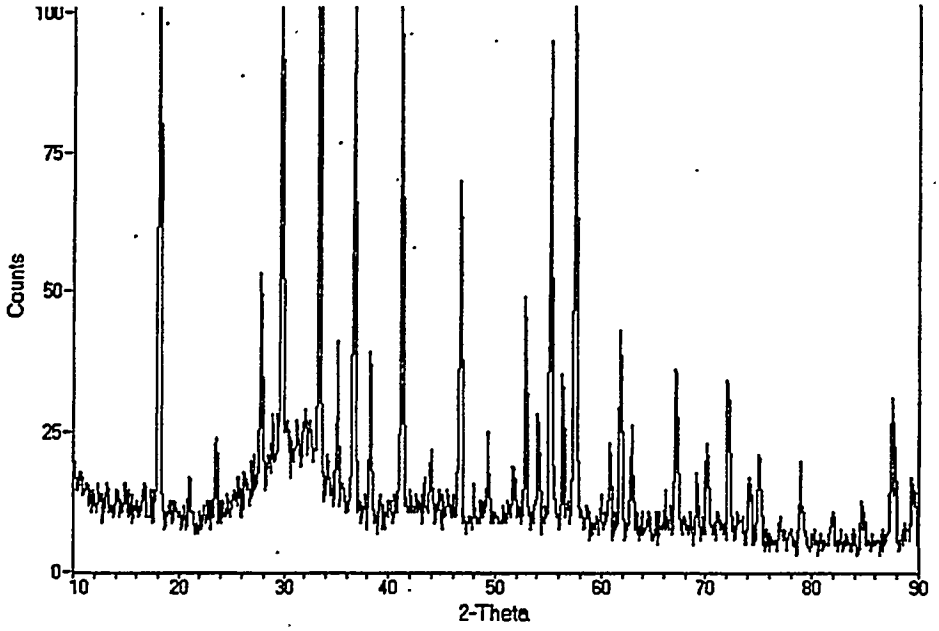

5.1.2.2.4. Evaluation of Chemical Skulling Methods

The primary objectives of these experiments include investigation of chlorinated CaO-Al_2O_3-SiO_2 compositions with a crucible and the effect of the metal/ceramic mixed region on the reactions at the metal/ceramic/refractory interface.

Two methods were investigated to characterize skull formation: 1) chemical reaction of a chlorinated ceramic layer with a crucible, and 2) interaction of a ceramic composition with chloride additions. The two methods for skull formation are outlined below.

Chemical Skull Method 1.

- Use of chlorinated CaO-Al_2O_3-SiO_2 ceramic layer that is very fluid at operating temperatures.
- Interaction of the ceramic layer with the crucible results in penetration of the ceramic melt into the surface layer of the crucible.
- Reaction of the penetrated ceramic melt with the crucible results in conditions in the ceramic phase that facilitate the precipitation reaction.
- The precipitation reaction results in a rapid increase in the viscosity of the ceramic layer, thus freezing off further penetration of the molten liquid into the crucible.
- The reaction layer acts as a barrier to further reaction between the crucible and the ceramic melt. In this case, the reaction layer (or chemical skull) consists of the penetration layer into the crucible.

This method of skull formation was evaluated for a variety of gas flow rates randing from essentially static to high gas flow rates. Increasing the gas flow rate results in an increase in the metal/ceramic 'mixed' region.

Chemical Skull Method 2:

- Use of a CaO-Al_2O_3-SiO_2 ceramic layer
- chloride additions were made either through gas injection into a fluid ceramic layer, or as a batch component to ceramic composition.
- Reaction of the Cl with the ceramic phase at high temperatures results in the precipitation reaction.
- The chlorinated ceramic material deposits or bonds to the surface of the crucible such that a barrier layer is formed between the crucible and the molten bath. In

this case, the reaction layer (or chemical skull) consists of a layer deposited on the crucible.

This method of skull formation can be viewed as a treatment to the crucible prior to beginning a process run.

5.1.2.2.4.1. Experiment Overview

Seven chemical skulling runs were conducted in a 10 lb. reactor with the basic containment configuration, which consists of a containment crucible with catchpot and spacers, and an insulated susceptor. The headspace of the reactor was insulated in each experiment. The gas handling train consisted of a cold trap, a coarse filter impinger, a HEPA canister, and two caustic scrubbers. Argon, hydrogen chloride, or a mixture of the two gasses at various flow rates were injected through a lance into an iron bath with a ceramic phase present. Four ceramic phase mixtures were used in the runs with chlorine either present or absent in the mixture. A summary of the seven runs is presented Table 5.23.

Table 5.23
Chemical Skulling Run Description

Skull Run #	MMT Run #	Refractory System	Ceramic Mix	Experimental Parameters
skull-1	R013-95-021	Alumina crucible	1	• $CaCl_2$ charge • Ar/HCl injection • small mixed region • foaming
skull-2	R013-95-022	Alumina crucible	1	• $CaCl_2$ charge • Ar/HCl, Ar injection • small mixed region
skull-3	R013-95-023	Alumina crucible	2	• Ar/HCl, Ar injection into fluid layer
skull-4	R013-95-025	Alumina crucible	3	• $CaCl_2$ • CaO $Al_2O_3SiO_2$ bulk addition
skull-5	R013-95-028	Alumina crucible	4	• no Cl • baseline
skull-6	R013-95-028	Alumina crucible	1	• $CaCl_2$ charge • Ar/HCl injection • large mixed region
skull-7	R013-95-029	Alumina crucible	1	• $CaCl_2$ charge • Ar/HCl injection • static case: minimal gas injection

5.1.2.2.5. Experimental Observations

5.1.2.2.5.1. General Comments

- Ar/HCI injection resulted in headspace fuming and/or foaming of the ceramic phase. Headspace fuming was a result of iron chloride formation, and resulted in reduced bath visibility.
- Hydrogen chloride injection was periodically secured to allow for visual observations of he bath. Securing HCI injection also reduced foaming of the bath.
- Ceramic phase foaming was minimized by decreasing the HCI flow.

5.1.2.2.5.2. Skull-1 (R013-95-021)

This experiment investigated the formation of a chemical skull between a high alumina refractory and chlorinated ceramic phase for a small mixed region (chlorides were added as $CaCl_2$ in the initial charge and HCl gas was injected into the bath.

- Section of the crucible revealed ceramic phase penetration on the interior and exterior wall surfaces, but no permeation through the entire wall thickness.
- A ridge formed in the crucible wall below the metal ceramic line. A white crystalline layer on the surface was observed on the crucible wall at the ridge and below.

5.1.2.2.5.3. Skull-2 (R013-95-022)

This experiment investigated skull formation with a layered mixed region by combining argon and hydrogen chloride to increase the gas flow during injection.

- Argon and Ar/HCl were injected into the bath.
- A frothy foam formation was observed with the submerged injection.
- When disassembled, no wetting was visible on the exterior of the crucible from ceramic phase penetration. The ceramic layer had frozen into two phases: a crystallized "bowl" with a transparent blue glass filling the center.
- The metal layer had formed a "mushroom" shape, with a ridge at the metal/ceramic interface. A white crystalline material was deposited on the crucible surface below the ridge and a darkening of the crucible bottom was observed (see Figure 5.46).

5.1.2.2.5.4. Skull-3 (R013-95-023)

This experiment investigated the formation of a skull by using Ar/HCl injection at high flow rates into a shallow, fluid ceramic layer. The mixing from the gas flow and reaction with HCl was intended to splash the ceramic layer on the crucible wall where it was expected to freeze and form a skull.

- During the cooling period, it was observed that the ceramic phase had formed a ring above the metal charge.
- During disassembly, it was discovered that the ceramic phase had formed a friable ceramic ring above the metal that easily broke from the crucible wall. Small beads of metal were dispersed throughout the ceramic ring.

- Sectioning of the crucible revealed slight permeation into the crucible wall, as evident by a small darkening. Unlike previous experiments, no darkening of the crucible bottom was observed, and the walls along the metal layer had few spots of white material.

5.1.2.2.5.5. Skull-4 (R013-95-025)

In this experiment, the formation of a skull between the crucible and ceramic layer containing $CaCl_2$ was investigated. The ceramic phase batch was mixed into a slurry and slip-cast on the interior of the crucible.

- The slip-cast coating on the crucible showed extensive cracking after it was dried. When the metal charge went molten, the coating spilled off of the crucible wall.

- The slip-cast coating had been dissolved to height of 1"-1 1/2" above the ceramic layer. The coating at the top of the crucible had a "peeled-paint" appearance with cracking and lifting, but it was still bonded to the crucible wall.

- The deepest ceramic phase penetration was found in the area coinciding with the liquid ceramic layer (bulk addition). the penetration depth decreased sharply below the ceramic layer.

- Below the metal/ceramic interface, the slurry coating was still present on the crucible, with a white-yellow crystalline build-up layer on the surface (see Figure 5.47).

Figure 5.46
Section of crucible wall below the metal/ceramic lines for Skull 2 (magnification = 20x, sample R013-95-022-R1-R2

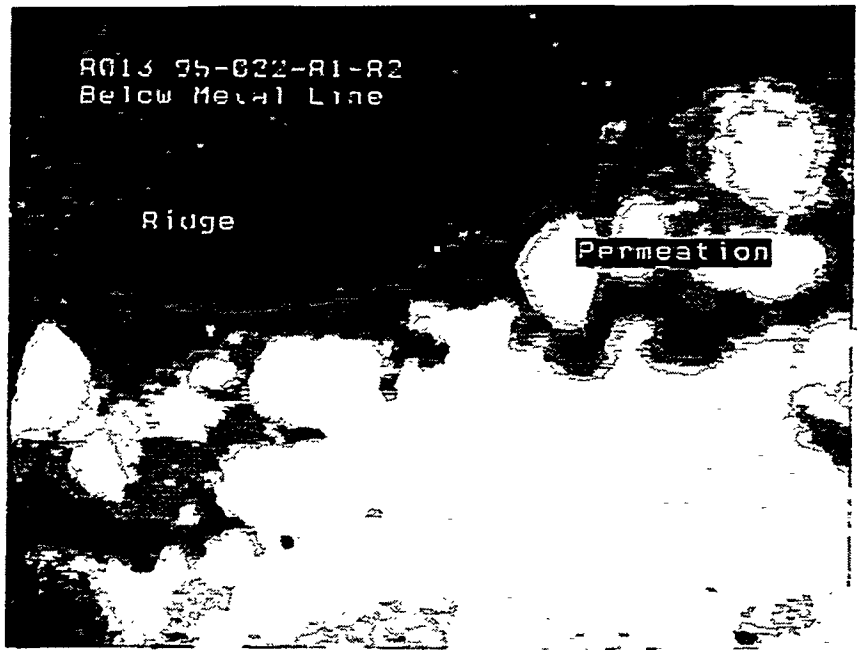

Figure 5.47
Section of crucible wall below the metal/ceramic line for Skull 4 (magnification = 20x, sample R013-95-025-R1-R2

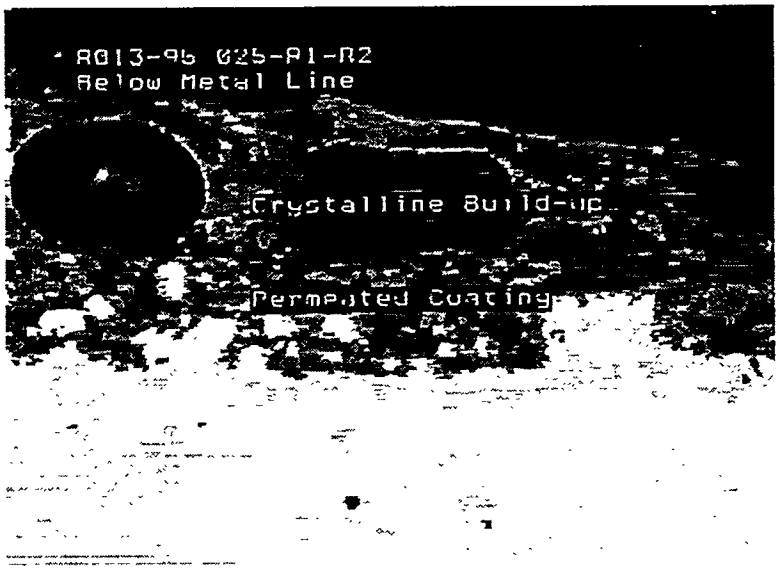

5.1.2.2.5.6. Skull-5 (R013-95-026)

This experiment was the baseline run for the crucible and CAS ceramic phase with no chlorine addition. Submerged injection of Argon was performed during this run.

- The ceramic phase was very fluid and no foam layer was observed.
- When the experiment was disassembled, the outside of the crucible had several wetted areas indicating deep permeation through the crucible wall.
- The interior wall of the crucible above the ceramic layer was pitted.
- The crucible walls near the metal layer showed no signs of white crystalline build-up.

5.1.2.2.5.7. Skull-6 (R013-95-028)

Skull-6 was similar to Skull-2, with the exception that higher gas flow rates were used to extend the metal/ceramic mixed region. The metal level was increased for this run to allow for a larger metal/ceramic mixed region (i.e., to minimize the effect of the bottom of the crucible).

- The interior wall of the crucible was pitted with visible white aggregate above and below the ceramic layer. It was speculated that this pitted area of the crucible wall represented the mixed region during the experiment. Penetration of the ceramic phase into the crucible wall in this area was observed with the deepest penetration at the metal/ceramic interface. (see Figure 5.48)
- The metal layer did not form a ridge as in previous experiments but did have visibly rounded sides in the mixed region. The bottom of the crucible showed slight ceramic permeation with deeper penetration into cracks attributed to the cooling period (see Figure 5.49)

Figure 5.48
Section of crucible wall from metal/ceramic mixed region for Skull-6
(magnification = 20x, sample R013-95-028-R1-R1)

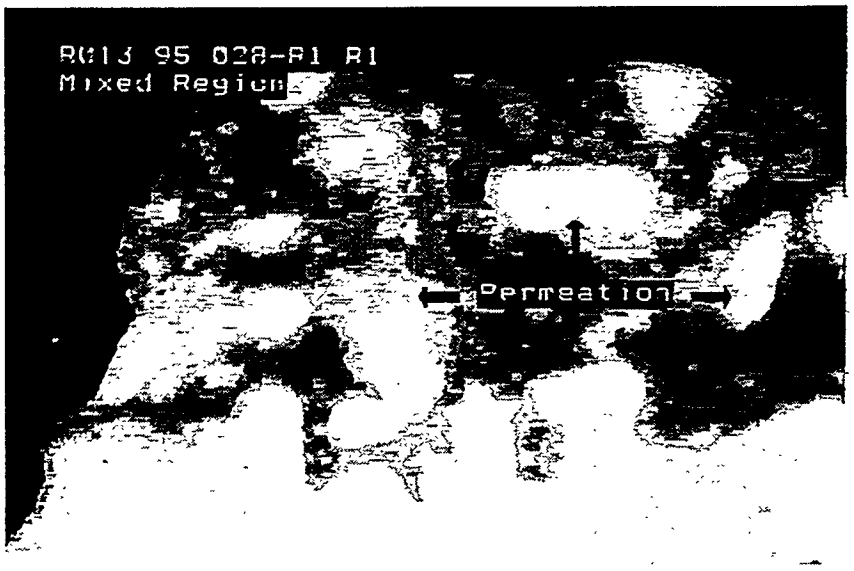

Figure 5.49
Section of crucible wall below the metal/ceramic line for Skull-6
(magnification = 20x, sample R013-95-028-R1-R1)

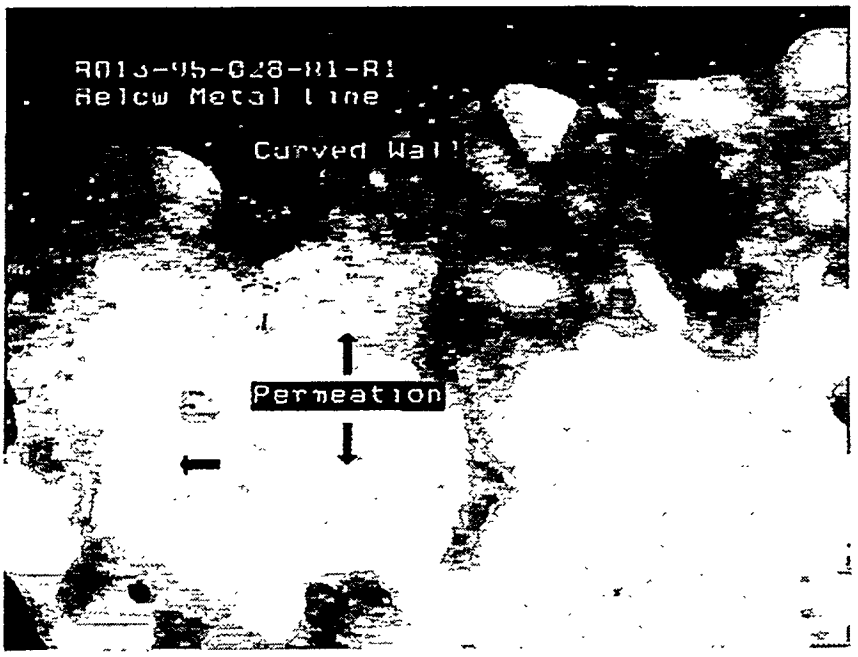

5.1.2.2.5.8. Skull-7 (R013-95-029)

Skull-7 investigated skull formation between the refractory and a CAS ceramic phase, with minimal gas injection for near-static conditions.

- When the crucible was removed during disassembly, two spots of wetting from ceramic phase permeation were discovered on the outside of the crucible.
- Ceramic phase penetration into the wall was found to be deepest from one inch below to one inch above the metal/ceramic interface.

5.1.2.2.6. Analytical Results

Chemical interaction between a non-chlorinated CAS ceramic phase and the alumina crucible was found to be extensive. The level of chemical interaction between the two was reduced by addition of chlorides to the system. The decrease in chemical interaction was attributed to formation of a barrier layer, or chemical skull.

Chemical analysis of various phases of the system are provided in Table 5.24. Post-run analysis of the ceramic phase layer and crucible surfaces provide insight to chloride retention/capture in the ceramic phase, as well as development of ceramic phase coatings on the crucible surfaces.

Table 5.24
Elemental analysis of ceramic phase and crucible samples using XRF with Uniquant. Compositions are given as normalized weight percent.

Sample ID	Description	Ceramic Mix	FeO	Cl
skull-1 R013-95-021-R1-C1	ceramic phase	1	0.72	8.4
skull-2 R013-95-022-R1-C3	ceramic phase	1	0.38	4.7
skull-2 R013-95-022-R1-R2	crucible surface layer: bottom	1	6.5	6.0
skull-3 R013-95-023-R1-C1	ceramic phase: friable layer	2	1.33	8.9
skull-4 R013-95-025-R1-C1	ceramic layer from bulk addition	3	0.47	3.7
skull-4 R013-95-025-R1-C2	slip cast crucible coating: side wall	3	0.97	4.27
skull-4 R013-95-025-R1-C2	crucible surface below metal line: side wall	3	0.41	0.93
skull-4 R013-95-025-R1-C3	crucible surface below metal line: bottom	3	0.83	1.98
skull-5 R013-95-026-R1-C1	ceramic layer	4	0.24	–
skull-6 R013-95-028-R1-C1	ceramic layer	1	0.26	3.73
skull-6 R013-95-028-R1-R3	crucible surface layer: bottom	1	3.22	0.10
skull-7 R013-95-029-R1-C1	ceramic layer	1	0.45	7.0

5.1.2.2.6.1. Chemical Skull Method 1

Chemical skull formation using the method 1 approach was observed for several runs, with the following statements summarizing the results.

- Ceramic phase penetration into the crucible was observed. the overall amount of penetration did not vary significantly as a function of gas injection flowrate. i.e., as a function of the metal/ceramic mixed region.

- The content of the post-run ceramic layer varied as a function of increasing the metal/ceramic mixed region (increasing the gas flowrate); i.e. there was increased wear of the inner crucible surface as the gas flowrate increased.

- Crucible wear for small metal/ceramic mixed region conditions was most severe at the metal/ceramic interface.

- Crucible wear for large metal/ceramic mixed region conditions was spread over a large region.

- Ceramic phase penetration below the metal line was highest for large metal/ceramic mixed region conditions.

The limited ceramic phase penetration into the crucible is attributed to the presence of chloride in the system. Microstructure analysis of the penetration region (i.e. barrier layer) will be performed to identify the phases present in the layer.

5.1.2.2.6.2. Chemical Skull Method 2

Two approaches were used to investigate Method 2 for chemical skull formation. The first approach looked into Ar/HCl gas injection into a fluid ceramic phase layer. Introduction of chloride to the fluid layer prompted the precipitation reaction. The precipitation reaction resulted in a friable crystalline material that contained significant amounts of Cl. This phase did not adhere well to the crucible wall; therefore, a chemical skull or barrier layer was not achieved.

The second approach to chemical skull formation utilized a slip-cast layer of ceramic phase batch material containing on the inner surface of the crucible. Upon heating, the precipitation reaction occurred and the layer was sintered to the surface of the crucible.

Once the barrier layer was formed, a ceramic phase was added to the system to study the effectiveness of the barrier layer. The slip cast layer was dissolved by the ceramic phase above the ceramic layer. Below the metal line; however, the slip-cast layer survived, with a thin layer of ceramic phase deposited on the surface of the barrier layer. This layer had a textured gold/green appearance. A small amount of deposited ceramic layer was also observed on the bottom surface of the crucible. Chemical analysis of this layer was similar to the batch composition of slip-cast layer.

5.1.2.2.7. Summary

The formation of a chemical skull, or barrier layer, was achieved by two methods: 1) chemical reaction of a chlorinated ceramic layer with crucible, and 2) interaction of a ceramic composition with chloride additions. Method 1 resulted in limited ceramic phase penetration into the crucible, with the penetration layer acting as the barrier for the further reaction between the molten ceramic phase and the containment system.

The Method 2 approach to skull formation was most successful when a slip-cast coating of chlorinated ceramic material was applied to the crucible surfaces. The performance of the barrier layer degraded when a non-chlorinated ceramic layer was added to the system. Below the metal line, a uniform coating was formed with additional ceramic phase material deposited on the surface of the coating; i.e. the barrier layer increased in thickness.

5.1.3. Ceramic Phase Stability

5.1.3.1. Introduction

The large variation in chemical composition and concentration of glass formers in waste streams presents a challenge in the development of a CEP ceramic phase which meets both operational and stability requirements. Experiments were conducted to determine the relationship between chemical composition and the stability of the ceramic phase. Various amounts of contaminants were added to the base glasses, including RCRA metals and uranium. These materials were then subjected to a variety of tests performed at the NYS College of Ceramics at Alfred University (AU), Vitreous State Laboratory (VSL), and MMT. The tests included determination of the volatility of certain components, DTA and viscosity measurements, and leach testing. Leach testing was performed using TCLP, PCT, and MMT's Leaching and Dissolution Resistance (LADR) test. The results unambiguously indicate that glasses based on a high silica composition of the CaO-Al_2O_3-SiO_2 (CAS) system are less susceptible to crystallization and are significantly more durable. Test results were also correlated with a modified form of the free energy of hydration model, which predicts (and experimental tests confirm) that the ceramic phase typically produced during CEP is more resistant to leaching than typical waste glass compositions.

5.1.3.1.1. CEP Ceramic Phase Generation

Ceramic phase generation during CEP operations is dependent on the chemical make-up of the wastestream and the desired partitioning of components to the ceramic phase. For instance, there are some cases where ceramic phase generation is negligible, and others where the ceramic phase is targeted for component capture (e.g. uranium capture in the ceramic phase).

The CaO-Al_2O_3-SiO_2 system has been targeted as the base ceramic phase system for CEP operations. This system satisfies many of the criteria for ceramic phase operability for typical CEP operating conditions. Operability issues include ceramic phase liquidus temperature and viscosity, as well as refractory compatibility. The CaO-Al_2O_3-SiO_2 system is also functional in terms of component incorporation in the ceramic layer; acid to basic compositions can be utilized, as well as addition of other constituents (such as B_2O_3, Li_2O, MgO), to facilitate partitioning of components to the ceramic phase.

As a first approximation, thermodynamics can be used to evaluate the partitioning of components to the ceramic phase for typical CEP operating conditions. Figure 5.50 shows the free energy of formation for the metal oxides of interest in this report with respect to CO generation. Under thermodynamic control, components that lie below the CO line will be oxidized to the ceramic layer, while those that lie above the CO line are reduced to the metal. This figure clearly shows that most RCRA metals are not favored to partition to the ceramic phase; curves for Se, Ag and Hg oxides fall above the curve

for PbO. While BaO is the only RCRA metal favored to partition to the ceramic phase for all temperatures, Cr oxidation to the ceramic phase is expected for temperatures below 1250°C or for excursions to higher oxygen potentials. All radionuclide surrogates and uranium are expected to oxidize and partition to the ceramic phase. It should be noted that this figure reflects a purely thermodynamic evaluation, and does not take into consideration mass transfer issues related to component capture in the ceramic phase.

5.1.3.1.1.1. Uranium Solubility

Uranium oxide has been successfully incorporated into a variety of glass-forming systems in amounts ranging from 15-50 wt%. The solubility of uranium in glass is strongly dependent on the glass melt composition, redox conditions during melting, melting temperature, and distribution of valence states of the uranium in glass. U^{+4}, U^{+5} and U^{+6} have been observed to be stable in glass, with the overall uranium solubility of the glass dependent on the redox equilibrium distribution. The redox equilibrium distribution is a function of the oxygen fugacity of the system. [Screiber-1982/1983]

Figure 5.50
Free Energy Of Formation For Selected Metal Oxides With Respect To CO Generation

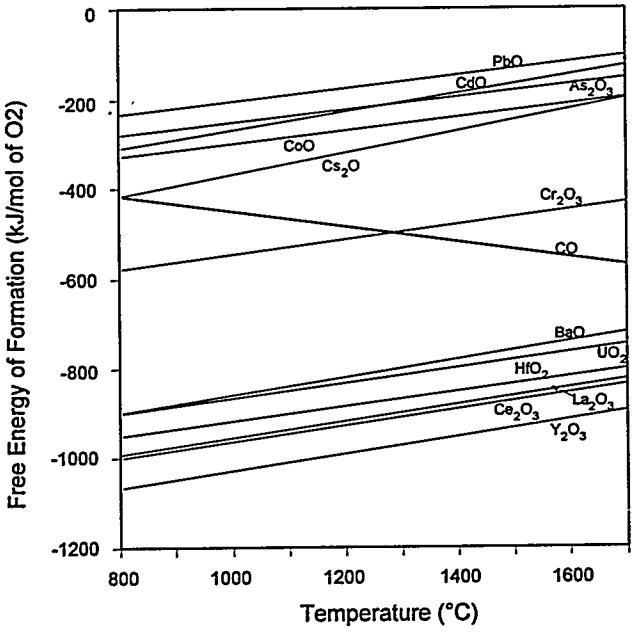

Uranium oxide solubility in glass is strongly dependent on the redox equilibrium distribution. In general, uranium solubility is highest when U^{+6} is present as discrete uranyl ions (UO_2^{2+}) in the melt. The solubility of uranium decreases tremendously as

U^{+6} is reduced to lower valence states. U^{+4}, in particular, appears to have a very low solubility in the glass-forming melt, with increasing U^{+4} content resulting in precipitation of UO_2 crystals in the melt. Typical uranium oxide solubilities for Aluminosilicate glasses equal 15 wt% for UO_3 (U^{+6}) and 5 wt% for UO_2 (U^{+4}). Given CEP operating conditions (i.e. low oxygen fugacity) uranium oxide will most likely be incorporated in the ceramic phase as UO_2 (U^{+4}), with a solubility limit of approximately 5 wt% UO_2. [Screiber-1982/1983]

5.1.3.1.2. Stabilization of the Ceramic Phase

One of the major objectives in development of the ceramic phase is "stabilization" of the ceramic phase. There are several areas in which stabilization of the ceramic phase may have different meanings in terms of the physical significance and the technical/analytical approach in the meeting the objectives. The areas of particular interest in developing the ceramic phase for CEP include: 1) structural stabilization, i.e. stabilization of components such as radionuclides or chlorides in the ceramic phase; 2) final form stabilization, which deals primarily with leachability of the ceramic phase product; and 3) vitreous phase stabilization, or the glass forming ability and stability of the melt.

5.1.3.1.2.1. Structural Stabilization

Structural stabilization of components, such as radionuclides or chloride, in the ceramic phase (both glass and crystalline forms) is a crucial objective to obtaining a high quality ceramic phase product. In this case, stabilization refers to a structural incorporation, or immobilization, of the component or element in the ceramic or vitreous phase. Incorporation of the component into the structure can be achieved by several means, such as: 1) bonding of the component within the network structure; 2) interstitial capture of the component within the network of the structure; 3) crystalline precipitation of the component, or complex, in the structure. While a glassy structure is often more accommodating in terms of component loading (i.e. incorporation), crystalline or partially crystallized structures can also immobilize waste components.

5.1.3.1.2.2. Final Form Stabilization

Ceramic phase final form stabilization deals primarily with the leaching characteristics of the final ceramic phase product. When discussing ceramic phase products or final form issues, the word stabilization refers to a non-leachable ceramic phase. Leachability of the ceramic phase can be determined through standard testing procedures as well as in-house screening leach tests (LADR).

The ceramic phase leachability testing requirements are determined based on the classification of the wastestream. For example, if the wastestream contains RCRA metals, the ceramic phase must be tested to ensure that the material is not classified as a RCRA hazardous material. The Toxicity Characteristic Leaching Procedure (TCLP) is a

standard, regulatory test used to determine if a material is classified as a RCRA hazardous waste. If the wastestream contains also contains radioactive components, i.e. a Mixed Waste, additional leachability testing is required. Currently, there is no disposal method or test procedure which is accepted and approved for mixed waste. The generally accepted practice is to perform both the TCLP test and a second test for radioactive waste forms. The Material Characterization Center-Test 1 (MCC-1) and Product Consistency Test (PCT) are extensively used to determine the relative leachability of glasses that contain radionuclides.

5.1.3.1.2.3. Vitreous Phase Stabilization

Vitreous phase stabilization deals with the glass forming ability and stability of the molten ceramic phase layer. While the term "ceramic phase" is used to describe the inorganic phase of the CEP, it encompasses the formation of both vitreous (glassy) and crystalline final form products. Stabilized vitreous phase indicates that the material is non-crystalline, i.e. a glass. The glass forming stability can be discussed in terms of the ceramic phase chemistry and the rate of cooling (i.e. mode of tapping).

5.1.3.1.3. Ceramic Phase Stabilization Experiments

Ceramic phase stability issues have been addressed by several development projects, with the combined results reported here. External development projects were conducted at the NYS College of Ceramics at Alfred University (AU), Vitreous State Laboratory (VSL), and MMT.

The AU study addressed stabilization of the ceramic phase for a variety of RCRA metals, radionuclide surrogates and chloride additions. This study focused on structural stabilization of components into a glassy matrix, and the effect of component addition on the glass forming stability. This study also provided samples for leachability testing using the TCLP and LADR testing protocols.

The AU study used two CaO-Al_2O_3-SiO_2 base glass compositions for component additions, one with a high silica composition and one with a low silica composition. These compositions represent ceramic phase regions for CEP operations. Characterization of the samples included: melt observations, thermal analysis (glass transformation temperature, T_g, and crystallization temperature, T_x), transition range viscosity measurements (10^{12}-10^9 poise), density, and refractive index measurements. X-ray diffraction (XRD) patterns and leachability data (TCLP and LADR) were obtained for selected samples.

The VSL study focused on composition development for Radioactive and Mixed Waste applications. Uranium and selected RCRA metal additions were made to several glass compositions; compositions were provided by both MMT and VSL. The compositions were determined based on uranium solubilities and typical CEP operating conditions.

Characterization of the samples included: verification of the uranium valence state (i.e. U^{4+}); glass stability evaluation using XRD and microanalysis, melt viscosity at 1200 to 1450°C, and leachability testing (PCT).

MMT ceramic phase stabilization studies have focused on component partitioning to the ceramic phase, where Hf and Cl have been the major components of interest, and development of an in-house leachability test (LADR). Selected information regarding structural incorporation and glass stability issues for either Hf or Cl incorporation has been integrated into this report

.

5.1.3.2. Component Incorporation and Glass Stability

5.1.3.2.1. Component Incorporation: AU, VSL and MMT

Radioactive and Mixed Waste component doping of ceramic compositions have been evaluated based on expected partitioning to the ceramic phase (see Figure 5.50). While most RCRA metals are not expected to concentrate in the ceramic phase under typical CEP operating conditions, minor component doping has been investigated to assess the effects of transient or metastable partitioning of the metals to the ceramic phase.

Table 5.25
Waste Component Dopants And Dopant Levels Used For Various Experimental Studies (AU, VSL, MMT)

Element	Waste Component	Dopant	Dopant Levels (wt%)	Base Glass
As	RCRA	As_2O_3	0.25, 0.5	A, B
Ba	RCRA	BaO	0.3, 1.5, 3.0	A, B
Cd	RCRA	CdO	0.1, 0.5, 1.0	A, B
Cr	RCRA	Cr_2O_3	0.3, 1.5, 3.0	A, B
Pb	RCRA	PbO	0.3, 1.5, 3.0	A, B
U	Radionuclide	UO_2	1.0, 3.0	A, B
Hf	RN-surrogate	Hf, HfO_2	1-5	A
Hf	RN-surrogate	Hf, HfO_2	1-3	B
Co	RN-surrogate	CoO	0.1, 0.5, 1.0	A, B
Ce	RN-surrogate	CeO_2	0.1, 1.5, 3.0	A, B
Cs	RN-surrogate	Cs_2O	0.1, 0.5, 1.0	A, B
Y	RN-surrogate	Y_2O_3	5.0	A, B
La	RN-surrogate	La_2O_3	3.0	A, B
Cl	Chlorinated	$CaCl_2$	8.0, 20.0	A
Cl	Chlorinated	$CaCl_2$	1.0, 1.25	B

Table 5.25 provides a listing of the ceramic phase dopants and dopant levels for various experimental studies. The component additions include the following elements of interest:

- RCRA metals: As, Ba, Cd, Cr, Pb
- radionuclide (RN) surrogates: Hf, Cs, Ce, Co, Y, La
- radionuclide: U
- halide: Cl.

Dopant additions were made to glass compositions that lie within two base CaO-Al_2O_3-SiO_2 compositions regions for CEP. These regions designate high silica compositions (region A) and low silica compositions (region B) that are commonly used for

processing wastestreams. The composition region required for processing a particular wastestream is dependent of the following factors:

- ceramic formers in the wastestream (e.g. Al, SiO_2, CaO/MgO)
- desired partitioning of particular components (e.g. uranium, chloride)
- final form specification (e.g. physical properties, leaching behavior).

In general, glasses were prepared by batching raw materials and melting in a crucible. Melting was performed in air for RCRA metal dopant additions, and a reducing atmosphere (i.e., CO bubbled through the melt) was used for uranium containing samples to ensure the U^{4+} valance state. Samples containing Hf were obtained through metal decontamination studies using bench scale testing at MMT.

Periodic in situ melt observations indicated that the component additions did not significantly alter the melting behavior and of the glass systems in terms of melting and fining times and fluidity at temperature. An exception to this statement was found for chloride additions to a region B glass composition. While small $CaCl_2$ additions ($\leq$1.25 wt%) did not alter the melt behavior, increased $CaCl_2$ additions resulted in an increase in the melt viscosity as determined by qualitative observations. It has been proposed that the rapid increase in viscosity with chloride addition is due to precipitation of a calcium aluminate crystalline phase.

5.1.3.2.2. Glass Forming Stability

When evaluating the glass forming ability (or stability) of a melt, the critical question is not whether the liquid will form a glass, but how fast must the liquid be cooled in order to avoid crystallization. In other words, a glass will be formed if the melt is cooled fast enough to avoid crystallization.

The glass forming ability relates to the critical cooling rate of the melt required to avoid crystallization, while glass stability is defined as the resistance of glasses towards devitrification upon heating. The glass forming ability and stability are often incorrectly considered to be synonymous. For this study glass forming ability was determined qualitatively by the severity of quench required to form a glass. Quench techniques varied from the simple removal of crucibles from the furnace to dipping the bottoms of hot crucibles in water.

Glass forming stability was determined using various thermal analysis techniques, i.e., Differential Thermal Analysis (DTA) and isothermal heat treatments of previously prepared glasses. DTA measurements are used to obtain the glass transformation temperature (T_g) and the crystallization temperature (T_x) for a given heating rate. The difference between T_g and T_x (i.e. T_x-T_g) is used as an indicator of the glass stability.

Large T_x-T_g values indicate good glass stability, while small T_x-T_g values indicate poor glass stability.

More than 70 glasses were prepared to determine the effect of component additions on the glass stability of two base CaO-Al_2O_3-SiO_2 compositions (i.e. high and low silica compositions). Glass forming ability Glass stability was determined by evaluating the effect of the component additions on T_x-T_g and the homogeneity of the sample.

The glass stability, or T_x-T_g, of the two base glasses varied significantly. The high silica glass composition displays excellent glass forming ability, with no crystallization peak observed in the DTA analysis. DTA analysis of the low silica composition), however, displayed a distinct crystallization peak, with a Tx-Tg value of 183°C. While this composition region shows reasonable glass forming ability (i.e. glass formation with moderate to fast quench rate for 20 gram glass batches), it is much more prone to devitrification than the high silica region.

All glasses prepared with the high silica composition showed excellent glass stability, i.e. no crystallization peak was observed for DTA analysis of the glass samples (heating rate of 20K/min). Homogeneous glass formation was observed for all component additions, with color variations indicative of the component addition (e.g. Cr_2O_3 additions resulted in green glass). Minimal effects were detected on the glass properties (i.e. T_g, transformation range viscosity) for most additions, with T_g variations ranging from 788 to 807°C and no crystallization peak detected. Chloride additions, however, resulted in decreases in T_g and transformation range viscosity. Chlorinated glass samples from an earlier study at AU showed a steady decrease in Tg from 786 to 657°C as the chloride content increased from 0 to 12.8wt% Cl, respectively. DTA analysis of the chlorinated glass samples did not show a crystallization peak, therefore, it appears that the glass stability of the chloride-doped samples was not compromised.

The low silica base glass (region B) inherently exhibits less glass-forming ability relative to the high-silica base glass, requiring a moderate to rapid quench rate for glass formation. Component additions to the low-silica glass showed minimal effects on glass stability for most components. However, decreases in glass stability were observed for Cr_2O_3 additions greater that 0.3wt%; T_x-T_g decreased from 203°C to 79°C as the Cr_2O_3 dopant level increased from 0.3 to 3.0 wt%, respectively. $CaCl_2$ additions greater than 1.25 wt% also decreased the glass forming ability, with the quenched samples showing devitrification. Chloride additions for similar low silica compositions has been shown to result in precipitation of a calcium aluminosilicate crystalline phase.[8]

Glass stability was also evaluated for selected VSL samples containing both RCRA metals and uranium (RCRA#1A and RCRA#2A). The glass samples were subjected to heat treatment to assess possible formation of crystal phases during the melting process; samples were heat treated at 1200°C for 20 hours. Following this heat treatment, quenched samples were examined by Scanning Electron Microscopy (SEM), coupled

with an Energy Dispersive X-Ray Spectrometer (EDXS), as well as optical microscopy to determine the amount and type of any crystal phases that may have formed. Sample RCRA#1A showed no apparent crystallization, while sample RCRA#2A contained approximately 1-1.5 volume percent crystallization. Elemental analysis of the crystalline phase revealed Cr as the primary component, suggesting that Cr_2O_3 or a Cr-rich phase was formed during the heat treatment process.

5.1.3.3. Ceramic Phase Leachability

One of the major concerns with component incorporation in the ceramic phase is final form stabilization, i.e. producing a non-leachable ceramic phase product. While the term product has different meanings for RCRA vs. Mixed Waste materials, the important issue is that the final material meets all regulatory and customer specifications with respect to leaching behavior.

5.1.3.3.1. Leaching and Leachability Testing

5.1.3.3.1.1. "Leaching" in Aqueous Solutions

Most commonly, the attack of glasses and ceramics by aqueous solutions is referred to as leaching. However, leaching is only part of the process, and it is probably more appropriate to refer to this attack as corrosion. The various stages of the corrosion of multi-component glasses are discussed below.‡

When glass is submerged in water, the first corrosion process is the leaching of mobile ions. Leaching proceeds by an ion exchange process where near-surface alkali (R^+) and (to a lesser extent) alkaline earth (R^{2+}) ions are replaced by hydronium (H_3O^+) ions. These hydronium ions diffuse inward from the glass surface while R^+ and R^{2+} ions diffuse outward. When the alkali or alkaline earth ions reach the surface, they exchange with more hydronium (H_3O^+) ions, and the process continues. This exchange results in an increase in the pH of the water and a weight loss of the submerged glass. When only leaching occurs, both the pH and weight loss increase linearly with the square root of time because the process depends on the diffusion of ions. Glasses with small inter-diffusion coefficients generally exhibit good resistance to leaching.

The second corrosion process is congruent dissolution. As the leaching of cations proceeds and the pH of the leachate increases, a point is reached were the overall network of the glass becomes susceptible to attack by the higher pH leachate. The network structure of glass is comprised of M-O-M bonds, where M is primarily Si(normally), but can also be Al, B, and P depending on composition. The M-O-M 'bridging' bond is attacked by OH^- ions, and the chemistry of this bond determines the

‡ In general, the majority of research on the corrosion of ceramic materials has focused on glasses, but much of the information can be applied to poly-crystalline ceramics as well.

pH where the attack begins, i.e. it is a function of glass composition. Attack of the M-O-M bonds results in a congruent dissolution of the glass and a corresponding increase in weight loss of the glass.

The congruent dissolution process does not have the same effect on pH as does leaching, i.e. the rate of increase in pH diminishes. This decrease in the rate of change of pH when the network of the glass begins to dissolve is the result of two factors. First, OH^- ions in the leaching are consumed by the formation of both soluble and insoluble $M(OH)_x$ complexes. Second, the insoluble $M(OH)_x$ complexes are deposited on the surface of the glass forming a passive layer. This layer acts as a diffusion barrier decreasing the leaching/exchange rate and therefore the rate of OH^- ion formation. The rates of consumption of OH^- ions and formation of the passive layer depend on the composition of the glass and can often result in the pH of the water/solution passing through a maximum during a static leach test.

In glasses with good leaching and dissolution resistance, the layer of deposited insoluble $M(OH)_x$ complexes forms a complete barrier preventing both further leaching and congruent dissolution. As a result, both the pH and the total weight loss reach steady-state values after a period of time. In general, experiments have shown that when the pH reaches a steady state value, the total weight loss has also reached a steady state value.

5.1.3.3.1.2. Toxicity Characteristic Leaching Procedure

The toxicity characteristic leaching procedure (TCLP) is a standard, regulatory test used to determine if a material is classified as a RCRA hazardous waste. This test is used to determine the mobility of both organic and inorganic analytes present in liquid, solid and multiphase materials. The TCLP tests for leachability (mobility) of heavy metals, semi-volatile, volatiles and pesticides. Because of the processing conditions inherent to CEP, RCRA metals are the only listed materials present in the ceramic phase, and therefore a TCLP test for RCRA metals is sufficient for regulatory purposes.

For the TCLP test, the sample of ceramic/glass is sized such that the smallest dimension is less than 1 cm. A 25 gram sample is placed in an extraction vessel and the appropriate amount of extraction fluid (acidic solution) is added: the weight of the extraction fluid equals 20 times the weight of the solid sample. The extraction vessel is sealed and rotated at 30±2 rpm for 18±2 hours at ambient temperature (23±2°C). On completion of this extraction procedure, the TCLP solution (extract) is filtered, pH is recorded, and the solution is analyzed for regulated substances (RCRA heavy metals). If the TCLP extract from a representative solid sample contains any listed contaminants at the concentration equal to or greater than the regulatory level, the solid exhibits the "characteristic of toxicity". See Table 5.26 for RCRA metals limits in TCLP extract. A solid waste that exhibits the characteristic of toxicity has the EPA Hazardous Waste Number which corresponds to the toxic contaminant causing it to be hazardous.

Table 5.26
Maximum Concentration of RCRA Metals for the Toxicity Characteristic.

EPA HW No.(†)	Contaminant Metal	Regulatory Level (mg/L)
D004	Arsenic	5.0
D005	Barium	100.0
D006	Cadmium	1.0
D007	Chromium	5.0
D008	Lead	5.0
D009	Mercury	0.2
D010	Selenium	1.0
D011	Silver	5.0

† Hazardous Waste No.

There are three critical factors which determine the performance of a glass or ceramic-phase product subjected to TCLP test; total heavy metal content, kinetic stability, and thermodynamic stability.

- **Total heavy metal content:** If the total mass of individual RCRA metals in the test sample is less than the quantity necessary to achieve the concentration limit in the given leachate volume, the sample will pass the TCLP test regardless of thermodynamics or kinetics. Specifically, the entire test sample could dissolve and the concentration of individual RCRA metals would still be less than the regulatory limits.

- **Kinetic stability:** If the kinetics of the leaching process are slow enough so that a sufficient quantity of individual RCRA metals cannot leach in the 18 hour testing time, the sample will pass the TCLP test regardless of the thermodynamic solubility limit.

- **Thermodynamic stability:** If the thermodynamic solubility limit of individual RCRA metals in the leachate is less than the regulatory limits, then the sample will always pass the TCLP test.

In addition to regulatory uses, the TCLP test can be used as a means of comparing the relative leachability of glasses. However, because of the test protocol, care must be taken in using the results of these tests as "feed-back" to materials engineering efforts. Specifically, changes in sample sizing will have dramatic effects on the amount of leached material. In addition, the use of the acidic leachate solution can cause selective removal of glass constituents and result in final leachate compositions which are non-representative of the true relative corrosion resistance of the glass.

5.1.3.3.1.3. Product Consistency Test

The PCT test was developed at the DOE's Westinghouse Savannah River Site (SRS) as a means of judging the success of their on site program to vitrify liquid high-level nuclear waste. However, it has found wider use in the characterization of mixed-waste glasses, and has been approved as a standard leach test by the American Society for Testing Materials (ASTM C26.13).

For the PCT test, a sample of glass is powdered to a size between -100/+200 mesh. One (1.0) gram or more of sample is placed in a container along with a quantity of leachate (deionized water) equal to 10 times the mass of the sample. The sample is then held at 90 °C for a period of 7 days. At the end of the test period, the leachate solution is analyzed using ICP-AES (inductively coupled plasma - atomic emission spectroscopy) to determine the concentration of all ions leached into solution. Different samples are compared by calculating a normalized elemental loss (N_i) for each element, using the equation,

$$N_i = \frac{\text{Mass}_{i(\text{leachate})}}{\text{MassFraction}_{i(\text{glass})} \cdot \text{Volume}_{\text{Leachate}}}$$

from the results of ICP-AES analysis.

The ultimate performance of samples subjected to PCT test are judged on a relative scale to a "reference" glass, e.g., West Valley WVCM62-2 glass. In general, the concentrations of primary components in the leachate are used for comparison of overall leach resistance of glasses. In addition, concentrations of specific ions, e.g., U or RCRA metals, are measured to analyze for selective leaching. It is important to note that there is no specific pass/fail criteria for this test because allowable leach levels will be site specific depending on the conditions of repositories selected in the future.

5.1.3.3.1.4. Leaching and Dissolution Resistance Test

The leaching and dissolution resistance (LADR) test was developed by MMT to provide feed-back to efforts directed at engineering a "stable" ceramic-phase product. The test

was designed to determine the contribution of ion exchange diffusion and material removal to the overall ceramic corrosion process. The parameters and procedure for this simple in-house test were derived by selecting the best components from existing standard durability and leachability tests.

For the LADR test, a sample is crushed and sieved to yield -25/+35 mesh particles. A portion of these sized particles is weighed and combined with leachate (water) such that the ratio of sample surface area (SA) to leachate volume(V) is 0.2 cm. The pH of the solution is measured as a function of time, and the test continues for at least seven days or until the $^{\delta pH}/_{\delta T} \rightarrow 0$. At the end of the test the leachate is decanted and particulate sample is filtered, dried and weighed. The leachate is reserved for subsequent optional elemental analysis using ICP-AES or similar. Samples can be judged on a relative scale by comparing initial $^{\delta pH}/_{\delta T}$, final pH, and total weight loss.

Table 5.27 compares the parameters from the LADR test with those from other durability tests. The most important feature of the LADR test is the fixed value of $(^{SA}/_{V})$. The ratio of $(^{SA}/_{V})$ is a critical factor in determining both the kinetics and magnitude of leaching and dissolution. In fact, experiment has shown that the amount of material leached/dissolved from a glass in a given quantity of time is directly proportional to the $(^{SA}/_{V})$. Therefore, to prevent erroneous conclusions, it is particularly important to fix this value when trying to compare the corrosion resistance of glasses with different densities. For example, if the ratio of sample weight to leachate volume is fixed, as in the case of the PCT, differences in densities exhibited by typical silicate glasses will result in variations in $(^{SA}/_{V})$ of >20%. Because, the chosen $(^{SA}/_{V})$ of 0.2 is relatively close to the minimum value for the TCLP test, the LADR test also has a potential use as a rough predictor of the performance of a sample subjected to TCLP testing.

5.1.3.3.2. Predicting Leachability: Free Energy of Hydration Model

Paul originally developed a model to explain composition dependence of the durability of oxide glasses in aqueous solutions [Paul-1977]. The model is based on the thermodynamic activity and stability for the component oxides of the glass and is often referred to as the free energy of hydration model. Jantzen subsequently demonstrated the predictive nature of this model for a wide range of silicate based glass compositions [jantzen-1992]. The free energy of hydration model treats a glass as a mixture of oxide species, e.g. $CaSiO_3$, Na_2SiO_3, SiO_2, Al_2O_3, etc. , which have known free energies of hydration. The stability of any glass is then assumed to be given by the summation of the free energy of hydration (ΔG_{hyd}) of the components weighted by the mole fraction of each [Plodinec-1984]. The calculated ΔG_{hyd} is a composition-dependent measure of the stability of the glass in aqueous solutions.

Table 5.27
Comparison Of Parameters Used For Leaching Characterization By The TCLP, PCT And LADR Tests

Test	SAMPLE			SOLUTION			PARAMETERS			Measured Quantity
	Configuration	Area (cm^2/g)	Amount(g)	Identity	Amount	SA/V(cm^{-1})	Temp (°C)	Agitation	Time	
TCLP	Crushed to <9.5mm	≥3.1	≥100	Acidic pH = 4.9	20x Sample Weight	≥0.155*	23(±2)	Tumble at 30Hz	18 hrs	• Concentration of RCRA metals (As, Cd, Cr, Hg, Se, Ag) in solution after test
PCT	Powdered to (-100/+200)	153 to 400	>1	Deionized Water	10x Sample Weight	≈27.5*	90(±0.5)	none	7 days	• Concentration of selected ions (normally Si, B, Li, Na, K) in solution after test, and • pH, initial and final
LADR	Crushed to (-25/+35)	≈40*	≈1*	Deionized Water	200 ml	0.2 (fixed)	25(±5)	none	≥7 days	• Weight, initial and final • pH, dpH/dT and final • Optional solution analysis

* These numbers vary with the density of the sample and were calculated assuming a density of 2.6 g/cm^3

Mechanistically, the model is applied as follows. Hydration reaction equilibria are written for each component of the glass, and the Gibbs free energy's of formation (ΔG_f) is used to calculate the free energy of hydration. For example, the hydration reaction equilibrium for vitreous silica,

$$SiO_2 + H_2O \leftrightarrow H_2SiO_3$$

gives a ΔG_{hyd} = 5.59 kcal/mol at 25°C. For multi-component glasses, the molar composition is rewritten in terms of specific compounds, and the total free energy of hydration is calculated from the free energy of hydration for these compounds from,

$$\Delta G_{hyd} = \sum_n \chi_n \delta G_n$$

where χ_n and δG_n are the mole fraction and free energy of hydration of constituent oxide compound n, respectively. Implicit in this summation is the assumption that the glass behaves as an ideal solution, and therefore the ΔG_{hyd} can be calculated as a linearly additive function of the free energies of hydration of the constituent compounds. Table 5.28 lists reaction equilibria and free energies of hydration (δG_n) for a number of compounds of interest.

Table 5.28:
Reaction Equilibria and Free Energy of Hydration (δG_n) for Constituent Compounds of Interest.

Reaction	δG_n (kcal/mol)
$La_2O_3 + 3H_2O \leftrightarrow 2La(OH)_3$	-31.14
$BaSiO_3 + 2H^+ \leftrightarrow Ba^{2+} + H_2SiO_3$	-30.57
$Na_2SiO_3 + 2H^+ \leftrightarrow 2Na^+ + H_2SiO_3$	-28.81
$Li_2SiO_3 + 2H^+ \leftrightarrow 2Li^+ + H_2SiO_3$	-22.74
$CaSiO_3 + 2H^+ \leftrightarrow Ca^{2+} + H_2SiO_3$	-16.12
$MnSiO_3 + 2H^+ \leftrightarrow Mn^{2+} + H_2SiO_3$	-14.87
$FeSiO_3 + 2H^+ \leftrightarrow Fe^{2+} + H_2SiO_3$	-14.61
$NiSiO_3 + 2H^+ \leftrightarrow Ni^{2+} + H_2SiO_3$	-14.34
$MgSiO_3 + 2H^+ \leftrightarrow Mg^{2+} + H_2SiO_3$	-13.89
$Y_2O_3 + 3H_2O \leftrightarrow 2Y(OH)_3$	-12.94
$CdSiO_3 + 2H^+ \leftrightarrow Cd^{2+} + H_2SiO_3$	-12.27
$B_2O_3 + 3H_2O \leftrightarrow 2H_3BO_3$	-9.93
$PbSiO_3 + 2H^+ \leftrightarrow Pb^{2+} + H_2SiO_3$	-8.81
$UO_3 + 2H_2O \leftrightarrow UO_2(OH)_2 \cdot H_2O$	-6.80
$Al_2O_3 + {}^1/_2H_2O \leftrightarrow AlO(OH)$	3.04
$SiO_2 + 2H_2O \leftrightarrow H_2SiO_3$	5.59
$CeO_2 + 4H^+ \leftrightarrow Ce^{4+} + 2H_2O$	11.34
$Cr_2O_3 + 3H_2O \leftrightarrow 2Cr(OH)_3$	37.36
$ZrSiO_4 + 2H_2O \leftrightarrow ZrO(OH)_2 + H_2SiO_3$	45.10

Jantzen applied the free energy of hydration model to a large number of silicate glasses. However, these glasses where primarily borosilicates with relatively low alkaline earth and alumina concentrations. The normal composition of MMT's ceramic phase product is outside the range of compositions where this model has been successfully applied. A modification of the free energy of hydration model has been developed which enables the calculation of ΔG_{hyd} for CaO and/or Al_2O_3 rich glasses.

With the high CaO-Al_2O_3 modification, the free energy of hydration model can be used to predict the relative leach resistance of vitreous ceramic-phase product. Typical

ceramic-phase product has a ΔG_{hyd} of -6.5 to -10 kcal/mol. This range of values compares favorably to that for typical waste glass compositions which have ΔG_{hyd} of -10 to -15 kcal/mol. Figure 5.51 illustrates the relative predicted leachability predicted from these values of ΔG_{hyd}. NL_{si} is the silicon content in solution normalized to the silicon content in the glass. The solid line in this figure represents the linear regression best fit to data for over 150 glasses tested by Jantzen. Jantzen found that the concentration of Si in solution increases as the free energy of hydration becomes more negative, i.e. as the thermodynamic driving force for hydration increases. It is clear from this figure that MMT ceramic phase should have superior leach resistance as compared to typical waste glasses.

Figure 5.51:
Illustration of the relative leachability of MMT Ceramic phase and typical waste glass compositions. Solid line represents the linear regression best fit to the data for >150 glasses tested by Jantzen. The dashed lines represent the range of NL_{Si} for the same data.

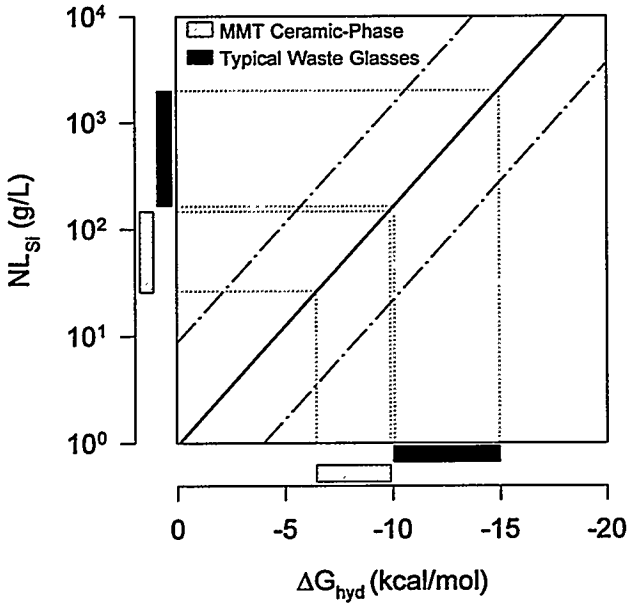

5.1.3.3.3. Leachability Test Results: AU, VSL, MMT

Leachability testing of various glass samples was performed using TCLP, PCT and LADR test methods. Two base composition regions were used with the following dopant additions:

- RCRA: BaO, CdO, Cr_2O_3, PbO (0.5 and 1.0 wt%)
- radionuclide surrogates: Y_2O_3, La_2O_3 (5 wt%)

- radionuclide: UO_2 (1 and 3 wt%)
- chloride: $CaCl_2$ (8-20 wt%).

Samples were prepared by AU and VSL, with the analyzed and batched glass compositions provided in Table 5.29- Table 5.31; note that only batched compositions were reported by VSL. The AU study used two CaO-Al_2O_3-SiO_2 base glass compositions, while the VSL glasses investigated composition variations within region A, including B_2O_3 and Li_2O additions.

Chemical analysis of the AU samples provided important information regarding retention of RCRA metals in the glass. Several glasses were doped (i.e. batch composition) with 0.5 wt% BaO, CdO, Cr_2O_3 and PbO. Component capture, or retention in the glass, was best for BaO and Cr_2O_3 (0.32-0.5 wt%) where volatilization of the components is not expected to be a problem. Capture of CdO and PbO was significantly lower, with samples containing chloride additions showing essentially no capture of CdO or PbO in the glass. The poor retention of CdO and PbO is attributed to volatilization of the components from the melts, with the presence of chloride enhancing volatilization of the components; i.e. chloride additions essentially strip Cd and Pb from the glass melt.

5.1.3.3.3.1. RCRA Materials

TCLP and LADR leachability tests were performed on the AU glass samples. Table 5.29 provides the results from TCLP testing (TCLP testing was performed at Alpha Analytical Laboratory). In addition to the eight RCRA metals, the leachate was also analyzed for Ca, Al and Si. While the TCLP test results are dependent only on the RCRA metal content of the leachate, measurement of the base glass components provides information on the chemical durability (leachability) of the glass network. This information is valuable when developing, or engineering, glass systems for component incorporation.

All glass samples passed the TCLP test, with sample AU-4 showing the lowest concentration of RCRA metals in the leachate solution (i.e. non-detection for all components). The test results were evaluated using the standard TCLP regulatory limits. The appropriate RCRA metals leachate limits must be considered for BDAT or delisting evaluation of the TCLP results.

Table 5.29
Oxide analyses for AU glass samples doped with selected RCRA metals, radionuclide surrogates and chloride (compositions gives as wt%). Samples were prepared for TCLP and LADR leachability testing.

Sample ID	Base Glass	BaO	CdO	Cr_2O_3	PbO	Y_2O_3	La_2O_3	Cl	ΔG_{hyd} (kcal/mol)
AU-1	A	---	---	---	---	---	---	---	-9.11
AU-2	A	0.41	0.28	0.50	0.35	---	---	---	-9.16
AU-3	A	0.32	0.01	0.48	0.005	---	---	2.1	-8.60
AU-4	A	0.32	0.006	0.38	0.006	---	---	5.8	-8.26
AU-5	B	---	---	---	---	---	---	---	-13.45
AU-6	B	0.42	0.19	0.56	0.28	---	---	---	-13.22
AU-7	B	0.43	0.11	0.50	0.23	5.2	---	---	-13.28
AU-8	B	0.51	0.11	0.47	0.20	---	5.2	---	-13.62

Table 5.30
Batch compositions for VSL samples doped with selected RCRA metals and Uranium (compositions given in wt%). Samples were prepared for TCLP and PCT leachability testing.

Sample ID	B_2O_3	Li_2O	FeO	NiO	Cr_2O_3	PbO	UO_2	ΔG_{hyd} (kcal/mol)
RCRA-1AR	---	---	1.0	1.0	1.0	1.0	1.0	-7.44
RCRA-2AR	6.3	1.1	1.0	1.0	1.0	1.0	1.0	-9.07

Table 5.31: Batch compositions for VSL samples doped with Uranium (compositions given in wt%). Samples were prepared for PCT leachability testing.

Sample ID	B_2O_3	Li_2O	FeO	UO_2	ΔG_{hyd} (kcal/mol)
VSL#1A	---	---	1.2	1	-7.28
VSL#1B	---	---	1.2	3	-7.35
VSL#2A	6.6	9.1	1.1	1	-10.2
VSL#2B	6.5	8.9	1.1	3	-10.19
MMT#1A	---	---	1.2	1	-8.79
MMT#1B	---	---	1.2	3	-8.79
MMT#2A	6.5	1.1	1.2	1	-6.39
MMT#2B	6.4	1.1	1.2	3	-6.38

The leachability results vary significantly for the two base glass systems, with the high-silica glasses (region A) showing generally superior leach resistance to the low silica glasses (region B). This behavior has been previously observed for leachability testing at AU, where the chemical durability of the CaO-Al_2O_3-SiO_2 base glass system was shown to degrade as the composition moved from the high silica region to the low silica region.

Leachability results of the high silica glass compositions can be evaluated in terms of the RCRA metals and the major components of the base glass (Ca, Al, and Si). Leaching of the RCRA metals was highest for glass AU-2 and decreased as chloride was added to the glass. Glass sample AU-4 showed the best results, with a non-detect for all RCRA metals. However, it should be noted that AU-2 had the largest concentration of RCRA metals captured in the glass, with chloride additions to the glass resulting in very low retention of both CdO and PbO (see Table 5.29).

The effect of component additions (RCRA metals and chloride) on the leaching characteristics of the glass can also be evaluated by looking at the concentration of the base glass constituents in the leachate (Ca, Al, and Si). The concentration of Ca, Al and Si in the leachate solution provides information regarding the integrity of the glass network; both leaching of cations (Ca) and dissolution of the network structure of the glass (Al and Si). Figure 5.52 shows the leachate concentrations of Ca, Al, and Si for the high silica glass compositions. The concentrations for Ca, Al and Si are highest for the base glass sample (AU-1: no component additions). The Ca, Al, and Si leachate concentrations decrease for RCRA metals additions and subsequent chloride additions, with the best results obtained for sample AU-4 (RCRA and high Cl capture). Note, that

there are also changes in the base glass components (e.g. CaO) that will most likely alter the leaching characteristics of the glass. At this stage, it is not possible to differentiate the effects of the dopant additions and small changes in the bulk chemistry on the leaching characteristics. Perhaps the most interesting result is the reduced leachant concentrations in the TCLP extract for the high chloride content sample (5.8wt% Cl, AU4). Further testing is recommended to determine the effect of increased chloride contents on leachability; chloride capture up to 15 wt% Cl have been achieved for high silica compositions.

TCLP analysis of the low silica glass compositions showed small variations in the leachate concentrations for all components; RCRA metal contents for the low silica glasses exceeded those for the high silica glasses for all samples. Figure 5.53 shows the leachate concentrations of Ca, Al, and Si for the low silica glass compositions. Small changes in the leaching characteristics were observed, however, no significant differences

Table 5.32
TCLP results for AU glass samples. The RCRA metals not shown (As, Hg, Se, Ag) all showed non-detect (ND) values.

Components	Base Glass	Sample ID	Ba	Cd	Cr	Pb
base glass	A	AU-1	ND	ND	ND	ND
Ba, Cd, Cr, Pb	A	AU-2	0.9	ND	0.4	0.5
Ba, Cd, Cr, Pb, Cl	A	AU-3	0.6	ND	0.3	ND
Ba, Cd, Cr, Pb, Cl	A	AU-4	ND	ND	ND	ND
base glass	B	AU-5	ND	ND	ND	ND
Ba, Cd, Cr, Pb	B	AU-6	1.7	0.5	1.2	0.9
Ba, Cd, Cr, Pb, Y	B	AU-7	2.1	0.4	1.4	0.7
Ba, Cd, Cr, Pb, La	B	AU-8	1.8	0.4	1.3	1.1
Regulatory Limits (mg/L) (detection limits (mg/L))			100 (0.5)	1.0 (0.1)	5.0 (0.2)	5.0 (0.5)

Figure 5.52
Ca, Al and Si leachate concentrations for high silica AU glass samples using TCLP testing protocols.

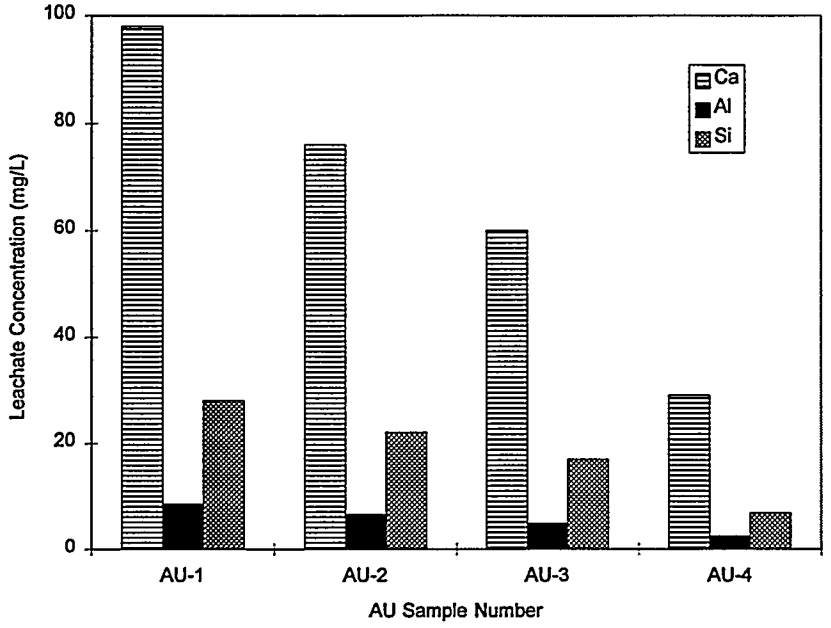

Figure 5.53
Ca, Al and Si leachate concentrations for low silica AU glass samples using TCLP testing protocols.

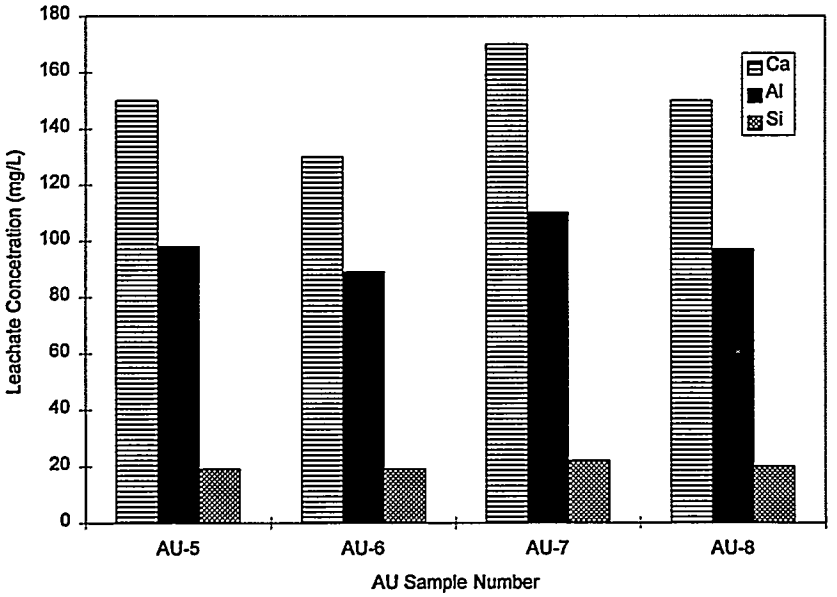

Figure 5.54
Normalized leachate concentration as a function of free energy of hydration for the AU glasses.

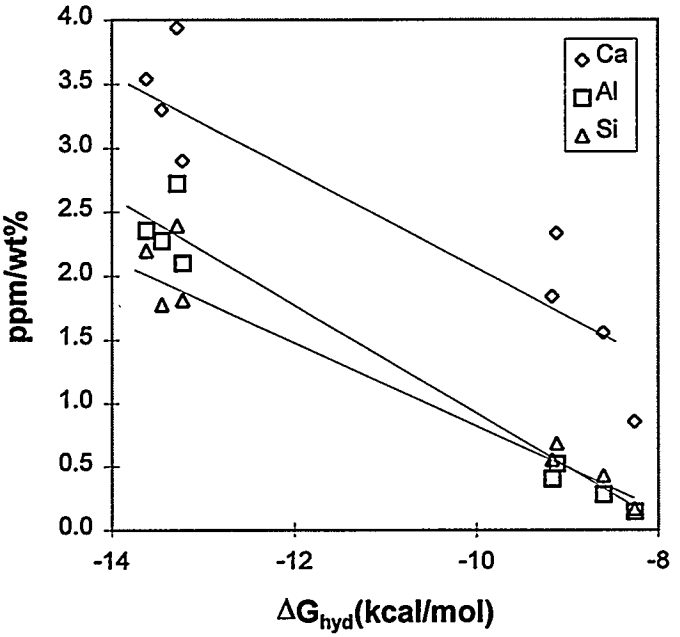

were measured for the RCRA metal or radionuclide surrogate additions (Y_2O_3 and La_2O_3). The latter results are a bit surprising since Y_2O_3 and La_2O_3 additions have been found to increase the chemical durability of aluminosilicate glasses in alkaline solutions. This apparent discrepancy can be attributed to the testing conditions of the TCLP test. The leachate for TCLP is an acidic solution, and one might expect different leaching behavior in this pH than for more basic (alkaline earth-rich) solutions.

An initial examination of the TCLP data for region A glasses indicates that the chemical durability of these glasses is improved as RCRA metals and chloride are added. It may be possible to attribute the improved leaching characteristics of these glasses to component incorporation into the glass structure. While the structural role of each component is not known at this time, addition of relatively large radius ions into the glass structure assists in blocking diffusion pathways in the glass network, hence decreasing the leachability of mobil ions (e.g. Ca). Consequently, the rate of dissolution of the glass network (e.g. Al, Si) decreases as well.

Although this explanation is plausible, it does not take into account the effects of variations in final compositions of these glasses. Specifically, there are substantial differences in CaO content of the high silica glasses which may be sufficient to significantly effect the leachability of these glasses. The effect of these composition variations can be determined by comparing the ΔG_{hyd} for these glasses.

Table 5.33
Weight loss and final pH data for AU glass samples tested for a total of 10 days using the LADR test protocol.

Sample No.	Weight Loss ($\times 10^{-3}$ g/cm^3)	Final pH
AU-1	0.0275	6.45 ± 0.05
AU-2	0.0375	6.42
AU-3	0.0275	6.66
AU-4	0.0150	6.58
AU-5	1.70	9.18
AU-6	1.74	9.60
AU-7	0.353	8.52
AU-8	0.385	8.84

The thermodynamic driving force for hydration decreases (ΔG_{hyd} becomes less negative) as the CaO content of the high silica glasses decreases. Figure 5.54 shows the normalized leachate concentration (ppm of leachate/ wt% of oxide in the glass) plotted as a function of the free energy of hydration for both high and low-silica glasses. This figure shows the expected behavior of increased leaching with increasing negative magnitude of ΔG_{hyd}. It is important to note that a linear dependence may not be appropriate for these data due to the TCLP test protocol which specifies a buffered acidic leachate and a relatively short test time.

The results of the LADR test for the AU-1 through AU-8 glasses are shown in Table 5.33. These data show relatively good agreement with the results of TCLP testing. The high silica glass samples showed very little weight loss and essentially no change in pH. The low silica glass samples showed moderate weight loss and significant changes in pH. It is interesting to note that glasses with Y and La, i.e., AU-7 and AU-8, show improved leach resistance when the LADR test protocol is used. These results are different than those from the TCLP test, and the difference can be attributed to the pH of the leachate solution. Specifically, Y and La have been shown to improve leach resistance in neutral and basic solutions, and therefore are expected to have a positive effect on leach resistance as measured by the LADR test.

A direct comparison of the LADR and TCLP results is shown in Figure 5.55. This figure shows that the concentrations of leached RCRA metal ions (Ba, Cd, Cr, and Pb) from the

TCLP test are roughly correlated with the glass durability (as measured by the total weight loss determination of the LADR test). This is an important result which shows the applicability of the LADR protocol as a screening test.

Figure 5.55
Comparison of LADR and TCLP test results for all AU glass samples. Lines are drawn as a guide to the eye.

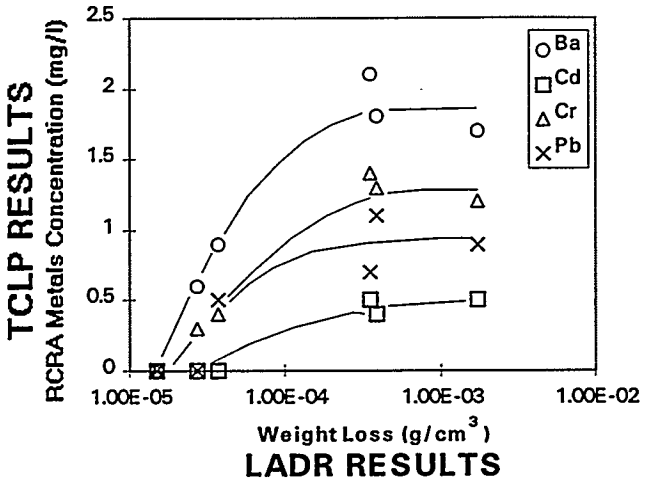

5.1.3.3.3.2. Radioactive and Mixed Waste Materials

As mentioned earlier, Mixed Waste materials are subjected to TCLP testing for RCRA components, and a second test for radioactive components; both the PCT and MCC-1 tests are used extensively to determine the relative leachability of glasses that contain radionuclides. Samples prepared at VSL were subjected to both TCLP and PCT testing at Catholic University, with 7- and 28-day PCT results obtained.

The leachability test results are shown in the following figures; test results are referenced to either the EPA requirements or a standard reference materials. TCLP testing results focused on Cr, Pb, Ni and U release from the glass, while PCT testing evaluated the U and Si release from the glass. The PCT test results are compared to the West Valley high-level nuclear waste reference glass (WVCM62-2), with the normalized Si release used to evaluate the performance of the glass.

Figure 5.56 and Figure 5.57 shows the TCLP leachate results for Cr, Pb and Ni for the RCRA glass series. While Ni is not classified as a RCRA metal, the leaching characteristics are of interest for ceramic phase delisting evaluations. The TCLP leachate concentrations for Cr and Pb fell well below the EPA requirements for both glasses.

Leachability results for Ni release were below the EPA requirement, with RCRA-2A displaying improved performance over RCRA-1A.

Figure 5.58 and Figure 5.59 shows the uranium TCLP leachate results for glasses doped with 1 or 3 wt% UO_2. The release of uranium from these glasses is compared with the permitted uranium in ingested water set by the DOE (DOE5400.5). The uranium release from all ten glasses was significantly lower than the DOE standard for ingested water. The uranium leachate concentration increased with increasing UO_2 content for all glass compositions.

Figure 5.56
TCLP leachate results for VSL samples doped with selected RCRA metals and 1 wt% UO_2: Cr and Pb leachate concentrations.

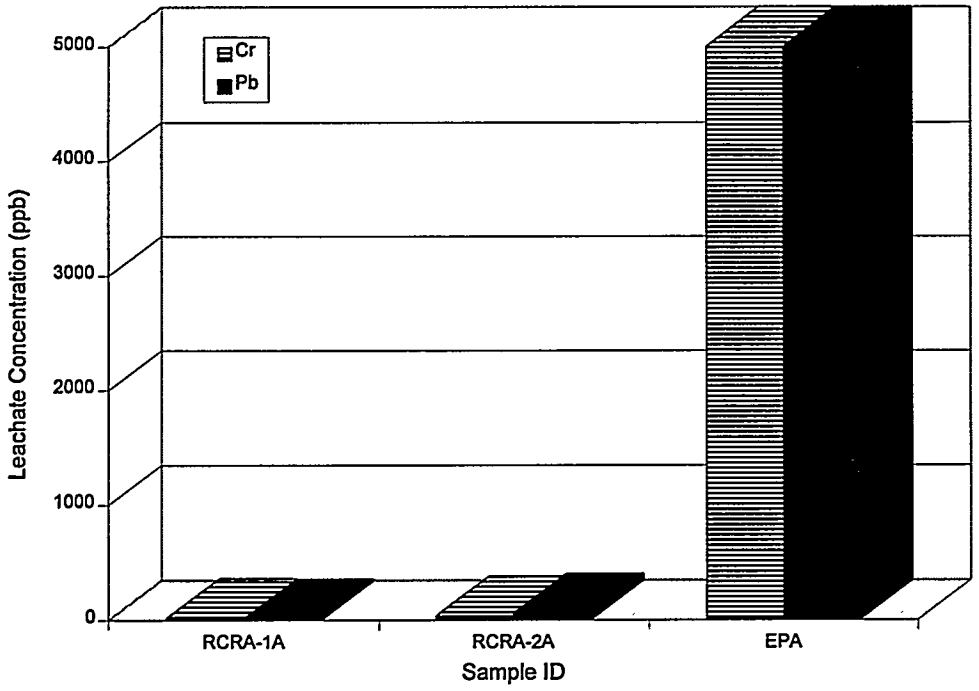

Figure 5.57
TCLP leachate results for VSL samples doped with selected RCRA metals and 1 wt% UO_2; Ni leachate concentrations.

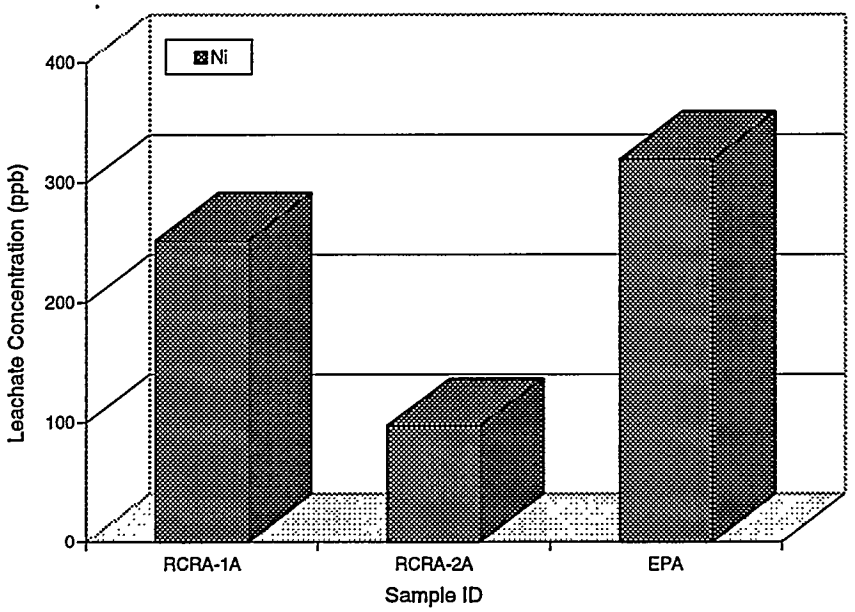

Figure 5.58
Uranium (U^{4+}) concentrations in TCLP leachate for VSL samples doped with UO_2; 1 wt% UO_2

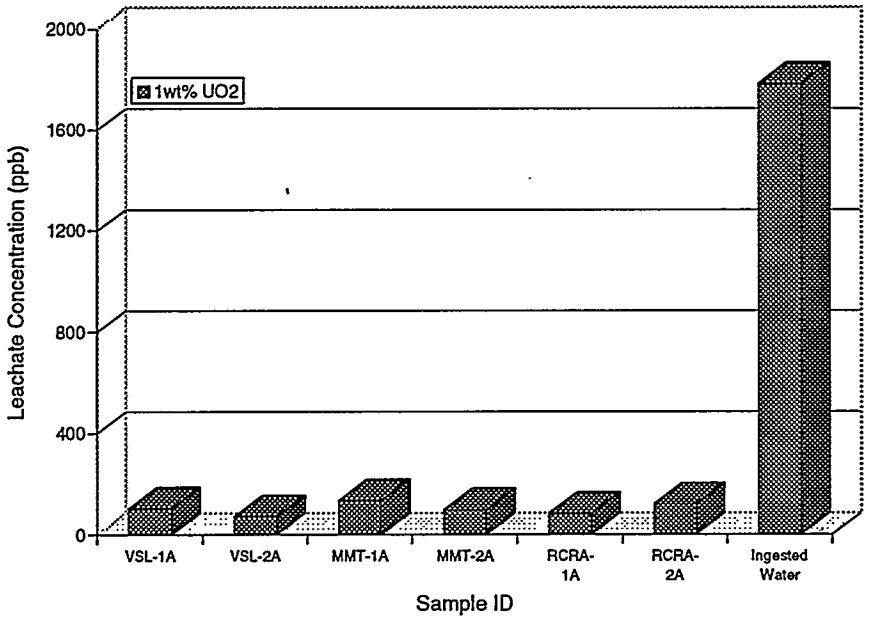

Figure 5.59
Uranium (U^{4+}) concentrations in TCLP leachate for VSL samples doped with UO_2; 3 wt% UO_2.

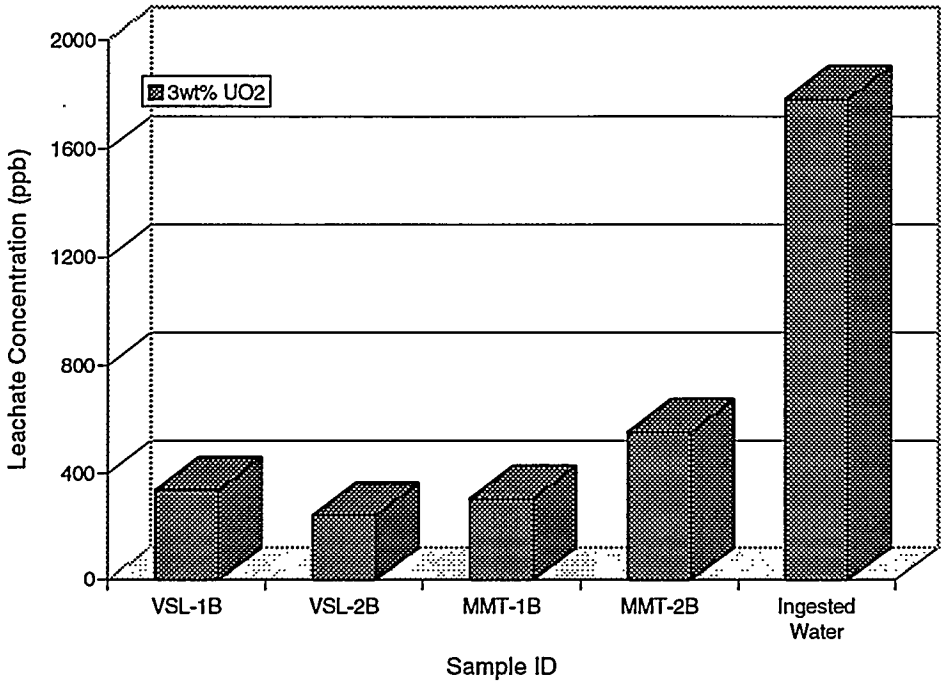

PCT testing results for VSL samples are shown in Figure 5.60 and 5.61 show the normalized elemental release of U and Si for 7 days of testing. All glasses showed substantially lower elemental release than the WVCM62-2 reference glass; the WVCM62-2 glass contains 0.6wt% uranium oxide. The role of glass composition/structure in determining the leachability of these glasses is best analyzed in terms of the free energy of hydration. (See Figure 5.62.) There is significant scatter in these data which might be attributed to departure of final glasses from the as-batched compositions. In spite of this scatter, this figure does shows that the expected increase in Si-release from these glasses with increasing negative magnitude of ΔG_{hyd}. (Statistically valid conclusion relating U-release and ΔG_{hyd} are impossible due to the scatter.)

Figure 5.60
PCT 7-day test results for VSL samples doped with UO_2; 1 wt%

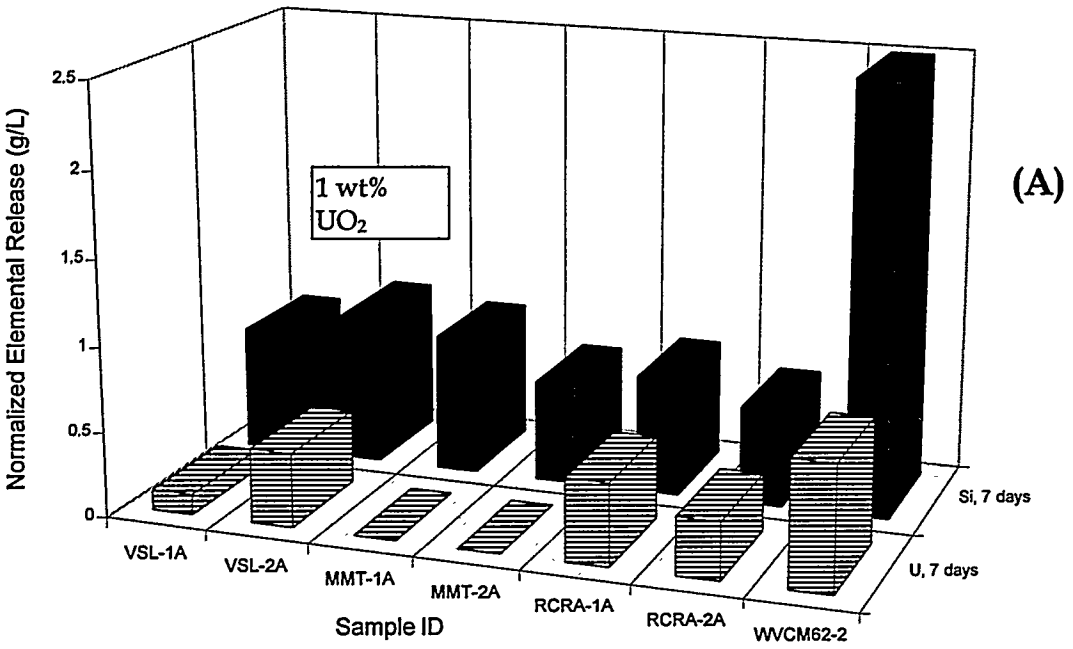

Figure 5.61
PCT 7-day test results for VSL samples doped with UO_2; 3 wt%

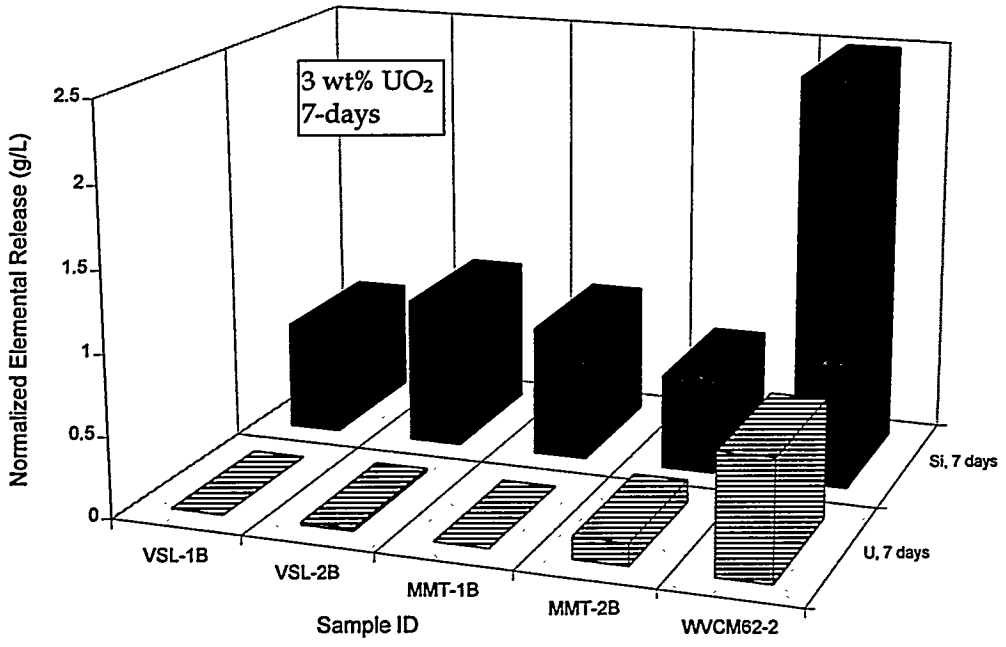

Figure 5.62
Leachate concentration as a function of ΔG_{hyd} for VSL glasses.

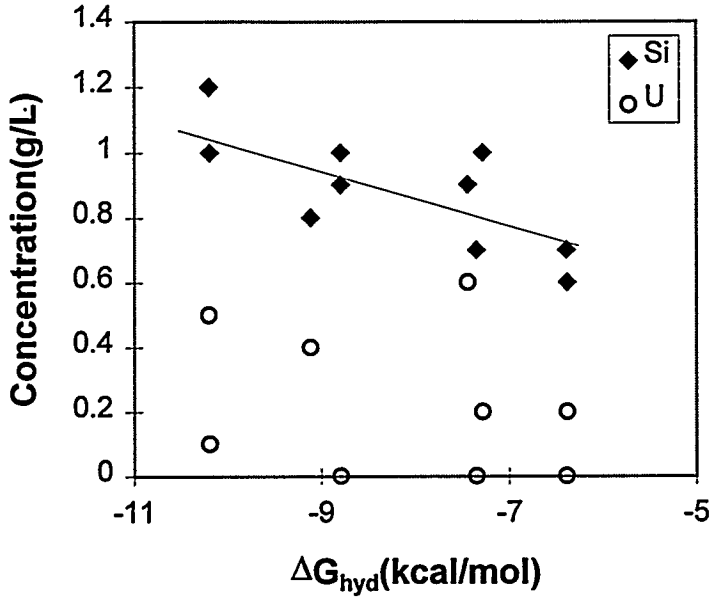

5.1.3.4. Summary

Experimental results around two base $CaO\text{-}Al_2O_3\text{-}SiO_2$ systems containing RCRA metals and uranium demonstrated the following:

1. RCRA metals, uranium, chlorine and other dopants could be incorporated into these glasses at various levels.

2. Chloride addition to the melt or glass has varied effects on component incorporation and glass stability. Chloride additions to the melt appears to increase the volatility of certain components (Cd, Pb) from the melt, hence lowering the amount of capture in the glass phase. The effect of chloride addition on glass stability varies for the high and low silica compositions; chloride is readily incorporated into high silica glasses, while chloride incorporation in low silica glasses results in an increase in the melt viscosity and decrease in glass stability.

3. As expected, DTA measurements show that the glass forming stability of the high silica (region A) glasses is significantly better than the low silica (region B) glasses. Both Cr and Cl can decrease glass stability of the low silica (region B) compositions.

4. All glasses passed TCLP testing. Test results were evaluated in terms of the leaching of both RCRA components and base glass components. Tentative correlations were made between compositions and observed leaching, but

further testing is required for definitive conclusions (due to some variations in base compositions).

5. A correlation was made between LADR and TCLP results, indicating that the LADR test may be useful as a rapid screening test for newly developed glasses.

6. All uranium-containing glasses passed both the TCLP and PCT. PCT results were compared to a standard reference glass. Standard, waste and site specific glasses will need to be developed in the future for this test.

Modeling results from the modified free energy of hydration model were also presented. These results suggested that the CEP glasses would display very low leachability, in agreement with the experimental data presented.

5.1.4. On-Line Ceramic Phase Characterization

5.1.4.1. Background

Ceramic phase viscosity is one of the most difficult properties to measure, yet it is one of the most critical properties to know for effective application of in waste recycling. Viscosity control is perhaps the most important task associated with maintaining the operability of the ceramic phase. Ceramic Phase Viscosity must be maintained within a specified range. If it is too low, it will provide suboptimal physical scrubbing performance and might lead to excessive corrosion of the refractory. If the viscosity is too high, it can result in excessive skulling, poor chemical scrubbing performance, and incompatibility with product removal (tapping) criteria.

A potential alternative to viscosity measurements is an electrical resistivity measurement. Combining two classic diffusion equations (Nernst-Einstein and Stokes-Einstein) yields the theoretical basis for this alternative measurement,

$$\eta = \frac{n(Ze)^2}{6\Pi r} \cdot \rho$$

In this equation, η is viscosity, ρ is resistivity, and n, Z, and r are the respective concentration, charge, and radius of the conducting ionic species. Although the N-E-S relationship holds exactly for some molten salts, experience has shown it must be modified with a proportionality constant for polymeric (glass-forming) melts.

A survey of available literature data indicates that for CaO-Al_2O_3-SiO_2 based melts, an exact solution of the N-E-S relationship is not necessary. Figure 5.63 shows the proportionality of viscosity and resistivity for CaO-Al_2O_3-SiO_2 (CAS), CaO-MgO-Al_2O_3-SiO_2(CMAS), CaO-FeO-SiO_2(CFS), and $CaCl_2$ and CaF_2 containing CaO-Al_2O_3-SiO_2. As shown in Figure 5.64, although not shown here, data for a broad range of CAS and

CMAS compositions maintain the linear correlation to at least 60 Poise/20 Ohm-cm. A least squares fit to these data gives,

$$\eta = 2.43\rho - 3.15$$

with a correlation coefficient (r^2) of 0.946.

The effects of anion additions on the viscosity of ceramics are critical when processing waste streams containing chlorine and sulfur, or when using fluorospar additions as a flux. Currently there is little data available for these effects. However, Figure 5.63 indicates that a relatively simple electrical resistivity measurement can provide these data.

The electrical resistivity measurement is not without its difficulties. Resistivity depends upon the measured resistance according to the relation,

$$R = C_c \rho$$

Figure 5.63
Relationship between viscosity and resistivity for CaO-Al_2O_3-SiO_2 based ceramics

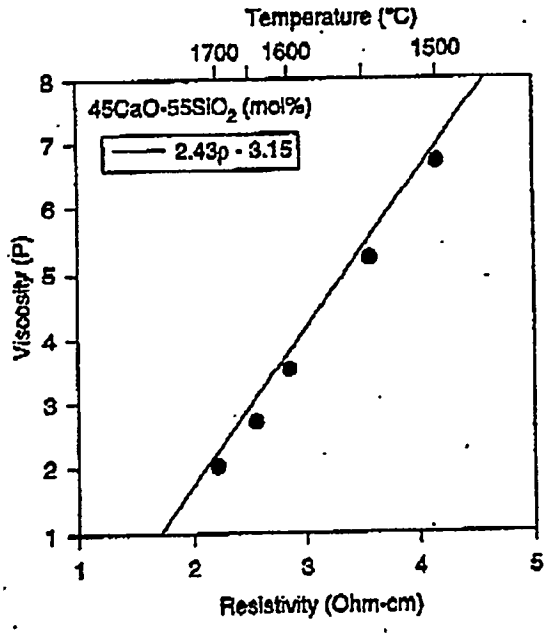

Figure 5.64
Relationship between viscosity and sensitivity for various ceramics

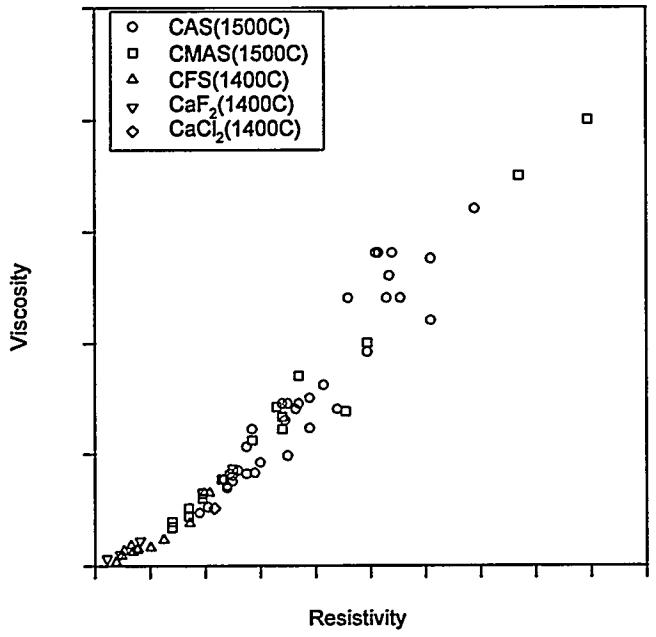

Where C_c is a cell constant. Determination of the absolute values for resistivity require either the use a well defined cell geometry or calibration with a liquid of known resistivity to determine cell constants. Difficulties arise in the determination of C_c.

Prior to addressing the very complex issue of cell design, it is appropriate to determine if a reproducible resistance measurement can be used to monitor changes in viscosity within the constraints imposed by the bench-scale and other CEP units. Specific issues include:

1. Detection limit with respect to total resistance, changes in composition, and changes in viscosity with temperature.

2. Effect of RF field on resistivity measurement.

3. Long term stability (2 to 4 hour time frame) of a simple cell made from high temperature metal wire (Pt or Mo).

4. Effect of entrapped gas bubbles on the measured resistance.

This study will address these and other issues using an electrode configuration similar to that used previously to determine foam height during ceramic foaming studies. See Figure 5.63.

These experiments represent the first step in developing an on-line ceramic phase monitoring device/system. The successful development of an appropriate electrode probe(s) and compilation of a data base will enable a single measurement of electrical resistivity (and temperature) to be used as an estimate of viscosity, composition, and the loading of captured species in the ceramic phase.

Figure 5.65
Schematic representation of configuration for 5lb unit for resistance measurements

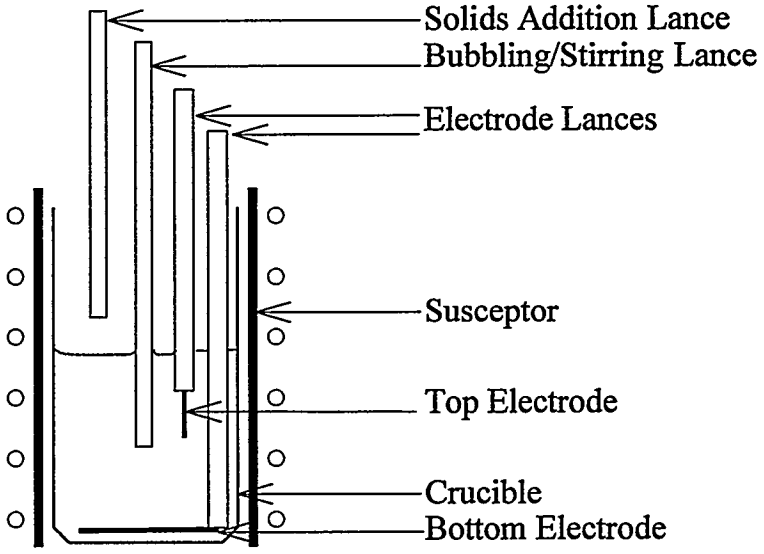

Figure 5.66
Schematic representation of electronic instrumentation for resistance measurement

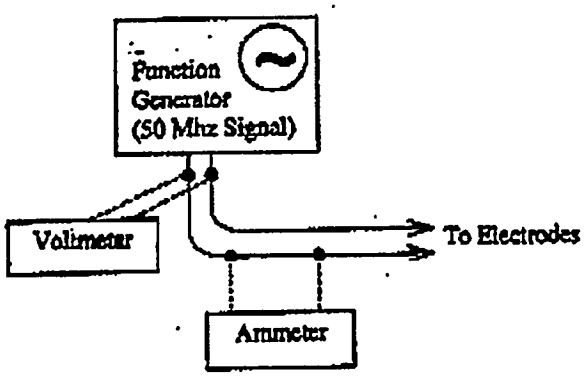

5.1.4.2. Study Objectives

The Primary Objectives of this Study Include:

- Feasibility study of resistance measurements in Bench Scale CEP Units.
  - Reproducibility
  - Electrode configuration
  - Other limitations
- Determine the effect of CaF_2, $CaCl_2$, and CaS additions on the electrical resistivity of a CaO-Al_2O_3-SiO_2 ceramic phase.
  - Detection limits
  - Correlation with known qualitative effects on viscosity
- Assess secondary effects on resistance measurement
  - Effect of entrapped bubbles
  - Effect of RF field

The Secondary Objectives of this Study Include:

- Determine efficiency of bulk flux additions at CEP operating temperature
- Prepare F, Cl, and S containing ceramic phase samples that can be used for leaching and dissolution resistance (LADR) testing

5.1.4.3. Summary of Experiments

- Testing with No Solids Additions
  - CaO-Al_2O_3-SiO_2 ceramic phase
  - Melt temperature range: 1400 to 1600°C
  - Measurement: Resistance as a function of time and temperature
    Resistance with and without RF field
    Resistance before and after bubbling

- These runs will allow a determination of the feasibility of the resistance measurement in bench-scale units. Other issues addressed include appropriate top electrode length and depth, response of resistance to changes in temperature and viscosity, long term stability of electrode, and effect of bubbling and RF field on the resistance measurement. These runs will also allow appropriate crucibles to be chosen for remainder of runs.

- Testing with CaO Additions

  - $CaO-Al_2O_3-SiO_2$ ceramic phase

  - Melt temperature range: 1400 to 1600°C

  - Measurement: Resistance as a function of composition

    Resistance as a function of temperature

    Resistance as a function of time

  – Additions: CaO, 2 to 4 additions of 2 to 5 wt% each.

  – These additions will traverse a composition line with T_{liq} <1400°C. The viscosity at 1500°C will vary by a factor of ~ 10, i.e. 40 Poise to <5 Poise. The measured resistance at 1500°C should vary by the same factor.

  – These runs will give specific information concerning the effect of ceramic phase composition (within the $CaO-A_2O_3-SiO_2$ system) on the measured resistance, i.e. detectability limits. Sampling of ceramic phase will allow a determination of the efficiency of flux addition from the top for the case of a relatively low volatility fluxing agent.

  - Final ceramic phase product will be used for LADR test samples.

- Testing with CaF_2, $CaCl_2$ and CaS Additions.

  - $CaO-Al_2O_3-SiO_2$ ceramic phase

  - Melt temperature range: 1400 to 1600°C

  - Measurement: Resistance as a function of composition

    Resistance as a function of temperature

    Resistance as a function of time

  – Additions: CaF_2, or $CaCl_2$ or CaS, 2 to 4 additions of 2 to 5 wt% each.

- These runs will give specific information concerning the effect of ceramic phase composition (within the $CaO-A_2O_3-SiO_2$ system) on the measured resistance, i.e. detectability limits. Sampling of ceramic phase will allow a determination of the efficiency of flux addition from the top for the case of a relatively low volatility fluxing agent.

- Final ceramic phase product will be used for LADR test samples.

5.1.4.4. Summary Results

Resistivity, was measured for three different compositions of $CaO-Al_2O_3-SiO_2$ ceramic phase. The viscosity for each composition was calculated from their respective resistivity measurements and compared with viscosity values obtained from literature. This comparison is presented in Figure 5.67.

Figure 5.67
Comparison of Ceramic Phase Viscosity

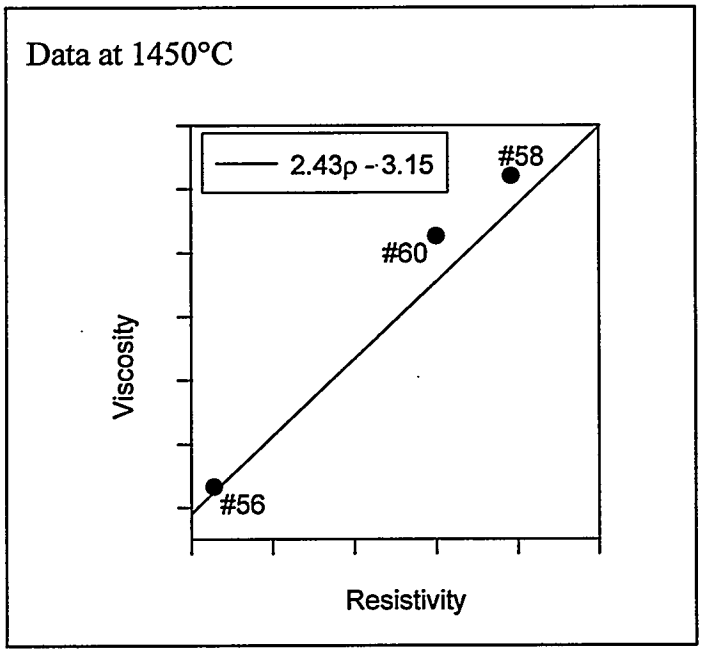

The agreement between measured viscosity (calculated from resistivity) and viscosity values from literature is considered to be very good.

An important factor in the potential application measuring the resistivity of the ceramic phase to determine its viscosity is the reproductivity of the resistivity measurement under various conditions. The experiments were conducted on a 10lb bench scale unit as shown in Figure 5.68.

Figure 5.68
Schematic Representation of Reactor Set-up

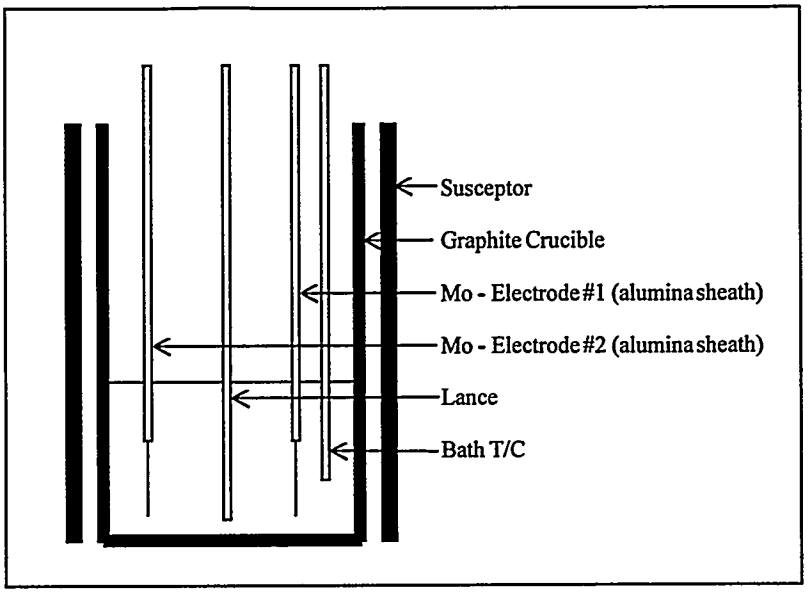

Resistivity was measured as a function of temperature, frequency of signal, and bath stirring. Data obtained from this experiment are presented in Figure 5.69 through Figure 5.76.

Figure 5.69
Measurements at 50kHz, t = 0, no stirring

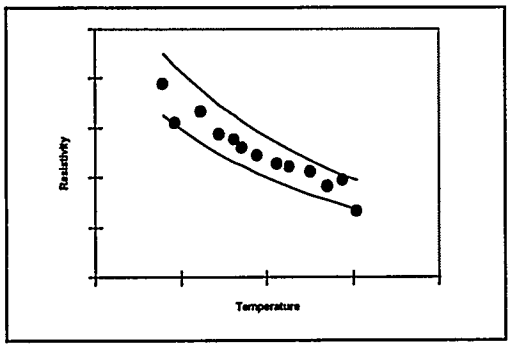

Figure 5.70
Measurements at 50kH$_2$, t=30 min, no stirring

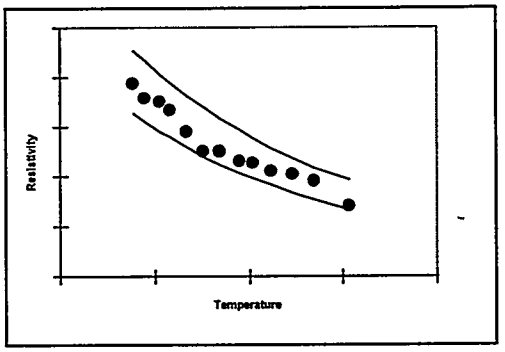

Figure 5.73
Measurements at 50kH$_2$, t=60 min, no stirring

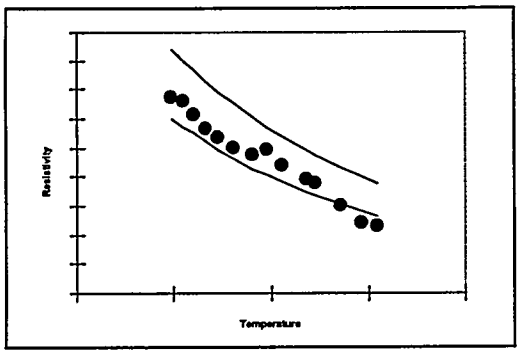

Figure 5.74
Measurements at 10kH$_2$, t=90 min, no stirring

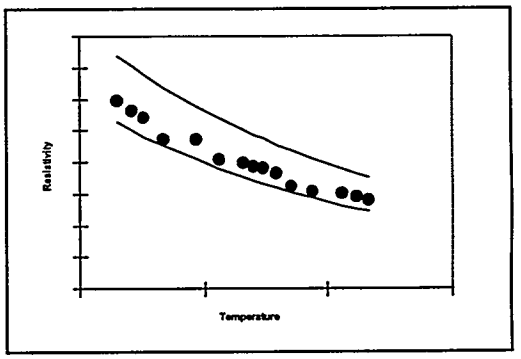

Figure 5.75
Measurements at 25kH$_2$, t=120 min, no stirring

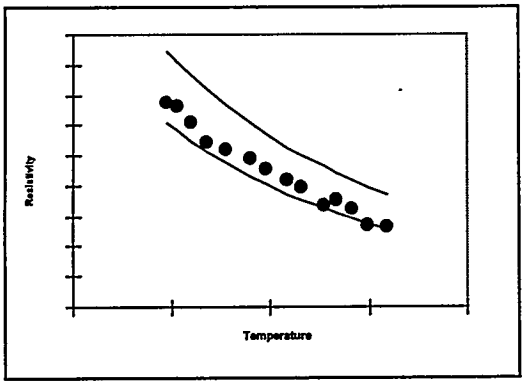

Figure 5.76
Measurements at 50kH$_2$, t=150 min, no stirring

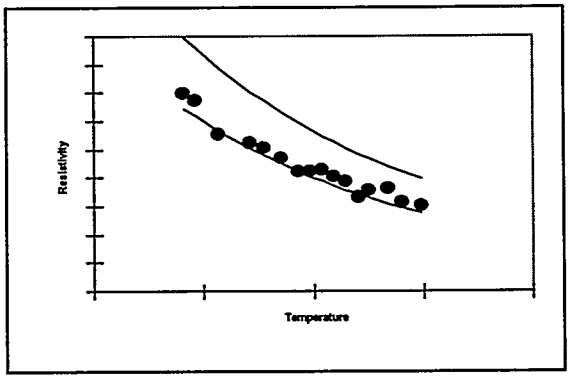

This data shows the excellent reproductivity of measuring ceramic phase resistivity under varying conditions. Resistivity, and hence its viscosity, remains in a relatively narrow range of values over a broad range of operating temperature.

5.1.4.5. Conclusions

Measuring resistivity to calculate the viscosity of the ceramic phase appears to be a viable approach to providing real-time control of the ceramic phase. It is highly compatible with current CEP control systems. Efforts are underway to redesign the electronics for instantaneous measurement of ceramic phase resistivity. The automated resistivity and temperature measurements will be combined with the empirical model for process control.

5.2. Optimization of the Containment System

5.2.1. Refractory Longevity

Minimizing refractory wear is important in CEP processing in order to maintain high on-stream factors. Refractory selection begins with an understanding of reactor chemistry and potential corrosion mechanisms for a particular application; one material is not ideal for all applications. An approach combining material selection with optimization of reactor operating conditions ensures maximum refractory operating life.

Figure 5.73 shows a schematic diagram of the refractory containment material for a typical vertical CPU reactor. Demonstration runs in 1994 and early 1995 confirmed that 90% of the total reactor refractory volume can be specified with high-quality industrial-grade materials that provide long working life under a wide range of operating conditions. Only 10% of the total refractory volume requires application-specific refractory selection. This critical area is in the region of the gas/liquid/refractory (GLR) interface, where metal, ceramic, and gas intermittently contact the refractory wall. The most aggressive conditions for refractory wear exist in this region, therefore extensive development work has focused on improving GLR performance.

Figure 5.73
Vertical CPU Schematic
Refractory Containment System

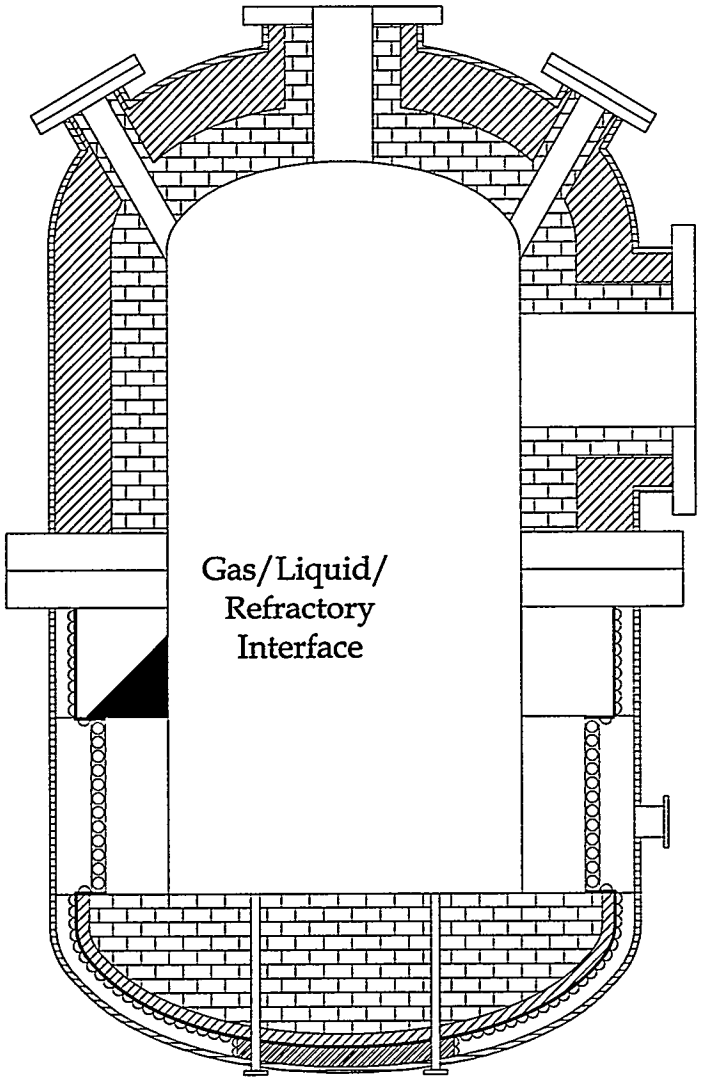

Two major refractory wear mechanisms have been identified: dissolution and corrosion. The first is primarily important in applications with feeds containing inorganic materials, while the second is particular to feeds containing chlorine. In each case, materials and operating conditions have been selected which minimize refractory wear.

5.2.1.1. Ceramic Phase Dissolution

Soils and sludges common in the DOE typically contain inorganic elements such as Ca, Al, and Si that partition to the ceramic product phase in CEP. This phase, which floats on top of the metal bath, causes corrosion where it contacts the refractory wall in the

upper throat of the reactor. The driving force for corrosion is the difference in chemical composition between the ceramic phase and the refractory material. This difference causes refractory wear by dissolution of refractory material into the ceramic melt.

Dissolution is minimized in two ways: control of ceramic phase composition through the addition of flux material, and selection of refractory materials with compositions and physical properties which are compatible with the ceramic phase. Demonstration runs have identified certain target ceramic compositions which exhibit superior properties for CEP operation. Flux is added to achieve the target composition, for which refractory performance is well understood.

5.2.1.1.1. Corrosion by Chlorine

The presence of chlorine in waste feed presents an additional mechanism of refractory wear. In the upper throat region, the refractory is intermittently contacted with both molten metal and headspace gases. In this GLR interface, chlorine from the feed is present as HCl in the gas, which can react with metal oxides in the refractory to cause corrosion. This reaction is only possible in the presence of carbon dissolved in the metal, $\underline{C}$, making this interface the only region susceptible to chlorine corrosion.

$$MO_x(s) + 2xHCl(g) + x\underline{C}(l) \rightarrow MCl_{2x}(g) + xH_2(g) + xCO(g).$$

5.2.1.2. Relative Performance of Selected Refractory Bricks Contacted with Hydrogen Chloride Gas

5.2.1.2.1. Summary

Initial observations on the APU during processing of chlorinated feeds showed apparent refractory corrosion from the contact of hydrogen chloride gas with the refractory lining underneath the metal level. It was postulated that the corrosion proceeds by a two step mechanism involving thermodynamically-limited reduction by carbon followed by highly-favored chlorination and volatilization of the metal chloride.

This mechanism has been reproduced adequately on the 20 lb refractory test rig. Considerable equipment challenges have been overcome to complete this testing, most notably development of a water-cooled lance capable of extended injection, a de-entrainment device for reducing splashing and a GHT capable of extended operation. Twelve different commercially available brick types have been tested.

Both thermodynamic and transport phenomena considerations have proven to be essential in interpreting the observations of the campaign.

5.2.1.2.2. Background

5.2.1.2.2.1. Reaction Mechanism

The following postulated mechanism of corrosion has been identified as having a significant impact on refractory longevity: $MO_x+2_xHCl(g)+_xC-MCl_{2x}(g)+xH_2(g)+xCO(g)$. This has been interpreted thermodynamically as a two-step process, a thermodynamically-limited reduction of oxide followed by very strongly-favored chlorination of any trace metal:

1. MO_x+xC - $M+xCO(g)$

2. $M+2xHCl(g)$ - $MCl_{2x}(g)+xH_2(g)$.

5.2.1.2.2.2. Prevalence of Reaction Below the Metal Line

In the headspace of a CEP reactor contact with hydrogen chloride gas occurs, with carbon monoxide gas behaving as a possible reducing agent, while in the melt the reducing agent is dissolved carbon. There are important differences between the headspace and melt regions which limit the driving force and corrosion reaction speed. These differences include temperature, concentration of corrodants and degree of agitation. However, the most important fundamental difference is that the headspace need not contact the metal melt which permits the use of different classes of materials in the headspace. Hence, materials such as carbon, which are superior in terms of gas-phase corrosion resistance can be used to virtually eliminate headspace corrosion as a concern.

5.2.1.2.2.3. Importance of Volatility of Chlorides

The nature of the chloride products is of critical importance to the corrosion phenomenon. Most refractory chlorides shown in Table 5.34 have generally ionic characteristics, while bonding in the low-boiling-point chlorides is more covalent. These boiling points are too low for the corrosion products to remain as a condensed phase product in nickel-based CEP operating systems. Hence, chemical passivation, the formation of an inert barrier of corrosion product [as is common with metals], is challenging. Corrosion products that exist as a vapor at operating temperatures probably will not remain in the refractory brick. Formation of corrosion-inhibiting surface layers (sometimes termed "chemical skulling")[1] is being investigated.

Table 5.34
Boiling Points of Selected Refractory Chlorides

B.Pt (°C)	Al	Cr	Sl	Zr	Mg	Ca
Chloride	178	1300	145	331	1412	>1600
Fluoride	1291	>100	-86	600	2239	2500
Oxide	2980	4000	2590	5000	3600	2850

5.2.1.2.2.4. Thermodynamic Predictions

In an earlier effort, a simplified thermodynamic analysis was performed for several oxide and nonoxide refractory candidates. Since that time, more detailed analysis has been performed using free-energy minimization for a variety of chemical systems. This analysis was expanded to include more species, such as other chlorides, fluorides, metal alloys, carbides, nitrides, borides, sulfides, and gas atmospheres.

For this effort, graphite was chosen as the primary material of due to the inherent resistance of carbon to chlorination.

Five materials are discussed here: Al_2O_3,ZrO_2,ThO_2,$MgO*Al_2O_3$,$Al_2O_3*3SiO_2$. Figures given depict the equilibrium concentrations of 1 mole of refractory oxide in contact with sufficient stoichiometric chloride and carbon to completely react it, and excess nickel as the medium.

The equilibrium conditions depicted in Figure 5.74 show that 1 mole of Al_2O_3 is reductively chlorinated to completion by stoichometric amounts of HCl and C as temperature increases to 1400°C. Even at 1000°C, the equilibrium condition consumes approximately 25% of the alumina. This is accompanied by the evolution of $AlCl_3$ as well as the alloys Ni_3Al and NiAl.

In Figure 5.75,1 mole ZrO_2 is seen to be 75% reductivity chlorinated at 1400°C by stoichiometric addition corrodants. This is accompanied by the evolution of $ZrC1_4$, ZrC which is expected to dissociates into solution, and other chlorides of zirconia.

In Figure 5.76, 1 mole of ThO_2 is seen to be only 50% reductivity chlorinated by 1400° C with stoichimetric corrodants. This is accompanied by evolution of $ThC1_4$ but essentially no alloy, metal or carbide is produced. Thorium forms the highest-melting-point oxide and the most stable one with respect to reductive chlorination.

In Figure 5.77, 1mole of spinel is seen to be completely deteriorated at 1200°C, accompanied by $A1C1_3$,$MgC1_2$,Ni_3A1, and NiA1.

In Figure 5.78, 5.1 mole of mullite is seen to be completely deteriorated at 1400°C, accompanied by the evolution of $AlCl_3$,Ni_3Al,NiAl,NiSi and $Ni_{.35}Si_{.65}$.

Although the thermodynamic calculations presented here are simplified and do not model the solution chemistry well, the results are highly relevant. Due to the overwhelming thermodynamic driving force it can be concluded that all oxide refractories will be attached by reductive chlorination at the operating conditions in the reaction zone of CEP. Thorium oxide represents the most stable oxide. Zirconia appears to be more stable than alumina, but it can be reduced into solution with the melt in the presence of carbon.

Figure 5.74
Equilibrium Concentrations of Species Originating from Al_2O_3/HCl/C/Ni Mixture in a Closed System

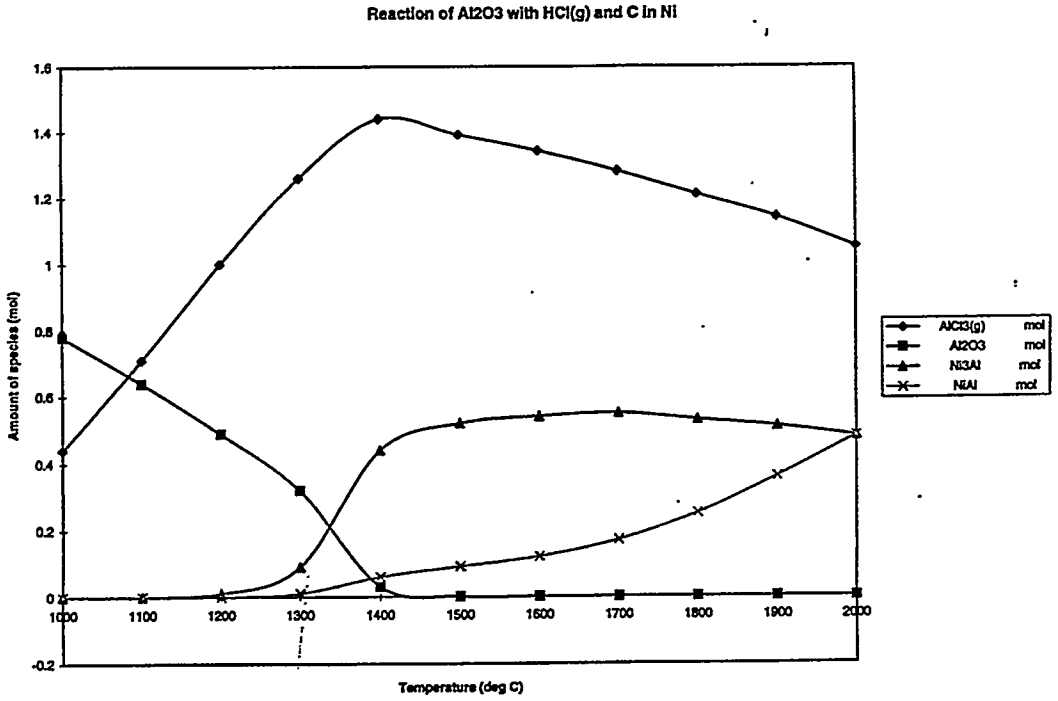

Figure 5.75
Equilibrium Concentrations of Species Originating from ZrO_2/HCl/C/Ni Mixture in a Closed System

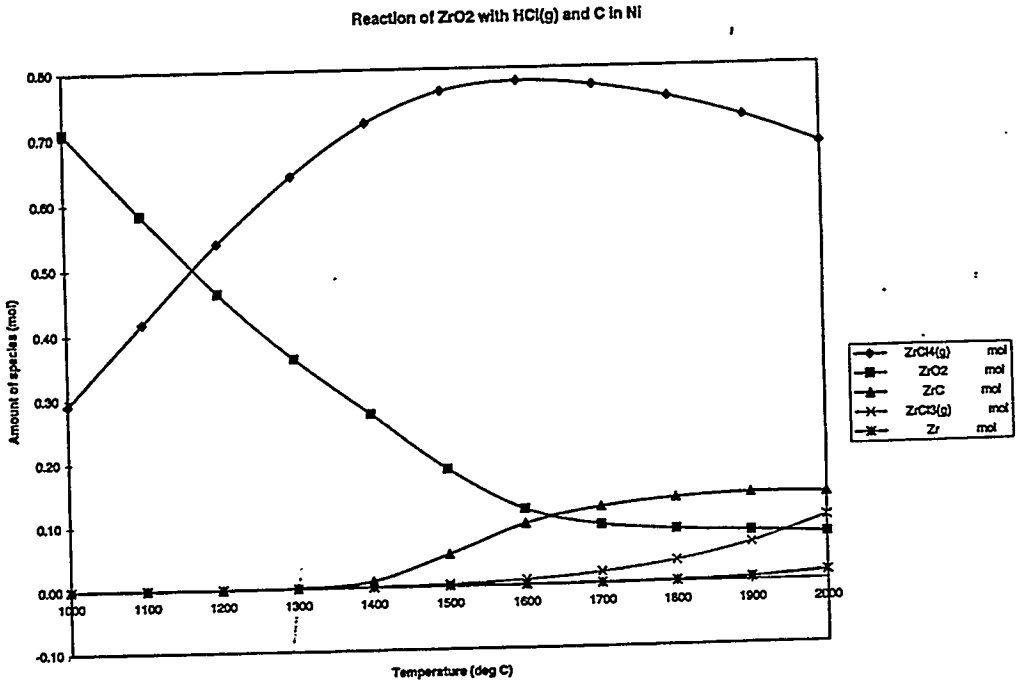

Figure 5.76
Equilibrium Concentrations of Species Originating from ThO_2/HCl/C/Ni Mixture in a Closed System

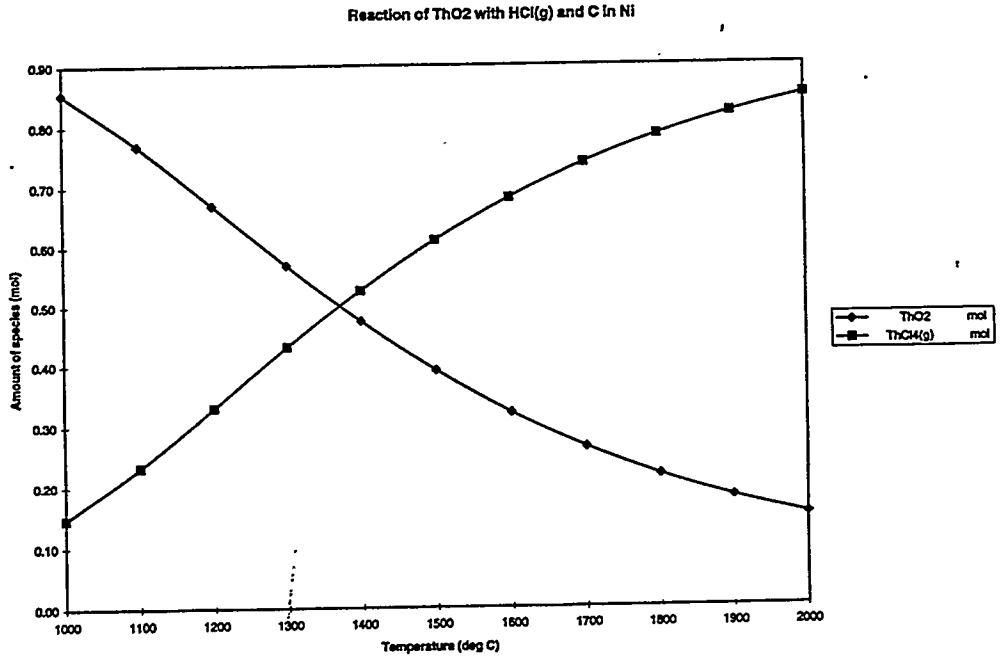

Figure 5.77
Equilibrium Concentrations of Species originating from $MgO*Al_2O_3$/HCl/C/Ni Mixture in a Closed System

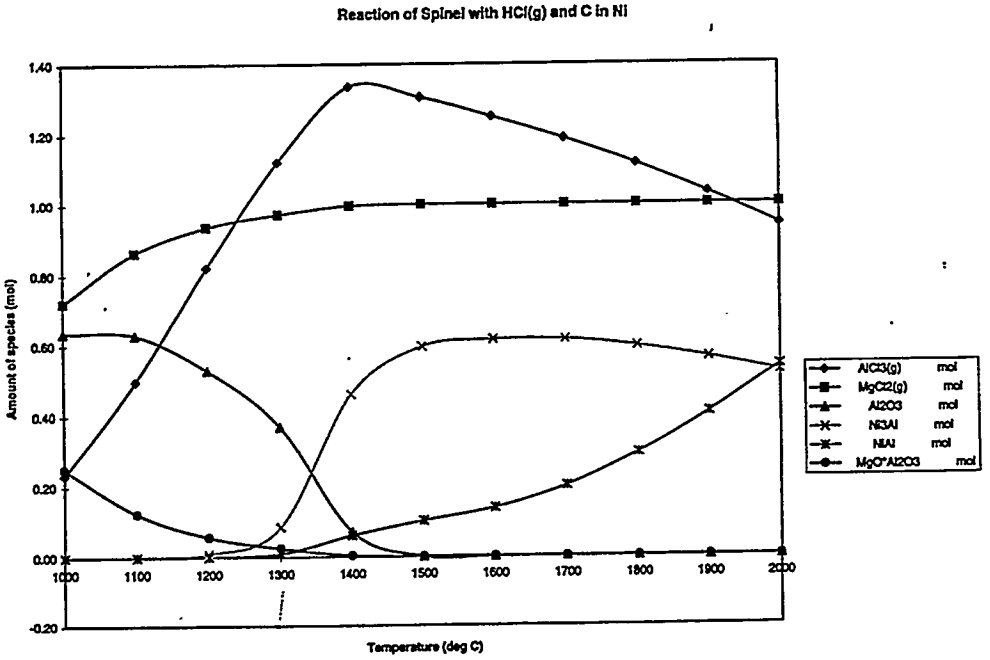

Figure 5.78
Equilibrium Concentrations of Species Originating from *3Al2O3*2SiO2/HCl/C/Ni Mixture in a Closed System

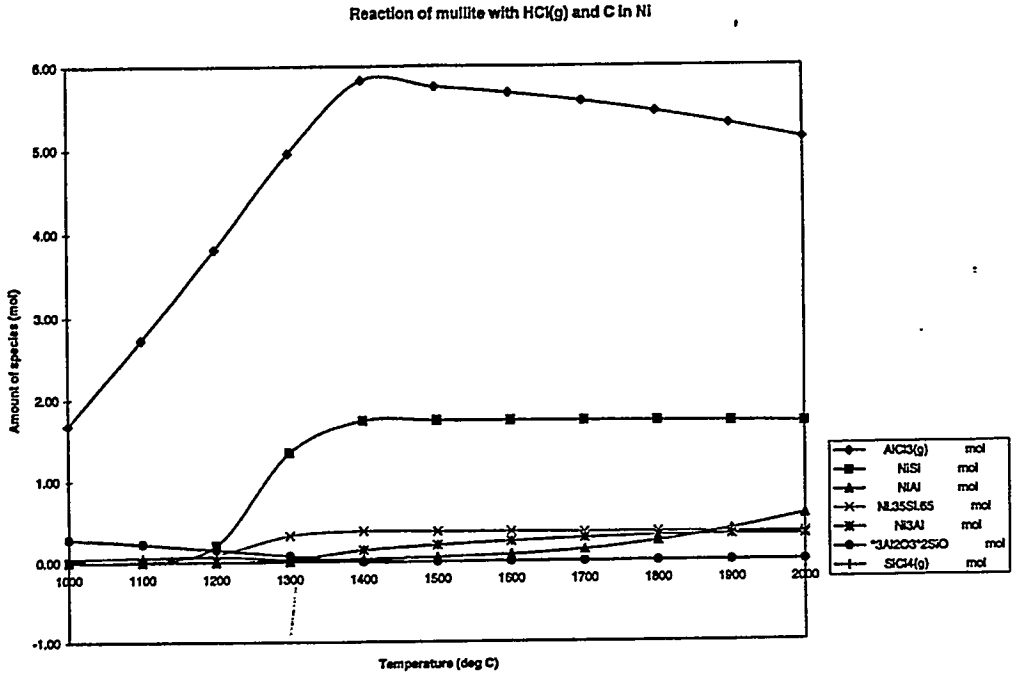

Table 5.35
Test Matrix

Day	Run	Brick 1	Brick 2	Brick3	Brick4	Temp (°F)	Rate (ccpm)	Time (hours)
11/1	57	Jargal	Taycor 512D	Aurex 75SR	HPCast Ultra	2700	200	2
11/12	58	Jargal	Zircoa 3004	Unicor 1	HPCast Ultra	2750	200	2
11/14	59	Jargal	Zircoa 3004	Unicor 1	HPCast Ultra	2850	750	6
11/17	60	BN	Mono-fraxL	Carbon	TiB_2	2850	750	6
11/21	61	BOF923	Aurex 75SR	ER 1195RT	Tribo-cor	2850	750	6
11/30	62	ER 1195RT	Zircoa 3004	Jargal	Mono-fraxL	2850	2500	11.5

5.2.1.2.3. Data

The results of the tests are presented here in terms of general appearance and, where available, apparent weight loss. The accuracy of weight loss is sometimes suspect due to adherence of foreign materials, but enough accurate information is available for comparative purposes in order to determine a relative ranking.

Tests were performed in Fall River on a dedicated refractory-testing system. In the system, refractory samples are suspended in a molten metal bath extending upwards into an atmosphere identical to that of a CEP reactor headspace. The refractory samples are spun rapidly in the molten bath and atmosphere to obtain accelerated wear data.

5.2.1.2.3.1. Test #2 (2hr. @200 cc/min, 2750°F)

This test was intended to compare several bricks of varying grades.

1. Jargal M. Fused-cast alumnia brick (with Na_2O bond)
2. Zircoa 3004. Sintered MgO-stabilized zirconia brick.
3. Unicor 1. Fused-cast AZS brick. The idea here was to duplicate more or less the physical form of Jargal M. but with a significant silica fraction.

4. HP Cast Ultra. High purity alumina castable similar to that in use in all large units (APU's and Demo Unit).

Below the samples are described.

- Jargal M. Sample showed a weight gain due to adhesion of material. Brick turned a sky-blue color to a depth of about 2mm.
- Zircoa 3004. Barely noticeable deterioration at metal line. Hardly any weight loss, even though sample was very clean.
- Unicor 1. Sample gives the impression of surface corrosion and noticeable deterioration at metal line although adhesion of substantial quantities of material gives an apparent weight gain.
- HP-Cast Ultra. Visual appearance of corrosion as matrix "fading" behind grains. The 6.9% recorded weight loss is probably inaccurate due to measurement errors, but does support the visual observation that significant corrosion did occur.

Table 5.36
Test #2 Results

Sample Number	LIMS Reference Number	Initial Sample Weight (grams)	Final Sample Weight (grams)	Final Sample Length (inches)	%Loss of weight
1	R006-94-058-R1-R1	371.18	219.32	4.125	gained
2	R006-94-058-R1-R2	514.90	370.89	5.062	0.4
3	R006-94-058-R1-R3	473.69	488.2	7	gained
4	R006-94-058-R1-R4	348.16	179.36	3.875	6.9

Our inability to get a quality visual impression led us to pursue a harsher test. Exposure time and HCl loading were therefore both increased. However, the equipment had proven to be robust in 20-94-058. The appearance of corrosion in sample 4 indicated that by increasing the severity of the test that a visual result would be obtained.

5.2.1.2.3.2. Test #3 (6hr. @750 cc/min, 2850°F)

This test was intended to compare the same bricks as in 20-94-058, but under more severe conditions.

1. Jargal M. Fused-cast alumnia brick (with Na_2O bond)

2. Zircoa 3004. Sintered MgO-stabilized zirconia brick.

3. Unicor 1. Fused-cast AZS brick. The idea here was to duplicate more or less the physical form of Jargal M. but with a significant silica fraction.

4. HP Cast Ultra. High purity alumina castable similar to that in use in all large units (APU's and Demo Unit).

Below the samples are described.

- Jargal M. Sample showed a weight loss in spite of adhesion of material. There was a definite cut at the metal line of >1mm in depth. Brick turned a sky-blue color to a depth of about 3mm.

- Zircoa 3004. Sample showed a weight loss in spite of adhesion of material. There was a definite cut at the metal line of >1mm in depth. It appeared that the surface was roughened as well, below the metal line.

- Unicor 1. Sample was terribly worn below the metal line, rounded near the tip. It gives the impression of drastic reduction of the material and bears visual resemblance to recent experience in the with silica-bearing refractory.

- HP-Cast Ultra. Visual appearance of severe corrosion as matrix "faded" behind grains. Corrosion was most severe at the metal line to a depth of >2mm, but corrosion was apparent at an above injection point of hydrogen chloride. At the metal line depth of corrosion was worse on the brick side away from the injection. Corrosion on this sample was definitely associated with the trajectory of injected gas. With an alumina basis the weight loss on this sample represents reaction to aluminum trichloride of 65% of the hydrogen chloride injected through the opposing hole.

Table 5.37
Test #3 Results

Sample Number	LIMS Reference Number	Initial Sample Weight (grams)	Final Sample Weight (grams)	Final Sample Length (inches)	%Loss of weight
1	R006-94-059-R1-R1	371.00	361.87	7	2.5
2	R006-94-059-R1-R2	541.20	394.84	5.375	5.0
3	R006-94-059-R1-R3	452.85	111.42	2	13.9
4	R006-94-059-R1-R4	356.99	216.85	4.9125	13.44

5.2.1.2.3.3. Test #4 (6hr. @750 cc/min, 1564°C)

This test was intended to compare assorted bricks, especially ones with BN content which had been touted as a possible binder material. Initial weights were not measured in this test. At the time of that test the intention was to comparatively screen materials and not attempt a mass balance.

1. BN. Theoretically stable to chlorination, this tested its susceptibility to dentrification and reaction with nickel to form nickel boride.

2. Monofrax L. Fused cast $MgO*Al_2O_3$ spinel.

3. (Hepworth) carbon brick. Calcined anthracite brick.

4. TiB_2/BN. Titanium diboride/boron nitride composite. Basically a test to see if the boride has enhanced properties over BN.

Below the samples are described.

- BN. Sample showed sèvere material loss below the metal line to a depth of about 2mm uniformly, consistent with the denitrification/nickel reaction mechanism.

- Monofax L. Sample showed clearly the path of hydrogen chloride gas passing over the brick surface due to coloration. There was a definite cut at the metal line of >1mm in depth.

- (Hepworth) carbon brick. Sample was barely worn at all, just at the metal line to a depth of <1mm in depth.

- TiB_2/BN. Sample showed severe material loss below the metal line to a depth of about 3mm uniformly above the point of injection, and about 1mm uniformly

consistent below the point of injection. Apparently there is more reaction with the corrosive gas than in the case of pure BN.

Table 5.38
Table #4 Results

Sample Number	LIMS Reference Number	Final Sample Weight (grams)	Final Sample Length (inches)
1	R006-94-060-R1-R1	144.17	5.25
2	R006-94-060-R1-R2	395.56	7
3	R006-94-060-R1-R3	98.25	4.8125
4	R006-94-060-R1-R4	199.46	5.25

5.2.1.2.3.4. Test #5 (6hr. @750 cc/min,1564°C)

This test was intended to complete the initial round of screening. Weights were not measured in this test.

1. BOF923 (MgO/C). Theoretically the carbon is stable to chlorination, but the MgO is not, and any metallic additions such as aluminum are also not.

2. Aurex 75SR. High chrome oxide brick.

3. ER1195RT. Fused-cast Zirconia Brick.

4. Tribocor. Nitrided titanium/tungsten/niobium alloy.

Photographs of the samples are shown in Figure 5.79. Below the samples are described.

- BOF923. Samples showed severe material loss at the metal line where there was corrosion depth over 10mm.

- Aurex 75SR. Sample maintained its shape, except at the metal line where there was corrosion >3mm deep. The material below the metal line however had become very soft and brittle to >1mm depth and could easily be scraped with a knife. Much deep pitting occurred just by handling the sample.

- ER1195RT. Sample was barely worn below the metal line but sustained severe wear at the metal line to a depth of >3mm. The sample cracked severely upon

cooling and became a tawny gold color which had not been observed with this material previously.

- Tribocor. Sample was destroyed wherever it contacted the melt.

Figure 5.79
Samples Run in Test 20-94-061

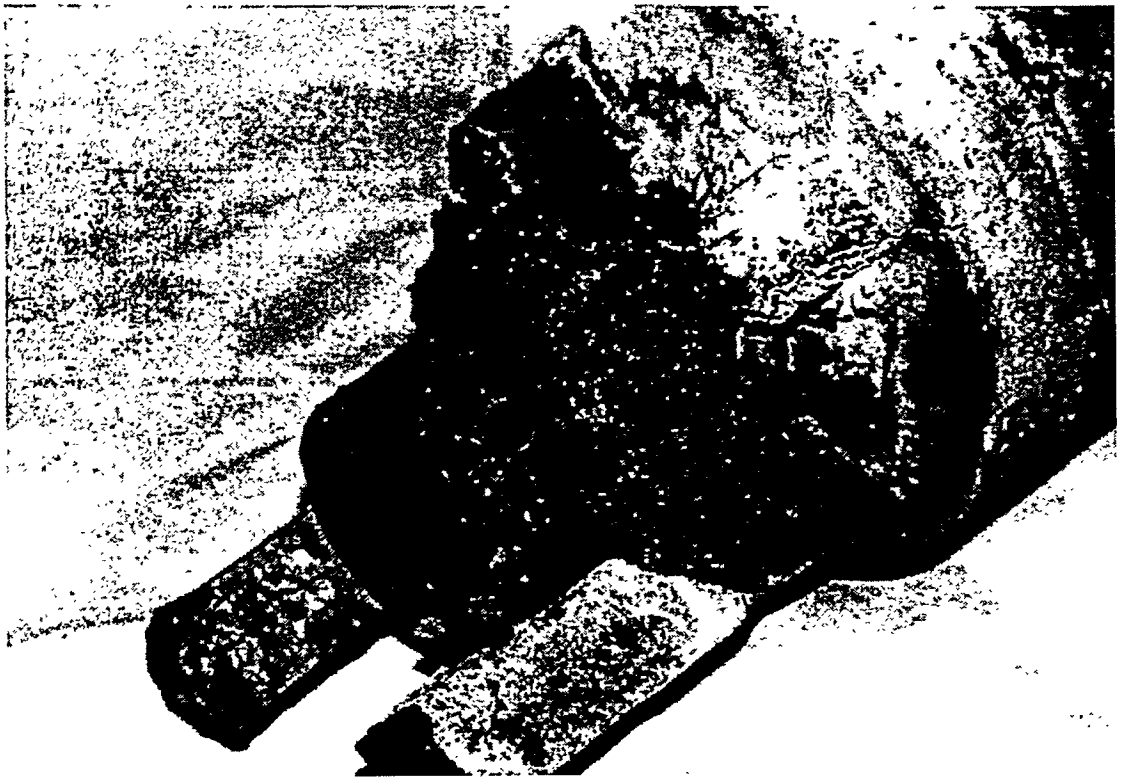

Table 5.39
Table #5 Results

Sample Number	LIMS Reference Number	Final Sample Weight (grams)	Final Sample Length (inches)
1	R006-94-061-R1-R1	138.93	5
2	R006-94-061-R1-R2	194.15	3.5
3	R006-94-061-R1-R3	567.63	7
4	R006-94-061-R1-R4		

5.2.1.2.3.5. Test #6 (11.5hr @2500 cc/min. 1564°C)

This test was intended to complete CTP-027. The initial round of screening had conclusively eliminated the worst performing materials. The top performing ones, used in this experiment, were:

1. ER1195RT. Fused-cast zirconia brick.
2. Zircoa 3004. Sintered MgO-stabilized zirconia brick.
3. Jargal M. Fused-cast alumina brick (with Na_2O bond).
4. Monofax L. Fused cast $MgO*Al_2O_3$ spinel.

Photographs of the samples are shown in Figure 5.80. Below the samples are described.

- ER1195RT. Severely corroded >4mm at metal line on faces not opposing injection. On injection face sample was severely sculpted >3mm at the splash zone about 1" from the metal line. No tawny color as in 20-94-061.
- Zircoa 3004. Severely corroded >4mm at metal line on faces not opposing injection. On injection face sample was severely sculpted >4mm at the splash zone about 1" from the metal line.
- Jargal M. Severely corroded >6mm at metal line on faces not opposing injection. On injections face sample was severely sculpted >5mm at the splash zone about 1" from the metal line.
- Monofrax L. Surface layers of about 1mm depth were spalling from this sample upon cooling. Severely corroded >4mm at metal line on faces not opposing injection. On injection face sample was severely sculpted >3mm at the splash zone about 1" from the metal line.

Figure 5.80
Samples Run in Test 20-94-062

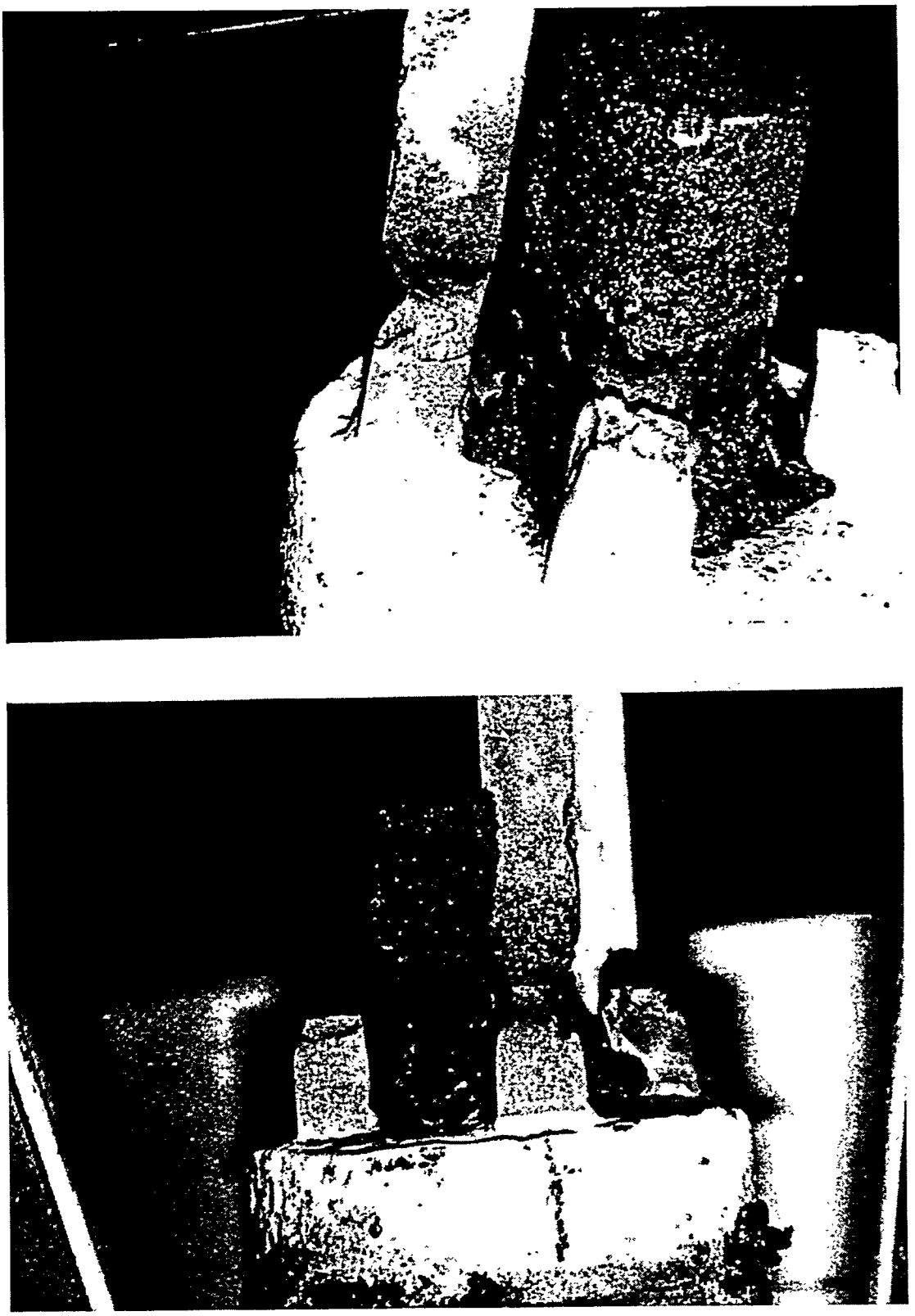

Table 5.40
Table #6 Results

Sample Number	LIMS Reference Number	Initial Sample Weight (grams)	Final Sample Weight (grams)	Final Sample Length (inches)	%Loss of weight
1	R006-94-061-R1-R1	545.83	514.4	7	5.8
2	R006-94-061-R1-R2	527.20	314.0	5.375	22.4
3	R006-94-061-R1-R3	374.9	136.9	3.75	31.8
4	R006-94-061-R1-R4	429.63	278.2	5.375	15.7

Accounting for all the weight loss as chloride is a reasonable assumption based on our proposed reaction mechanism. Comparing the amount of chloride to the chlorine in the feed results in a yield of 16.0% of chlorine fed into the reactor as metal chloride originating from the refractory. This is actually much less than the 65% figure computed for HP-Cast Ultra.

The relevance of these numbers will be discussed below.

5.2.1.2.4. Discussion

5.2.1.2.4.1. Qualitative Ranking of Refractory Bricks via Visual Inspection

There were clearly three tiers of brick performance as measured by visual appearance. The top tier included only one material, which was carbon.

The second tier, including "acceptance" performance., listed in order of decreasing performance was:

1. ER1195RT
2. Zircoa 3004
3. Monofrax L (lower than Zircoa 3004 due to surface spalling)
4. Jargal M

The remaining bricks were found to be categorically inferior to the other five. Ranked in order of decreasing apparent performance they are;

1. Aurex75SR
2. BN
3. HP Cast Ultra
4. Unicor 1

5. TiB_2/BN
6. MgO/C
7. Tribocor

5.2.1.2.4.2. Quantitative Ranking of Refractory Bricks via Weight Loss Measurement

Using the weight loss data shown in the section 3.6, a quantitative ranking was compiled. The data are renormalized to reflect the percentage of the total sample lost due to corrosion. In the experiments prior to section 3.6 the intention was to compare performance based on physical appearance, and to eliminate obvious poor choices.

For this reason, only the result from 20-94-62 is shown in Figure 5.81. The plot shows the performance not completely in agreement with the qualitative ranking. The discrepancy is due to the appearance of the post-test Monofrax L which exhibited significant surface delamination and spalling, and this was not reflected in the weight loss measurement.

Figure 5.81
Relative Ranking of Materials in Test 20-94-062

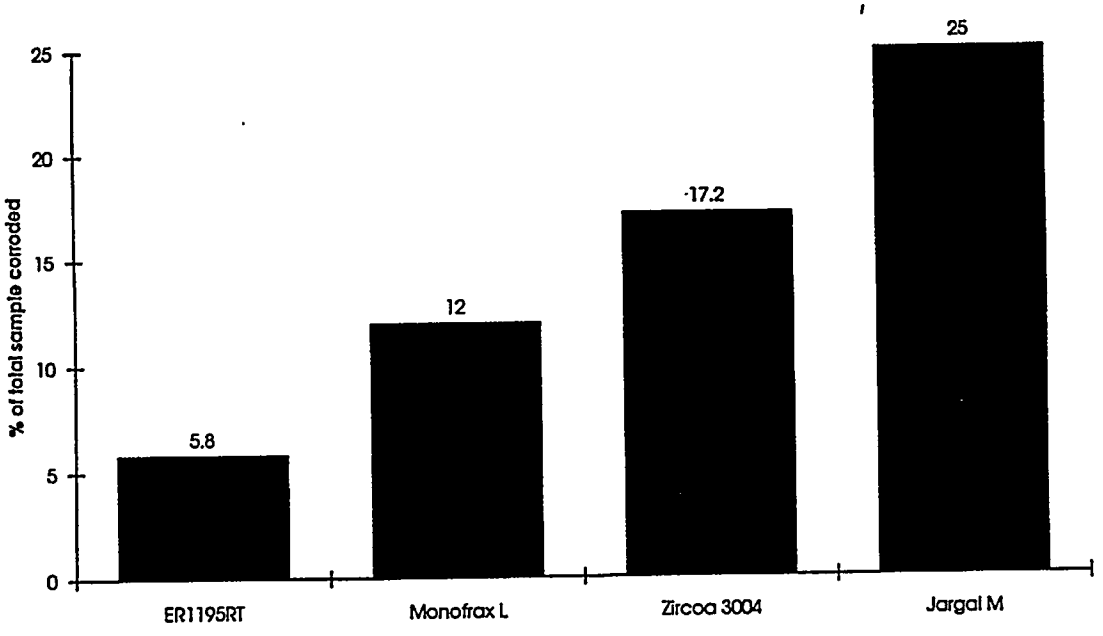

5.2.1.2.4.3. Effect of HCl Loading

The effect of increasing HCl loading was to increase the severity of the test. This observation was consistent both in changing from 200cc/min for 2 hours to 750cc/min for 6 hours, and again in changing to 2500cc/min for 11.5 hours. Since there was no

quantitative measurement of corrosion in the earlier experiments, there is no attempt to draw a quantitative relationship here.

5.2.1.2.4.4. Equilibrium Thermochemistry

Equilibrium thermochemistry is seen to play an important role in these experimental results, although the differences in performance are sometimes very subtle and may be due to the chemical interactions of the minor constituents of the refractories. The relatively poor performance of Aurex75SR, BN, Unicor 1, TiB_2/BN,MgO/C and Tribocor are readily explicable by mechanisms listed below:

Table 5.41
Corrosion Mechanisms for Selected Refractories

Material	Major/minor constituent	Mechanism of corrosion
Aurex75SR	chromia/alumina	reduction of chromia
Unicor 1	Alumina-zirconia-silica	reduction of silica
BN	boron nitride/boric oxide	denitrification, NiB formation
TiB_2/BN	titanium dibordie/boron nitride	denitrification, NiB formation
MgO/C	magnesia/carbon	chlorination of magnesia
Tribocor	niobium/tungsten/titanium	dissolution into nickel

The ranking of the top fused-cast materials, i.e..

1. Zirconia (minor phase silica)

2. Spinel (almost no minor phase) and alumina (minor constituent soda) is more difficult to explain thermodynamically, especially so with respect to the good performance of the spinel material relative to the fused-cast alumina. The relative weakness of the fused-cast alumina may be its soda fraction, while the spinel material is more pure. The periclase-rich nature of the spinel is definitely susceptible to direct chlorination, but this does not appear to be a major problem, compared to the poor performance of MgO/C. The relative inertness of the fused zirconia compared to either the fused-cast alumina or the fused-cast spinel was expected.

5.2.1.2.4.5. Refractory Microstructure

The microstructure and open porosity of refractory materials has probably played a role as well. Strong evidence of the benefit of lowering porosity is provided by the improved performance of Jargal .M as compared to HP-Cast Ultra as well as the improved performance of ER1195RT over Zircoa 3004.

5.2.1.2.4.6. Fluid Dynamics and Mass Transport

The corrosion in the top-performing bricks occurred in zones of intermittent gas/metal contact. In particular, severe corrosion has occurred where the fluctuating melt level contacts the bricks and where entrained metal droplets contact the bricks.

The important conclusion is that neither gas velocity near a refractory surface nor metal velocity near a refractory surface has a direct influence on the deterioration due to reductive chlorination. Rather, the deterioration is promoted when the gas/metal interface near a refractory surface is in fluctuating motion such that the refractory surface frequently alternates between contact with gas and metal media. This notion follows directly from the postulated mechanism of corrosion and has been also borne out by the morphology of corroded samples in the experiments.

5.2.1.2.5. Conclusions

5.2.1.2.5.1. Results of the Experiments

- Materials ranked in order of performance in this campaign:
  1. Carbon (practical only as a headspace material)
  2. ER1195RT (fused zirconia)
  3. Zircoa 3004 (sintered MgO-stabilized zirconia_
  4. Monofrax L (fused spinel)
  5. Jargal-M (fused alumina)
- all others performed in a significantly inferior manner
- the results can be explained with thermochemical and transport arguments

5.2.1.2.5.2. Implications for Commercial Application

- thermodynamics appears to dictate that materials selection alone will not eliminate corrosion due to the presence of both chloride and carbon with a fluctuating melt/gas interface.

5.2.1.2.6. References

1. Shaw, Cathy, CTP-94-022, "Chemical Skulling", pp 1-7, (October 1994).

5.2.1.3. Refractory Performance in Contact With Hydrogen Chloride Gas

5.2.1.3.1. Overview

Several runs have been conducted to probe the effects of selected process and design variables on refractory performance applications of CEP to chlorinated feeds processing. In these experiments both carbon level and temperature have been treated as variables. According to MMT's "reductive chlorination" model of corrosion, decreasing the carbon level should dramatically reduce the corrosion rate, while reducing the temperature should also reduce the rate of corrosion, but less markedly.

Our experiments on the 20 lb refractory test unit confirm these predictions. A factor of 10 improvement was obtained by lowering bath carbon level from saturation to effectively zero, while a factor of 13 improvement was obtained by lowering bath temperature from 1564°C to 1370°C.

5.2.1.3.2. Background

Analysis of refractory corrosion for chlorinated feeds has focused on the simultaneous chlorination of metal in the metal oxide of the refractory with oxidation of carbon as the primary chemical pathway.

The simplest way to minimize this corrosion is to lower the carbon activity. The driving force achieved in this way is depicted in Figure 5.82. At high carbon activity, alumina and zirconia refractories are intrinsically unstable, reacting to completion in Figure 5.82 at 1200°C; no substantial difference in performance would be expected at high carbon levels. At very low carbon activity, the refractories are stable, with little reaction detected at 2000°C. At intermediate carbon activities (ac~0.1) it is seen that zirconia is more stable than alumina.

Figure 5.82
Equilibrium Reaction of 1g of Al_2O_3 and 1 g of ZrO_2 with 25L HCl, 25L CO, 1000g Ni and 20g C

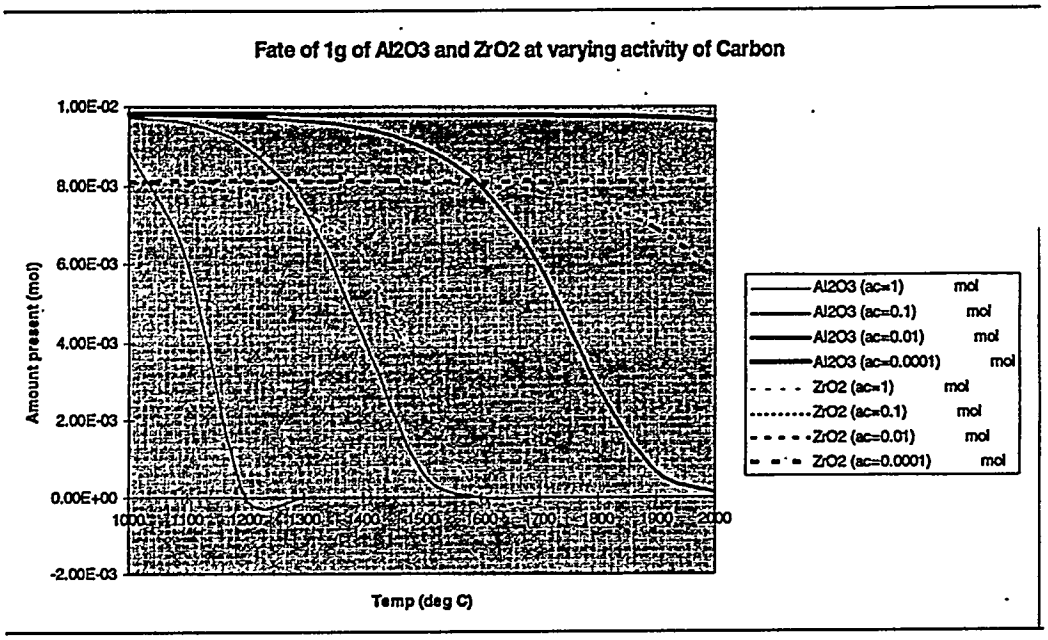

Each of the equilibrium curves in Figure 5.82 has zero slope at low temperature where little or no reaction occurs, and an essentially constant slope until it reacts to extinction. Individual refractory chemicals can be ranked, at a given carbon activity, by the temperature where significant reaction occurs. Figure 5.82 shows that zirconia has a higher reaction temperature for intermediate carbon activities.

It has been recognized that the operating wall temperature may play a significant role in minimizing corrosion rate. At intermediate carbon activities a temperature drop of 200°C at the wall can drastically alter the thermodynamic driving force for corrosion. we have not attempted to independently distinguish the effect of temperature on (gas-phase) intrinsic reaction kinetics or fluid phase mass transfer.

5.2.1.3.3. Test Program

A test plan was developed to test six types of refractory materials with four lances under various conditions. A summary of the test plan is presented in Table 5.42.

Table 5.42
Test Matrix

Run	Carbon	Lance	Brick 1	Brick 2	Brick 3	Brick 4	Temp. (°C)	Rate (ccpm)	Time (hours)
1	Low	A	G	I	J	K	1564	1370	10
2	Low	B	H	J	I	G	1633	1370	4
3	Low	C	H	J	G	L	1647	1370	6
4	Sat'd	D	H	J	G	L	1370	1370	6
5	Sat'd	D	H	J	F	L	1370	1370	6

5.2.1.3.4. Data

The results of the tests are presented here in terms of general appearance and, where available, quantitative measures of material loss.

5.2.1.3.4.1. Run 1 - Bohr. @ 1564°C, Low Carbon, Lance A

This test was intended to provide the first data points at low carbon levels. Lance A was chosen due to its ease of machining. However, the lance deteriorated very quickly and was discharging onto the bath surface rather than in submerged mode. The addition of boron to the melt in some sense defeated the purpose of the test, as boron is an effective scavenger of oxygen and is expected to promote reductive chlorination of the refractory.

The exposed samples are shown in Table 5.43. The two zirconia materials tested (G and I) were corroded, but less than that observed on a previous run which operated for 12 hours at carbon saturation. The fused-cast alumina (J) exhibited corrosion only where the metal droplets splashed on the sample surface. The material had grown a thick protective skull at the bath level. The fused-cast spinel (L) showed greater corrosion than in a previous run, which was the opposite trend of the other materials. Apparently this material is sensitive to the presence of boron or does not require carbon to be present for corrosion to occur.

Table 5.43
Run 1 Summary of Results

Sample	Description
G	• sample was definitely corroded at the gas/metal interface • corrosion was less than in a previous run
I	• sample was definitely corroded at the gas/metal interface • corrosion was less than in a previous run
J	• sample was corroded where metal droplets had splashed onto refractory surface • sample was not corroded and had grown a thick ceramic skull at the metal level
K	• sample was much more severely corroded at the gas/metal interface than in a previous run

5.2.1.3.4.2. Run 2 - 4 hr. @ 1634°C, Low Carbon, Lance B

The exposed samples are shown in Table 5.44. All samples were corroded, but much less so than previous runs at carbon saturation. In all cases, the degree of corrosion could not be measured with certainty, being less than 2mm at the corners. This is certainly much less than was established with a carbon-saturated bath at 1564°C during CTP-027.

Table 5.44
Run 3 Summary of Results

Sample	Description
G	• corrosion evident <lmm depth at sample corners
L	• corrosion evident <lmm depth at sample corners
J	• corrosion evident <lmm depth at sample corners
H	• corrosion evident <lmm depth at sample corners

5.2.1.3.4.3. Run 5 - 6 hr. @ 1564°C, Saturated Carbon Lance D

Sample	Description
G	• corrosion evident 4-5mm depth at sample corners
L	• corrosion evident 4-5mm depth at sample corners
J	• corrosion evident 4-5mm depth at sample corners
H	• corrosion evident 4-5mm depth at sample corners

5.2.1.3.5. Discussion

5.2.1.3.5.1. Effect of Varying Carbon Concentration

Carbon appeared to have a marked effect on the rate of corrosion of refractory bricks in contact with nickel and hydrogen chloride gas. Data indicates that an order-of-magnitude improvement in the corrosion rate is attainable by minimizing the amount of bath carbon present. This may be attributed to the much smaller thermodynamic driving force for chlorination in the absence of carbon.

An important observation concerns the widening of oxide injection nozzles, both alumina and zirconia, which were nominally in contact with hot HCl gas only in the conspicuous absence of contact with the melt. It has been postulated that a nonzero amount of chlorine gas as Cl_2 is evolved which reacts at the high temperatures of those tests.

5.2.1.3.5.2. Effect of Varying Bath Temperature

There appears to be significant effect of temperature on the speed of corrosion as well. A change in bath temperature from 1370°C to 1564°C approximately tripled the corrosion rate of refractory materials operating in a carbon-saturated bath.

5.2.1.3.6. Conclusions

Minimizing bath carbon concentration may substantially reduce refractory corrosion since an order-of-magnitude improvement in corrosion rate has been evidenced in laboratory tests, as measured by elemental ratios in baghouse dust. Subsequently this data was further corroborated on the pilot-scale APU unit. Reducing wall temperature may also reduce refractory corrosion. An apparent three-fold decrease in corrosion rate has been produced in the laboratory with a drop in temperature of 177°C. The implications of these results on CEP reactor design are important. Matching the refractory to the operating condition is essential. Refractory oxides should be chosen as containment materials only when the carbon concentration in the bath at the gas/metal/wasll interface is low. There is significant advantage to minimizing the

operating temperature at the gas/metal/wall interface. There are also significant benefits to a lower wall temperature even before the freezing point of the melt is reached.

5.2.2. Containment for Low Surface Tension Melts

5.2.2.1. Refractory Deterioration Modes

5.2.2.1.1. Melt Permeation

The addition of sulfur into the iron melt forms an iron sulfide (FeS) matte phase. The presence of sulfur reduces the liquid surface tension, causing uniform "soaking" permeation of the matte into the refractory. Inductive heating of the penetrated matte can result, which leads to abnormal sintering and increased reaction with sulfur (see Section 5.2.2.1.2). High-alumina refractories are particularly susceptible to this effect. Use of a silica-containing mullite reduces permeation through the generation of a non-wetting vitreous phase at the containment surface. Mullite is also less susceptible to reactions with sulfur, making it an optimal material for sulfur applications.

5.2.2.1.2. Reaction with Sulfur

Refractory oxides are susceptible to chemical reaction with sulfur. This reaction is only possible in the presence of carbon dissolved in the metal, $\underline{C}$. Basic metal oxides such as magnesia (MgO) are especially reactive by the following mechanism,

$$MgO + FeS + \underline{C} \rightarrow MgS + Fe + CO\,.$$

This reaction is very similar to the carbochlorination process seen in processing of chlorinated organics. Unlike carbochlorination, which affects only the gas/liquid/refractory interface, the entire wetted surface is subject to sulfur reaction. Permeation effects caused by low surface tension combine with chemical corrosion processes to produce significant damage in MgO-containing materials. Even low percentages of MgO can facilitate degradation, since the FeS matte travels along MgO grains in the refractory matrix. Silica-containing refractories (SiO_2) are relatively acidic and have demonstrated resistance to corrosion by this mechanism.

5.2.2.1.3. Molten Oxide Ceramic Phase Dissolution

The presence of oxidizing conditions can cause the formation of iron oxide (FeO) and other metal oxides in the melt. Buildup of a molten oxide ceramic phase (MOCP) can cause refractory degradation where it contacts the refractory wall. The driving force is the difference in chemical composition between the ceramic phase and the refractory material, which causes dissolution of refractory material into the ceramic melt.

High-alumina refractories containing MgO are known to minimize the corrosive effects

of MOCP dissolution. These materials are unfavorable due to sulfur corrosion and FeS permeation. Silica-rich materials are resistant to both permeation and sulfur reactions but suffer increased vulnerability to MOCP dissolution. Mullite-based materials with an intermediate silica concentration have emerged as an optimal material to minimize all deterioration modes.

5.2.2.1.4. Mechanical Stress

Heating of pre-cast refractory materials to high temperature can cause thermal stresses due to differential heating. Stress cracks often result through which the melt can permeate. This mode is most prevalent in pre-manufactured crucible designs. Dry-vibratable refractories are installed as an unfired powder to alleviate this problem. "Dry-vibe" is nearly immune to cracking on a single thermal cycle because a solid body is not formed until the operating temperature has been reached.

5.2.2.2. Refractory Development Program

Original refractory materials for sulfur-containing feeds were very similar to those which have shown good performance in non-sulfur CEP applications. These refractories contain metal oxides such as alumina and magnesia which were found to suffer from permeation and chemical degradation in the presence of sulfur. Materials were developed to resist not only this mode of deterioration, but also MOCP dissolution, melt permeation, and mechanical stresses. An additional constraint in material selection is the need for a free-standing, replaceable crucible. The presence of radionuclides in mixed-waste feeds requires the containment shell to be easily replaceable and portable.

5.2.2.2.1. Pre-Manufactured Crucibles

The need for a free-standing, replaceable crucible necessitated a preference toward pre-manufactured crucibles in initial development work. Several materials were investigated, starting with high-alumina refractory that had been demonstrated in several non-sulfur applications. The thermal stress associated with heating the crucible to operating temperature caused major cracking to occur. Pre-manufactured ceramics were deemed unsuitable for this application based on cracking in demonstration runs.

An additional type of pre-manufactured containment system investigated was the graphite crucible. This is a traditional form of containment in high-temperature applications, and its advantages include high mechanical strength and resistance to cracking. Demonstration runs showed poor operability in this application, because the oxidizing atmosphere associated with high sulfur concentrations causes steady oxidization of the graphite wall to carbon monoxide.

5.2.2.2.2. Operating Conditions

Optimization of reactor operating conditions was investigated as a means to minimize the reactivity of sulfur melts. Operation at very low carbon concentration had proven very successful in processing of chlorinated organics. This operational change only reduced corrosion at lower sulfur concentrations. Very low carbon operation also caused an unacceptably high level of MOCP dissolution due to the higher oxygen potential. An additional operational change which had limited success was addition of manganese to partition sulfur out of the melt as MnS.

5.2.2.2.3. Material Selection

Original materials containing alumina and MgO were unsuitable due to high reactivity with FeS in the presence of dissolved carbon. Adjustment to low-carbon operation had only limited success in minimizing wear rates with MgO-containing materials. Several materials were then evaluated for longevity in sulfur applications with higher bath carbon.

Silica was found to be resistant to sulfur reactions due to its relative acidity. The susceptibility of silica to MOCP dissolution required an optimization of the refractory composition. Alumina-bonded mullites containing moderate amounts of silica showed good results but were weakened by dissolution in low carbon, high oxygen potential melts. Adjustment to high carbon alleviated dissolution wear. A dry-vibratable mullite was specially developed in cooperation with the vendor to take advantage of its crack resistance.

5.2.2.2.4. Results

Dry-vibratable mullite combined with relatively high carbon concentration emerged as the optimal formulation. This material combines the advantages of mechanical strength, resistance to sulfur corrosion, and resistance to MOCP dissolution in a form applicable to modular, free-standing crucible design. Demonstration of mullite refractory has shown high performance at carbon saturation and a wide range of sulfur concentrations up to saturation (pure FeS).

The mechanical strength properties of dry-vibratable mullite were also confirmed. Reliable sintering has been achieved at the lower temperatures associated with high sulfur operations. Sintering was also demonstrated above the bath level at these conditions, showing that dry-vibratable refractory can be applied in both the lower and upper regions of the reactor.

5.2.2.3. Mullite Confirmation Program

After studying various classes of refractory materials and operating conditions in sulfur applications, mullite-based materials showed the highest level of performance in a

broad range of Fe-S-C ternary compositions. A series of additional test campaigns was performed to further establish the performance of these materials with sulfur-containing feeds.

Several test campaigns were developed to demonstrate mullite performance over a range of operating conditions. The first test was designed to provide an accurate benchmark of mullite behavior in sulfur-containing melts. This run tested the dry-vibratable material used in demonstration runs. Performance was demonstrated in sulfur concentrations up to saturation (pure FeS).

Other tests investigated the same material in the presence of a melt simulating typical high-sulfur applications. The melt included Fe, S, and C, along with additional elements like Na, K, Zn, B, P, and Ba. This testing showed that mullite materials are compatible with the additional elements and specific operating conditions required for mixed-waste and other sulfur-containing feeds. Castable materials were also shown to have potential in applications requiring both sulfur resistance and high mechanical strength such as the reactor bottom block.

5.2.2.4. Free-Standing Modular Crucible Design

The overall motivation for use of a modular crucible is to facilitate removal and replacement of refractory components due to accumulation of radioactive species during mixed-waste processing. A fracture-proof ceramic crucible is of particular importance to the safe operability of mixed-waste processing facilities. Concerns about volume reduction prevent utilization of additional crucible layers to overcome cracking problems. Alternative crucible designs with higher mechanical strength have been evaluated, such as graphite, metal "stealth" shell support and water-cooled cold-crucible technology. These options have been found to include unfavorable operational and cost concerns. Dry-vibratable refractories have emerged as the ideal material for modular crucibles. A structural shell is needed in this application to hold the dry-vibe before firing and to act as a backup containment structure.

A key component of the free-standing modular crucible is the structural shell made of continuous fiber-reinforced ceramic composite (CFCC). This novel material falls under the general category of "tough ceramics." Tough ceramics are non-brittle composites, reinforced with ceramic fibers for unusual mechanical strength and resiliency. Their physical and chemical composition makes them well-suited to withstand thermally and chemically stressful environments. The continuous fiber network of CFCC provide superior performance within the class of tough ceramics.

The modular crucible design consists of unfired, dry-vibratable refractory installed between two containment linings. The inner lining is a consumable metal mandrel composed of the bath metal element. A CFCC shell is used to support the outer edge of the dry-vibe refractory. A layer of lightweight compressible insulation is included between the dry-vibe and CFCC shell to absorb radial strain produced by thermal

expansion. The entire crucible is installed intact in the reactor. Springs beneath the crucible absorb axial strain from thermal expansion. After reaching operating temperature, the mandrel melts into the bath as the refractory sinters into a removable solid shell.

5.2.3. Evaluation of Refractory-Ceramic Compatibility

5.2.3.1. Introduction

To bring MMT's experience with refractory systems to bear on the specific issue of DOE waste processing, evaluations of several candidate refractory materials were made as part of the contract effort. These materials were considered for use with the ceramic compositions discussed earlier which are being developed for the stabilization of radionuclide species and hazardous components. This study is also motivated by the fact that deposition on crucible walls was observed in earlier experiments.

Refractory/ceramic compatibility was evaluated with the refractory materials in the form of crucibles in bench-scale experiments. Five different types of refractories were used in this study in combination with six different ceramic compositions. For the majority of the experiments, a high alumina crucible was used as the base material. However, this report also briefly details consideration and use of alternative materials. This includes fabrication of several crucibles from castable materials.

5.2.3.2. Summary of Materials Tested

Several different materials were considered for use in these tests. The actual materials selected were chosen primarily on the basis of chemical composition and physical properties. However, these tests were designed to be integrated into decontamination experiments of radioactively contaminated metals. This meant that there was also the practical issue of using materials which could be purchased in the correct form as a crucible or, alternatively, using a material from which a crucible could be fabricated in-house.

The series of crucible materials actually used in this study were the following:

- CRUC1: high alumina,
- CRUC2: high alumina,
- CRUC3: high zirconia,
- CRUC4: high alumina (castable), and
- CRUC5: high alumina (castable).

The chemical constitutents of the refractories used are shown in Table 5.45 with a qualitative description of their amounts. With the exception of the high zirconia crucible, all materials were very high in Al_2O_3 content. The base crucible used in Task 1.3 experiments was a high alumina crucible. This material was chosen as it has proven in past bench-scale CEP experiments to be capable of withstanding severe heating and cooling rates. It is also generally corrosion and erosion resistant to many of the typical CaO-Al_2O_3-SiO_2 ceramic compositions used.

The ZrO_2-SiO_2 crucible was included in this study because it was believed to have excellent compatibility characteristics with borosilicate glasses and other more acidic ceramics.

Table 5.45
Refractory Compositions

Oxide	CRUC1	CRUC2	CRUC3	CRUC4	CRUC5
Al_2O_3	high	high	low	high	high
SiO_2	medium	low	medium	low	low
TiO_2	low	low	low		low
Fe_2O_3	low	low	low	low	low
CaO	low	low		low	low
MgO	low	low		low	
Na_2O	low	low		low	low
K_2O	low	low			
ZrO_2			high		
others			low		

5.2.3.3. Refractory Evaluation

5.2.3.3.1. Processing conditions

As the refractory evaluation in this phase was scoping in nature, the majority of the runs were done with the CRUC2 crucible. The primary, common conditions experienced by the crucible materials were the following: all contained both a molten metal bath and a molten ceramic mixture all were subjected to typical CEP operating temperatures (from 1375 °C to 1575 °C), baths were agitated with gas injected through a lance at a known flow rate (accelerating refractory wear), and the materials were

usually subjected to the extreme heating and cooling rates typical of bench-scale CEP experiments. Table 5.46 summarizes the operating conditions used in each experiment.

Table 5.46
Summary of Operating Conditions

Run	Metal	Crucible	Ceramic	Temp (°C)	Injection (min)[1]
05-93-083	Fe	CRUC2	None	1500	75
05-93-084	Fe	CRUC2	CAS2	1475	70
05-93-085	Fe	CRUC2	CAS1	1575	62
05-93-087	Fe	CRUC2	CAS2	1550	67
05-93-089	Fe	CRUC2	CAS2	1550	97
05-93-090	Fe	CRUC2	CAS1	1450	114
05-93-091	Ni	CRUC2	CAS1	1525	60
05-93-092	Ni	CRUC2	CAS1	1525	73
05-93-093	Ni	CRUC2	CAS2	1575	30
05-93-094	Ni	CRUC2	CAS2	1500	31
05-94-001	Ni	CRUC1	CAS1	1550	75
05-94-002	Fe	CRUC2	CAS1	1550	71
05-94-006	Fe	CRUC2	BSG1	1550	61
05-94-009	Fe	CRUC2	BSG2	1550	60
05-94-010	Fe	CRUC2	BSG3	1525	67
05-94-013	Fe	CRUC3	BSG4	1375	66
05-94-020	Ni	CRUC5	BSG4	1550	60
05-94-021	Ni	CRUC4	BSG4	1550	61

[1]Total gas injection time.
CAS1: Calcium Alumino-silicate composition No. 1
CAS2: Calcium Alumino-silicate composition No. 2
BSG1: Borosilicate No.1
BSG2: Borosilicate No.2
BSG3: Borosilicate No.3
BSG4: Borosilicate No.4

5.2.3.3.2. General Results for Different Refractories

Qualitative comparison of refractory performance was made by visual inspection of the crucibles after the run. The principal areas of concern and evaluation for refractory degradation are at the ceramic/metal line, in the ceramic layer itself and at the lance (or tuyere on larger units). Little deterioration is ever observed in the metal layer, as the chosen refractories are all specified to be compatible with the molten metal, especially under reducing conditions. Crucible deterioration is expected to be a function of multiple variables including operating temperature, ceramic composition, ceramic viscosity, ceramic quantity, bath size, gas injection rate, gas injection time and injection method (e.g., two versus four hole lance). Several conclusions can be drawn from visual observations. Post-run photos including interior and exterior views were taken after each run. In addition, measurements of ceramic penetration were made at various crucible positions for a more quantitative evaluation.

5.2.3.3.3. Ceramic Penetration Rates for Different Operating Conditions and Refractories

While qualitatively the crucibles can be evaluated visually, a quantitative comparison is more desirable. Therefore, measurements were made of ceramic penetration through the crucible wall at various crucible positions. These positions included the base of the crucible, the crucible in contact with the metal layer only, the crucible at the metal/ceramic boundary and the crucible in contact with the ceramic layer only. In transferring these data to another system, the operating conditions must be carefully considered. These factors include the fact that with the bench-scale reactor, a graphite susceptor was used. This means that the temperature is at a maximum towards the outer part of the crucible, i.e., the hottest part of the reactor is actually outside of the crucible. Therefore the temperature effect may increase ceramic penetration rate as a function of penetration position. The opposite effect is expected in larger reactors as the ceramic is expected to reach cooler zones as it penetrates the refractory, potentially decreasing total penetration rate.

5.2.3.4. Conclusions

This study provided an overview of initial ceramic/refractory compatibility evaluations. Five different types of refractories were used in this study in bench-scale experiments in conjunction with six different ceramic compositions. Several other refractory compositions were also considered. Particularly explored was the interaction of a high alumina crucible with two calcium aluminosilicate ceramics, one with a low alumina content and the other with a high content. This compatibility was investigated under a range of operating conditions. A series of borosilicate glasses of widely differing compositions were also used in this study. Several crucibles were also made from castable materials and used in these experiments. The following conclusions were reached:

- Composition CAS2, with a low alumina content, caused significant crucible degradation. The observed wear was essentially independent of operating temperature. Use of CAS1, containing a higher alumina content, resulted in minimal crucible wear.

- The high zirconia crucible performed very well. However, this was only tested in one experiment. It warrants further consideration, especially with borosilicates or more acidic glasses.

- The CRUC4 castable crucible performed better than the CRUC5 castable. This comparison was done only for one ceramic composition and may be extended to others in the future.

- Making crucibles from castable materials proved to be a feasible project. In the future, the crucible quality could be much improved when the dimensions are not constrained. Specifically, increasing the wall thickness is expected to significantly improve ease of fabrication.

- Ceramic penetration rates were presented for several different ceramic compositions used with different crucibles. These indicate that in the conditions used on the bench-scale reactor, ceramic wear may be more severe than on larger reactors.

5.2.4. Relation of Refractory Wear to Agitation Rate

5.2.4.1. Introduction

The scoping nature of the refractory-ceramic compatibility experiments (Section 5.2.3) necessitated that more experiments be designed where the effect of certain process variables can be isolated and fully investigated. Agitation rate of the metal-ceramic melt has been known to influence the rate of refractory wear. For this reason, refractory samples belonging to one material were exposed to different agitation rates in a metal-ceramic melt mixture of fixed composition

It was the objective of this study to establish a prototypical relationship for the variation of wear rate of refractory material with melt agitation rate.

Controlled wear testing was performed on three samples of identical material at differing agitation rates of 0.15-0.35 m/s (superficial velocity). The material chosen was a high-alumina refractory.

5.2.4.2. Test Matrix

Table 5.47 lists the experiments successfully completed in this test plan. The molten ceramic phase used was in all cases a prefused calcia-alumina-silica mixture. All tests were done under reducing conditions with a known carbon concentration in molten

iron. The rotation rate was varied through a narrow range in order to have a stable melt surface and avoid fluid dynamic transitions.

Table 5.47
Experimental Conditions

Material	Temperature (°F)	RPM	Duration (h)
High alumina	2,750	50	5
High alumina	2,750	75	2.5
High alumina	2,750	100	2.5

5.2.4.3. Summary of Results

A summary of the experimental data is given in Table 5.48. The maximum penetration rate is defined as the maximum depth divided by the exposure time. Breadth of the molten ceramic/metal cut is defined as the axial distance over which wear is at least 0.1 inches. Cross-sectional wear rate is defined as the integrated wear profile divided by the exposure time. Increased agitation was clearly seen to have an increasing effect on the two metrics of wear rate.

Table 5.48
Summary of Experimental Results

Agitation Rate (m/s)	Maximum Penetration Rate (in/h)	Breadth of Molten Ceramic/Metal Cut (in)	Cross-Sectional Wear Rate (in^2/h)
0.17	MMT Proprietary	MMT Proprietary	MMT Proprietary
0.25	MMT Proprietary	MMT Proprietary	MMT Proprietary
0.33	MMT Proprietary	MMT Proprietary	MMT Proprietary

The maximum penetration rate in Figure 5.83 was seen to vary in a nonlinear fashion with agitation rate in the range studied. The nonlinearity suggests that the rate of actual material loss may be linear and the curvature be accounted for by the decreasing sample diameter during the course of the experiment. This possibility is tested by the plot in Figure 5.85.

Figure 5.83
Variation of Maximum Wear Rate with Agitation

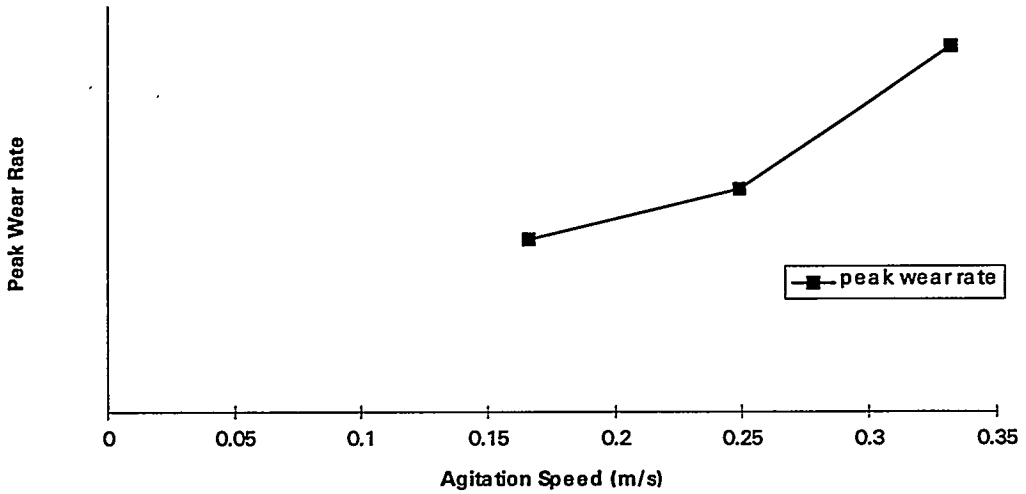

The width of the molten ceramic/metal cut was practically invariant with agitation rate in the range studied as shown in Figure 5.84. The slight increase can be attributed to inaccuracy of the measurements which were rounded to the nearest 0.1 inch, measured perpendicular to the original face. The invariance of this span verifies that the fluid dynamic regime probed by these experiments was indeed stable.

Figure 5.84
Variation in Width of Molten Ceramic/Metal Cut with Agitation

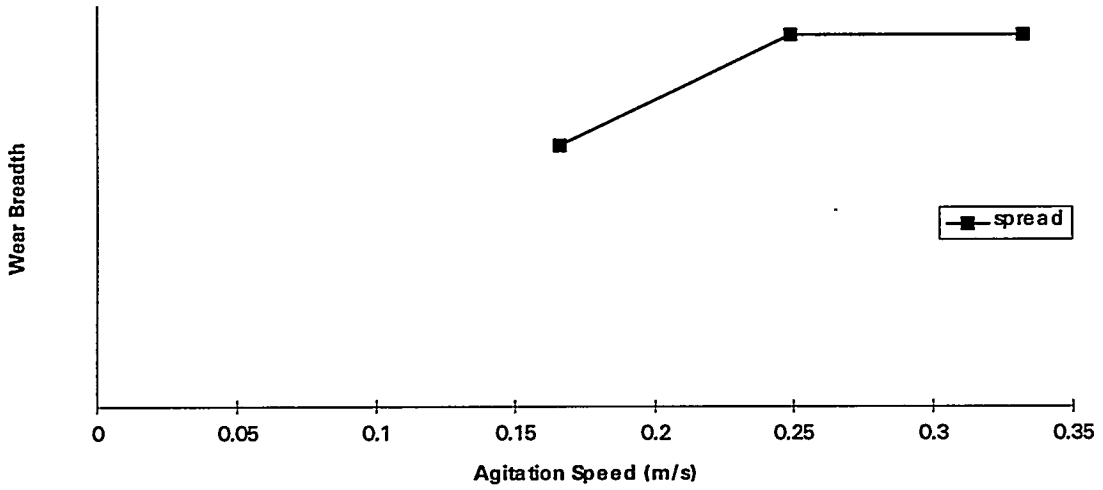

Importantly, the integral wear on the specimen was seen to vary in a nearly linear fashion with agitation rate in the range studied as shown in Figure 5.85. The linearity

could result as a product of a thinner controlling boundary layer and increased energy in the multiphase region. These two are typically scaled with the square-root of velocity and the square of velocity, respectively. The relationship was still nearly linear when an artificial data point of zero wear at zero agitation rate is added.

Figure 5.85
Variation in Integral Wear Rate with Agitation

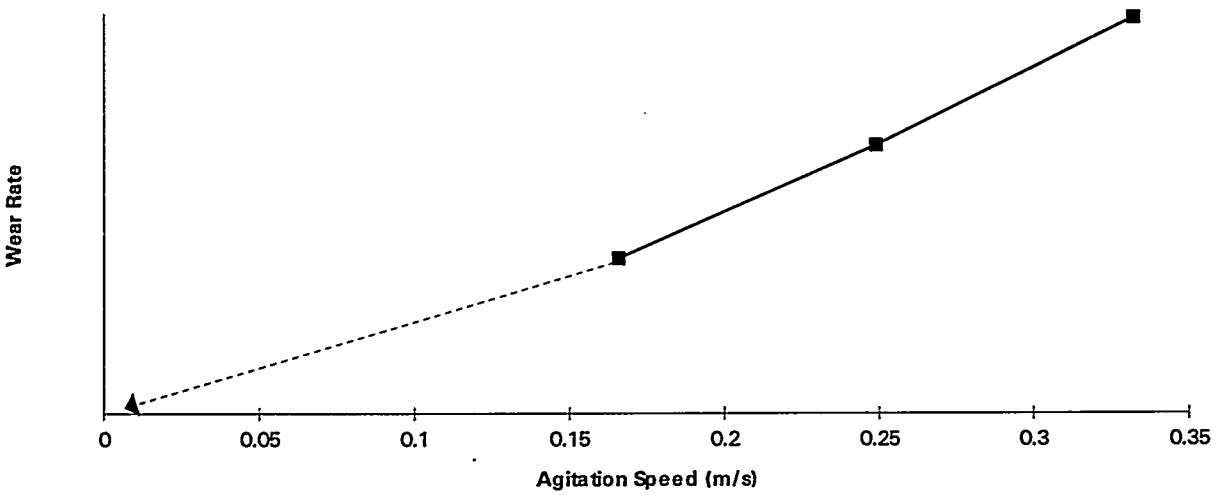

5.2.4.4. Conclusions

The conclusions of this experimental study can be summarized as follows:

- The integral rate of wear of high alumina refractory tested in this study was nearly linear with the differential velocity between the sample and the molten ceramic/metal melt.
- It is expected that in CEP systems, the rate of wear of refractory in contact with molten ceramic/metal mixtures would vary linearly with (downcomer) velocity.

However, it is presently unclear as to whether this result is caused primarily by:

- Increased heat transfer to the reactive sample and ceramic which are not isothermal under conditions of this experiment, yielding a higher effective ceramic/sample interface temperature, or
- Increased mass transfer of corrosive materials from the molten bulk ceramic to the sample outer surface and corroded material from the surface to the bulk.

In current CEP practice, each mechanism may play a role as the reactor walls are never isothermal and a corroded layer is always observed.

Therefore, future materials testing at MMT will provide an isothermal hot zone option in order to provide insight into the relative importance of (not having) interphase heat transfer. These tests will then be done at varying agitation rates to provide insight into the importance of mass transfer unaffected by thermal gradients.

5.2.5. Modeling of Refractory Lining Wear

5.2.5.1. Introduction

Refractory wear is the most important physical phenomenon faced in the CEP containment development program, as gradual wear processes will ultimately determine the longevity of CEP units. The factors involved in refractory lining wear are therefore being addressed experimentally (Sections 5.2.3 and 5.2.4) and theoretically.

An integrated program aimed at refractory wear minimization has been developed. The program focus is on improving the containment system design methodology, optimizing refractory materials selection, and developing a theoretical understanding of the mechanisms controlling lining degradation.

Analysis of refractory materials that have been experimentally tested on bench-, pilot- and demonstration-scale units has led to predictions about the controlling mechanism, and hence to the development of a thermal model for describing refractory lining wear.

5.2.5.2. Containment System Design

Containment system design is the most important component effort for combating refractory lining deterioration. Much of the initial development work in CEP containment has been focused on improving design methodology. Refractory reliability has shown a steady increase over the course of the contract. This has been due to a combination of improvements to refractory layout, heatup practice, shell design and temperature control (setpoint derived from laboratory experiments).

Important design efforts are being made on an ongoing basis. Basic induction furnace design has been changed in cooperation with the manufacturer. A prototype new furnace has been installed and successfully operated on the pilot- and demonstration-scale systems with copper barrier plates. These barrier plates prevent molten metal penetration through the joint or throat from reaching the area behind the coils.

The CPU refractory system was completely overhauled as its reaction cavity was resized. The design of this containment system involved some collaboration with the refractory manufacturer. One important observation for the new containment system was the effect of reduced agitation on observed wear trends. Laboratory experiments (Section 5.2.4) have shown that increased agitation velocity yields an approximately linear increase in wear rate under specific nonisothermal conditions. In addition, the

ability of the monolith to accept individual test bricks is a clear benefit, since it will allow testing of different bricks to be performed routinely.

5.2.5.3. Refractory Materials Selection

Presently, most CEP refractories are selected based on chemical composition and strength measurement. Alumina-based refractories have been predominantly chosen because of alumina's consistent performance against varying molten ceramic phase composition. When a fixed molten ceramic phase is present, a refractory composition can be chosen which may be less reactive and may not be alumina-based. MMT laboratory testing has shown that different refractory materials perform differently with a relevant molten ceramic phase. The compatibility of refractory materials with MMT-developed ceramic phases has been systematically investigated. The findings are outlined in Section 5.2.3.

5.2.5.4. Microstructure of Refractories

Microstructure consists of the arrangement of mineral phases, metals and porosity which determine the refractory's properties. It can be thought of as describing the:

- size gradation of aggregates in the refractory,
- size gradation of porosity in the refractory,
- spatial orientation of minerals, glass and porosity in the refractory, and
- orientation and concentration of microcracking in the structure.

The growth of mineral phases in situ results in an evolving microstructure for any given refractory. For even identical chemical compositions the microstructure may differ significantly. The microstructure of the refractory has a most profound effect on mechanical properties. Mechanical properties are particularly important as regards mechanical failure, thermal shock--sometimes described as "spalling"--resistance and erosion resistance. Mechanical failure of the refractory material is remedied through design and material changes. Mechanical failure occurs only during thermal cycling. Contraction associated with cooldown results in tensile stress which exceeds the tensile limits of refractories. The formation of these cracks from a monolithic surface is seen any time a reactor lined with a monolithic dry vibratable or castable refractory is cooled to ambient. An independent effort by an outside contractor has been undertaken to model the thermal stresses in the CEP reactor to pinpoint potential stress concentration areas.. However, for a properly designed and continuously-operating CEP unit, thermal cycles do not exist and hence, mechanical failure is not anticipated to occur.

Importantly, microstructure exerts control on the rate of chemical or mineralogical evolution of the refractory by limiting transport rates and surface area available for

reaction. First an isothermal non-equilibrium situation is considered to illustrate this. The spatial orientation of porosity, for example, affects the transport of corrosive materials into the refractory structure and corrosion products out of the refractory structure. This transport through pores may be the rate-limiting step determining refractory wear (when competing mechanisms of kinetics and convection are relatively faster). The relation for effective diffusivity in a porous medium, where ε is the porosity and τ is the tortuosity factor, is classically used to describe surface reactions in porous media:

$$D_{eff} = \frac{\varepsilon}{\tau} D_{liq}$$

where D_{liq} is the diffusion coefficient in the bulk liquid and D_{eff} the effective diffusion coefficient.

The microstructure directly determines both porosity and tortuosity, as well as available surface area for reaction. When the equations of transport are solved for an isothermal porous semi-infinite plate, two related parameters borrowed from catalysis literature can be defined.

An effectiveness factor η is the ratio of actual reaction rate to the theoretical reaction rate where no concentration gradients exist in the pores. A Thiele modulus ϕ is the relative weighting of reaction kinetics versus diffusion speed, where k_{rxn} is a first-order reaction rate constant and x_{mal} is the penetration depth of corrosion into the refractory:

$$\eta = \frac{\tanh \varphi}{\varphi}$$

$$\varphi = x_{mal} \sqrt{k_{rxn} / D_{eff}}$$

Where porous diffusion resistance is significant the effectiveness factor is less than one. A gradient of spatially-averaged concentration exists within the porous structure. Where porous diffusion is dominant, the effectiveness factor becomes closer to zero than one and the importance of the microstructure as quantified by porosity and tortuosity is evident:

$$\eta \approx \frac{1}{\varphi} \propto \sqrt{\frac{\varepsilon}{\tau}}.$$

In addition, integral reaction rates may vary approximately with surface area. Thus the volume contained in a grain is affected at a rate inversely proportional to the square of its diameter, and the reaction rate per unit mass is inversely related to the average diameter. This accounts for the lack of apparent affect on the large alumina grains as seen in most CPU runs and other high wear conditions. The transport through pores is also controlled by surface wetting, and the distribution of a nonwetting phase in the refractory is therefore important in determining transport rates.

A low-porosity material, which may be appropriate for molten ceramic phase applications, is being prepared for tuyere plugs and material test panels. It will be contrasted with castable and prefired bricks, and tested in the multiplexed wear test and integrated containment test facility. Ultimately a knowledge of unused refractory microstructures is relevant for the zoning of a lining.

5.2.5.5. Isothermal Chemical Reactions and Dissolution (Corrosion)

On an atomic level chemical transformations control the evolution of chemical species. On an integral scale these chemical reactions control the evolution of constituent mineral phases in the refractory. The penetrated region near the hot face is a result of the evolution of the component mineral phases and is therefore a product of the chemical reactions including dissolution.

Refractories can be thought of as chemically having two phases, aggregate and a matrix. These two can be treated separately. The corrosion rates due to metal are orders of magnitude less than those due to molten ceramic phase, with the exception of the reduction of chromic oxide which has been observed in CEP.

The refractory can be viewed as a single or two-component material. Upon exposing the refractory to a molten ceramic phase, transport of corrosive agents into the refractory begins, governed by the relationships involving porous diffusion as discussed above. Simultaneous dissolution of the solid material begins to occur. Several interfaces which may be in local equilibrium can evolve:

1. between unaltered solid refractory material and solid reaction products that appear as adjacent minerals in the appropriate compatibility region on a ternary phase diagram. For example, alumina (A) may react to form interfaces with anorthite (CAS2) and CA6, except at low V-ratios where mullite A3S2 may be formed.

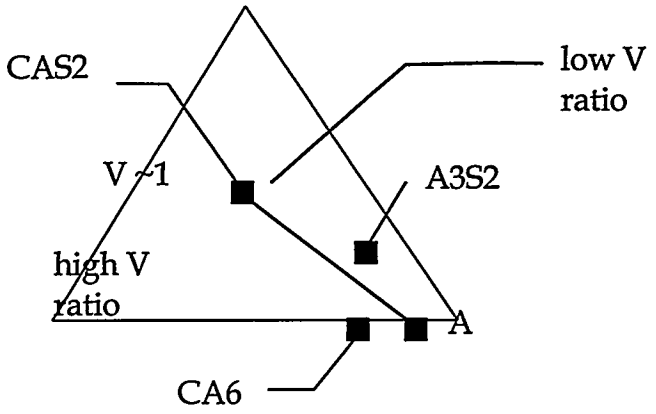

2. between altered solid refractory minerals, and minerals that are the products of further reactions, such as an interface between CA6 and CA2 phase formed by subsequent reaction of CA6 with lime or between CA6 and C2AS.

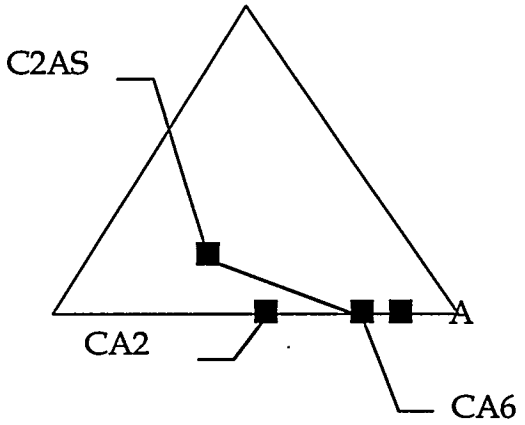

3. this process continues until either the original mineral or a product of reaction is the primary mineral in a region of compatibility that also includes the molten ceramic phase composition at the operating temperature. The melting point of the mineral must exceed the operating temperature. An interface occurs between this solid mineral and the melt, at a composition which is given on the phase diagram approximately by the intersection of the straight line joining the solid mineral composition with the bulk molten ceramic phase composition and the liquidus surface. A mass transport layer occurs in the melt, the composition at the end points of the layer being the equilibrium melt composition and the bulk molten ceramic phase composition.

The melt/solid interface or "hot face" advances as a moving boundary, as does the maximum depth of penetration. The hot face is located approximately where the composition is at its melting point. In the absence of erosion the rate of advance is controlled by the balance of chemical kinetics and mass transfer, as reflected in the value of the Thiele modulus explained earlier.

Given a batch system, transport of material occurs until the molten ceramic phase composition equals the equilibrium composition and dissolution stops. For a laboratory experiment, the amount and composition of phases at equilibrium can be calculated using the lever rule on a ternary phase diagram. If there is enough corrosive molten ceramic phase present, the entire sample will be consumed. In an isothermal laboratory experiment with a large excess of molten ceramic phase the exposed sample will always be consumed eventually. In reality even inert coatings can only delay the approach to equilibrium. For this reason laboratory experiments are of short duration.

The importance of temperature control in CEP becomes immediately apparent. The more thermally stable reaction intermediates that exist, the better. This fact is especially relevant when these intermediates have compositions close to that of the bulk of the molten ceramic phase. Very little dissolved refractory can then form a large amount of saturated corrosion product. For example, solid anorthite will be formed at 1500°C as a reaction product when the refractory is alumina and the molten ceramic phase is primarily calcium silicate. At 1600°C no solid diffusion boundary layer of anorthite is formed and the alumina dissolves readily into the molten ceramic phase.

In addition, the intrinsic kinetics of reaction typically increase with temperature exponentially as in an Arrhenius expression:

$$k_{rxn} = A_0 e^{-E_a/RT}$$

where k_{rxn} is the reaction rate constant, A_0 the preexponential factor, E_a the activation energy, R the universal gas constant, and T the temperature.

Experiments have been performed in the laboratory which confirmed the dramatic increase of wear rate with temperature. Data are shown in Figure 5.86 plotted alongside a curve given by the relation $k = 2.84 \times 10^{17} \exp(-78000/T)$, where T is in Kelvin. However, those were not isothermal experiments and the intrinsic effect of temperature may have been greatly underestimated.

A multisample wear test unit has been constructed at MMT to remove non-isothermal effects on the sample performance and study isothermal corrosion rates of samples.

Figure 5.86
Wear Rate of a Specific Refractory Material at 350 rpm

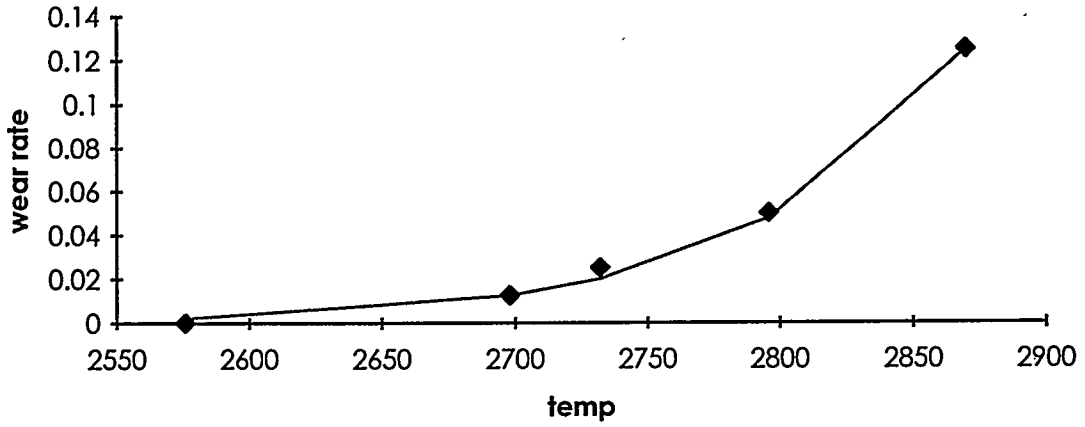

5.2.5.6. Mechanical Wear of Corroded Solid and Adhered Molten Ceramic Phase (Isothermal Erosion)

While unreacted refractory is practically immune to erosion in CEP, much of the mechanically weak solid corrosion products and adhered glasses will be exfoliated by high shear before they react to an equilibrium liquid. Their reaction proceeds in the bulk. When this happens the hot face evolves according to a balance of mechanical equilibrium, rather than thermodynamic (melting point) equilibrium.

In an isothermal situation when diffusional transport is rate-limiting, varying agitation can have a most profound effect on the rate of wear. Erosive wear comprises species transport from the surface to the bulk where the melt/solid interface is determined by mechanical, not chemical, equilibrium. Diffusion of materials in the remaining corroded layer is balanced by erosion which conveys material to the bulk. The diagram below contrasts an interface at chemical equilibrium where the surface average concentration is at the liquidus concentration, with an interface at mechanical equilibrium.

The erosion can be approximated by an erosive mass transfer coefficient at the surface h_s:

$$h_s(c - c_s) = D_{eff}(\nabla c)_s$$

where c_s is the vector of component concentrations at the melt/solid interface, and $(\nabla c)_s$ is the concentration gradient at the surface. An overall effectiveness factor can be written, where η' is based on the penetration depth x'_{mal} under conditions of mechanical equilibrium which is reduced from the earlier x_{mal} which was based on thermodynamic equilibrium alone:

$$\frac{1}{\eta_{overall}} = \frac{1}{\eta'} + x'_{mal}\frac{k_{rxn}}{h_s}$$

The effectiveness factor $\eta_{overall}$ will approach η' when the penetration depth becomes very small due to high erosion, and then the limiting rate will become the intrinsic chemical reaction kinetics. In an isothermal situation increasing the agitation rates to the point of most severe erosion will result in corrosion becoming the wear rate-limiting factor.

Tests have already been done in the laboratory to observe the effect of increasingly erosive condition on wear rate. The results shown below may actually overestimate the effect of erosion, because the tests were nonisothermal and the results may reflect simply increased heat transfer, which may dominate erosion. Isothermal tests at varying agitation rates can be performed in the multisample test apparatus to determine the effect of true erosion on the wear rate.

Figure 5.87
Integral Wear Rate versus Agitation Speed

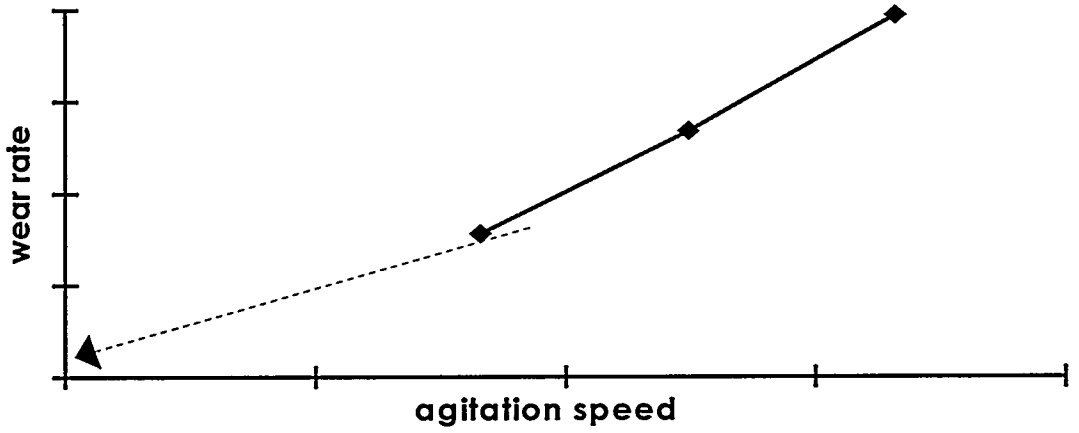

5.2.5.7. Synthesis of Mechanisms in Realistic Service (Nonisothermal Wear)

5.2.5.7.1. The Thermal Profile and the Existence of an Equilibrium Refractory Thickness

The thermal profile and thermal properties of the containment can independently be varied to dictate the manner in which individual wear mechanisms affect the overall wear of containment. A quasi steady-state one-dimensional heat transfer model neglecting interfacial resistance is sufficient to illustrate the coupling.

Heat is transferred from the bulk of the melt to the containment lining. This is modeled with an effective heat transfer coefficient, and a driving force proportional to the difference between the melt temperature (T_m) and the surface temperature (T_s). When the transfer coefficient h_m is large compared to conduction through the lining, then the surface temperature T_s becomes nearly equal to the bulk melt temperature T_m.

$$Q = h_m A(T_m - T_s)$$

where Q is the rate of heat conduction and A is the surface area.

Heat is conducted through the affected layer, composed of corrosion products, and located on the hot face surface. This is approximated with linear conduction. The thickness of the layer, x_{mal}', can be a function of mechanical erosion. The temperature T_c is defined as the temperature at the point where unaffected refractory forms (the maximum penetration of corrosive material). Areas closer to the shell are below this temperature and no solid state reactions are occurring there.

$$Q = \frac{k_{mal}}{x_{mal}} A(T_s - T_c)$$

Through these first two layers, the heat conduction may be expressed as:

$$Q = \frac{1}{\frac{1}{h_m} + \frac{x_{mal}}{k_{mal}}} A(T_m - T_c)$$

Similarly, heat loss through the refractory layer, safety lining, insulation and shell can be written, where T_∞ is the ambient temperature.

$$Q = \frac{1}{\frac{x_r}{k_r} + \frac{x_{safety}}{k_{safety}} + \frac{x_{ins}}{k_{ins}} + \frac{x_{shell}}{k_{shell}} + \frac{1}{h_\infty}} A(T_c - T_\infty)$$

Given enough time, the lining will wear toward an equilibrium thickness. At system equilibrium the affected layer stops at a location with temperature T_c^*, where T_c^* is a critical temperature below which either reaction or transport rates become negligible. Sometimes this isotherm is referred to as a molten ceramic phase freeze plane. This temperature is dependent upon the specific chemical corrosion reaction or the

diffusivity of a corrosive component. The hot face is arrested at a point where mechanical shear forces are insufficient to further erode the surface affected layer, which obtains a thickness x_{mal}*.

The equations above can be solved for the thickness of working refractory at system equilibrium conditions, x_r*. The larger that x_r* becomes, the more resilient the refractory lining is to system fluctuations. By doing this mathematical transformation the variables which directly affect equilibrium refractory thickness can be easily identified. Immediately apparent is that a large insulation thickness can yield a zero or unachievable negative value for equilibrium refractory thickness. Physically, this means that the refractory lining will be completely consumed before equilibrium is reached.

$$x_r^* = k_r\left[\frac{(T_c^* - T_\infty)}{(T_m - T_c^*)}\left(\frac{1}{h_m} + \frac{x_{mal}^*}{k_{mal}}\right) - \frac{x_{safety}}{k_{safety}} - \frac{x_{ins}}{k_{ins}} - \frac{x_{shell}}{k_{shell}} - \frac{1}{h_\infty}\right],$$

$$x_r^* \geq 0$$

These factors are summarized in the table below.

Table 5.49

Process variables which increase x_r*	**Process variables which decrease x_r***
1. low melt temperature T_m	1. high melt temperature T_m
2. inert molten ceramic phase composition with high T_c*	2. reactive molten ceramic phase composition with low T_c*
3. low mechanical erosion giving thick x_{mal}*	3. high mechanical erosion giving thin x_{mal}*
4. low wall convection giving low h_m	4. high wall convection giving large h_m
Design variables which increase x_r*	**Design variables which decrease x_r***
1. high refractory thermal conductivity k_r	1. low refractory thermal conductivity k_r
2. high heat transmission behind the working refractory to ambient	2. insulation behind the working refractory
3. large bath diameters giving low h_m	3. small bath diameters giving large h_m

A more sophisticated two-dimensional model is presently being developed and will be used to profile the predicted equilibrium thickness in an actual reactor shape. In a qualitative sense, the observed lining wear profile in the demonstration-scale CPU agrees with the fact that the lining is simply wearing back to approach an equilibrium thickness.

Experimentally, a main focus of the Integrated Containment Test Facility (ICTF) will be to isolate optimal combinations of refractory and heat transfer situation for optimizing refractory lining loss. In addition, experiments to be conducted on the CPU will compare thermally conductive backup lining to thermally insulating backup lining.

Three types of lining selections could emerge:

1. A well-insulated lining can be chosen that will eventually wear out completely but its rate of failure will be very slow (continuous nonequilibrium wear). This may be the most advantageous for the purposes of energy efficiency and frequent shutdown time.

2. A conductive lining could be installed with a thickness equal to or even less than its equilibrium thickness to entirely eliminate wear. This is probably the best in terms of contamination from the melt due to wear of the lining and process control.

3. A lining could be installed which has an expendable wear face, and will recede to equilibrium. This may be the best compromise for most long-term applications since rates of wear close to equilibrium are very slow, and the lining retains more insulation to aid in the energy cost.

5.2.5.7.2. Refractory Wear as an Approach to Equilibrium

As a first-order approximation a refractory lining may wear at a rate proportional to the departure from equilibrium thickness (x_r^*), where A is a constant determined by the transient mechanisms of wear:

$$\frac{dx_r}{dt} = -A(x_r - x_r^*)$$

That governing equation would yield the following relationship of thickness (x) versus time (t):

$$x_r = x_r^* + (x_r^{t=0} - x_r^*)e^{-At}$$

Observations of temperature in the CPU have shown real-time trends, such as that shown in Figure 5.88, which could be fitted with such an exponential relationship. The exact value of the rate constant A is determined by the overall effectiveness factor, the Thiele modulus evaluated at surface conditions, the thermal gradient and the activation energies for reaction and diffusion.

Figure 5.88

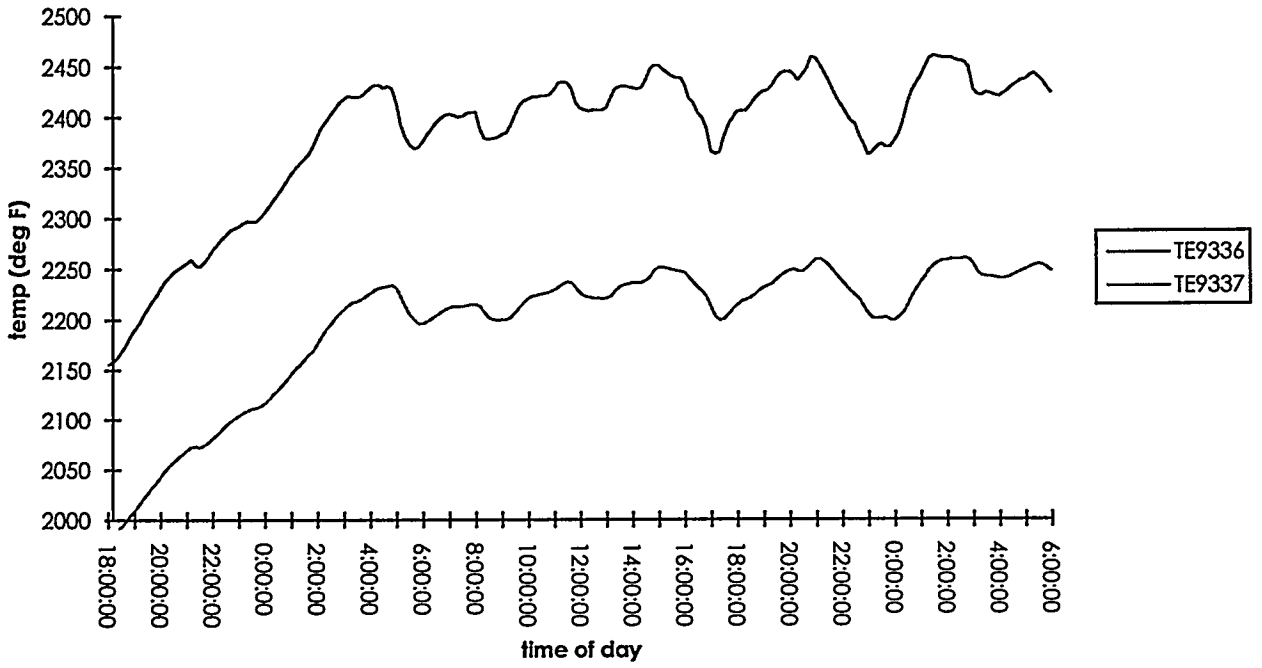

In reality, there are multiple phases in the refractory which may delay the lining wear. If a second phase having rate constant A_2 is introduced to protect the dissolving phase which has rate constant A_1, the wear may proceed as consecutive reactions of two phases, and the following approximate trend for refractory thickness would apply. It can be seen that if the protecting phase reacts slower than the original refractory ($A_2<A_1$), then the time required to reach equilibrium thickness is considerably delayed by the slower reaction. The equation demonstrates the usefulness of an inert coating or shrouding phase for slowing the approach to equilibrium.

$$x_r = x_r^* + (x_r^{t=0} - x_r^*)\frac{A_1 e^{-A_2 t} - A_2 e^{-A_1 t}}{A_1 - A_2}$$

5.2.5.8. Conclusions

The wear of refractory materials has been discussed. It is recognized that factors controlling wear are the thermal profile, chemistry, mechanical erosion and refractory

microstructure. In a real application it is seen that a lining can be designed for steady wear, for zero wear, or for wear rates decreasing toward equilibrium thickness. The most important parameter for design of containment with a given material is heat transfer. The individual mechanisms of corrosion and erosion can be identified through isothermal experiments, where sample materials' wear is simulated. Post-mortem examinations of worn refractory are key for identifying wear mechanisms in the field.

Efforts are underway on several fronts to advance understanding of refractory wear and minimize wear rates on linings. These efforts are summarized in Table 5.50.

Table 5.50

Focus Area	Description Of Present Efforts
Design	• induction furnace design with barrier plate • CPU redesign with Narco
Material Selection	• evaluation of test coupons in CPU compared to baseline wear • new tuyere plug materials • expansion of refractory vendor contacts
Micro-structure	• evaluation of low-porosity materials as tuyere plug for CPU and molten ceramic phase line for integrated facility
Corrosion	• isothermal experiments of multisample wear test
Erosion	• isothermal experiments of multisample wear test at varying rotation rate
System Design	• integrated containment test facility for equilibrium wear experiments • model development for prediction of equilibrium thickness profiling • post-mortem work to determine controlling mechanism of wear or equilibrium thickness development

The existence of a theoretical equilibrium refractory thickness has been shown with the aid of a simple thermal model. This quasi-steady state thickness depends critically on heat transfer and, specifically, heat conduction through the refractory lining. The key design variables in achieving stable refractory thickness are:

- thermal properties (conductivity) of the refractory and outer containment,
- equilibrium chemistry (thermodynamics) of the corrosive agents, and

- agitation (erosion).

Given a containment design and materials selection, the key process-related variables determining the rate at which wear occurs until equilibrium is reached are:

- speed of mass transport through the reacted layer,
- chemical kinetics of the corrosive agents, and
- agitation (erosion).

5.3. Delisting of Product Phases

MMT has prepared a draft petition for the ceramic product generated by the Q-CEP™ processing of mixed waste which is presented as exhibit (1). The following strategy was used in preparing the petition:

- Identification of the most common DOE mixed waste streams and the most commonly found hazardous waste constituents within those streams
- Formulation of a surrogate the evaluation of the surrogate was based on the property of elemental partitioning (i.e., the elemental compositions determine the processing efficiency).
- Provision of additional data to support CEP's efficiency in processing other hazardous constituents (primarily organics data)
- Mapping unprocessed material to existing data (i.e., transfer of data based on elemental conversion and partitioning).

MMT representatives met with EPA headquarters representatives in January 1996 to discuss the delisting petition review process. EPA headquarters indicated that due to fiscal constraints, headquarters personnel would no longer participate in the delisting petition review process. MMT was instructed to contact EPA Region IV to conduct the delisting petition review. MMT representatives subsequently met with EPA Region IV representatives in February 1996 regarding the conduct of a review of the delisting petition. EPA Region IV has indicated that it will perform a review of the delisting petition. MMT plans to conduct an informal review of the petition with Region IV representatives prior to formal submission of the delisting petition.

6. Task 1.5 Experimental Testing of Resource Conservation and Recovery Act (RCRA) Wastes

6.1. Pilot-Scale Processing of RCRA-Listed Waste

6.1.1. Overview

Chlorinated waste is a major element of concern for RCRA wastes under regulations. In addition, the increasing awareness of dioxins' and furans' effects on human health makes success in processing chlorinated organics a crucial factor to demonstrate CEP's effectiveness in processing RCRA wastes. Starting from the scoping tests carried out under the chlorine study campaign, major goals to be achieved are outlined as shown in Table 6-1. On-going studies were designed to set up the path to solve these problems.

Table 6-1
Chlorine Study Strategy

Goals	Evaluation Method	Methodology
Destruction of Hazardous Chlorinated Organics:	• Feed and system output quality analysis: off-gas, ceramic, metal, particulate, scrubber water detection for feed hazardous materials	• System design to ensure complete conversion of feed materials to products
Capture of Chlorine in Stable Final Form	• Chlorine Partitioning • Mass Balance Closure • Ceramic and Metal Phase Analysis	• Operation conditions design and control for steady state operations • Ceramic composition design for capture of Cl
Minimal Byproducts Formation	• Off-gas Quality Characterization	• GHT design precluding byproducts formation and providing appropriate sampling location • Analytical methods and sampling protocol to represent accurately the performance of the process

6.1.2. VPR and APU Studies on Chlorine

6.1.2.1. Introduction

The bench-scale scoping studies outlined the possibilities of chlorine capture in CEP based on fundamental principles and verified by experimental data. Potentially, chlorine can be captured in either the gas phase as HCl, calcium chloride if calcium is present in the system, or in the ceramic phase with a ceramic composition that has a high retention of chlorine. The first set of pilot-scale experiments focused on processing in an iron bath in order to evaluate chlorine partitioning, off-gas quality, and mass balance closure. The data generated from the bench- and pilot-scale will be used to develop conditions of optimal design and operation of demonstration-scale CEP reactors for effective processing of chlorinated hazardous waste.

6.1.2.1.1. Experimental Setup

Experiments were carried out in the Advanced Processing Units (APU). The APU1 is comprised of a refractory based (crucible) system enclosed in a stainless steel containment vessel. APU2 is a refractory lined system with the capability to inject feed material either through a submerged lance or a tuyere. Both furnaces are heated by induction. Solids and/or gases are conveyed into the metal bath via the fluidizer or the screw feeder through either a submerged lance or tuyere. Product gases are withdrawn with a vacuum pump from each reactor through a gas handling train (GHT). The GHT consists of a dust trap, a high efficiency particulate (HEPA) filter, and an acid gas scrubber common for both reactors. Solid injection into the APU2 was carried out in a single pipe tuyere along with argon carrier gas. For the APU1, feed materials were injected through the refractory lined lance along with argon carrier gas.

6.1.2.1.2. Gas Analysis method

Product gases were analyzed semi-continuously by on-line gas chromatography via thermal conductivity detection (GC/TCD). The concentrations of hydrocarbons, H_2, CO, CO_2, and O_2 were measured during each injection. The primary gas species and HCl concentrations (before scrubber) were measured continuously by mass spectrometer (whenever available) as a check for GC. Gas samples (of selected tests) collected in SUMMA canisters were analyzed for volatile organic compounds by combined gas chromatography/mass spectromety. These analyses were performed by an independent third party using EPA Method TO-14. Total hydrocarbons in the off-gas were measured continuously during later experiments.

6.1.2.2. Operational procedure

Table 6-2 summarizes processing test conditions.

Table 6-2
Processing Conditions in APUs Experiments

Process Variable	Description
Chlorinated Surrogate	CH_3Cl (g) PVC (s)
Metal depth	Proprietary
Carbon level	Proprietary
Bath Temperature	Proprietary
Feed Rate	Proprietary
Particle size	Proprietary
Ceramic System	(Ca-Al-Si) System
Injection Method	VPR: gas-cooled, refractory-lined lance APU: Tuyere

The experimental campaign was divided into three sections. APU1 runs were mainly for compliance purposes which set up the limits for chlorine injection and emission limits. A second set of experiments on the APU2 focused more on gas product generation and used pure surrogate in the experiments. The third set of runs, also on the APU2, further confirmed chlorine partitioning, and examined off-gas trace quality.

The following analyses were performed during the runs:

- DEP compliance testings for chloride injection and chlorine off-gas emission
- Evaluation of injection procedure
- Gas Chromatography and on-line mass spectrometer data collection for CO, H_2, CO_2, HCl, NO_x, SO_x, HCN, H_2O, etc.
- Ceramic layer observations
- Metal, ceramic, and particulate sample analysis
- C_1-C_3 off-gas concentration analysis
- VOC (Volatile Organic Constituent) detection in the off-gas
- SUMMA and XAD samples collection for dioxins measurement

6.1.2.3. Processing Results

6.1.2.3.1. HCl Generation

Thermodynamically, chlorine is expected to partition evenly to HCl and ferrous chloride under the given test conditions. The experiments were designed to verify the theoretical predictions. The amount of HCl generated from the feed was quantified by analysis of chloride ion concentration in the scrubber solution and the amount of HCl detected from off-gas using mass spectrometry, SUMMA, and XAD analysis. The experiments in the APU1 for DEP compliance were of short duration and limited injection consistency, hence resulted in a low generation rate of HCl. The HCl recovery in the gas phase during the APU2 runs was found to be consistently in the range 50-60%. Table 6-3 summarizes the distribution and recovery of chlorine as HCl during the APU runs. The results shown originated from a wide variety of feed materials: APU2 15,16, 36-39 used pure chlorine surrogates, APU2 40-41 included Ni, Pb, Zn, and Ag in the system, and APU2 42 include Hf in addition to the above listed elements.

Table 6-3
HCl Generation and Distribution

Run #	Cl Feed (g)	Cl as Particulate (g)	HCl in Scrubber (g Cl-)	HCl in Gas Sampling Stream (g)	Total HCl (g Cl-)	Total HCl Recovery (%)[3]
100-94-APU15	459.43	[1]	224	105.38	329.38	71.69
100-94-APU17	439.58	[1]	322.1	66.56	388.66	88.41
100-94-APU36	284.86	41.5	61.25	20.73	81.98	28.78
100-94-APU37	712.16	81.3	317.8	114.06	431.86	60.64
100-94-APU38	474.78	87.17	335.14	93.59	428.73	90.3
100-94-APU39	593.47	87.06	122.42	163.84	286.26	48.23
100-94-APU40	483.25	149.73	159.82	33.5	193.32	40.00
100-94-APU41	850.8	177.88	274.3	98.37	372.67	43.8
100-94-APU42	385.41	87.42	221.48	17.35	238.83	61.97
100-94-APU43	332.34	29.57	235.65	[2]	235.65	70.91

[1] Unknown dust quantity due to frequent filter change.
[2] Mass Spec was under repair, hence no gas sampling stream data.
[3] Variation in HCl recovery may be due to sampling error from the scrubber water.
Note: Overall recovery of chlorine will be presented in the mass balance section

6.1.2.3.2. Chlorine Partitioning

The distribution of chlorine shown in Table 6-3 indicated the partitioning of chlorine as HCl gas and ferrous chloride particulate, which agreed with the theoretical predictions. Potentially, the ferrous chloride will be reinjected into the system during long term processing. The development of ceramic systems with high chloride retention potential will be the subject of further testing.

6.1.2.3.3. Product Gas Composition

Product gases during APU2 tests were analyzed both by a mass spectrometer and a gas chromatograph. The mass spectrometer (MS) measures major gas components such as CO, H_2, HCl, O_2, N_2, CO_2 every twenty seconds; while the gas chromatograph via thermal conductivity detection (GC/TCD) measures all the above components and hydrocarbons every five minutes. Table 6-4 summarizes the off-gas analysis using GC and MS analytical results. Low concentrations of C_1-C_3 were detected, consistently. The composition of H_2, CO, and HCl varied depending on the feed materials.

Table 6-4
Off-Gas Composition

		Vol. (%) Balance by Argon							
Run#	Off-gas[1]	H_2	CO	CO_2	CH_4	C_2H_2/ C_2H_4	C_2H_6	C_3H_6/ C_3H_8	HCl
APU14	GC	4.74	0.62	0.065	0.001	0.0007	0.0001	0.00	-
	MS	5.7	0.00	0.029	0.00	-	-	-	2.53
APU 20	GC	6.70	10.19	-	0.00	0.00	0.00	0.00	-
	MS	6.37[3]	13.17[3]	0.44	0.00	-	-	-	2.17
APU 36	GC	3.53	0.33	0.13	0.00[1]	0.00[2]	0.00[2]	0.00[3]	
	MS	2.58	1.34	0.28	0.00	-	-	-	0.52
APU37	GC	6.82	0.35	0.17	0.00	0.00	0.00	0.00	-
	MS	5.88	2.06	0.14	0.00	0.00	0.00	0.00	2.86
APU39	GC	11.77	0.51	0.17	0.00	0.00	0.00	0.00	-
	MS	9.18	1.90	0.04	0.00	-	-	-	4.94
APU40	GC	5.40	45.03	0.23	0.00	0.00	0.00	0.00	-
	MS	7.08	45.14	0.26	0.00	-	-	-	1.26
APU41	GC	4.29	23.03	0.76	0.00	0.00	0.00	0.00	-
	MS	5.09	24.26	0.72	0.00	-	-	-	1.85

[1] Gas Composition balanced by argon as carrier gas
[2] Hydrocarbons below detection limit
[3] H2 and CO ratio were in agreement with the feed rate

6.1.2.3.4. Off-Gas Trace Quality

The gas samples of selected tests were collected in SUMMA canisters and analyzed for volatile organic compounds by combined gas chromatography and mass spectromety. These analyses were performed by an independent third party using EPA Method TO-14.

The off-gas from the APU1 tests were analyzed only by GC/TCD. Hydrocarbons present were predominantly methane and C_2 with a range of 10-100 ppm. The C_3-C_4 compounds were always found to be below the detection limit (Lower Detection Limit (LDL) = 10 ppm). Low concentrations of hydrocarbons were found during the APU1 runs, consistently. Total hydrocarbon (THC) analyses were obtained continuously in

several APU1 runs via Flame Ionization Detection (FID) with a detection of methane on the order of 10-100 ppm. CH_4 concentrations in Run APU1 14-21 were all in the low ppm range (10 ppm by GC/TCD). The concentrations of C_2-C_4 were below the detection limit (< 1 ppm). SUMMA samples were analyzed for hydrocarbons and TO-14 species. Methane was detected in the range of 10-80 ppm, while light hydrocarbons (C_2-C_4) were detected only in very low ppm range (0.1-1 ppm). Other chloro-organic compounds under the EPA method TO-14 were found to be in single digit ppb level or not detected (LDL = 10-20 ppb). Presence of methane, although in very low concentrations, was attributed to reformation reactions in the headspace. Further design modifications would make sure that the reformation of hydrocarbons will be minimal.

DRE Calculations were performed using the formula:

$$DRE = 1 - (ppb * DF/10^9 ppb) * 100\%$$

where DF was assumed to be 4. Calculated DRE's for CH_3Cl and vinyl chloride were > 99.9999%.

6.1.2.3.5. Mass Balance

Mass balance closure was carried out on elemental carbon, hydrogen, and chlorine based on off-gas flow and analysis, feed rate, and feed elemental analysis. The amount of hydrogen and chlorine injected was based on the amount of feed material fed and the stoichiometric elemental ratio. Since carbon was present in the metal bath throughout the experiment, the amount of carbon contributed to a particular run was the difference between the sum of initial bath carbon and injected carbon (based on stoichiometric feed composition) and the final bath carbon concentration. The amount of each element in the off-gas was determined by the mass spectrometer results (% of off-gas flow) and the measured off-gas flow. The mass balance closure is the ratio between the amount detected in the off-gas over the amount contributed to the run. Table 6-5 summarizes the experimental amount in and out of the reactor, and Table 6-6 summarizes the elemental balance for C, H, Cl.

Table 6-5
Material Accounting In and Out

Run #	Carbon Change based on Analysis (initial + feed - final)	Carbon Recovered (CO & CO_2) in the off-gas analysis	Hydrogen Fed (based on injected feed)	Hydrogen Recovered (H_2) in the off-gas	Chlorine Fed (based on injected feed)	Chlorine Recovered (include off-gas, particulate, and ceramic as specified)
VPR18	460	394	120	104.47	NA[3]	NA
VPR20	220	221	280	259	NA	NA
APU15	NA	NA	290.3	271.26	NA	NA
APU17	NA	NA	277.8	271.7	439.58	388.66[1]
APU37	NA	NA	450	449.56	712.16	513.16
APU40	1115	1235	305.35	275.24	483.25	343.05
APU41	1380	974	539.75	655.99	850.8	550.55
APU43	802	523	210	217.05	332.34	265.22+C[2]

[1] Unknown dust quantity due to frequent filter change
[2] Include 14.12% Cl-capture in ceramic layer
[3]NA=Not Analyzed

Table 6-6
Mass Balance for Elemental C, H, Cl

Run #	C Balance (%)	H Balance (%)[2]	Cl Balance (%)[3]
VPR18	85.7	87.06	N.A.
VPR20	100.0	92.5	N.A.
APU15	N.A.[4]	93.4	N.A.
APU17	N.A.	97.8	88.4
APU37	N.A.	99.9	72.1
APU40	110.8	90.1	71.0
APU41	70.6	121.5	64.7
APU43	65.2[1]	103.4	*78.1*

[1] Variability of feed flow made mass balance calculations difficult
[2] Mass Balance for H was usually >90% except the VPR runs where flow rate of CH3Cl was varied due to increased pressure in the dust trap
[3] Overall Cl balance was in the range of 70-80%. The remaining Cl is expected to be associated with refractory which contain Ca and Mg. The amount of dust, which was difficult to quantify, also affected the mass balance closure
[4]N.A.=Not Analyzed

6.1.2.4. APU/VPR Summary Results

Pilot-scale studies on chlorine focused on processing chlorinated organic materials in an iron bath. Off-gas analysis indicated the formation of hydrogen and carbon monoxide in gas stream. Volatile organic compounds C_2-C_4 in the off-gas were in the low ppm

(0.3-1) range. DRE of chloro-organic compounds were > 99.9999%. Chlorine was partitioned to HCl and ferrous chloride which was collected in the GHT. Further studies on the capture of chlorine in the ceramic phase are warranted. The high quality of off-gas indicated the effective processing of organic chlorinated materials.

6.2. Thermochemistry of Chloride/Fe/Ni System

Under CEP conditions, chlorine can be partitioned to the gas phase as hydrogen chloride and/or metal chloride, or a ceramic system can be designed with a high chloride retention capacity. Metal/ceramic systems were evaluated in this experimental campaign for their ability to capture chlorine. Chloride partitioning was quantified for chlorinated gas injection into metal/ceramic phase systems. Moreover, the effect of ceramic phase composition on chloride saturation values was examined. The run parameters shown in Table 6-7 were used for this campaign.

Table 6-7
Experimental Runs

Run No.	Metal	Ceramic Phase CaO-Al_2O_3-SiO_2	Injection Gas Mix	Crucible
test 1	none	none	$HCl/CO/H_2$	graphite
test 2	none	none	$HCl/CO/H_2$	graphite
1	Fe	none	$HCl/CO/H_2$	graphite
2	Ni	none	$HCl/CO/H_2$	graphite
3	Fe	MMT Proprietary	$HCl/CO/H_2$	graphite
4	Fe	MMT Proprietary	$HCl/CO/H_2$	graphite
5	Fe	MMT Proprietary	$HCl/CO/H_2$	graphite
6	Fe	MMT Proprietary	$HCl/CO/H_2$	graphite
7	Fe	MMT Proprietary	$HCl/CO/H_2$	graphite
8	Ni	MMT Proprietary	$HCl/CO/H_2$	graphite
9	Ni	MMT Proprietary	$HCl/CO/H_2$	graphite
10	Fe	MMT Proprietary	$HCl/CO/H_2$	graphite
11	Ni	MMT Proprietary	$HCl/CO/H_2$	graphite

The $HCl/CO/H_2$ gas mixture was used to simulate injection of chlorinated organic compounds, such as those found contaminating much DOE scrap metal. Titration data were obtained using the first scrubber, which contained NaOH solution. Once the titration of the first scrubber was complete, the gas stream was diverted to the second gas train and injection continued. The titration curves from the first scrubber were used to determine the relative concentration of HCl in the gas stream, which will be referred to as HCl generation.

Chloride partitioning was determined by analyzing the total HCl in the gas phase (using both scrubbers), and the chloride content of the dust and ceramic phases. The ceramic phase analysis was performed by both MMT's XRF Uniquant and an independent third-party analytical laboratory which utilized XRF for the major components, ICP for minor components, and ion selective electrode for chloride analysis. Titration data (curves) and chloride partitioning data were used to characterize the behavior of metal and metal/ceramic systems.

HCl in the off-gas stream was measured using strong acid/base titrations. Comparisons can be made between data (see Table 6-8) with common process parameters, and general conclusions can be drawn from features of the titration curves. In particular, extended delay times in the titration curves indicate chloride capture in the ceramic phase. During this time there was minimal HCl generation and dust formation. The actual delay time of the titration (i.e., chloride capture before HCl generation) was dependent on the ceramic phase composition and the process conditions. At a particular chloride concentration in the ceramic phase, HCl was detected in the off gas; this point was identified by the onset of deflection of the titration curve. The slope of the titration curve indicates the rate of HCl generation; the steeper the slope of the curve, the greater the HCl concentration in the gas stream.

Table 6-8
Comparisons of Titration Onset and Completion Times for Various Metal/Ceramic Systems Shown in Figure 6.1

Metal/Ceramic System	Onset of Titration[1] (minutes)	Final Titration Time (minutes)
Fe	7.5	27.5
Fe/ Phase 1 Ceramic System	19	68.5
Fe/ Phase 2 Ceramic System	60	109
Fe/ Phase 3 Ceramic System	81	137

[1]The onset on titration was determined using a slope intercept method.

6.2.1. Results

Figure 6.1 shows the gas titration data for Fe and Fe/ceramic systems. The figure illustrates the effect of ceramic phase composition on chloride partitioning. The curves in Figure 6.1 display a wide variation in titration delay times and final titration times as a function of ceramic composition. The delay times are indicative of chloride capture in the ceramic phase, but do not represent the time to reach the chloride capacity of the ceramic phase. As the HCl concentration in the gas stream increases, the slope of the titration curve increases. The relative partitioning of the input Cl^- (i.e., Cl^- in the gas stream vs. Cl^- in the ceramic and dust phases) can be estimated by comparing the slopes of the process titration curves.

Figure 6.1
$HCl/CO/H_2$ Gas Injection into Iron and Iron/Ceramic Phase Systems
Ceramic Phase Compositions (Mol%) CaO-Al_2O_3-SiO_2

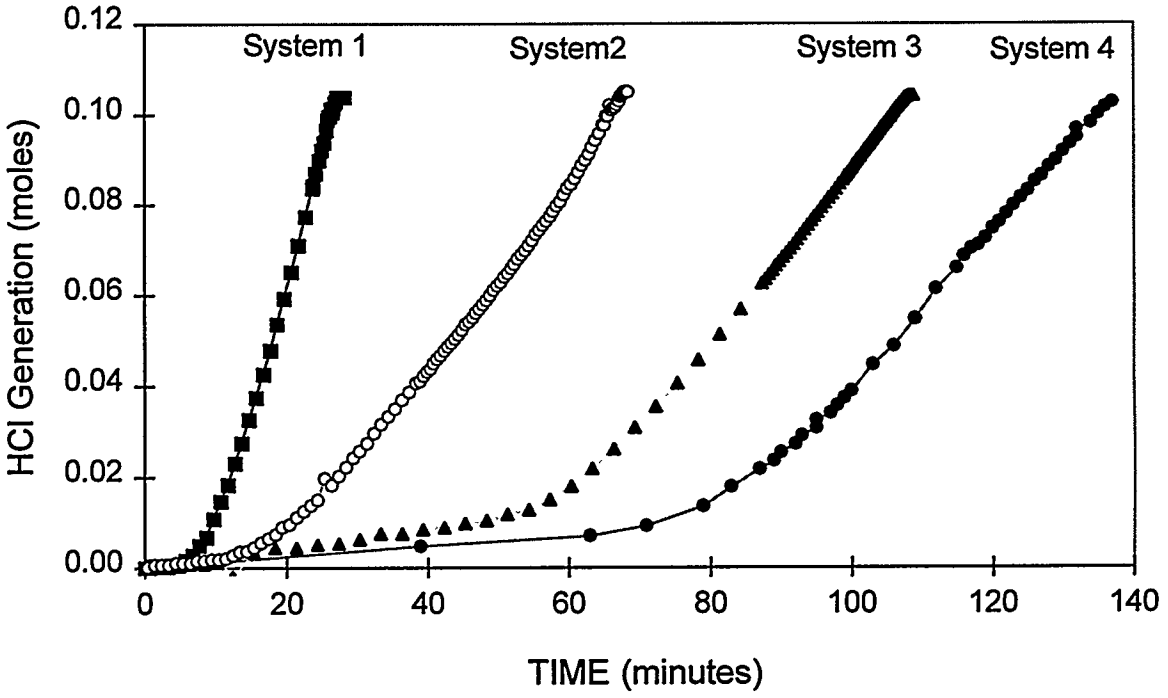

6.3. Demonstration Unit Processing of RCRA-Listed F024 Waste

6.3.1. Introduction

RCRA listed chlorinated waste F024 was processed successfully in MMT's demonstration-scale unit. The experimental campaign was carried out successfully as outlined below:

- steady state processing was demonstrated as evidenced by consistent feed injection and reliable product gas with steady volumetric flow and a consistent synthesis gas H_2/CO ratio;
- excellent total (99%) and component (100 ± 5% for C, H, O) mass balance closure;
- effective conversion of hazardous organics with DREs ≥ 99.9999% and no evidence of dioxin formation to the targeted regulatory limit of 0.1 ng TEQ/Nm^3;
- no organic constituents detected in the ceramic and metal phases which satisfied the regulatory limits for final form of materials (non-leachable).

6.3.2. Feed Composition

F024 (EPA RCRA-listed waste) is a mixture of chlorinated aliphatic hydrocarbons having carbon chain lengths ranging from one through five, with varying amounts and positions of chlorine substitution. Detailed analysis of the F024 waste was carried out to identify its hazardous constituents. Major volatile constituents, shown in Table 6-9, included 1,1,2-trichloroethane, chlorobenzene, 1,1,2,2-tetrachloroethane, and trichloroethane, which are mainly chlorinated aromatic compounds. Volatile compounds comprised nearly 99% of the feed, indicating its high toxicity.

Table 6-9
Major Constituents of F024 Waste (1T-94-09-S3)

Volatile Organics	µg/ℓ
1,1,2-Trichloroethane	18,000,000
Tetrachloroethane	9,700,000
Chlorobenzene	12,000,000
1,2-Dichloroethane	6,800,000
1,1,2,2-Tetrachloroethane	11,000,000
Trichloroethene	24,000,000
Xylenes	610,000
1,1,1,2-Tetrachloroethane	1,000,000
Sec-Butylbenzene	540,000
Tert-Butylbenzene	2,000,000
Hexachlorobutadiene	3,600,000
P-Isopropyltoluene	870,000
Naphthalene	900,000
1,2,4-Trimethylbenzene	1,100,000

An ultimate analysis test was performed to characterize the F024 waste. The analytical results are shown in Table 6-10.

Table 6-10
Ultimate Analysis of F024

Element	Wt%
C	31.15
H	2.73
N	< 0.5
S	0.077
Cl	67.30
Ash	0.1535
O	< 0.5
Moisture	549 ppm
Volatile Matter	99.12%
S.G.	1.4190
BTU/lb.	5,539

The F024 waste stream was mixed with fuel oil, chlorotoluene, and chlorobenzene before injecting into the CPU to emulate the processing of a heterogeneous waste feed. Table 6-11 summarizes the content of the mixture and the final elemental composition of the feed processed.

Table 6-11
Elemental Composition of the Feed Mixture

Element	Wt. %
C	72.5
H	9.76
O	0.1
Cl	17.63
The feed mixture consisted of: 21.6 wt% F024 63.6 wt% Fuel Oil 5.0 wt% Chlorotoluene 9.8 wt% Chlorobenzene	

6.3.3. Sampling Procedures

The samples taken and the analyses conducted during the F024 processing are outlined below:

Gas sampling: Samples of product gases were taken at the Baghouse using on-line summa canisters once every hour. Analysis of the summa canister gas samples was carried out using EPA method TO-14. Mass spectrometer samples were drawn on-line in two locations: before the gases entered the scrubber and after they exited the aftercooler. Measurements of the gas composition were taken every twenty seconds and logged into the PLC. A modified EPA method 23 was used to measure dioxins in the off-gas.

Metal sampling: Metal samples were collected before and after the injection by lowering a sealed sampling probe through the top of the reactor. The carbon concentration of metal samples was monitored using a LECO analyzer. Analyses of metal samples were carried out using an optical spectrometer capable of identifying the composition of a metal containing up to 16 elements. In addition, pre, during, and post injection samples were analyzed by using EPA method 8260 for volatile organics, 8270 for semi-volatile organics. Total halides and sulfur were analyzed for.

Ceramic sampling: Ceramic samples were collected before, and after feed injection. These samples were analyzed using EPA methods 8260, 8270 for organics.

Scrubber Water sampling: Scrubber water samples were collected at the discharge of the scrubber pump before, after, and once every hour during injection. Samples were analyzed by EPA methods 8260, 8270 for organics; total halides and sulfur.

6.3.3.1. Operational Issues

The processing of F024 was carried out on 30 June 1994 from 0:05:00 to 9:15:00. A total of 666 lbs of F024 mixture was processed continuously in 9 hours and 10 min. Approximately 3000 lbs of metal iron was melted in the CPU prior to processing the F024. The feed material was first loaded in a holding tank and then injected into the CPU reactor through the bottom tuyere. The weight of the holding tank was monitored to measure the amount of material injected into the system. Together with the feed, oxygen was injected as a co-reactant, methane as a cooling gas, nitrogen as purge gas, and argon as a tracer gas.

The temperature of the CEP system was maintained at 2700°F by thermocouple measurements and computerized control of heat addition of the induction coil. The carbon concentration (2.69%-2.82%) in the metal was monitored by a feed-forward control loop, hourly sampling, and on-line LECO carbon content analysis.

F024 was first mixed and loaded to the feed liquid tank before injection. Figure 6.2 shows the change in the weight of the feed liquid tank during injection. The curve shows a steady rate of liquid feed flow.

Figure 6.2
F024 Feed Injection

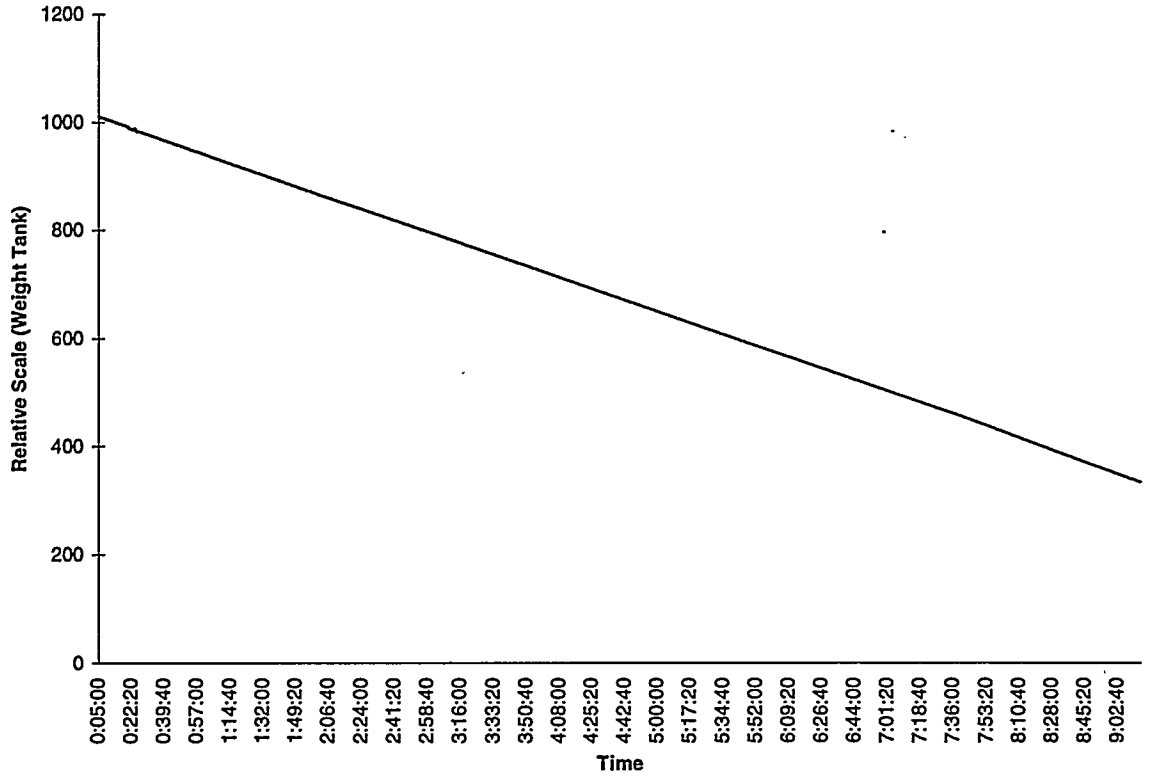

6.3.4. Steady State Operation

6.3.4.1. Off-Gas Flow and Composition

Figure 6.3 shows the process product gas flow. Steady flow of the off-gas stream was consistent with previous demonstration campaigns and validated that steady feed rates lead to steady product gas flows. Argon gas was used as the tie for determining output gas flow rates. The calculated product gas flow was compared with the gas flow to the reheater, which showed a direct correlation.

Figure 6.3
Off-gas Flow Rate during Processing of F024

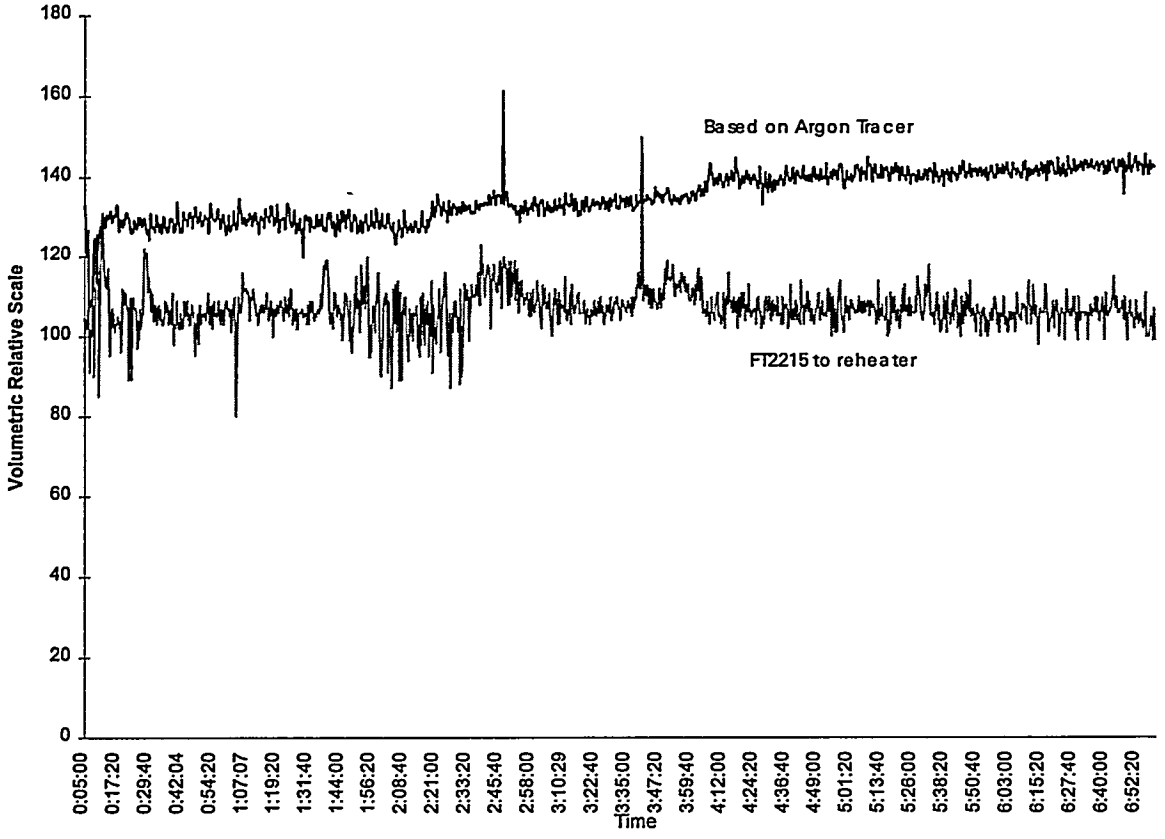

Figure 6.4 shows the flow of hydrogen, carbon monoxide, carbon dioxide, and hydrogen chloride throughout the run. Steady flow of hydrogen and carbon monoxide was achieved at the beginning of the demonstration run. Carbon dioxide flow decreased as the system approached steady state. Hydrogen chloride evolution began 2 hours after start of feed injection. The delay is attributed to the formation and volatilization of iron chloride particulates, which were then condensed in the gas handling train.

Figure 6.4
F024 Processing Product Components

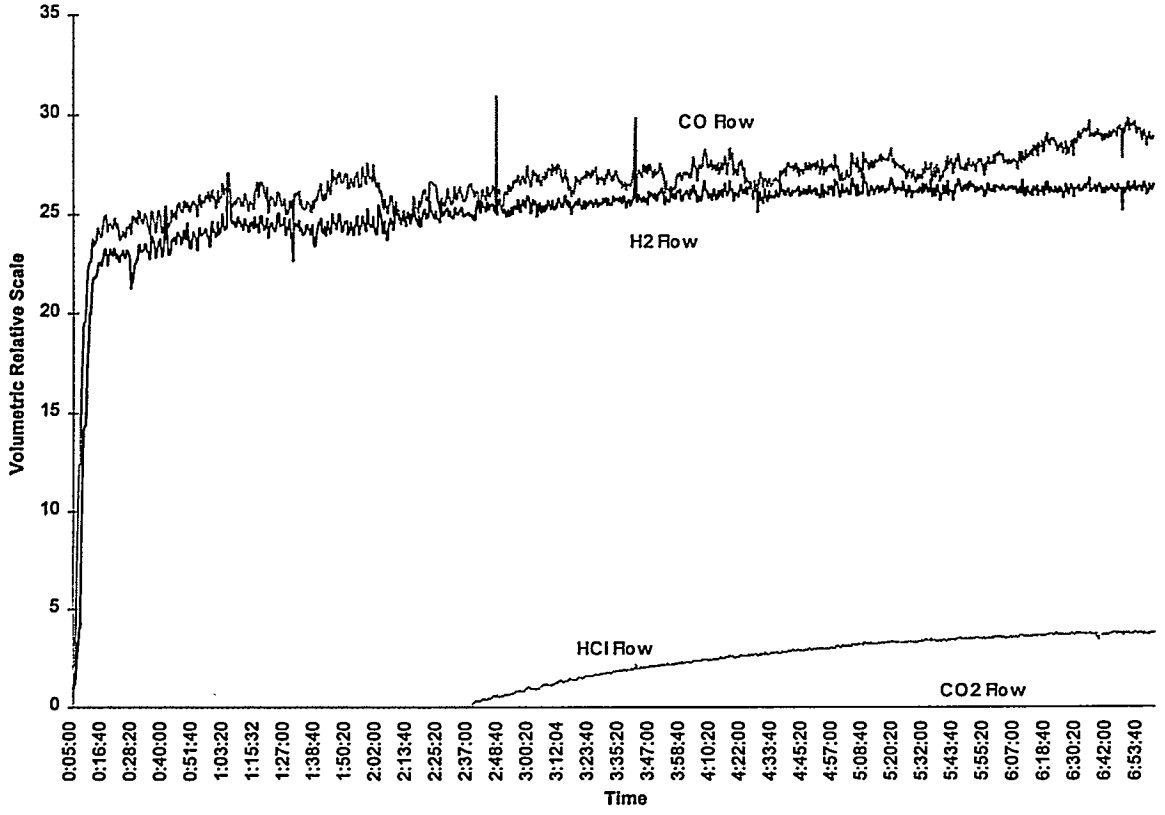

Consistent synthesis gas quality is illustrated by the constant H_2/CO ratio as shown in Figure 6.5. Moreover, the CO/CO_2 ratio was observed to increase during approach to steady-state conditions, which is a consistent phenomenon throughout CEP demonstration campaigns.

Figure 6.5
F024 Processing H_2/CO Ratio

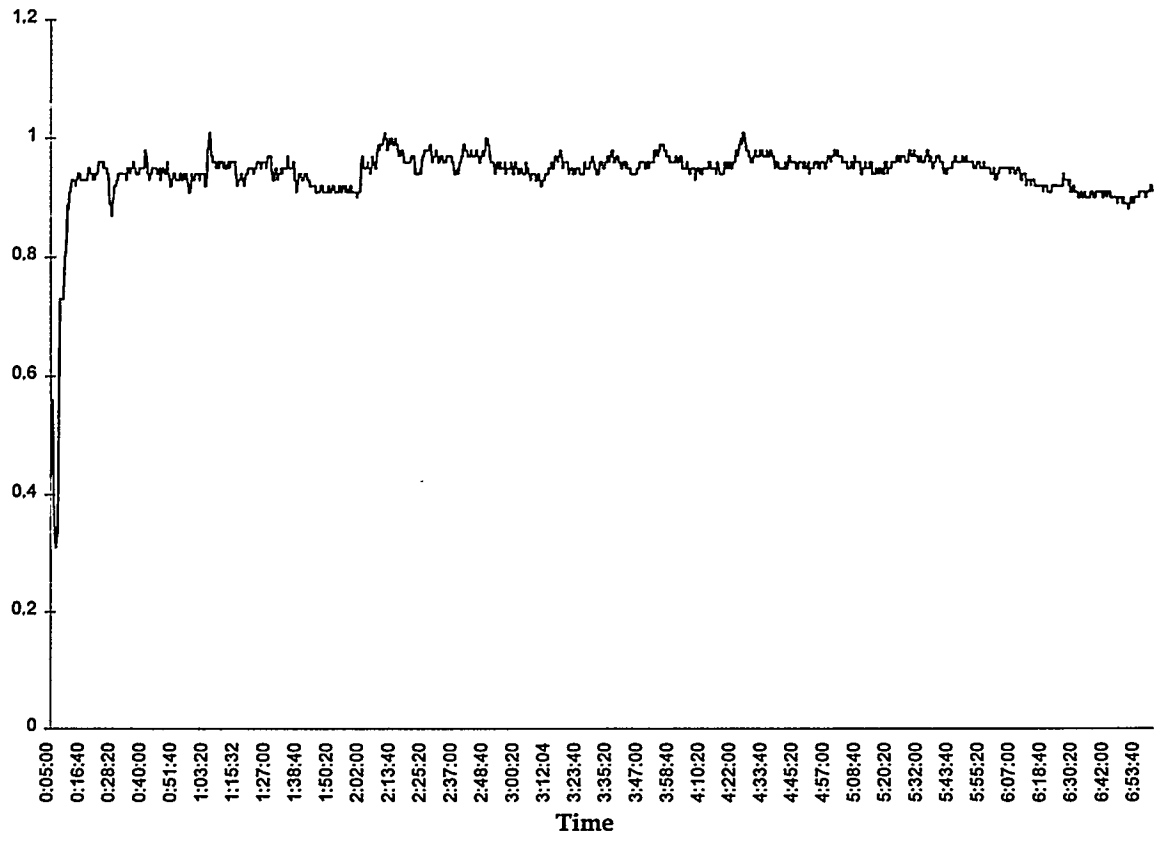

6.3.4.2. Off-Gas Quality

6.3.4.2.1. DRE Discussion

DRE calculations compare the amount of a tracer molecule in the feed with the amount of the same tracer molecule detected in the off-gas. Several SUMMA canisters were filled with off-gas samples at the baghouse outlet during feed injection and the canisters were analyzed for trace organics using EPA Method TO-14. According to 'Guidance Manual for Hazardous Waste Incinerator Permits" (US EPA, PB 84-10057, July 1983, Page 2-15), POHC selection has to be based on consideration of two factors: (1) the degree of incinerability as represented by the Heat of Combustion (ΔH_C) value, and (2) the concentration of the constituent in the feed. Hence, DRE calculations were carried out for the constituents with both high concentration and high ranking as POHC (refer to Table D1, Guidance on Setting Permit Conditions and Reporting Trial Burn Results, January 1989). Chlorobenzene was ranked the highest among all the POHC present in the feed, and trichloroethene exhibited the highest concentration in the feed material. These components were both non-detectable in the off-gas. A DRE of $\geq$ 99.9999% was achieved for all samples as shown in Figure 6.5.

Table 6-12
DREs for Chlorobenzene and Trichloroethene

Sample No.	Sampling Time	Date	DRE for Chlorobenzene (POHC)	DRE for Trichloroethene
1T-94-009-BO-12	0:39	Jun 30	≥99.9999	≥99.9999
1T-94-009-BO-13	1:39	Jun 30	≥99.9999	≥99.9999
1T-94-009-BO-14	1:39	Jun 30	≥99.9999	≥99.9999
1T-94-009-BO-15	2:42	Jun 30	≥99.9999	≥99.9999
1T-94-009-BO-16	2:42	Jun 30	≥99.9999	≥99.9999
1T-94-009-BO-17	3:50	Jun 30	≥99.9999	≥99.9999
1T-94-009-BO-18	3:50	Jun 30	≥99.9999	≥99.9999

Note: Chlorobenzene and trichloroethene were non-detectable in the off-gas. DRE's were limited by the lower detection limit (LDL)

6.3.4.2.2. Total Hydrocarbons

Total hydrocarbon data were taken using an on-line analyzer with a flame ionization detector (FID) throughout the run. Composition of the THC can be obtained both from summa canister and GC data. Methane, the major component in the THC measurement, was generally in the range of 70 ppm or lower. This level of methane is thermodynamically predicted under the operating conditions of CEP. C_{1+} concentrations were typically < 10 ppm.

6.3.4.2.3. Trace/Dioxins

A modified EPA method 23 was used to measure the dioxin and furan concentrations. During processing of F024, as shown in Table 6-13, dioxins concentration was not detected to the stringent German (and US targeted) regulatory limit of 0.1 ng 2,3,7,8 TCDD TEQ/Nm^3.

Table 6-13
Trace Analysis

Date		6/30/94	6/30/94
Time	Initial:	0:54	2:50
	Final:	2:18	4:03
Gas Meter Volume (ft^3)	Initial:	319.26	339.35
	Final:	339.35	360.65
Gas Meter Outlet (°F)	Initial:	70	70
	Final:	70	70
Total Sample Volume	SCF	20.09	21.30
	Nm^3	0.53	0.56
Analytes (ng)*	2378-TCDD	(ND)	(ND)
	12378-PeCDD	(ND)	(ND)
	123478-HxCDD	(ND)	(ND)
	123678-HxCDD	(ND)	(ND)
	123789-HxCDD	(ND)	(ND)
	1234678-HpCDD	(ND)	(ND)
	OCDD	(ND)	(ND)
	2378-TCDF	(ND)	(ND)
	12378-PeCDF	(ND)	(ND)
	23478-PeCDF	(ND)	(ND)
	123478-HxCDF	(ND)	(ND)
	123678-HxCDF	(ND)	(ND)
	234678-HxCDF	(ND)	(ND)
	123789-HxCDF	(ND)	(ND)
	1234678-HpCDF	(ND)	(ND)
	1234789-HpCDF	(ND)	(ND)
	OCDF	(ND)	(ND)
	Total TCDD	(ND)	(ND)
	Total PeCDD	(ND)	(ND)
	Total HxCDD	(ND)	(ND)
	Total HpCDD	(ND)	(ND)
	Total TCDF	(ND)	(ND)
	Total PeCDF	(ND)	(ND)
	Total HxCDF	(ND)	(ND)
	Total HpCDF	(ND)	(ND)

*ND= Not Detected to the targeted regulatory standard of 0.1 ng TEQ/Nm^3 or lower

6.3.4.3. Ceramic Quality

The composition (in weight %) of the ceramic product was measured at the beginning and end of the run as shown in Table 6-14. The amount of ceramic product was estimated based on complete oxidation of ceramic formers (e.g., Al_2O_3, MgO, CaO, and SiO) in the system.

Table 6-14
Ceramic Composition

				Major Components					Trace Components					
Sample	Note	Date	Time	CaO	Al_2O_3	SiO_2	MgO	FeO	K[1]	Na[1]	P[1]	Cr	S	Cl
1T-94-009-S19	Pre-Injection	6/29	21:30	20.7	54.6	19.0	2.61	0.86	0.02	0.16	0.06	0.03	0.714	<0.02
1T-94-009-S22	Post-Injection	6/30		18.5	57.7	18.6	2.12	1.84	0.01	0.03	0.07	0.03	0.304	0.38

[1] minor fluctuations in K, Na, P are attributable to flux additions during the process.
[2]S reduced and recovered in the metal. Feed halogen captured using lime in the ceramic phase.

Ceramic samples taken before and after injection of the liquid feed were analyzed using EPA methods 8260 for volatile organics, and 8270 for semi-volatile organics. No feed hazardous organic materials were detected (Table 6-15), and the ceramic phase passed the TCLP test for RCRA metals (Table 6-16).

Table 6-15
Organic Constituents in the Ceramic Product

Volatile Organics	Feed Composition (µg/l)	Ceramic Product Result (µg/kg)	LDL (µg/kg)	EPA NonWastewater Regulation (mg/kg)
,1,2-Trichloroethane	18,000,000	ND	7.5	6000
'etrachloroethane	9,700,000	ND	7.5	6000
:hlorobenzene	12,000,000	ND	18	6000
,2-Dichloroethane	6,800,000	ND	7.5	6000
,1,2,2-Tetrachloroethane	11,000,000	ND	5.0	6000
'richloroethene	24,000,000	ND	5.0	6000
;ylenes	610,000	ND	5.0	3000
,1,1,2-Tetrachloroethane	1,000,000	ND	25	6000
ec-Butylbenzene	540,000	ND	25	6000
'ert-Butylbenzene	2,000,000	ND	25	6000
Iexachlorobutadiene	3,600,000	ND	25	5600
'-Isopropyltoluene	870,000	ND	25	6000
Japhthalene	900,000	ND	25	5600
,2,4-Trimethylbenzene	1,100,000	ND	25	6000

Table 6-16
Full TCLP of Tapped Ceramic Product

Sample ID	As	Ba	Cd	Cr	Pb	Hg	Se	Ag
Regulatory Limits (mg/l)	**5.0**	**100**	**1.0**	**5.0**	**5.0**	**0.2**	**1.0**	**5.0**
Pre-Injection 1T-94-09-S14	ND[1]	ND	ND	0.9[2]	ND	ND	ND	ND
During Injection 1T-94-09-S11	ND	ND	ND	0.4[2]	ND	ND	ND	ND
Post-Injection 1T-94-09-S13	ND	ND	ND	0.4[2]	ND	ND	ND	ND

Notes:
[1]ND = not detected
[2]Cr_2O_3-Al_2O_3 refractory bricks were present during these runs which provides a source of Cr. Total Cr was measured in the ceramic phase. Cr^{+6} is not formed under CEP operating conditions. Cr within the CEP system has been analyzed and no hexavalent Cr^{+6} has been detected.

6.3.4.4. Metal Quality

The composition of the metal was analyzed both before and after liquid injection. Changes in composition were found to be minimal with only a slight decrease in carbon concentration. Table 6-17 shows the final composition of metal. The final metal weight was calculated from nickel tracer data.

Table 6-17
Tapped Metal Composition

Sample	Note	Date	Time	Fe	Al	Ca	Mg	Na	K	Ni	P	S	Si	Cl
1T-94-009-M38	Pre-Injection	6/29	21:20		0.01	6.2	1.67	<0.01	<0.01		<0.01	0.258		
1T-94-009-M41	Tapped Metal	6/30			0.14	0.01	0.01	<0.01	<0.01		1.66	0.295		
1T-94-009-S41 (analytical)	Tapped Metal	7/01	08:06	85.73	0.04	0.08	0.09	0.11	0.83	0.93	1.67	0.11	0.33	<0.0008

Table 6-18
Organic Constituents in the Metal Phase

Volatile Organics	Feed Composition (µg/l)	Result (µg/kg)	LDL (µg/kg)	EPA NonWastewater Regulation (µg/kg)
1,1,2-Trichloroethane	18,000,000	ND	7.5	6000
Tetrachloroethane	9,700,000	ND	7.5	6000
Chlorobenzene	12,000,000	ND	18	6000
1,2-Dichloroethane	6,800,000	ND	7.5	6000
1,1,2,2-Tetrachloroethane	11,000,000	ND	5.0	6000
Trichloroethene	24,000,000	ND	5.0	6000
Xylenes	610,000	ND	5.0	3000
1,1,1,2-Tetrachloroethane	1,000,000	ND	25	6000
Sec-Butylbenzene	540,000	ND	25	6000
Tert-Butylbenzene	2,000,000	ND	25	6000
Hexachlorobutadiene	3,600,000	ND	25	5600
P-Isopropyltoluene	870,000	ND	25	6000
Naphthalene	900,000	ND	25	6000
N-Propylbenzene	33,000,000	ND	25	6000
1,2,4-Trimethylbenzene	1,100,000	ND	25	6000

6.3.4.5. Scrubber Water

During processing of F024, no hydrogen chloride gas was separated before emission, so a caustic scrubber was used to capture the acid gases including HCl, from the off-gas. Analysis of a scrubber water sample, shown in Table 6-19, indicated that no VOCs were present.

Table 6-19
Scrubber Water Analysis

Constituents	Feed Composition (mg/l)	Scrubber Water (mg/l)	UTS Waste Water (mg/l)
1,1,2-Trichloroethane	18,000	ND (0.0015)	0.054
Tetrachloroethene	9,700	ND (0.0015)	0.056
Chlorobenzene	12,000	ND (0.0035)	0.057
1,2-Dichloroethane	6,800	ND (0.0015)	0.21
1,1,2,2-Tetrachloroethane	11,000	ND (0.001)	0.057
Trichloroethene	24,000	ND (0.001)	0.054
Xylenes	610	ND (0.001)	0.32
1,1,1,2-Tetrachloroethane	1,000	ND (0.001)	0.057
Hexachlorobutadiene	3,600	ND (0.001)	0.055
Naphthalene	900	ND (0.001)	0.059
ND = Not Detected (Lowest Detection Limit)			

6.3.5. Material Closure for Major Components

A vigorous mass balance was attempted on the major elements carbon, oxygen, hydrogen, and chlorine. Based on the material accounting data and operation log book, the source of elements added to the system were determined. On-line MS provided information for the gas composition. Analytical results indicated the composition of the metal and ceramic phase, which, when considered with estimations on the ceramic and metal phase amounts, allow an estimation of the amount of elements found in the product. Excellent mass balance was achieved on carbon (94.54%), hydrogen (103.55%) and oxygen (100.09%). Gas phase chlorine closure (on-line detection limited) was only

73% due to partitioning of the chlorine to metal chloride. Commercially, these metal chlorides would be recycled to the reactor for further conversion. The particulate matter was collected at the end of the entire demonstration campaign and therefore contained contributions from other waste processing experiments. Hence, the halogens attributable specifically to the F024 processing were not isolated due to the nature of the experimental conditions.

Table 6-20
Mass Balance for Major Components in F024 Processing
(Material Balance Closure Period I)

		Elemental Basis							
Components	**lbs.**	**C**	**O**	**H**	**Cl[8]**	**Fe**	**Ca**	**Al**	**Si**
Waste Feed[1]	666	482.85	0.67	65	117.42				
Methane[2]	32	24		8					
Oxygen[2]	668.13		668.13						
Iron Melt[3]	3510	98.28				3411.02			
Ceramic in Bath	800		335.46		0.16	5.35	118.29	231.25	70.93
Other Ceramic Additions	65		30.59					34.41	
Total Input	5741.13	605.83	1034.85	73	117.58	3416.37	118.29	265.66	70.93
Hydrogen[4]	73.27			73.27					
Carbon Monoxide[4]	1097.69	470.44	627.25						
Carbon Dioxide[4,7]	29.47	8.04	21.43						
Hydrogen Chloride[4]	84.88			2.33	82.56				
Ferro Alloy Product[5]	3505	94.28				3423.67			
Ceramic Product[6]	905		387.05		3.44	0.38	101.10	104.06	110.74
Total Output	5695.31	572.76	1035.73	75.79	86	3423.67	119.59	276.45	78.55
Closure	**99%**	**94.54**	**100.09**	**103.55**	**73.14**	**100.21**	**101.10**	**104.06**	**110.74**

[1] Based on feed composition and total amount of feed measured by change in Remacor solid feed tank weight
[2] Co-feeds measured by on-line flowmeters
[3] Based on pre-injection metal analysis and known weight of metal added to bath
[4] Calculated by MS (Mass Spectrometer) product analysis and argon as tracer gas
[5] Based on post-injection metal analysis and estimate of total weight tapped from bath
[6] Based on post-injection ceramic analysis and estimate of total ceramic tapped from bath
[7] Attributable to startup conditions. As steady-state is approached, carbon dioxide concentrations become negligible.
[8] Some chlorine is partitioned to metal chlorides as particulate matter. Since the particulate was collected at the end of the entire demonstration campaign and contained contributions from other waste processing, the halogens attributable to the F024 Processing was not possible to determine under the aforementioned conditions due to the integral nature of the experimental conditions.

6.4. Demonstration Unit Processing of RCRA-Listed K027 Waste

RCRA-listed K027 waste was processed in the demonstration-scale CEP prototype unit. The demonstration confirmed CEP's effectiveness in processing actual RCRA wastes and validated the predictions of high standards of environmental performance, highlighted by:

- Steady feed injection and off-gas generation;
- A high quality off-gas with total hydrocarbons <100 ppm with C_{2+} hydrocarbons, NO and SO_2, and principal organic hazardous constituents from the feed (i.e., 1,1,2 trichloroethane, 1,2 dichloroethane, and 1,2 dichlorobenzene) non-detectable to lowest detection limits (LDL);
- Ceramic product which passed full TCLP tests for both RCRA metals and organics;
- Metal product with non-detectable hazardous organic constituents (EPA Method 8260 and 8270).

6.4.1. Feed Material

K027 is an EPA RCRA-listed hazardous waste stream containing highly toxic chlorinated aromatic compounds. The major constituents in K027 are listed in Table 6-21, as analyzed according to EPA Methods 8260 and 8270 (volatile and semi-volatile hazardous constituents). The ultimate elemental analysis is shown in Table 6-22.

Table 6-21
Component Analysis of K027

Component		Concentration
2,4 Toluene Diisocyanate		5,100 mg/kg
Metals	Nickel	1,200 mg/kg
	Sodium	640 mg/kg
	Zinc	7.2 mg/kg
	Chromium	7.2 mg/kg
	All Others	Nondetect
Volatile Organics	1,1,2 Trichloroethane	7.5 mg/kg
	1,2 Dichloroethane	7.5 mg/kg
Semi-Volatile Organics	1,2 Dichlorobenzene	20 mg/kg

Table 6-22
Ultimate Analysis of K027 Feed Processed

Elemental Constituent	Wt%
Carbon	54.39
Hydrogen	6.01
Chlorine	3.26
Sulfur	0.012
Nitrogen	15.25
Ash	0.26
Oxygen (by difference)	20.82

6.4.2. Processing Summary

The K027 waste material was mixed with graphite in the ratio of 31.5% feed and 68.5% graphite. The feed mixture was sampled to analyze its toxicity, loaded in the solids holding tank, and pneumatically injected into the reactor through the tuyere. The tuyere is "triple-concentric" and allows injection of feed, oxygen, and methane through separate pipes. Oxygen was injected stoichiometrically with carbon in the feeds. Methane provided localized cooling for temperature control in the injection region. Argon was used as the carrier gas for the pneumatically-injected feed. The flow rate of the gases and the weight of the holding tank were monitored continuously to determine the amount of material injected. Inorganic co-reactants (mainly lime) were added to the reactor prior to feed injection to form a minimal ceramic phase that would capture trace amounts of sulfur and chlorine in the feed.

Throughout the demonstration, the operating conditions of the CEP system were closely monitored and controlled. Temperature was monitored using embedded thermocouples in the containment refractory. The temperature of the bath was maintained between 2700°F and 2800°F using the induction coil for heat addition. The carbon concentration in the liquid metal was monitored by hourly sampling and analyzed for carbon content using the on-site LECO equipment. It was maintained between 2.8 wt% and 3.0 wt% throughout the experiment.

6.4.3. Sampling Protocol

General sampling equipment and methods are described in the previous section; the specific samples taken and analyses conducted in this demonstration are outlined below:

- Gas sampling: Gas sampling protocol was designed to measure off-gas impurities to evaluate CEP's hazardous conversion efficiency. Product gases were sampled over a period of an hour near the headspace of the reactor (the 'Dutchman') using on-line SUMMA™ canisters. Analysis of the SUMMA™ canister gas samples was carried out by third party laboratories based on EPA Method TO 14 and a gas chromatography/flame ionization detector (GC/FID). Two SUMMA™ canisters samples were taken on-line during the TDI/TDA processing. Mass spectrometer samples were drawn on-line in two locations: before the gases entered the scrubber and after they exited the aftercooler. Measurements of the gas composition were taken every twenty seconds and logged into the PLC. The mass spectrometer was calibrated using standard gases before and after the injection.

- Metal sampling: Metal samples were collected every hour by lowering a sealed sampling probe through the top of the reactor. The carbon concentration of metal samples was monitored using a LECO analyzer available in MMT's analytical laboratory. Analyses of metal samples were carried out using an optical spectrometer capable of identifying the composition of a metal containing up to 16 elements. In addition, pre- and post-injection samples were packaged according to standard EPA procedure and then sent out for third party metal composition analyses using EPA method 6010 for RCRA 8 metals.

- Ceramic sampling: A ceramic sample was collected at the completion of the injection. The ceramic was first visually observed for color and consistency. An in-house optical spectrometer was used to measure ceramic composition. Samples were also taken for third party analyses for composition and TCLP metals and organics. Specifically, EPA methods 6010 and 7410 were used for RCRA metals and methods 8260, 8270 and 8150 for organics.

6.4.4. Off-Gas Trace Analysis

Gas produced in the CEP unit was monitored by an on-line mass spectrometer (MS). The MS sampled the gas every 20 seconds and analyzed it for 16 constituents, including CO, H_2, HCl, and Ar. Due to mass spectrometer interference between CO and N_2, the amount of synthesis gas produced (CO and H_2) could not be quantified precisely to allow mass balance closure. Additional instrumentation has since been installed (IR analyzer) to provide an independent assessment of CO and CO_2 concentrations and to verify the accuracy of the mass spectrometers.

Samples of off-gas were collected in SUMMA™ canisters. Total hydrocarbon (THC) was detected at less than 100 ppm throughout the run based on FID results. The off-gas quality was also determined by third party analysis using both GC/FID and EPA Method TO-14. A range of common C_{2+} hydrocarbons, which are potential products of gas-phase reformation reactions, were not detected down to ppm levels as illustrated in Table 6-23.

Table 6-23
Off-Gas Analysis - Hydrocarbons
(K027 Waste Processing)

Method: GC/FID		
Analyte	**Result (ppm)**	**Detection Limit (ppm)**
Methane[1]	22	0.2
Ethylene	ND	0.2
Acetylene	ND	0.2
Ethane	ND	0.2
Propylene	ND	0.2
Propane	ND	0.2
Methyl Acetylene	ND	0.2
Isobutane	ND	0.2
Isobutylene	ND	0.2
1,3-Butadiene	ND	0.2

[1]This level of methane is thermodynamically predicted in a syngas environment under CEP operating conditions.

Table 6-23
Off-Gas Analysis - Hydrocarbons
(K027 Waste Processing)
(Cont'd)

Method: GC/FID		
Analyte	**Result (ppm)**	**Detection Limit (ppm)**
n-butane	ND	0.2
trans-2-Butene	ND	0.2
2,2-Dimethylpropane	ND	0.2
Ethyl Acetylene	ND	0.2
cis-2-Butene	ND	0.2
Isopentane	ND	0.2
1-Pentene	ND	0.2
2-Methyl-1-Butene	ND	0.2
n-Pentane	ND	0.2
Isoprene	ND	0.2
trans-2-Pentene	ND	0.2
cis-2-Pentene	ND	0.2
2-Methyl-2-Butene	ND	0.2
2, 2-Dimethyl Butane	ND	0.2
2-Methyl Pentane	ND	0.2
3-Methyl Pentane	ND	0.2
n-Hexane	ND	0.2
trans-2-Hexene	ND	0.2
cis-2-Hexene	ND	0.2
Methyl Cyclopentane	ND	0.2
Cyclohexane	ND	0.2
Isoheptane + 2,3-Dimethyl Pentane	ND	0.2
3-Methyl Hexane	ND	0.2
n-Heptane	ND	0.2
Isooctane	ND	0.2
2,3,4-Trimethylpentane	ND	0.2

Table 6-24 shows the principal organic hazardous constituents in the feed that were included in gas-phase analysis by EPA Method TO-14. A gas-phase SUMMA™ canister sample was collected during TDI processing and analyzed using Method TO-14. None of the hazardous TO-14 compounds in the feed were detected to lowest detection limits.

Table 6-24
Off-Gas Analysis
Principal Hazardous Organic Constituents
(K027 Waste Processing)

Hazardous Feed Constituent[1]	Feed Concentration (ppb)	Off-Gas Concentration (ppb)	Off-Gas Detection Limit (ppb)
1,1,2 Trichloroethane	7,500	ND[2]	0.93
1,2 Dichloroethane	7,500	ND	1.2
1,2 Dichlorobenzene	20,000	ND	0.84

[1] Based on principal hazardous constituents in the waste feed that are analyzed using EPA Method TO-14.
[2] ND = not detected to lowest detection limits (LDL) using EPA Method TO-14 on SUMMA™ canister samples.

Oxidation byproducts NO and SO_2 were monitored using the on-line mass spectrometer. No NO or SO_2 were detected to an LDL of 100 ppm. These data are consistent with data from other Fall River demonstrations for a variety of waste and waste surrogate materials.

6.4.5. Ceramic Product

Inorganics were added to the CEP reactor at the beginning of the run as co-reactants for the capture of trace amounts of chlorine and sulfur in the feed. The composition of the ceramic product was analyzed extensively using both in-house and third party analysis. In addition, analysis according to standard EPA methods for TCLP (both RCRA metals and organics) showed that the ceramic phase passed the TCLP test, as shown in Table 6-25 and Table 6-26.

Table 6-25
TCLP Metals Analysis on Ceramic Samples
(K027 Waste Processing)

SAMPLE ID	As	Ba	Cd	Cr	Pb	Hg	Se	Ag
Regulatory Limits (mg/l)	**5.0**	**100**	**1.0**	**5.0**	**5.0**	**0.2**	**1.0**	**5.0**
Post Run Sample	ND	ND	ND	ND	ND	ND	ND	ND

Table 6-26
TCLP Organics Analysis on Ceramic
(K027 Waste Processing)

Sample ID	TCLP Result (mg/L)	Regulatory Limits (mg/L)
Pesticides		
Chlordane	ND	0.03
Endrin	ND	0.02
Heptachlor	ND	0.008
Heptachlor Epoxide	ND	0.008
Lindane	ND	0.4
Methoxychlor	ND	10.0
Toxaphene	ND	0.5
Herbicides		
2,4-D	ND	10.0
2,4,5-TP	ND	1.0
ND = Not Detected at lowest detection limit		

Table 6-26
TCLP Organics Analysis on Ceramic
(K027 Waste Processing)
(Cont'd)

Sample ID	TCLP Result (mg/L)	Regulatory Limits (mg/L)
Volatile Organics		
Benzene	ND	0.5
Carbon Tetrachloride	ND	0.5
Chlorobenzene	ND	100.0
Chloroform	ND	6.0
1,4-Dichlorobenzene	ND	7.5
1,2-Dichloroethane	ND	0.5
1,1-Dichloroethylene	ND	0.7
Tetrachloroethylene	ND	—
Trichloroethylene	ND	0.5
Vinyl Chloride	ND	0.2
Methyl Ethyl Ketone	ND	200.0
Semi-Volatile Organics		
Cresol, Total	ND	200.0
2,4-Dinitrotoluene	ND	0.13
Hexachlorobenzene	ND	0.13
Hexachloro-1,3-Butadiene	ND	0.5
Hexachloroethane	ND	3.0
Nitrobenzene	ND	2.0
Pentachlorophenol	ND	100.0
2,4,5-Trichlorophenol	ND	400.0
2,4,6-Trichlorophenol	ND	2.0
Pyridine	ND	5.0

ND = Not Detected at lowest detection limit

6.4.6. Metal product

The metal bath was used as the solvent for the conversion of feed materials to products and the media to capture trace levels of chromium and nickel from the feed. The composition of metal product from the demonstration is shown in Table 6-27. Detection of chromium and nickel in the metal samples indicated the capture of these metals as predicted thermodynamically.

Table 6-27
Metal Product Composition
(K027 Waste Processing)

Elements	Concentration (wt%)
Aluminum	0.172
Chromium	0.228
Cobalt	0.026
Copper	0.481
Nickel	0.132
Lead	0.017
Sulfur	0.137
Iron	92.4
Organic Matter	0%
Note: metals including Co, Cu, Pb, Al (which were absent from the K027 feed) originated from material processed prior to K027 injection	

During a bench-scale K027 Recycling Demonstration, the post-injection metal samples were tested for organic constituents using EPA Methods 8260 and 8270. No organic compounds were detected in the metal, which passed current EPA non-wastewater disposal regulations.

6.4.7. QA/QC Sample Analysis

Pursuant to the Sampling and Analysis Plan, the following additional samples were taken. A trip blank sample containing distilled/de-ionized (DI) water and preservative was placed in the transportation cooler to determine whether any VOC contamination occurred. The results indicate that no VOC contamination occurred. A field blank sample was also obtained by pouring DI water into a sample bottle next to the commercial-scale CEP prototype during processing. The purpose of the field blank sample was to determine the presence of any air contamination. No air contamination occurred.

6.5. Demonstration Unit Processing of RCRA-Listed K019/K020 Waste

6.5.1. Introduction

RCRA-listed hazardous waste K019/20 was processed in the demonstration-scale CEP unit. The purpose of the experimental run was to demonstrate the effectiveness of CEP in processing actual RCRA hazardous waste. Standard analytical sampling protocols designed to meet EPA regulatory requirements were used in the campaign. Ceramic and metal samples were taken for analysis. The major findings are:

- Off-gas trace analysis showed: DREs for major hazardous constituents ≥ 99.999% (analytically limited), THC < 100 ppm throughout the run, NO_X and SO_X not detected to the LDL of 100 ppm;

- Ceramic and metal phase samples showed absence of organic constituents, and the ceramic phase passed the TCLP test;

- Chloride was partitioned as hydrogen chloride and metal chloride. Hydrogen chloride was removed in the scrubber. In a commercial plant, the metal chloride would be recycled to the reactor for further processing.

6.5.2. Feed Analysis

K019/20 is a RCRA-listed waste stream whose major hazardous constituents include 1,1,2,2-Tetrachloroethane, 1,1,2-Trichloroethane, tetrachloroethene, 1,2-Dichloroethane, and chlorobenzene as shown in Table 6-28. Prior to feed injection, the K019/20 material was mixed with fuel oil and chlorobenzene. An ultimate analysis test was performed on a feed sample. The analytical results are shown in Table 6-29.

Table 6-28
Major Constituent in K019/020

Compound	Concentration (μg/kg)
1,1,2-Trichloroethane	220,000
Tetrachloroethene	4,400
1,2-Dichloroethane	160,000
1,1,2,2-Tetrachloroethane	5,600
Chlorobenzene	22,000

Table 6-29
Elemental Composition of the Feed Mixture

Element	Wt. %
Carbon	68.1
Hydrogen	8.2
Chlorine	22.8
Sulphur	0.3
The feed mixture injected had a composition (wt%):	
Fuel Oil	48.9%
Chlorobenzene	31.6%
K019/20	19.5%

6.5.3. Operational Issues

The processing of K019/20 was carried out on 20 November, 1993 from 0:04:00 to 3:40:00. Approximately 3000 lbs of metal iron was melted in the CPU prior to feed injection. The feed material was first loaded in a holding tank and then injected into the reactor through the bottom tuyere. The weight of the holding tank was continuously monitored to measure the amount of liquid feed injected into the bath. Together with the feed, oxygen was injected as a co-reactant, methane as a cooling gas, nitrogen as purge gas, and argon as a tracer gas.

6.5.4. Mass Balance

Mass balance closure for carbon, oxygen, hydrogen, and chlorine were found to be 100.39%, 112.46%, 125.74%, and 28.78%, respectively. Low chlorine closure was due to the unknown amount of chlorine captured in the gas handling train as ferrous chloride. Particulate samples were collected after various feeds had been processed, so the particulate composition could not accurately represent a particular feed performance.

6.5.4.1. DRE Calculations

The DREs of major hazardous constituents in the K019/20 (1,1,2,2-Tetrachloroethane, 1,1,2-Trichloroethane, Tetrachloroethene, 1,2-Dichloroethane, and Chlorobenzene) were calculated based on the analytical results of the SUMMA canister samples. The SUMMA canister data were collected for 1 hour during injection. These constituents were not detected to the lowest detection limit of 10 $\mu g/M^3$, which resulted in DREs $\geq$ 99.999% (analytically limited).

6.5.4.2. Off-Gas Trace Analysis

Potential by-products like NO_X and SO_X were measured using on-line analyzers. NO_X was measured using a chemiluminescent analyzer. SO_2 was analyzed using an ultraviolet-photometric device. Both NO_X and SO_X were not detected to the LDL of 100 ppm. More accurate devices were used in more recent runs, which showed no NO_X and SO_X detection to the LDL of 3 ppm and 1 ppm, respectively.

Total hydrocarbon data were taken using an on-line analyzer via a flame ionization detector (FID). The THC was in the range of 100 ppm for samples taken from both the Dutchman and the baghouse, consistent with data from previous runs.

6.5.5. Ceramic Quality

Ceramic samples were taken before and after feed injection and were analyzed for their metal composition. As shown in Table 6-30, TCLP analytical test results for RCRA metals, acids/base/neutral extractables, and pesticides/herbicides showed that the ceramic phase passed the TCLP test. The tapped ceramic phase was also analyzed for volatile organics (Method 8260), semi-volatile organics (Method 8270), and chlorinated organics (TOX). No chlorinated organic constituents were detected.

Table 6-30
Ceramic Composition for K019/20 Processing

mg/kg	Al	Ca	Cr	Co	Cu	Fe	Pb	Ni	Si	S	Sn	Zn	Zr
Pre (L9309570-05)	228000	180000	1190	5.5	976	37200	374	44.2	10300	724	ND	123	210
Post (L9309570-06)	172000	138000	1020	50.5	9660	193000	66.7	703	19700	1000	ND	9.0	272
Note: A highly heterogeneous organometallic feed was processed prior to K019/20 processing, resulting high concentration of metals which were not present in the actual K019/20 material.													

Table 6-31
Full TCLP Results for K019/20 Processing

Parameter	Results	Detection Limit
RCRA Metals (mg/ℓ)		
Arsenic	ND	1.0
Barium	ND	0.5
Cadmium	ND	0.1
Chromium	0.3[1]	0.2
Lead	ND	0.5
Mercury	ND	0.005
Selenium	ND	0.5
Silver	ND	0.1
Acid/Base/Neutral Extractables (mg/ℓ)		
Total Cresol	ND	0.029
2,4-Dinitrotoluene	ND	0.015
Hexachlorobenzene	ND	0.011
Hexachloro-1,3-butadiene	ND	0.032
Hexachlorobenzene	ND	0.020
Nitrobenzene	ND	0.0076
Pentachlorophenol	ND	0.0368
2,4,5-Trichlorophenol	ND	0.019
2,4,6-Trichlorophenol	ND	0.011
Pyridine	ND	0.1
Pesticides/Herbicides (mg/ℓ)		
Chlorodane	ND	0.01
Endrin	ND	0.001
Heptachlor	ND	0.001
Heptachlor epoxide	ND	0.001
Lindane	ND	0.001
Methoxychlor	ND	0.002
Taxaphene	ND	0.01
2,4-D	ND	0.005
2,4,5-TP	ND	0.005

ND=Not Detected

[1] Cr_2O_3-Al_2O_3 refractory bricks were present during these runs which provides a source of Cr. Total Cr was measured in the ceramic phase. Cr^{+6} is not formed under CEP operating conditions. Cr within the CEP system has been analyzed and no hexavalent Cr^{+6} has been detected. The detected concentration was a full order of magnitude below the regulatory limit 5 mg/ℓ.

6.6. Demonstration Unit Processing of Chlorinated Scrap Metal

6.6.1. Summary

The CEP viability to process waste streams containing chlorinated organic contaminants has been investigated. The waste feed mixtures consisted of metals and organic materials, prepared to simulate DOE's contaminated scrap metal. Trace quantities of volatile heavy metals were also added to the feed mixtures. The conversion efficiency of organic components, consisting primarily of chlorinated polymeric materials, was quantified through extensive off-gas sampling and using EPA method TO-14 for analysis of volatile and semi-volatile organic components. High conversion of chlorinated organic materials exceeding EPA's standards (99.9999%) was achieved. Total hydrocarbon content (THC) in the off-gas was consistently measured below 100 ppm. Ceramic samples were taken for each experimental campaign and TCLP testing of RCRA metals was performed. The TCLP test results indicate that metal leaching levels were non-detectable or below regulatory limits. Material balance closure for C, H, and O were performed and presented.

6.6.2. Experimental Campaign 1T-93-015 Summary

A feed mixture containing organic material and metals was processed on October 16, 1993. The final organic content of the feed was 22.5%. The organic fraction of the feed was selected to model chlorinated waste streams. Metals comprised 47.7% of the feed. Lead and zinc were added to the feed to simulate waste contaminated with volatile heavy metals (VHM). The conversion efficiency of organic materials into a stable off-gas product was examined. The Composition of the feed mixture is shown in Table 6-32.

Table 6-32
Composition of Feed Mixture for Run 1T-93-015
with and without Accounting for Final Three Components

Component	Lbs.	Prior to Flux Addition		After Flux Addition	
		wt%	mol%	wt%	mol%
Aluminum	55	7.2	16.4	5.0	11.6
Chromium	10	1.3	1.5	0.9	1.1
Copper	264	34.4	33.5	24.2	23.6
Iron	158	20.6	22.8	14.5	16.1
Nickel	10	1.3	1.4	0.9	1.0
Lead	10	1.3	0.4	0.9	0.3
Zinc	10	1.3	1.2	0.9	0.9
Silver	4	0.5	0.3	0.4	0.2
Tetrachlorobenzene	6	0.8	0.2	0.5	0.2
Polyvinyl Chloride[1]	70	9.1	9.0	6.4	6.4
Polystyrene[1]	170	22.2	13.2	15.6	9.3
SiO_2	CONFIDENTIAL				
CaO	CONFIDENTIAL				
FeS_2	CONFIDENTIAL				
TOTAL	1,091				

[1]Mole calculations use monomer forms of $-[C_2H_3Cl]_n-$ and $-[C_8H_8]_n-$.

A sample was taken to perform an ultimate analysis testing. A summary of the results is shown in Table 6-33.

Table 6-33
Ultimate Analysis of (1T-93-015) Feed

Element	Composition (wt%)
Carbon	27.21
Hydrogen	2.55
Nitrogen	< 0.5
Oxygen	< 0.5

6.6.2.1. Feed Injection

The metal bath was initially charged with approximately 1600 lb of iron. During heatup, additional iron was added to the bath as were flux-forming materials. In addition, ceramic-formers (CaO, SiO_2, and FeS_2) were mixed with the solid feed to minimize dependence on top additions during feed injection. Measurements taken prior to feed injection showed a bath temperature of 2871°F and a carbon level of 3.19%. Waste powder injection began at 14:31 on 10/16/94. The feed was transported to the reactor using argon as the carrier gas. Oxygen was injected as a co-reactant and methane was injected as a cooling gas. Feed was continuously injected for 90 minutes before it was interrupted temporarily. There were then subsequent injection periods of 282 minutes and 30 minutes. The total amount of feed injected was 853.6 lb. Solid feed flow rates were in general steady. A summary of the feed injection periods and the amounts injected is presented in Table 6-34.

Table 6-34
Summary of Feed Injection for Run 1T-93-015

Injection Period	Duration (minutes)	Surrogate Injected (pounds)
14:31:40-16:02:00	90	173.2
16:43:40-21:25:20	282	607.0
22:03:40-22:34:20	30	73.4
Totals	402	853.6

Throughout the run, bath temperature and carbon levels were periodically measured. Gas, ceramic, and metal products were sampled as prescribed in the sampling plans. Several metal samples were successfully taken before, during, and after feed injection. In addition, post-run dust and scrubber samples were taken at various points in the gas handling train. Operational conditions precluded pre-injection ceramic sampling. However, post-tap ceramic samples and one ceramic sample during waste processing were obtained.

6.6.2.2. Off-Gas Trace Analysis

Product gas samples were taken over a period of time from the reactor headspace (Dutchman) and from the baghouse outlet stream using on-line SUMMA canisters. The gas samples were analyzed for volatile organic compounds by combined gas chromatography/mass spectrometry according to EPA Method TO-14. The samples collected and sampling time and location are summarized in Table 6-35. The data was used to calculate destruction efficiencies of organic compounds.

Table 6-35
Summa Canister Samples

Sample No	Sampling Time	Date	Sampling Location
Summa 1-5, # 9646B	17:36	10/16/93	Dutchman
Summa 1-6, # 9639B	18:10	10/16/93	Dutchman
Summa 1-7, # 9638B	18:41	10/16/93	Dutchman
Summa 3-5, # 9644B	17:36	10/16/93	Baghouse outlet
Summa 3-6, # 9645B	18:10	10/16/93	Baghouse outlet
Summa 3-7, # DE-7	18:41	10/16/93	Baghouse outlet

Off-gas product NO and SO_2 levels were monitored using an on-line mass spectrometer. Samples were drawn on-line downstream of the baghouse and downstream of the aftercooler. No NO or SO_2 were detected at a lower detection limit of 100 ppm. These data are consistent with results from other experiments carried out on a variety of waste feed streams.

6.6.2.3. Destruction of Organics

Normal destruction and removal efficiency (DRE) calculations compare the amount of a tracer molecule in the feed with the amount of the same tracer molecule detected in the off-gas stream. When the tracer molecule is a solid material that does not volatilize in the reactor, a normal DRE calculation cannot be performed. Polyvinyl chloride (PVC) and polystyrene, both components in the feed, are polymeric molecules that do not volatilize and therefore, will not be detected in the off-gas. Tetrachlorobenzene, also a feed component, is not analyzed for by EPA Method TO-14.

A modified approach for calculating DRE values is based on the assumption that PVC can be modeled as vinyl chloride (CH_2CHCl) or as chloroethane (CH_3CHCl), which are very similar structurally to the PVC monomer (-[CH_2CHCl]-). Similarly, polystyrene (-[CH_2-$CH(C_6H_5)$]-) can be modeled as styrene (CH_2=$CH(C_6H_5)$) or as ethyl benzene ($CH_3CH_2(C_6H_5)$). The destruction efficiency for tetrachlorobenzene was calculated by accounting for all chloride-benzene (C_6H_5-Cl) compounds on the TO-14 list. Representative destruction and removal efficiency values for PVC, polystyrene, and tetrachlorobenzene are displayed in Table 6-36.

Table 6-36
DRE` Summary for PVC, Polystyrene and Tetrachlorobenzene

Sample No	Sampling Time	Date	Location	Tracer	Compound	DRE`
Summa 1-5	17:36 - 18:06	10/16/93	Dutchman	Vinyl Chloride	PVC	> 99.99999%[1]
Summa 1-5	17:36 - 18:06	10/16/93	Dutchman	Chloroethane	PVC	99.99990%
Summa 3-5	17:36 - 18:06	10/16/93	Baghouse	Vinyl Chloride	PVC	> 99.99999%
Summa 3-5	17:36 - 18:06	10/16/93	Baghouse	Chloroethane	PVC	99.99998%
Summa 3-6	18:10 - 18:40	10/16/93	Baghouse	Vinyl Chloride	PVC	> 99.99999%
Summa 3-6	18:10 - 18:40	10/16/93	Baghouse	Chloroethane	PVC	99.99998%
Summa 3-7	18:41 - 19:10	10/16/93	Baghouse	Vinyl Chloride	PVC	99.99999%
Summa 3-7	18:41 - 19:10	10/16/93	Baghouse	Chloroethane	PVC	99.99998%
Summa 1-5	17:36 - 18:06	10/16/93	Dutchman	Styrene	Polystyrene	> 99.99999%
Summa 1-5	17:36 - 18:06	10/16/93	Dutchman	Ethyl Benzene	Polystyrene	99.99999%
Summa 1-6	18:10 - 18:40	10/16/93	Dutchman	Styrene	Polystyrene	> 99.99999%
Summa 1-6	18:10 - 18:40	10/16/93	Dutchman	Ethyl Benzene	Polystyrene	99.99999%
Summa 1-7	18:41 - 19:10	10/16/93	Dutchman	Styrene	Polystyrene	> 99.99999%
Summa 1-7	18:41 - 19:10	10/16/93	Dutchman	Ethyl Benzene	Polystyrene	99.99996%
Summa 3-7	18:41 - 19:10	10/16/93	Baghouse	Styrene	Polystyrene	> 99.99999%
Summa 3-7	18:41 - 19:10	10/16/93	Baghouse	Ethyl Benzene	Polystyrene	99.99991%
Summa 1-6	18:10 - 18:40	10/16/93	Dutchman	Cl-C_6H_5 bonds[2]	Tetrachloro-benzene	> 99.99990%

[1] The ">" signs indicate that the tracer molecules were non-detectable in the summa canister samples. Lower detection limits (LDL) for those compounds were used to calculate their DRE.
[2] The compounds containing a Cl-C_6H_5 bond on the TO-14 list were chlorobenzene, m-dichlorobenzene, p-dichlorobenzene, o-dichlorobenzene, and 1,2,4-trichlorobenzene.

6.6.2.4. Ceramic Product

Prior to feed injection, inorganic ceramic-forming materials (85 lb) containing CaO, SiO_2, and FeS_2 were added to the CEP reactor. In addition, ceramic-forming materials were blended with the feed mixture to minimize dependence on top additions. The cumulative amount of flux materials added was 452.3 lbs. Visual observation of

samples and of the tapped ceramic layer at the end of the run indicated entrainment of refractory materials. The erosive effect of the tuyere jet on the refractory walls is believed to have caused and accelerated particle entrainment. These observations were confirmed by analyzing ceramic samples for their major components. Subsequent re-design of the reactor throat have eliminated jet impingement on the refractory.

A toxicity characteristics leaching procedure (TCLP) testing of RCRA metals was performed on the ceramic sample marked 1T-93-015-S2. The TCLP test results indicate that metal leaching levels were non-detectable or below regulatory limits as shown in Table 6-37.

Table 6-37
TCLP Analysis on Ceramic Sample

Metal	1T-93-015-S2	Regulatory Level, (mg/L)
As	ND[1]	5.0
Ba	ND	100
Cd	ND	1.0
Cr	0.81[2]	5.0
Pb	ND	5.0
Hg	ND	0.2
Se	ND	1.0
Ag	ND	5.0

[1] ND = Not detected

[2] Cr_2O_3-Al_2O_3 refractory bricks were present during these runs which provided a source of Cr_2O_3 to the ceramic phase. Refractory composition has been optimized to preclude this occurrence in commercial installations.

6.6.2.5. Mass Balance

Mass balance calculations were performed for the major components (C,H, and O) for appropriate injection periods. Table 6-38 summarizes the results of the calculations. Sources of data for the mass inputs include gases fed through the tuyere (methane and oxygen) and the organic components of the feed as measured by ultimate analysis. The output mass data were calculated using mass spectrometer results. Argon gas was used as the tie for determining output gas flow rates.

Table 6-38
Carbon, Hydrogen and Oxygen Overall Mass Balance

In	C	H	O
Total Mol	14,551.46	7,845.10	6,074.35
Total Lbs.	384.62	17.28	214.07
Out	**C**	**H**	**O**
Total Mol	14,859.96	7,398.55	7,946.11
Total Lbs.	392.77	16.30	280.04
Percent Recovered	102.12	94.31	130.81

Table 6-38 shows that good mass closure for carbon and hydrogen were achieved. The high oxygen recovery can be attributed to oxygen infiltration into the reactor during sampling and error associated with calculating oxygen contained in the ceramic product (typically calculated by difference). Table 6-39 summarizes the overall recovery of organic constituents, carbon, hydrogen, and oxygen during waste processing. "% Feed" represents the amount of elements in the feed (organic) potentially available for formation of synthesis gas. "% Recycled" represents the amount of elements actually present in the synthesis gas based on measured gas flow rates in the off-gas product stream. "% Recovered" is the ratio of % Recycled to % Feed. Conversion of organics to syngas product exceeded 99%.

Table 6-39
Experimental Recovery for Synthesis Gas

Synthesis Gas Formers (wt% Feed)			% Feed	% Recycled	% Recovered
C	H	O			
27.21	2.55	0.50	30.26	30.08	99.42

6.6.3. Experimental Campaign 1T-93-018 Summary

A feed mixture containing organic material and metals was processed. The final metal content of the feed was 64.5%. Lead and zinc were added to the feed to simulate VHM-contaminated waste. The organic fraction comprised 20.2% of the feed. The conversion

efficiency of organic materials into a stable off-gas stream was quantified. The composition of the feed is shown in Table 6-40.

Table 6-40
Feed Composition for Run 1T-93-018

		Prior to Flux Addition		After Flux Addition	
Component	Lbs.	wt%	mol%	wt%	mol%
Aluminum	48	7.8	19.5	6.6	16.1
Chromium	11	1.8	2.3	1.5	1.9
Copper	232	37.9	40.0	32.1	33.0
Iron	141	23.0	27.7	19.5	22.8
Nickel	10	1.6	1.9	1.4	1.5
Lead	10	1.6	0.5	1.4	0.4
Zinc	10	1.6	1.7	1.4	1.4
Silver	4	0.7	0.4	0.6	0.3
Organic	146	23.9		20.2	
SiO_2	10			1.4	1.5
CaO	100			13.9	16.1
TOTAL	576				

Elemental composition of the feed was calculated and is summarized in Table 6-41. Approximate chemical formulae were used for the polymeric organic fraction of the feed.

Table 6-41
Elemental Composition (Wt%)

	C	H	O
Non-flux	19.29	1.71	1.69
With flux	16.35	1.45	0.34

6.6.3.1. Feed Injection

The metal bath was initially charged with approximately 2100 lbs of iron and 15 lb of lime and heated to about 2600°F. Fifteen-pound charges of metal were then added per minute over a period of 2.5 hours, interrupted by periods of addition of flux materials and graphite. Ceramic-formers added included lime and calcium aluminate (CaO, MgO, Al_2O_3, SiO_2). The total metal weight in the reactor prior to the initial injection was 3838 lbs. The feed was transported to the reactor using argon as the carrier gas. Oxygen was injected as a co-reactant and methane was injected as a cooling gas. Feed mixture injection began at 13:16 on 11/19/93. At 14:28, feed injection was temporarily interrupted for minor maintenance work. It was re-started at 15:02 and was stopped at 18:47. The total amount of feed injected was 585 lbs. Ceramic formers accounted for 89.1 lbs, while the actual feed material injected was 495.9 lbs. Solids feed flow rates were in general steady. A summary of the feed injection periods and the amounts injected is presented in Table 6-42.

Table 6-42
Summary of Feed Injection for Run 1T-93-018

Injection Period	Duration (minutes)	Feed Injected (lbs)
13:16:20-14:27:40	71	123.2
15:02:40-18:47:20	224	461.8
Totals	295	585

6.6.3.2. Off-Gas Product

Output component gas flows and total gas flow rates were calculated using mass spectrometer data. In this method, argon gas was injected into the reactor as a tie component whose flow rate was known. The argon concentration in the off-gas measured by the MS was combined with the known input argon flow rate to calculate the total off-gas flow rate. Using this value, the flow rate of other gas components detected by the MS were calculated.

The off-gas flow rate during the second feed injection period was maintained steady, following an initial transient period. The off-gas composition was also calculated during feed injection. Steady CO vol% and H_2 vol% were observed, indicating steady solids feed, O_2 co-feed, and methane feed flow rates. The CO/H_2 ratio on a volume basis in the off-gas was maintained relatively constant (1.4 +/- .1) over the time period of interest.

6.6.3.3. Off-Gas Trace Analysis

Total hydrocarbon data, taken using an on-line analyzer with a flame ionization detector (FID), are summarized in Table 6-43. The THC samples were taken from the baghouse outlet stream, and were analyzed according to EPA Method 25A. Low THC concentration levels of < 60 ppm in the off-gas were demonstrated.

Table 6-43
Total Hydrocarbon Analysis Results at the Baghouse Outlet (ppm)

THC Analyzer Results		SUMMA Canisters	
Average Total Hydrocarbons or C_1-C_4	Maximum THC	Ethylene	Acetylene
35	60	0.8	0.4

In addition, product gases were sampled over a period of time at the baghouse outlet stream using on-line SUMMA canisters. The gas samples were analyzed for volatile organic compounds by combined gas chromatography/mass spectrometry according to EPA Method TO-14.

Off-gas product NO and SO_2 levels were monitored using an on-line mass spectrometer. Samples were drawn on-line downstream of the baghouse and downstream of the aftercooler. No NO or SO_2 were detected at a lower detection limit of 100 ppm. These data are consistent with results from other experiments carried out on a variety of waste feed streams.

6.6.3.4. Ceramic Product

Prior to feed injection, inorganic ceramic-forming materials containing CaO and SiO_2 were added to the CEP reactor. In addition, ceramic-forming materials (89 lbs) were blended with the feed mixture to minimize dependence on top additions.

A toxicity characteristics leaching procedure (TCLP) testing of RCRA metals was performed on the ceramic sample marked 1T-93-018-S2b. The TCLP test results indicate that metal leaching levels were non-detectable or below regulatory limits, as shown in Table 6-44.

Table 6-44
TCLP Analysis on Ceramic Sample

Metal	1T-93-018-S2b	Regulatory Level, (mg/L)
As	ND[1]	5.0
Ba	ND	100
Cd	ND	1.0
Cr	0.5[2]	5.0
Pb	ND	5.0
Hg	ND	0.2
Se	ND	1.0
Ag	ND	5.0

[1] ND = Not detected

[2] Cr_2O_3-Al_2O_3 refractory bricks were present during these runs which provided a source of Cr_2O_3 to the ceramic phase. Refractory composition has been optimized to preclude this occurrence in commercial installations.

6.6.3.5. Mass Balance

Mass balance calculations were performed for the major components (C,H, and O) for appropriate injection periods. Table 6-45 summarizes the results of the calculations. Sources of data for the mass inputs include gases fed through the tuyere (methane and oxygen) and the organic components of the feed as calculated. The output mass data were calculated using mass spectrometer results. Argon gas was used as the tie for determining output gas flow rates.

Table 6-45
Carbon, Hydrogen and Oxygen Overall Mass Balance

In	C	H	O
Total Mol	14,784.62	5,054.22	5,763.99
Total Lbs.	390.78	11.13	203.14
Out	**C**	**H**	**O**
Total Mol	13,599.04	7,060.49	6,918.31
Total Lbs.	359.45	15.55	243.82
Percent Recovered	91.98	139.69	120.03

Table 6-45 shows that good mass closure for carbon was achieved. The high oxygen recovery can be attributed to oxygen infiltration into the reactor during sampling and error associated with calculating oxygen contained in the ceramic product (typically calculated by difference). In addition, excess hydrogen and oxygen may have resulted from the fact that feed chemical composition was calculated from approximate chemical formulae as no ultimate analysis was performed. Table 6-46 summarizes the overall recovery of organic constituents, carbon, hydrogen, and oxygen during waste processing. "% Feed" represents the quantities of elements in the feed (organic) potentially available for formation of synthesis gas. "% Recycled" represents the quantities of elements actually present in the synthesis gas based on measured gas flow rates in the off-gas product stream. "% Recovered" is the ratio of % Recycled to % Feed. Conversion of organics to synthesis gas product exceeded 94%.

Table 6-46
Experimental Recovery for Synthesis Gas

Synthesis Gas Formers (wt% Feed)			% Feed	% Recycled	% Recovered
C	H	O			
19.11	1.76	4.22	25.09	23.76	94.69

6.6.4. Experimental Campaign 1T-94-003 Summary

Mixtures of graphite/divinyl benzene (DV) and graphite/polystyrene were processed on the demonstration-scale CEP reactor. The experimental run was designed to demonstrate the conversion efficiency of organic materials into a stable off-gas stream. Lead and zinc were added to the graphite/DV feed mixture in trace quantities to simulate waste contaminated with volatile heavy metals (VHMs). Trace amounts of polyvinyl chloride (PVC) and cobalt were added to the graphite/polystyrene mixture to model metal-containing chlorinated waste streams. The chlorine content of this feed was 0.57%. The feed mixtures components are summarized in Table 6-47.

Table 6-47

Feed	Feed Components
Graphite/DV	28.4% Graphite, 68.8% Divinyl benzene, 1% Zinc, 1% Lead, 0.8% Cobalt
Low PVC	78.4% Graphite, 19.6% Polystyrene, 1% PVC, 1% Cobalt

6.6.4.1. Feed Composition

As per the experimental plan, the graphite/DV feed mixture was prepared by mixing known amounts of graphite with divinyl benzene. Pre-determined trace amounts of zinc, lead, and cobalt were added to the mixture. The low PVC feed mixture was prepared by blending known quantities of polyvinyl chloride and cobalt with a mixture of graphite and polystyrene to yield a 1% PVC feed mixture. All materials were pre-treated by grinding and sifting to reduce their particle size to less than 70 mesh in order to meet the solids feed system requirements. Ultimate analysis results of the feed components were used to calculate the elemental composition of the feed mixtures as shown in Table 6-48.

Table 6-48
Feed Mixture Elemental Composition (Wt%)

Element	IX Resin	Low PVC
Carbon	49.90	95.79
Hydrogen	7.06	1.63
Nitrogen	1.79	0.09
Chlorine	-	0.57
Ash	0.09	0.24
Oxygen	38.36	0.68
Cobalt	0.8	1.0
Zinc	1.0	-
Lead	1.0	-

6.6.4.2. Feed Injection

The metal bath was initially charged with approximately 921 lbs of iron and 15 lb of flux-forming materials and heated to about 2800°F. During heatup, incremental amounts of iron were added to the bath at a rate of 15 lbs/min over a period of 4.5 hours. Metal addition was interrupted by periods of addition of flux materials and graphite. The amount of ceramic-formers added prior to feed injection was 225 lbs. The total metal weight in the reactor prior to the initial injection was 4526 lbs. Measurements taken prior to feed injection showed a bath temperature of 2651°F and a bath carbon concentration of 2.52%. The feed was transported to the reactor using nitrogen as the carrier gas. Oxygen was injected as a co-reactant and methane was injected as a cooling gas.

Graphite/DV feed injection began at 22:18 on 3/15/94. At 1:59, feed injection was temporarily interrupted in order to "deskull" the reactor. Deskulling involves the directed addition of oxygen at sampling and viewing ports to react away any carbon accumulation forming on the ports. Feed injection was re-started at 6:27. Approximately, 776 lbs of solids feed was injected in 6 hours and 24 minutes. Feed flow rates to the reactor were in general steady during the two injection periods.

The graphite/polystyrene feed mixture was injected (beginning at 21:15 on 3/16/94) for 6 hours and 45 minutes, at which point feed flow was stopped for deskulling operations. The total feed amount injected during this period was 603 lbs. Feed flow was interrupted at 22:31 for 36 minutes to carry out decarburization experiments.

Decarburization is a process that involves reducing the carbon content of the metal bath by interrupting solids feed flow to the reactor.

There was then a subsequent injection period during which 294.4 lbs of feed was processed in 2 hours and 42 minutes. Solid feed flow rates for the graphite/polystyrene feed were generally steady. The total feed injection times and quantities are summarized in Table 6-49.

Table 6-49
Summary of Feed Injection for Run 1T-94-003

Feed	Injection Time	Amount Injected (Lbs)
IX Resin	3 hrs, 40 min	436.8
IX Resin	2 hrs, 44 min	339.2
Totals	**6 hrs, 24 min**	**776.0**
Graphite/PS	6 hrs, 45 min	603.0
Graphite/PS	2 hrs, 42 min	294.4
Totals	**9 hrs, 27 min**	**897.4**

It should be mentioned that the data presented in this report were collected according to a detailed experimental plan, whose main objective is to study CEP performance for processing a wide range of waste streams. As such, the reactor operation is not optimized for a commercial environment since the primary goal is to maximize data collection through sampling, testing, and manipulating operating conditions. This entails feed interruption and performing of tasks that normally would not be required under normal operating conditions.

6.6.4.3. Off-Gas Product

Total output gas flow rates were calculated using mass spectrometer (MS) data. Argon gas is injected into the reactor as a tie component at a known flow rate. Off-gas argon concentration measured by the MS is combined with the known input argon flow rate to calculate the total off-gas flow rate. Using this value, the flow rates of other gas components detected by the MS are calculated.

A profile of product off-gas flow rate during processing of both feed mixtures was plotted against time. A steady off-gas flow rate has been maintained during feed injection, indicating a steady solids feed flow rate.

Under steady feed conditions of solids, oxygen, and methane, the CO/H_2 ratio was also maintained steady, an indication of the consistency in converting organic materials into a stable off-gas stream.

6.6.4.4. Off-Gas Trace Analysis

Product gases were sampled over a period of time at the baghouse outlet stream using on-line SUMMA canisters. The gas samples were analyzed for volatile organic compounds by combined gas chromatography/mass spectrometry according to EPA Method TO-14. The analytical results were used to calculate destruction and removal efficiencies (DREs) of organic compounds. The samples collected and sampling times and locations are summarized in Table 6-50.

Table 6-50
Summa Canister Samples

Sample No	Sampling Time	Date	Sampling Location
IER-BO	00:48	3/16/94	Baghouse outlet
DRE-1-BO	1:10	3/17/94	Baghouse outlet
DRE-2-BO	3:50	3/17/94	Baghouse outlet
CW-1-BO	13:57	3/17/94	Baghouse outlet
CW-2-BO	14:10	3/17/94	Baghouse outlet
CW-3-BO	14:43	3/17/94	Baghouse outlet
CW-4-BO	14:50	3/17/94	Baghouse outlet

Mass spectrometer samples were also drawn on-line downstream of the baghouse and downstream of the aftercooler. No NO or SO_2 were detected at a lower detection limit of 100 ppm.

Total hydrocarbon content data were taken using an on-line analyzer with a flame ionization detector (FID). The THC samples were taken from the reactor headspace and from the baghouse outlet stream, and were analyzed according to EPA Method 25A. The CH_4 level was typically below 60 ppm.

6.6.4.5. Destruction of Organics

System destruction and removal efficiency (DRE) calculations were performed using a modified procedure (outlined earlier) to account for the fact that polyvinyl chloride (PVC) and polystyrene are polymeric molecules that do not volatilize and therefore,

will not be detected in the off-gas stream. In addition, divinyl benzene which makes up the bulk of the organic matter is not detected for by EPA Method TO-14.

PVC was thus modeled as vinyl chloride (CH_2CHCl) and as chloroethane (CH_3CHCl), which are very similar structurally to the PVC monomer (-[CH_2CHCl]-). Similarly, polystyrene (-[CH_2-$CH(C_6H_5)$]-) was modeled as styrene (CH_2=$CH(C_6H_5)$) and as ethyl benzene ($CH_3CH_2(C_6H_5)$). The destruction efficiency for divinyl benzene was calculated by comparing the number of moles of benzene rings in the solids feed with the number of moles of benzene rings contained in the TO-14 compound list. The resulting DREs for PVC, polystyrene, and divinyl benzene for representative samples are displayed in Table 6-51.

Table 6-51
DRE` Summary for PVC and Polystyrene

Sample No	Sampling Time	Date	Tracer	Compound	DRE`
IER-BO	00:48-00:49	3/16/94	Benzene/ Toluene	(IXR) Divinyl benzene	99.99990%
CW-1-BO	13:52-13:57	3/17/94	Vinyl chloride	PVC	>99.99980%[1,2]
CW-1-BO	13:52-13:57	3/17/94	Chloroethane	PVC	>99.99981%[2]
DRE-1-BO	1:05-1:10	3/17/94	Styrene	Polystyrene	>99.99999%
DRE-1-BO	1:05-1:10	3/17/94	Ethyl benzene	Polystyrene	>99.99999%
CW-3-BO	14:42-14:44	3/17/94	Styrene	Polystyrene	>99.99999%
CW-3-BO	14:42-14:44	3/17/94	Ethyl benzene	Polystyrene	>99.99999%
CW-4-BO	14:42-14:52	3/17/94	Styrene	Polystyrene	>99.99999%
CW-4-BO	14:42-14:52	3/17/94	Ethyl benzene	Polystyrene	99.99999%

[1] The ">" signs indicate that the tracer molecules were non-detectable in the SUMMA canister samples. Lower detection limits (LDL) for those compounds were used to calculate the DREs.
[2] DRE calculation analytically limited by LDL.

6.6.4.6. Ceramic Product

Prior to feed injection, inorganic ceramic-forming materials containing Wollastonite, $CaAlO_4$, and CaO were added to the CEP reactor. The cumulative amount of flux materials added was 254 lbs.

A toxicity characteristics leaching procedure (TCLP) testing of RCRA metals was performed on the ceramic sample marked 1T-94-003-S11. The TCLP test results indicate

that metal leaching levels were non-detectable or below regulatory limits as shown in Table 6-52.

Table 6-52
TCLP Analysis on Ceramic Sample

Metal	1T-94-003-S11	REGULATORY LEVEL, (Mg/L)
As	ND	5.0
Ba	ND	100
Cd	ND	1.0
Cr	ND	5.0
Pb	ND	5.0
Hg	ND	0.2
Se	ND	1.0
Ag	ND	5.0

6.6.4.7. Metal Product

Metal samples were collected during feed injection by lowering a sealed sampling probe through the top of the reactor. Pre- and post- injection metal samples were taken and analyzed for metal concentration and composition. The analysis indicated that there was no organic constituents in the metal samples.

6.6.4.8. Mass Balance

Mass balance calculations were performed for the major components (C,H, and O) during injection of the graphite/DV. Sources of data for the mass inputs include gases fed through the tuyere (methane and oxygen) and the organic components of the feed as measured by ultimate analysis. The output mass data were calculated using mass spectrometer results. Argon gas was used as the tie for determining output gas flow rates. Table 6-53 summarizes the results of the calculations.

Table 6-53
C, H, and O Material Balance

Run 1T94-003				Major Element Balance		
Graphite/DV	SCF	Moles	Lbs.	C	H	O
Mass In						
Methane	327.9	0.87	13.84	10.38	3.46	
Oxygen	3415.4	9.01	288.37			288.37
Feed Mixture			651.20	326.15	46.14	250.72
Iron Melted (2.53 wt% C)			4986	126.15		
Total				462.68	49.6	539.09
Mass Out						
Hydrogen	8554.1	22.57	45.14		45.14	
Carbon Monoxide	10823.9	28.56	799.65	342.71		
Carbon Dioxide	233.9	0.62	27.15	7.41		456.95
Ferro bath at end (3.06 wt% C)			4986	153.0		19.75
Total				503.12	45.14	476.70
% Closure				108.7%	91.0%	88.4%

6.6.5. Experimental Campaign 1T-94-004 Summary

Graphite/polystyrene (PS) feed mixtures containing low PVC and high PVC levels were processed on the demonstration-scale unit. The experimental run was designed to demonstrate the conversion efficiency of organic materials into a stable synthesis gas. Polyvinyl chloride (PVC) was added to the feed mixtures to model chlorinated waste streams. Lead and zinc were added to the high PVC feed mixture in trace quantities to simulate waste contaminated with volatile heavy metals (VHMs). The feed mixtures components are summarized in Table 6-54.

Table 6-54

Feed	Feed Components
Low PVC	78.4% Graphite, 19.6% Polystyrene, 1% PVC, 1% Cobalt
High PVC	70% Graphite, 7% Polystyrene, 20% PVC, 1.5% Zinc, 1.5% Lead

6.6.5.1. Feed Composition

As per the experimental plan, pre-determined amounts of polyvinyl chloride (PVC) were blended with a mixture of graphite and polystyrene to yield a 1% PVC and a 20% PVC feed mixtures. Trace quantities of metals were added to both feed mixtures. All materials were pre-treated by grinding and sifting to reduce their particle size to less than 70 mesh in order to meet the solids feed system requirements. Ultimate analysis results of the feed components were used to calculate the elemental composition of the feed mixtures. Table 6-55 shows the calculated final composition of the feed mixtures.

Table 6-55
Feed Mixture Elemental Composition (Wt%)

Element	Low PVC	High PVC
Carbon	95.79	83.17
Hydrogen	1.63	1.56
Nitrogen	0.09	0.08
Chlorine	0.57	11.36
Ash	0.24	0.22
Oxygen	0.68	0.61
Cobalt	1	-
Zinc	-	1.5
Lead	-	1.5

6.6.5.2. Feed Injection

The metal bath was initially charged with approximately 1289 lbs of iron and 20 lbs of flux-forming materials and heated to about 2629°F. During heatup, incremental amounts of iron were added to the bath at a rate of 15 lbs/min over a period of 2 hours. Metal addition was interrupted by periods of addition of flux materials and graphite. Flux-forming materials were also added during injection of the solids feed to optimize the composition of the ceramic layer. The total amount of ceramic-formers added during the run was 411 lbs. The total metal weight in the reactor prior to the initial injection was 3179 lbs. Measurements taken prior to feed injection indicated a bath temperature of 2686°F and a bath carbon concentration of 2.36%. The feed was transported to the reactor using nitrogen as the carrier gas. Oxygen was injected as a co-reactant and methane was injected as a cooling gas.

Feed injection of the low PVC mixture began at 17:28 on 3/19/94. Feed was injected for 10 hours and 41 minutes before it was interrupted temporarily in order to perform decarburization experiments. There were then two subsequent injection periods of 10 hours and 2.75 hours. The approximate total amount of low PVC feed injected was 1467 lbs. Changes in the weight of the Remacor solid feed tank were in general steady indicating a steady feed flow rate.

The high PVC feed mixture was injected continuously for 4 hours and 45 minutes. The total feed amount injected during this period was 313.8 lbs. The total feed injection times and quantities are summarized in Table 6-56.

Table 6-56
Summary of Feed Injection for Run 1T-94-004

Feed	Injection Time	Amount Injected (Lbs)
Low PVC	10 hrs, 41 min	676.4
Low PVC	10 hrs	622.4
Low PVC	2 hrs, 45 min	168.4
Totals	**23 hrs, 26 min**	**1467.2**
High PVC	4 hrs, 30 min	313.8

It should be mentioned that the data presented in this report were collected according to a detailed experimental plan, whose main objective is to study CEP performance for processing a wide range of waste streams. As such, the reactor operation is not optimized for a commercial environment since the primary goal is to maximize data

collection through sampling, testing, and manipulating operating conditions. This entails feed interruption and performing of tasks that normally would not be required under normal operating conditions.

6.6.5.3. Off-Gas Product

Total output gas flow rates were calculated using mass spectrometer (MS) data. Argon gas was injected into the reactor as a tie component at a known flow rate. The argon concentration in the off-gas measured by the MS was combined with the known input argon flow rate to calculate the total off-gas flow rate. Using this value, the flow rates of other gas components detected by the MS were calculated.

A profile of product off-gas flow rate during feed processing was plotted. A steady off-gas stream flow rate has been maintained for both feed mixtures. The CO/H_2 ratio (on a volume basis) was highly dependent on feed flow rates of solids and oxygen co-feed, as predicted. Under steady feed conditions of solids, oxygen, and methane, the CO/H_2 ratio remained within a stable range, indicating a consistency in converting organic materials into a stable gas phase.

6.6.5.4. Off-Gas Trace Analysis

Product gases were sampled over a period of time at the baghouse outlet stream using on-line SUMMA canisters. The gas samples were analyzed for volatile organic compounds by combined gas chromatography/mass spectrometry according to EPA Method TO-14. The analytical results were used to calculate destruction and removal efficiencies (DREs) of organic compounds. The samples collected and sampling times and locations are summarized in Table 6-57.

Table 6-57
Summa Canister Samples

Sample No	Sampling Time	Date	Sampling Location
DRE-03-BO	19:35	3/19/94	Baghouse outlet
DRE-04-BO	20:10	3/19/94	Baghouse outlet
DRE-05-BO	22:32	3/19/94	Baghouse outlet
DRE-06-BO	00:21	3/20/94	Baghouse outlet
DRE-07-BO	1:34	3/20/94	Baghouse outlet
DRE-08-BO	4:04	3/20/94	Baghouse outlet
DRE-09-BO	6:46	3/20/94	Baghouse outlet
DRE-10-BO	9:04	3/20/94	Baghouse outlet
DRE-11-BO	10:33	3/20/94	Baghouse outlet
DRE-12-BO	12:53	3/20/94	Baghouse outlet
DRE-13-BO	14:12	3/20/94	Baghouse outlet
DRE-14-BO	15:40	3/20/94	Baghouse outlet
DRE-15-BO	18:45	3/20/94	Baghouse outlet
DRE-16-BO	1:49	3/21/94	Baghouse outlet
DRE-17-BO	4:14	3/21/94	Baghouse outlet

Mass spectrometer samples were also drawn on-line downstream of the baghouse and downstream of the aftercooler. No NO or SO_2 were detected at a lower detection limit of 100 ppm. HCl gas in the off-gas was not detected by the mass spectrometer.

6.6.5.5. Destruction of Organics

System destruction and removal efficiency (DRE) calculations were performed using a modified procedure (outlined earlier) to account for the fact that polyvinyl chloride (PVC) and polystyrene are polymeric molecules that do not volatilize and therefore, will not be detected in the off-gas stream.

PVC was thus modeled as vinyl chloride (CH_2CHCl) and as chloroethane (CH_3CHCl), which are very similar structurally to the PVC monomer (-[CH_2CHCl]-). Similarly, polystyrene (-[CH_2-$CH(C_6H_5)$]-) was modeled as styrene (CH_2=$CH(C_6H_5)$) and as ethyl benzene ($CH_3CH_2(C_6H_5)$). The resulting destruction efficiencies for PVC and polystyrene for representative samples are displayed in Table 6-58.

Table 6-58
DRE` Summary for PVC and Polystyrene

Sample No	Sampling Time	Date	Tracer	Compound	DRE`
DRE-16-BO	1:49-2:33	3/21/94	Vinyl chloride	PVC	>99.99998%
DRE-16-BO	1:49-2:33	3/21/94	Chloroethane	PVC	>99.99998%
DRE-17-BO	4:14-4:50	3/21/94	Vinyl chloride	PVC	>99.99998%
DRE-17-BO	4:14-4:50	3/21/94	Chloroethane	PVC	>99.99998%
DRE-16-BO	1:49-2:33	3/21/94	Styrene	Polystyrene	>99.99994%
DRE-16-BO	1:49-2:33	3/21/94	Ethyl benzene	Polystyrene	>99.99993%
DRE-17-BO	4:14-4:50	3/21/94	Styrene	Polystyrene	>99.99994%
DRE-17-BO	4:14-4:50	3/21/94	Ethyl benzene	Polystyrene	>99.99994%

[1]The ">" signs indicate that the tracer molecules were non-detectable in the SUMMA canister samples. Lower detection limits (LDL) for those compounds were used to calculate the DREs.
[2]DRE calculation analytically limited by LDL.

6.6.5.6. Ceramic Product

Prior to feed injection, approximately 20 lbs of inorganic ceramic-forming materials were added to the CEP reactor. Additional flux materials containing Wollastonite, $CaAlO_4$, and CaO were added prior to injection of the high PVC feed. The ceramic layer composition was not optimized for processing highly chlorinated feed. The high content of Al_2O_3 (both dissolved and entrained) in the ceramic phase precluded capture of any significant amount of chlorine.

A ceramic sample was collected at the completion of feed injection and marked 1T-94-004-S9. A toxicity characteristics leaching procedure (TCLP) testing of RCRA metals was performed. The TCLP test results indicated that metal leaching levels were non-detectable or below regulatory limits as shown in Table 6-59.

Table 6-59
TCLP Analysis on Ceramic Sample

Metal	1T-94-004-S9	Regulatory Level, (mg/L)
As	ND[1]	5.0
Ba	ND	100
Cd	ND	1.0
Cr	0.30[2]	5.0
Pb	ND	5.0
Hg	ND	0.2
Se	ND	1.0
Ag	ND	5.0

[1] ND = Not detected
[2] Cr_2O_3-Al_2O_3 refractory bricks were present during these runs which provided a source of Cr_2O_3 to the ceramic phase. Refractory composition has been optimized to preclude this occurrence in commercial installations.

6.6.5.7. Metal Product

Metal samples were collected during feed injection by lowering a sealed sampling probe through the top of the reactor. Pre- and post- injection metal samples were taken and analyzed for metal concentration and composition. The analysis had indicated that there were no organic constituents in the metal samples.

6.6.5.8. Mass Balance

Mass balance calculations were performed for the major components (C,H, and O) in each feed and for the total materials. Sources of data for the mass inputs include gases fed through the tuyere (methane and oxygen) and the organic components of the feed as measured by ultimate analysis. The output mass data were calculated using mass spectrometer results. Argon gas was used as the tie for determining output gas flow rates. Table 6-60, Table 6-61, and Table 6-62 summarize the results of the calculations.

Table 6-60
C, H, and O Material Balance

Run 1T94-004				Major Element Balance		
Low PVC	SCF	Moles	Lbs.	C	H	O
Mass In						
Methane	6247.5	16.48	263.75	197.8	65.9	
Oxygen	32260.6	85.12	2723.85			2723.9
Feed Mixture			1467.2	1405.4	23.9	10.0
Carbon added to bath				280.0		
Iron Melted (2.63 wt% C)			3179	75.0		
Total				**1958.2**	89.8	**2733.9**
Mass Out						
Hydrogen	18616.1	49.1	98.2		98.2	
Carbon Monoxide	53562.1	141.3	3957.1	1695.9		2261.2
Carbon Dioxide	1307.5	3.5	151.8	41.4		110.4
Ferro bath at end (3. 6 wt% C)			3179	114.4		
Total				**1851.7**	**98.2**	**2371.6**
% Closure				**94.6%**	**109.3%**	**86.7%**

Table 6-61
C, H, and O Material Balance

Run 1T94-004				Major Element Balance		
High PVC	SCF	Moles	Lbs.	C	H	O
Mass In						
Methane	1155.25	3.05	48.77	36.6	12.2	
Oxygen	5762.60	15.20	486.55			486.6
Feed Mixture			313.8	261.0	4.9	1.9
Iron Melted (3.74 wt% C)			3179	118.9		
Total				**416.5**	**17.1**	**488.5**
Mass Out						
Hydrogen	3570.06	9.42	18.84		18.8	
Carbon Monoxide	9594.93	25.32	708.86	303.8		405.1
Carbon Dioxide	169.14	0.45	19.64	5.4		14.3
Ferro bath at end (3. 8 wt% C)			3179	120.8		
Total				**430.0**	**18.8**	**419.4**
% Closure				**103.2%**	**109.9%**	**85.9%**

Table 6-62
Overall Material Balance

Run 1T94-004	Low PVC	High PVC	SCF	Lbs.
Mass In				
Methane (SCF)	6247.50	1155.25	7402.75	312.5
Oxygen (SCF)	32260.60	5762.6	38023.2	3210.4
Feed Mixture (lbs.)	1467.2	313.8		1781.0
Carbon added to bath (lbs.)				280
Flux additons (lbs.)				411
Iron melted				3179
Refractory				280
Total				9453.9
Mass Out				
Hydrogen (SCF)	18616.1	3570.1	22186.2	117.1
Carbon monoxide (SCF)	53562.1	9594.9	63157.0	4666.0
Carbon dioxide (SCF)	1307.5	169.1	1476.6	171.4
Hydrogen chloride (SCF)				
Metal/ceramic tapped (lbs.)				3918
Total				9017.0
% Closure				95.4%

6.6.6. Experimental Campaign 1T-94-005 Summary

A feed mixture containing graphite, organic material, and metals was processed on the demonstration-scale unit. The heterogeneous mixture consisting of small pieces of colored plastic, bits of metal and wire, and grains of these materials was prepared to simulate scrap metal contaminated with organic waste matter. A 70 mesh size material was prepared by sifting and grinding for tuyere injection. Because of the decrease in total metal content upon grinding, aluminum, iron, and copper were added to the 70 mesh powder. Lime (ceramic-former) was also added to the powder material to minimize dependence on top additions during feed injection. The new mixture was composed of 58% 70 mesh powder, 14% additional metals (Al, Fe, Co), and 28% lime.

Finally, graphite was mixed with the 70 mesh powder material to ensure sufficient carbon source in the feed.

Large size materials, which were not sifted through the 4 mesh screen, were chopped into 1/8" or smaller pieces in a radial knife grinder. This material was selected for injection through the bulk solids lance. The remaining 1" material was selected for top charging to the reactor. The metal composition for all feed materials is shown in Table 6-63.

Table 6-63
Metal Composition of Feed Materials for Run 1T-94-005 (Wt%)

Component	70 mesh powder	Tuyere Injection[1]	Tuyere Injection[2]	Bulk Solids Lance[3]	Bay Funnel[4]
Aluminum	14.8	8.39	4.11	16.93	84.68
Chromium	0.4	0.23	0.11	0.24	0.004
Copper	5.2	2.95	1.45	15.25	0.013
Iron	6.0	3.40	1.67	1.18	0.053
Nickel	1.1	0.62	0.30	0.24	0.036
Lead	1.1	0.62	0.30	0.36	0.0013
Zinc	0.8	0.45	0.22	0.51	0.008
Silver	0.086	0.05	0.02		< 0.001
Tin	0.8	0.45	0.22	0.45	
Barium	0.3	0.17	0.08		
Cobalt	0.3	0.17	0.08		
Cadmium	0.023	0.01	0.00		
Manganese	0.1	0.06	0.03		
Molybdenum	0.06	0.03	0.01		
Titanium	0.2	0.11	0.05		
Total Metals (lbs.)	31.269	17.71	8.65	35.08	84.7963

[1]Composed of 207 lbs. of the 70 mesh mix and 158 lbs. of graphite.
[2]Material injected during the combined tuyere/bulk solids lance injection. Consisted of 144.2 lbs. of the first tuyere-injected material and 150 lbs. of graphite.
[3]Composition of 1/8" pieces injected through the bulk solids lance.
[4]Composition of 1" pieces added through the bay funnel.

The measured and calculated carbon, hydrogen, and oxygen levels for the material injected through the tuyere and the bulk solids lance are shown in Table 6-64. These

were determined from the ultimate analysis of the 70 mesh powder and the ultimate analysis of the 1/8" material. No ultimate analysis for the 1" material was performed. However, based on the metal composition, the C, H, and O levels are not expected to exceed 15 wt%.

Table 6-64
Carbon, Hydrogen and Oxygen Levels in the Feed (Wt%)[1]

	C	H	O
70 mesh powder	32.09	3.46	0.10
Tuyere injection #1[2]	53.85	1.14	0.03
Tuyere injection #2[3]	77.38	0.559	0.015
Bulk solids lance[4]	38.63	5.00	0.5

1 There was no ultimate analysis for the 1" material.
2 Composed of 207 lbs. of the 70 mesh powder mix and 158 lbs. of graphite injected through the tuyere.
3 Used during the combined tuyere/bulk solids lance injection.
4 Composition of 1/8" pieces injected through the bulk solids lance.

6.6.6.1. Feed Injection

The bath was initially charged with approximately 3,200 pounds of metal. The bath temperature measured just prior to injection was approximately 2700°F. Tuyere injection began at approximately 8:32 on 4/21/94 and was stopped at 10:41. An additional 150 lb of graphite was added to the Remacor tank as planned. Bay funnel additions of the 1" material began at approximately 11:30. This continued until about 12:00, at which time funnel additions were stopped (pending arrival of a third party analytical service). The measured bath temperature at this time was 2687°F, and the carbon level was 2.2 wt%. Funnel additions were re-started at 13:55 and continued until 14:50 (final temperature=2717°F, carbon=1.87 wt%). A total of 45 lbs of the 1" Sandia material were added through the bay funnels. Throughout the run, additional ceramic formers, metals, iron and graphite were added to the bath.

A bulk solids lance was put into position and pre-heated at 19:14. Bulk solids injection of the 1/8" material began at about 20:10 and continued until 20:56. At 20:13 it was observed that the tip of the submerged lance was just above the bath. Material addition through this lance continued without adjustment.

The combined injection experiments began at 21:28 with tuyere injection of the 70 mesh powder mixture. Bulk solids injection then started at 21:39 and ended at 22:26. Tuyere

injection was stopped at 22:29. The total amounts of feed added to the bath were 45 pounds of the 1" material (bay funnel), 56.6 pounds of the 1/8" material (bulk solids lances) and 362 pounds of the 70 mesh powder/graphite mixture.

6.6.6.2. Off-Gas Trace Analysis

Total hydrocarbon data, taken using an on-line analyzer with a flame ionization detector (FID), are summarized in Table 6-65. The THC samples were taken from the baghouse outlet stream, and were analyzed according to EPA Method 25A. Low THC concentration levels of < 20 ppm in the off-gas were demonstrated.

Table 6-65
Total Hydrocarbon Analysis Results at the Baghouse Outlet (ppm)

	THC Analyzer Results			SUMMA Canisters	
Run	Average Total Hydrocarbons or C_1-C_4	Maximum THC	Non-Methane Hydrocarbons	Ethylene	Acetylene
1T-94-005[1]	8	20	NA	ND	ND

[1]Includes data from the first tuyere injection period, only.
NA = Not analyzed
ND = Not detected

In addition, product gases were sampled over a period of time at the baghouse outlet stream using on-line SUMMA canisters. The gas samples were analyzed for volatile organic compounds by combined gas chromatography/mass spectrometry according to EPA Method TO-14. As shown in Table 6-65, ethylene and acetylene were not detected in the off-gas product stream.

Off-gas product NO and SO_2 levels were monitored using an on-line mass spectrometer. Samples were drawn on-line downstream of the baghouse and downstream of the aftercooler. No NO or SO_2 were detected at a lower detection limit of 100 ppm.

6.6.6.3. Ceramic Product

Prior to feed injection, inorganic ceramic-forming materials (85 lbs) were added to the CEP reactors. In addition, ceramic-forming materials (66 lb) were blended with the feed mixture to minimize dependence on top additions.

A toxicity characteristics leaching procedure (TCLP) testing of RCRA metals was performed on the ceramic sample marked 1T-94-005-TS2. The TCLP test results indicate

that metal leaching levels were non-detectable or below regulatory limits as shown in Table 6-66.

Table 6-66
TCLP Analysis on Ceramic Sample

Metal	1T-94-005-TS2	Regulatory Level, (mg/L)
As	ND[1]	5.0
Ba	ND	100
Cd	ND	1.0
Cr	0.3[2]	5.0
Pb	ND	5.0
Hg	ND	0.2
Se	ND	1.0
Ag	ND	5.0

[1] ND = Not detected
[2] Cr_2O_3-Al_2O_3 refractory bricks were present during these runs which provided a source of Cr_2O_3 to the ceramic phase. Refractory composition has been optimized to preclude this occurrence in commercial installations.

6.6.6.4. Mass Balance

Mass balance calculations were performed for the major components (C,H, and O) for appropriate injection periods. Table 6-67 summarizes the results of the calculations. Sources of data for the mass inputs include gases fed through the tuyere (methane and oxygen) and the organic components of the feed as calculated. The output mass data were calculated using mass spectrometer results. Argon gas was used as the tie for determining output gas flow rates.

Table 6-67
Carbon, Hydrogen and Oxygen Overall Mass Balance

In	C	H	O
Total Mol	6,566.21	5,054.22	5,763.99
Total Lbs.	173.56	11.13	203.14
Out	**C**	**H**	**O**
Total Mol	6,551.19	7,060.49	6,918.31
Total Lbs.	173.16	15.55	243.82
Percent Recovered	99.77	139.69	120.03

The Table 6-67 shows an outstanding mass closure for carbon. The high oxygen recovery can be attributed to oxygen infiltration into the reactor during sampling and error associated with calculating oxygen contained in the ceramic product (typically calculated by difference). Table 6-68 summarizes the overall recovery of organic constituents, carbon, hydrogen, and oxygen during waste processing. "% Feed" represents the quantities of elements in the feed (organic) potentially available for formation of synthesis gas. "% Recycled" represents the quantities of elements actually present in the synthesis gas based on measured gas flow rates in the off-gas product stream. "% Recovered" is the ratio of % Recycled to % Feed. Conversion of organics to syngas product exceeded 97%.

Table 6-68
Experimental Recovery for Synthesis Gas

Synthesis Gas Formers (wt% Feed)			% Feed	% Recycled	% Recovered
C	H	O			
32.09	3.46	23.37	58.86	57.46	97.62

6.6.7. Experimental Campaign 1T-94-006 Summary

Feed mixtures of graphite, polyethylene, and polystyrene were successfully processed on the demonstration-scale unit. The Feed mixtures and their compositions are described in Table 6-69. Feed (1), consisting of graphite and polyethylene, was processed to demonstrate the conversion efficiency of organic constituents into a stable

gas phase. After processing of feed (1) was completed, dust material from the baghouse was mixed with unprocessed feed (1). The new feed mixture (feed (2)) was processed to demonstrate the viability of recycling process dust. Feed (3), comprised of graphite, polystyrene, polyvinyl chloride (PVC), trichlorobenzene (TCB), and trace amounts of heavy metals, was processed to demonstrate the applicability of CEP to processing chlorinated organic feed streams. PVC and TCB were added to feed (3) mixture to model the chlorinated portion of the waste stream. Zinc and lead, present in trace quantities, were added to the feed to simulate volatile heavy metals-contaminated waste.

Table 6-69

Feed	Feed Components
Feed (1)	83.3% Graphite, 16.7% High Density Polyethylene (HDPE)
Feed (2)	64.3% (83.3% Graphite, 16.7% HDPE), 35.7% Recycled Dust
Feed (3)	66.8% Graphite, 4.5% Polystyrene, 25.7% PVC, 1.0% Zinc, 1.0% Lead, 1.0% TCB

6.6.7.1. Feed Composition

As per the experimental plan, graphite was mixed with high density polyethylene to yield a 83.3% graphite and 16.7% HDPE feed (1) mixture. Feed (2) mixture was prepared by mixing recycled baghouse process dust that had accumulated from previous runs with unprocessed feed (1) mixture. Feed (3) was prepared by blending polyvinyl chloride (PVC) with a mixture of graphite and polystyrene. Trichlorobenzene, lead, and zinc were added in trace quantities to the feed mixture. The elemental composition of all three feed mixtures is shown in Table 6-70. All materials were treated by grinding and sifting to reduce the particle size to less than 70 mesh in order to meet the solids feed system requirements.

Table 6-70
Feed Mixtures Composition

Element	Feed (1) wt%	Feed (2) wt%	Feed (3) wt%
Carbon	96.29	70.35	80.28
Hydrogen	2.27	1.64	1.65
Chlorine	-	2.10	15.20
Nitrogen	0.10	0.24	0.08
Sulfur	0.05	0.49	-
Ash	0.28	22.79	0.21
Oxygen	1.01	2.39	0.58
Zinc	-	-	1.0
Lead	-	-	1.0

6.6.7.2. Feed Injection

The metal bath was initially charged with 1321 lbs of iron and 10 lbs of lime and heated to about 2500°F. During heatup, additional charges of iron were added to the bath at a rate of 25 lbs/min over approximately 1.5 hours. Additional flux-forming materials and graphite were also added. Measurements taken prior to feed injection showed a bath temperature of 2637°F and a carbon level of 3.02%. Waste powder injection began at 2:42 on 4/24/94. The feed was transported to the reactor using nitrogen as the carrier gas. Oxygen was injected as a co-reactant and methane was injected as a cooling gas. Feed was continuously injected for 14 hours and 50 minutes with a few interruptions in order to carry out decarburization experiments. The total amount of feed (1) injected was 787 lbs.

Feed (2) injection was started at 21:42 after an amount (205 lbs) of recycled baghouse process dust was mixed with feed (1) in the Remacor tank. The amount of feed (2) mixture injected was 229 lbs. The feed was continuously injected for 3 hours. The steady feed flow indicates that process dust would be acceptable material for recycle.

Feed injection of the high PVC mixture was started at 4:57 on 4/25/94. Approximately 600 lbs of feed was injected in 9 hours and 8 minutes. The total feed injection times and quantities are summarized in Table 6-71.

Table 6-71
Summary of Feed Injection for Run 1T-94-006

Feed	Injection Time (hr)	Amount Injected (lbs)
Feed (1)	14 hr, 50 min	787.4
Feed (2)	3 hr	229
Feed (3)	9 hr, 8 min	600

6.6.7.3. Off-Gas Product

Total output gas flow rates were calculated using mass spectrometer (MS) data. Argon gas was injected into the reactor as a tie component whose flow rate was known. The argon concentration in the off-gas measured by the MS was combined with the known input argon flow rate to calculate the total off-gas flow rate. Using this value, the flow rates of other gas components detected by the MS were calculated.

A steady off-gas flow rate has been maintained during injection of all three feed mixtures, indicating a very steady solids feed flow rate. The off-gas flow rate correlated closely with changes in feed conditions. A steady CO/H_2 ratio was observed during feed injection, indicating consistent conversion of organic materials into a stable gas phase. Moreover, the steady off-gas flow and composition during processing of the graphite/HDPE/recycled dust feed demonstrate the viability of recycling process dust to the CEP reactor.

6.6.7.4. Off-Gas Trace Analysis

Product gases were sampled over a period of an hour at the baghouse outlet stream using on-line SUMMA canisters. The gas samples were analyzed for volatile organic compounds by combined gas chromatography/mass spectrometry according to EPA Method TO-14. The samples collected and sampling times and locations are summarized in Table 6-72. The data were used to calculate destruction and removal efficiencies (DREs) of organic constituents.

Table 6-72
SUMMA Canister Samples

Sample No	Sampling Time	Date	Sampling Location
Mix 3-1	6:30	4/24/94	Baghouse outlet
Mix 3-2	8:52	4/24/94	Baghouse outlet
Mix 3-3	10:47	4/24/94	Baghouse outlet
Mix 3-4	12:51	4/24/94	Baghouse outlet
Mix 3-5	15:20	4/24/94	Baghouse outlet
Mix 3-6	17:16	4/24/94	Baghouse outlet
Mix 2-1	7:25	4/25/94	Baghouse outlet
Mix 2-2	11:30	4/25/94	Baghouse outlet

Mass spectrometer samples were also drawn on-line downstream of the baghouse and downstream of the aftercooler. No NO or SO_2 were detected at a lower detection limit of 100 ppm. Hydrogen chloride gas was detected by the mass spectrometer in the baghouse outlet stream during injection of the high PVC feed (feed (3)).

Total hydrocarbon content data were taken using an on-line analyzer with a flame ionization detector (FID). The THC samples were taken from the baghouse outlet stream, and were analyzed according to EPA Method 25A. THC levels measured were consistently low (< 50 ppm).

6.6.7.5. Destruction of Organics

System destruction and removal efficiency (DRE) calculations were performed using a modified procedure (outlined earlier) to account for the fact that polyvinyl chloride (PVC) and polystyrene are non-volatile and hence will not be detected in the off-gas stream.

PVC was thus modeled as vinyl chloride (CH_2CHCl) and as chloroethane (CH_3CHCl), which are very similar structurally to the PVC monomer (-[CH_2CHCl]-). Similarly, polystyrene (-[CH_2-$CH(C_6H_5)$]-) was modeled as styrene (CH_2=$CH(C_6H_5)$). The resulting destruction efficiencies are displayed in Table 6-73.

Table 6-73
DRE` Summary for PVC and Polystyrene

Sample No	Sampling Time	Date	Tracer	Compound	DRE`
Mix 2-1	7:25	4/25/94	Vinyl chloride	PVC	99.99989%
Mix 2-2	11:30	4/25/94	Vinyl chloride	PVC	>99.99999%
Mix 2-1	7:25	4/25/94	Chloroethane	PVC	99.99983%
Mix 2-2	11:30	4/25/94	Chloroethane	PVC	>99.99999%
Mix 2-1	7:25	4/25/94	Styrene	Polystyrene	>99.99989%
Mix 2-2	11:30	4/25/94	Styrene	Polystyrene	>99.99995%

[1]The ">" signs indicate that the tracer molecules were non-detectable in the SUMMA canister samples.
[2]Lower detection limits (LDL) for those compounds were used to calculate their DRE.

6.6.7.6. Mass Balance

Mass balance calculations were performed for the major components (C,H, and O) in each feed and for the total materials in all three feeds. Sources of data for the mass inputs include gases fed through the tuyere (methane and oxygen) and the organic components of the feed as measured by ultimate analysis. The output mass data were calculated using mass spectrometer results. Argon gas was used as the tie for determining output gas flow rates. Table 6-74 and Table 6-75 summarize the results of the calculations.

Table 6-74
C, H, and O Material Balance

Run 1T94-006	Feed (1)	Feed (2)	Feed (3)	Major Element Balance		
				C	H	O
Mass In				(lbs.)	(lbs.)	(lbs.)
Methane (SCF)	3777.05	434.35	2135.30	87.4	67.0	
Oxygen (SCF)	18972.75	2160.65	11002.75			2713.3
Feed Mixture (lbs.)	787.4	229.0	600	1401.0	31.5	16.9
Carbon added to bath (lbs.)	140.0		40.0	180.0		
Iron Melted (lbs.)	92.42	97.6	97.40	287.4		
Total				1955.8	98.5	2730.2
Mass Out						
Hydrogen (SCF)	13785.6	1828.20	6546.27		116.9	
Carbon Monoxide (SCF)	30486.76	3863.86	17586.56	1644.5		2192.6
Carbon Dioxide (SCF)	805.62	69.54	90.84	30.6		81.6
Hydrogen Chloride (SCF)			903.48		2.4	
Ferro bath at end (lbs.)	99.43	96.11	111.69	307.2		
Total				1982.3	119.3	2274.2
Closure %				101.4%	121.1%	83.3%

Table 6-75
Overall Material Balance

Run 1T94-006	Feed (1)	Feed (2)	Feed (3)	SCF	lbs.
Mass In					
Methane (SCF)	37771.1	434.4	2135.3	6346.8	267.9
Oxygen (SCF)	18972.8	2160.7	11002.8	32136.3	2713.3
Feed Mixture (lbs.)	787.4	229.0	600.0		1616.4
Carbon added to bath (lbs.)	140		40		180
Flux additons (lbs.)	40	20	2		62
Iron melted	3229	15	15		3259
Total					8098.6
Mass Out					
Hydrogen (SCF)	13785.6	1828.2	A.	22160.1	116.9
Carbon monoxide (SCF)	30486.8	3863.9	17586.6	51937.3	3837.1
Carbon dioxide (SCF)	805.6	69.5	90.8	965.9	112.1
Hydrogen chloride (SCF)			903.5	903.5	87.0
Metal/ceramic tapped (lbs.					3684
Dust (lbs.)					99.6
Total					7936.7
Closure %					98.00%

6.6.8. Experimental Campaign 1T-94-009 Summary

Biosludge residuals, modeling contaminated sludge, were processed successfully via the CEP commercial prototype. This demonstration was performed continuously for more than 72 hours. Results from the demonstration campaign are highlighted by the following:

- excellent conversion efficiencies of ≥ 99.9999% with no evidence of dioxin formation as measured against the stringent German dioxin standard of 0.1 ng/Nm^3 TEQ;
- minimal levels of trace impurities (e.g., NO_X, SO_X < 3 and 1 ppm respectively) in the off-gas;
- a ceramic phase which passed EPA's TCLP (Toxicity Characteristics Leaching Procedure);

- excellent overall mass balance closure of 97%, with a carbon mass balance closure of 99%;
- steady state operation meeting and surpassing over 40 operational criteria; and
- an on-stream factor >90%.

6.6.8.1. Feed Composition

A total of five samples of the biosludge feed (as received) were taken from several drums and from within a common drum. Ultimate analysis was performed on the samples to determine the feed composition. The average composition of the biosludge is given in Table 6-76. The range of compositions for the five samples are also listed in Table 6-76. The compositional variation is within ± 5% for all elements except oxygen which varied nearly ± 10%. These data ranges indicate that the feed composition was fairly consistent at different locations within a single drum and among samples from multiple drums.

Table 6-76
Biosludge (as Received) Ultimate Analysis

Element	Average Composition (wt%)	Range of Compositions (wt%)
Carbon	45.7	43.9 - 47.4
Hydrogen	6.6	6.29 - 6.88
Oxygen	26.7	24.38 - 29.38
Nitrogen	9.2	8.77 - 9.53
Sulfur	1.2	1.16 - 1.22
Chlorine	0.05	0.02 - 0.069
Ash	10.6	9.78 - 10.86
Total	100.0	

The metal content of the ash (10.6% of the total biosludge material) was determined on four of the feed samples. The ash data summary is provided in Table 6-77.

Table 6-77
Metals Content of the Biosludge Ash (no PVC)

Element	Average Composition (wt%)	Range of Compositions (wt%)
Phosphorus	12.8	12.48 - 13.05
Silicon	3.5	2.8 - 4.31
Iron	2.6	2.46 - 2.93
Aluminum	0.5	0.42 - 0.58
Titanium	0.02	0.005 - 0.035
Calcium	8.2	7.66 - 8.79
Magnesium	1.9	1.82 - 1.91
Sulfur	2.9	2.85 - 3.10
Potassium	5.9	5.27 - 7.06
Sodium	17.4	10.48 - 21.90
Other (Balance)	44.3	
Total	100.0	

The remainder of the ash composition (balance of 44.3 wt%) was assumed to be oxygen.

Polyvinyl chloride (PVC) was blended with the biosludge in order to "spike" the feed with some chlorine. This provides a method to evaluate CEP processing ability of simulated sludge contaminated with chlorinated organic waste. The quantity of PVC added was equal to 2% of the total weight of the blended feed (PVC + biosludge). Table 6-78 shows calculated final feed (as injected) compositions that were calculated for the 2 wt% PVC blend with biosludge using the average biosludge composition (Table 6-78) and the PVC composition as analyzed. Through the rest of this section the terms "Biosludge" or "Biosludge Feed" shall refer to this blended feed material which contains biosludge waste and 2 wt% PVC.

Table 6-78
Biosludge Blend Composition with 2% PVC

Element	Average Composition (wt%)
Carbon	45.5
Hydrogen	6.6
Oxygen	26.4
Nitrogen	9.0
Sulfur	1.2
Chlorine	0.9
Ash	10.4
Total	100.0

6.6.8.2. Feed Injection

Figure 6.6 shows the time spent on various operations during the biosludge injection period. "Solid Injection" refers to the time spent feeding biosludge to the reactor. The remaining operations shown on the chart took place when the solids were not feeding. "Material Addition" corresponds to time spent adding fluxing materials or carbon to the reactor. "Feed Loading" addresses the time spent refilling the solids weigh tank with additional solids feed. "Other" applies to miscellaneous operations such as bath temperature sampling, or routine maintenance activities. The remainder of the demonstration system was fully operational and capable of processing biosludge feed during all re-loading periods. Hence an on-stream factor > 90% on-stream time can be calculated from this demonstration.

Figure 6.6
Biosludge Demonstration-Scale Injection

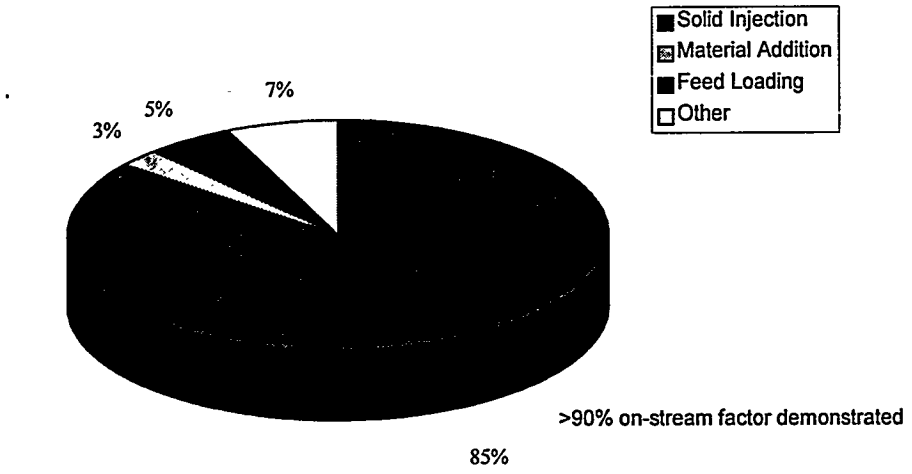

6.6.8.3. Steady State Operation

6.6.8.3.1. Off-Gas Flow and Composition

The off-gas flow rates and CO and H_2 volume ratio in the syngas product for a steady feed period are shown in Figure 6.7 and Figure 6.8. The off-gas composition and rate show generation of a steady syngas product of consistent composition.

Figure 6.7
Biosludge Off-Gas Flow (Steady State III)
(Demonstration-Scale Processing)

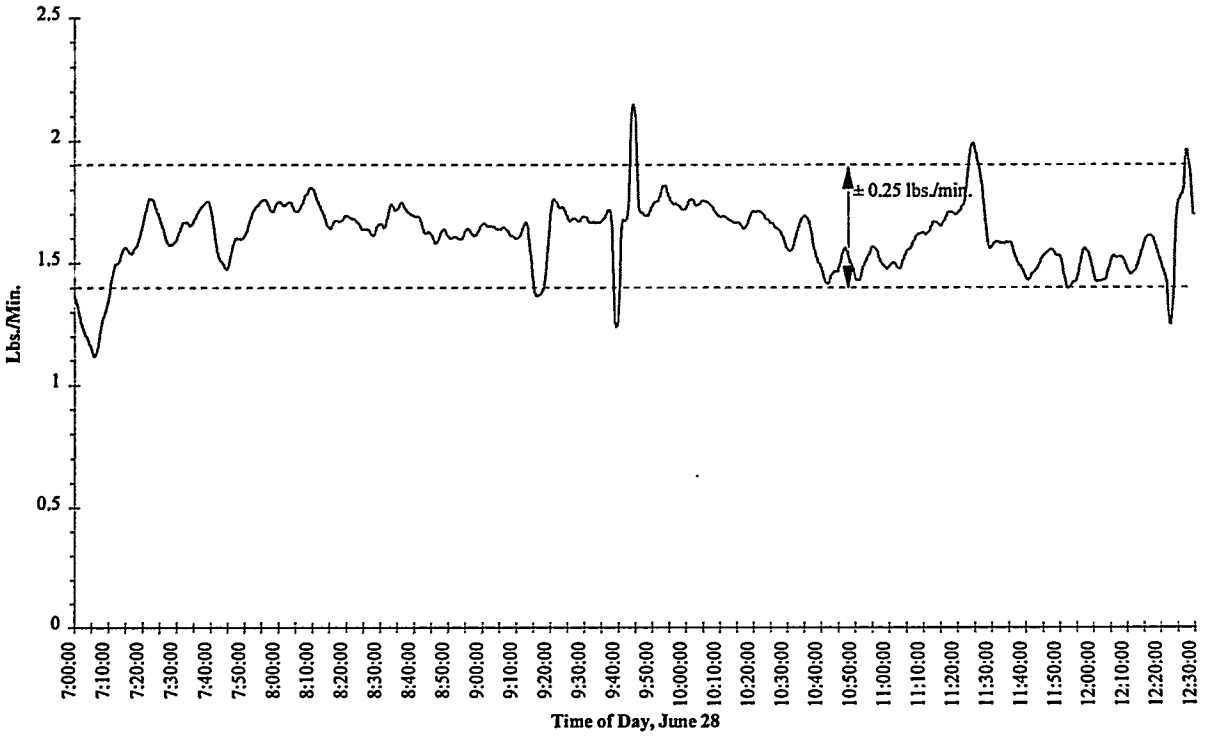

Figure 6.8
Biosludge Processing - Off-Gas H_2/CO Ratio

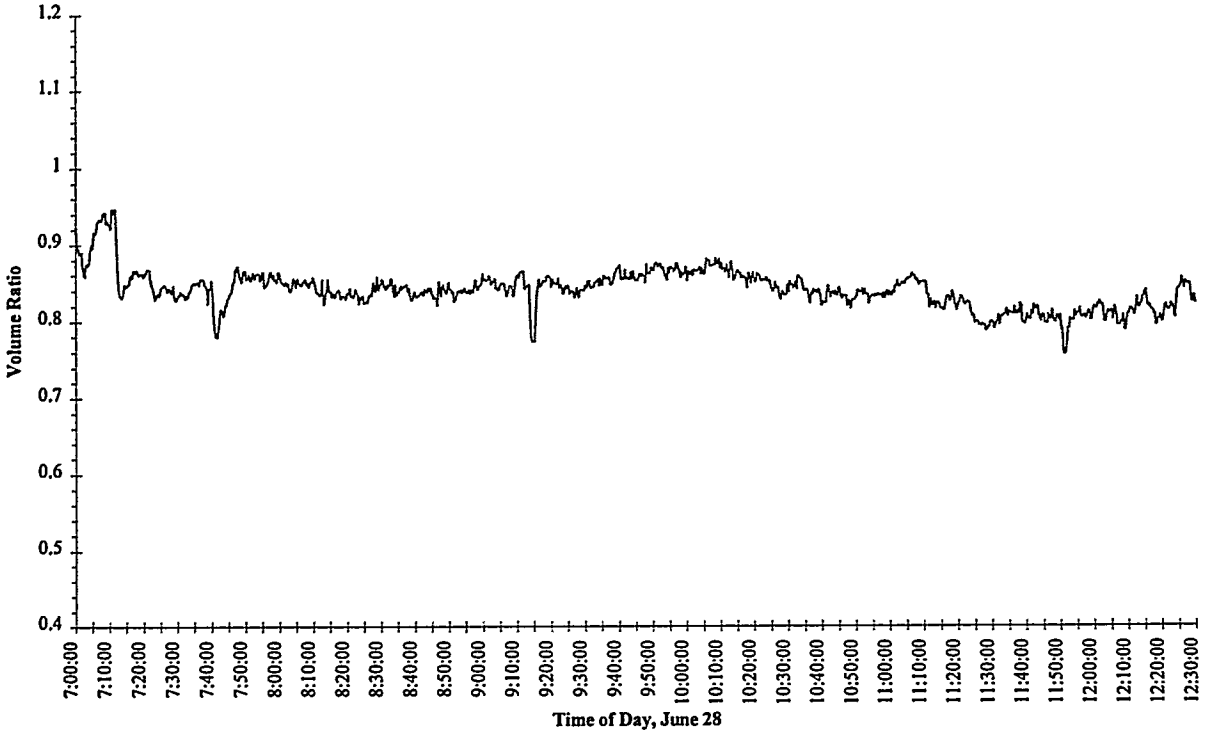

6.6.8.3.2. Off-Gas Quality

6.6.8.3.2.1. Conversion of Organics

Polyvinyl chloride (PVC) was blended with the biosludge feed to increase the chlorine level to near 1.0 wt%. It is difficult to make a traditional destruction efficiency ("DRE") calculation when using a solid material as a tracer. Normal DRE calculations compare the amount of a tracer molecule in the feed with the amount of the same tracer molecule detected in the off-gas. Since PVC polymer will not volatilize in the reactor it will not be detected as PVC in the off-gas. Alternative destruction efficiency calculations were made assuming that the PVC added to the biosludge can be modeled as vinyl chloride (CH_2CHCl) or chloroethane (CH_3CH_2Cl) which are very similar in structure to the PVC monomer segment, $[-CH_2CHCl-]_n$. Both vinyl chloride and chloroethane were analyzed in the off-gas by the TO-14 method. The corresponding destruction efficiencies, DREs, for these two models are provided in Table 6-79.

Table 6-79
Destruction Removal Efficiency (DRE) for PVC Monomer
(Biosolids Demonstration-scale Processing)

Sample	Date	Time	DRE Using Vinyl Chloride Tracer	DRE Using Chloroethane Tracer
SUMMA™-1	6/27	17:24	≥ 99.9999	≥ 99.9999
SUMMA™-2	6/27	20:30	≥ 99.9999	≥ 99.9999
SUMMA™-3	6/28	8:25	≥ 99.9999	≥ 99.9999
SUMMA™-4	6/28	19:17	≥ 99.9999	≥ 99.9999
SUMMA™-5	6/28	20:35	≥ 99.9999	≥ 99.9999
Note: Vinyl chloride & chloroethane were not detected in the CEP gas product. DREs are limited by the lower detection limits (LDLs)				

The "≥" signs are included in Table 6-79 since vinyl chloride and chloroethane were non-detectable in these SUMMA™ canister samples. The detection limits for these two compounds were used to calculate the DREs. All of the data are consistent with prior experience with the CEP reactor which consistently provides a ≥ 99.9999% DRE.

6.6.8.3.2.2. NO_X and SO_2

Two analytical techniques were used to monitor key off-gas impurities during the run. Samples were pulled from the baghouse using Draeger tubes and analyzed for NO_X. On-line analyzers were used on the second two days of the run to continuously monitor the gas for NO, NO_X, and SO_2. NO_X were measured using a chemiluminescent analyzer. SO_2 was analyzed using an ultraviolet-photometric device.

SO_2 was below detection limits (LDL = 1 ppm) throughout the run. NO_X was also at lower detection limit level (LDL = 3 ppm), measured at less than 3 ppm by the on-line analyzer; the Draeger tube samples (LDL = 2 ppm) did not detect any NO_X in the gas. These results are expected and consistent with the highly reducing environment of the reactor. The minimal production of NO_X and SO_X has been demonstrated in many trials on the demonstration reactor.

6.6.8.3.2.3. Total Hydrocarbons

Total hydrocarbons data were taken from an on-line analyzer with a flame ionization detector (FID) for the entire biosludge run. The THC results are reported as "THC ppm as methane". The CH_4 level was typically less than 50 ppm throughout the run. These levels of methane are thermodynamically predicted in a syngas environment under

CEP operating conditions. C_2H_4, C_2H_2 and other hydrocarbons were typically non-detectable throughout the run.

6.6.8.3.2.4. Trace/Dioxins

Four gas samples were collected with XAD traps at the Dutchman using a modified version of EPA Method 23. The result of these dioxin analyses on the samples is given in Table 6-80 below. The results are given in the most common U.S. and European dioxin toxicity equivalent units.

Table 6-80
XAD Trap Results 2,3,7,8-TCDD Toxicity Equivalents (TEQ)
(Biosolids Demonstration-Scale Processing)

Sample	Date	Time	EPA-1989 or NATO	UBA (German)
XAD-1	6/27	13:27 to 14:00	ND	ND
XAD-2	6/27	18:34 to 19:12	ND	ND
XAD-3	6/28	10:02 to 11:02	ND	ND
XAD-4	6/28	19:14 to 19:42	ND	ND
ND = Not Detected to stringent regulatory limits of 0.1 ng/Nm^3 TEQ.				

6.6.8.3.3. Ceramic Quality

TCLP (Toxicity Characteristics Leaching Procedure) RCRA metals analysis was performed on three ceramic samples taken after the biosludge injection. In all cases, the metal leaching levels were non-detectable (Table 6-81) and the ceramic material passes the TCLP for metals leachability.

Table 6-81
TCLP Metals Analysis on Ceramic Samples
(Biosolids Demonstration-Scale Processing)

Sample ID	As	Ba	Cd	Cr	Pb	Hg	Se	Ag
Regulatory Limits (mg/l)	**5.0**	**100**	**1.0**	**5.0**	**5.0**	**0.2**	**1.0**	**5.0**
C8	ND	ND	ND	ND	ND	ND	ND	ND

TCLP organics analysis was performed on the ceramic phase, C11, taken after the biosludge injection, with results given in Table 6-82. In all cases, the volatile and semi-volatile organic leaching levels were below regulatory limits, indicating that the ceramic material passes the TCLP for organics leachability.

Table 6-82
TCLP Organics Analysis on Ceramic
(Biosolids Demonstration-Scale Processing)

Sample ID	Sample C11 TCLP Result (mg/L)	Regulatory Limits (mg/L)
Pesticides		
Chlordane	ND	0.03
Endrin	ND	0.02
Heptachlor	ND	0.008
Heptachlor Epoxide	ND	0.008
Lindane	ND	0.4
Methoxychlor	ND	10.0
Toxaphene	ND	0.5
Herbicides		
2,4-D	ND	10.0
2,4,5-TP	ND	1.0
ND = Not Detected at lowest detection limit		

Table 6-82
TCLP Organics Analysis on Ceramic
(Biosolids Demonstration-Scale Processing) (Cont'd)

Sample ID	Sample C11 TCLP Result (mg/L)	Regulatory Limits (mg/L)
Volatile Organics		
Benzene	ND	0.5
Carbon Tetrachloride	ND	0.5
Chlorobenzene	ND	100.0
Chloroform	ND	6.0
1,4-Dichlorobenzene	ND	7.5
1,2-Dichloroethane	ND	0.5
1,1-Dichloroethylene	ND	0.7
Tetrachloroethylene	ND	---
Trichloroethylene	ND	0.5
Vinyl Chloride	ND	0.2
Methyl Ethyl Ketone	ND	200.0
Semi-Volatile Organics		
Cresol, Total	ND	200.0
2,4-Dinitrotoluene	ND	0.13
Hexachlorobenzene	ND	0.13
Hexachloro-1,3-Butadiene	ND	0.5
Hexachloroethane	ND	3.0
Nitrobenzene	ND	2.0
Pentachlorophenol	ND	100.0
2,4,5-Trichlorophenol	ND	400.0
2,4,6-Trichlorophenol	ND	2.0
Pyridine	ND	5.0
ND = Not Detected at lowest detection limit		

6.6.8.3.4. Metal Quality

A summary of the metals analysis for the tapped metal sample is given in Table 6-83:

Table 6-83
Metals Analysis: Tapped Metal Sample
(Biosolids Demonstration-Scale Processing)

Element	Weight %
Sulfur	0.11
Aluminum	0.04
Calcium	0.08
Iron	85.7
Potassium	0.83
Magnesium	0.09
Nickel	0.93
Phosphorus	1.67
Silicon	0.33
Sodium	0.11
Chlorine	< 0.0008
Total	**89.9%**

6.6.8.4. Material Closure for Major Components

Material balances were performed for the major components (carbon, hydrogen, and oxygen) and for the total material fed. Table 6-84 and Table 6-85 summarize the results of such calculations.

Table 6-84
Biosludge Demonstration Carbon, Hydrogen, Oxygen Balance
(Material Balance Closure)

	Feed Components			Major Element Balance		
Biosolids Feed	**SCF**	**Moles**	**Lbs**	**C**	**H**	**O**
MASS IN						
Methane	4159	10.97	175.58	131.68	43.89	
Oxygen	23959	63.22	2022.92			2022.92
Feed Mixture			4684.00	2135.90	313.83	1391.15
Carbon added to bath			380.00	380.00		
Iron (3.06% C)			3180.00	97.31		
TOTAL				**2744.90**	**357.72**	**3414.07**
MASS OUT						
Hydrogen	71825	189.51	379.02		379.02	
Carbon monoxide	79134	208.80	5846.31	2505.56		3340.75
Carbon dioxide*	3416	9.01	396.58	108.16		288.42
Ferro bath at end (3.15% C)			3225.00	101.59		
TOTAL				**2715.31**	**379.02**	**3629.17**
Closure%				**98.92**	**105.95**	**106.30**

*Attributable to startup conditions. As steady-state is approached, carbon dioxide concentrations become negligible.

Table 6-85
Biosludge Demonstration Global Material Balance
(Material Balance Closure)

	Feed Components		
Biosolids Feed	**SCF**	**Moles**	**Lbs.**
MASS IN			
Methane	4159	10.97	175.58
Oxygen	23959	63.22	2022.92
Feed Mixture			4684.00
Carbon added to bath			380.00
Flux additions			218.00
Iron			3180.00
TOTAL			**10660.50**
MASS OUT			
Hydrogen	71825	189.51	379.02
Carbon monoxide	79134	208.80	5846.31
Carbon dioxide*	3416	9.01	396.58
Metal product			3225.00
Ceramic product			410.00
TOTAL			**10256.92**
Closure%			**96.21**

*Attributable to startup conditions. As steady-state is approached, carbon dioxide concentrations become negligible.

6.7. Demonstration of Toxicity Destruction of 2-Chloroethyl Ethyl Sulfide

6.7.1. Test Plan Overview for 2-Chloroethyl Ethyl Sulfide

An experimental program was designed to demonstrate the destruction and removal efficiency (DRE) of CEP for 2-chloroethyl ethyl sulfide (CEES) via a systematic bench-scale study. It is a chlorinated organic material with a disulfide bond. The objectives of the experimental program were:

- Assessing the DRE of the bench-scale CEP reactor for 2-chloroethyl ethyl sulfide (CEES).
- Assessing the performance of the bench-scale CEP reactor for other surrogate liquid feeds in order to obtain information pertaining to scale-up.

6.7.2. Feed Materials

A spectrum of materials with similar elemental composition as CEES are shown in Table 6-86. These materials were injected in either pure form for DRE analysis or in concentrated mixtures that captured the elemental composition of CEES for the overall chemistry assessment. DMSO (Dimethyl Sulfoxide) was used as an elementally analogous surrogate for CEES. A mixture of 55/45 hexane/methylene chloride was used as a compositionally analogous surrogate for CEES. All the surrogates that are being considered were organic molecules with C-H, C-Cl, C-S and C-C bonds.

Table 6-86
Feed Composition for Planned Array of 2-Chloroethyl Ethyl Sulfide

Materials	Density (g/cm^3)	MW	%C	%H	%Cl	%S	%O
n-Hexane	0.659	86	83.72	16.28	0.00	0.00	0.00
Methylene Chloride	1.336	85	14.12	2.35	83.53	0.00	0.00
Dimethyl Sulfoxide	1.101	78	30.77	7.69	0.00	41.03	20.51
CEES	1.07	124.5	38.55	7.23	28.51	25.70	0.00

6.7.3. Analytical

The analytical protocol was designed to obtain appropriate data to determine the DRE of a sulfur-bond chlorinated compound (CEES). The analyses are summarized as follows:

- CO/CO_2 infrared monitors, which monitor the background CO levels, and the off-gas if oxygen is co-fed.
- Mass Spectrometer (MS) which provides the H_2, CO, CO_2, Ar, HCl, H_2S levels in the offgas.

- Gas Chromatography/Thermal Conductivity/Detector (GC/TCD), Flame Ionization Detection (FID). Electron Capture Detector (ECD), Flame Polarization Detector (FPD). The TCD will be used for CO, H_2 analysis and a FID will yield information about any trace hydrocarbons present in the off-gas. The ECD and FPD will be used to lower the detection limits to the tens of ppb range to yield the required DRE information.

- CEES trapping train, including third party (Battelle) XAD traps and Tenax traps with lower detection limits of $0.5*10^{-6}$ and $3*10^{-6}$ g respectively.

6.7.4. Results

The processing of CEES provided the background operational knowledge to access accurately CEP of toxic materials. Specially, in-house analysis demonstrated the destruction removal efficiency (DRE) of CEP systems: surrogate compounds were not detected in GC analysis. A two-step third party (Battelle) product gas analysis was utilized to accurately assess the performance of CEP in CEES processing. A trapping train using Battelle specified traps (XAD and Tenax traps) was used to trap all feed CEES and any semivolatile species before the offgas entered the analytical equipment. A separate distribution manifold for the analytical instruments was then used to evaluate the product gas, including GC, TCD/FID, CO/CO_2 monitor, and Perkin Elmer Mass Spectrometer. CEES species were not detected in the XAD and Tenax traps to the lower detection limits of $0.5*10^{-6}$ g and $3*10^{-9}$ g, resulting in DREs ≥99.9999% and 99.9999999%, respectively. Table 6-87 summarizes the experimental results for individual feed surrogates.

Table 6-87
2-Chloroethyl Ethyl Sulfide & Surrogates Experimental Results

Feed Injected	Objectives	Operational Parameter	Performance
Hexane/Methylene chloride	Demonstrate conversion of chlorinated liquid with an elemental composition similar to CEES	Nickel bath Crucible	No detection of the feed compounds in the GC analysis (LDL=1ppm)
Dimethyl Sulfoxide (DMSO)	Demonstrate conversion and operability while processing sulfur compounds	Nickel bath Crucible	No detection of DMSO in the FPD analysis (LDL=40 ppb)
2 Chloroethyl Ethyl Sulfide (CEES)	Obtain DRE data for processing CEES	Nickel bath Crucible	≥99.9999999%[1]

[1] As confirmed by third party analytical using Battelle equipment to lower detection limits on the order of 10^{-8} g/ml of concentrated effluent.

6.7.5. Hexane/Methylene Chloride Performance

A 55/45 mixture of hexane (C_6H_{14}) and methylene chloride (CH_2Cl_2) with a weight composition of 40.2% C, 7.6% H, and 52.2% Cl was processed in a series of experiments. This composition resembled the composition of CEES (excluding the sulfur). Both GC and mass spectrometer were used to evaluate the off-gas quality. The composition of the synthesis gas were summarized in Table 6-88, indicating the consistency between theoretical and experimental off-gas generation. GC and FID analysis indicated that feed compounds were not detected on-line to the detection limits of 1 ppm.

Table 6-88
Off-gas Analysis for Hexane/Methylene Chloride Processing

Experiment	Hydrogen (vol %)	Carbon Monoxide (vol %)	Hydrogen Chloride (vol %)	Hydrogen Sulfide (vol %)
Experiment 1	19[1] (15.61)[2]	4.3 (2.57)	5 (7.11)	0
Experiment 2	12.5[1] (13.9)	11 (12.47)	4.7 (5.6)	0
Experiment 3	10.3[1] (10.9)	9.7 (14.4)	4.4 (5.3)	0
Experiment 4	9.6[1] (11)[2]	11 (11)	1.5 (3.5)	0.4 (0.25)

Off-gas composition balanced by argon carrier gas.
[1]Actual vol. %
[2]Predicted vol. % based on feed composition.

6.7.6. Dimethyl Sulfoxide Performance

Dimethyl Sulfoxide (DMSO) was injected with co-reactants in a nickel bath. The experiment was set up in a similar way as that of hexane/methylene chloride processing. The mass spectrometer indicated the off-gas composition was 12 vol.% CO and 17 vol.% H_2, which followed closely with the predicted off-gas composition (12 vol.% CO, 17.2 vol.% H_2). FPD analysis indicated that DMSO was not detected to the detection limit of 40 ppb.

6.7.7. CEES Performance

CEES was injected with co-reactants into the 10-lb CEP reactor. A nickel bath was used for CEES processing. Table 6-89 summarizes the off-gas composition of the CEES processing, demonstrating consistent agreement between theoretical and experimental data.

Table 6-89
Off-gas Analysis for CEES Processing

Experiment	Hydrogen (vol. %)	Carbon Monoxide (vol.%)	Hydrogen Chloride (vol. %)
Experiment 1	10[1]	8.7	2.6
	(10.53)[2]	(7.15)	(2.58)
Experiment 2	7[1]	8.4	1.72
	(7.73)[2]	(8.24)	(1.9)

Off-gas composition balanced by argon carrier gas.
[1]Actual vol. %
[2]Predicted vol. % based on feed composition.

A two-step, third-party product gas analysis was used to accurately assess the performance of CEP in CEES processing. A CEES trapping train using Battelle-specified traps (XAD and Tenax traps) was used to trap all CEES and any semivolatile species before the off gas entered the analytical equipment. These traps were removed from on-line after the experiment and sent to Battelle for analysis. The processing of CEES resulted in DREs ≥99.9999999%. CEES was non-detectable in the XAD trap with a GC/FPD analysis LDL (lower detection limit) of 0.5 μg, resulting in a DRE for CEES ≥99.99999%. Another sample showed CEES non-detectable in the Tenax trap (LDL=3 ng), resulting in a DRE for CEES ≥99.9999999%.

7. Task 1.6: Conceptual Design of a CEP Facility

7.1. Overview

This conceptual design is of a CEP system in which organic sludges, inorganic sludges, scrap metals, soils, construction debris, and organic debris could be processed through the reactor at feed rates compatible with the natures of the various waste compositions, and in such a manner as to inform the future decisions that will be required for the subsequent scale-up to a full-scale CEP system.

The CEP system components are arranged into three general areas: Feed Handling, Reactor Systems, and Gas Handling Train. All systems or components in these areas will be designed for transportability by incorporating multiple features into modules or skids.

The Feed Handling area is comprised of equipment needed to off-load and handle incoming containers, safely remove the contents, and condition the feed for pneumatic or slurry injection or bulk feeding into the reactor. Each step of the feed handling operation will be engineered to isolate and protect the operating staff in accordance with MMT standards that meet or exceed all other health and safety requirements.

Reactor System designs will be based on operating units at MMT's Fall River facility and will incorporate the latest innovations and improvements. The reactor will contain approximately 1,100 lbs (as determined during the design phase) of molten iron and a proportional amount of ceramic in the horizontal section. The reactor is equipped with a 600 kW induction coil power supply and additional heat capacity required to preheat the vessel and to supplement heating the horizontal section during tapping operations, lance operations, or to deskull the reactor interior surfaces.

The capability to sample the metal and ceramic phases, observe key parts of the bath in operation, and to monitor all aspects of the reactor's performance will be designed into the unit. Upon shutdown, the automatic injection of inert purge gases assures that safe conditions are maintained throughout the system. Ancillary systems for the reactor include a means for discharging the bath contents into a closed container which will prevent the potential spread of radioactive contamination and a system for discharging accumulated ceramic product during extended operations. All reactor component designs are based on modular concepts to facilitate future alterations needed for feed streams different than those currently identified.

The Gas Handling Train (GHT) will be capable of handling a broad spectrum of gas compositions generated from the incoming feeds. The GHT will have the capability to filter or scrub any carryover particulate, collect potentially reactive dusts and

volatile heavy metals safely, and to condition gases for potential re-use. All off gas will be passed through a series of absorbents and filters to assure that no radioactive or hazardous component is discharged into downstream systems. The entire process will be expertly monitored to assure safe operations for employees and the community.

CEP typically generates hydrogen and carbon monoxide product gases during routine operations. Handling these gases is an important safety issue and appropriate design considerations based on multiple years of experience within MMT and the practices established by the government and other industries handling these gases will be applied. GHT system components will also be designed to minimize the generation of secondary wastes and will include the option to recycle most of the secondary waste streams generated through CEP.

In support of the three key areas (feed handling, central processing reactor, and gas handling train) noted above, the facility infrastructure will require the design and installation of necessary support items such as a nitrogen supply, oxygen supply, staff facilities, offices, etc.

The following table outlines the expected staging of waste streams. The functional requirements for each waste stream are included. This table will be used to set the boundaries for the Conceptual Design.

Table 7.1
System Functionality by Waste Stream

Waste Stream	Functionality
Soil	• Screening/sizing of clay material with organic and radionuclide contamination • Blending of soil with co-feeds • Tuyere feeding at average 125 lbs soil per hour[1] • Destruction of PCBs/organics • Non-continuous ceramic phase removal during run • VHM capture in GHT • Capture of radioactive and reactive particulates in GHT • Safe containment of radionuclides, VHM, H2/CO • Demonstrate potential for reuse of syngas[2] • Process instrumentation and control • Analytical support equipment
Sediment	In addition to above: • Screening/sizing of sandy materials with high mercury and radionuclide contamination • Significant VHM capture
Inorganic Sludge	In addition to above: • Removal of excess water in presence of organics and mercury • Processing of wastes with high water content (>20 wt%)
Organic Sludge	In addition to above: • Filtering of organic sludges with high solids content • Chlorine capture in ceramic phase • Adequate refractory lifetime for chloride wastes
Scrap Metal Processing Equipment	In addition to above: • Bulk feeding of metal pieces up to 6-8 inches • Non-continuous bulk feeding of metal pieces • Non-continuous metal tapping during run • Sufficient residence time to flux minor radionuclide contamination • Sufficient power to reactor to process 50 lbs/hr
Construction debris	In addition to above: • Sizing/sorting sufficient for bulk feeding (2-4 inches) • Sufficient residence time for formation of ceramic phase with desired properties
Spent Activated Carbon	• Tuyere feeding of dusty solids with high gas generation • Feeding of bulk solids with high gas evolution rates
Personal Protective Equipment	• Shredding/sizing of clothing, plastics, etc.

7.2. Emission Limits and Environmental Issues

Representative Wastewater Effluent Treatment Standards for the Host Site:

- **Oils and Grease** - less than 100 mg/l in the stream and nothing becoming viscous between 32 and 150 degrees Fahrenheit.
- **Explosive Mixtures** - less than 5% of LEL (Lower Explosive Limit) for liquids, solids, or gases which by reason of their nature or quantity may cause an explosion or fire hazard.
- **Noxious Materials** - malodorous materials prohibited.
- **Improperly Shredded Garbage** - particles must be 1/2" or less and will freely suspend under flow conditions.
- **Solid or Viscous Wastes** - no discharge that may hinder flow or cause an obstruction to the sewage facilities.
- **Excessive Discharge Rate** - flow rate not to exceed design of pre-treatment facilities during discharge to system.
- **Toxic Substances** - any toxic substances, chemical elements, phenols, or other taste or odor producing substances that may interfere with downstream treatment.
- **Corrosive Wastes** - pH value should be in the range of 6 to 9.
- **Thermal Discharge** - Under no conditions shall the temperature at the point of discharge exceed 120 F.
- **Human Hazard** - no waste which causes hazard to human life or creates public nuisance.

7.2.2. Environmental Issues

Facility Siting - Siting will be within existing zoned industrial property. A complete due diligence of environmental issues will be performed. The review of site conditions will be performed to identify existing contamination, proximity to population, surface and groundwater resources, past land uses, etc.

7.2.3. Federal Codes and Authorities

The authority for the federal codes is the US Environmental Protection Agency, and they are responsible for implementing the Federal Resource Conservation and Recovery Act (RCRA), the Clean Air Act (CAA) and the Clean Water Act (CWA).

Federal Resource Conservation and Recovery Act (RCRA) - The following issues may be of concern to the federal officials involved with RCRA:

Confirmation that the proposed CEP unit will be engaged in legitimate recycling activity -- This determination will be the responsibility of the state environmental regulators, although the environmental regulators may ask EPA to provide assistance in the determination. Classification of the CEP unit as a legitimate recycling process is critical, as the CEP unit will then be exempt from RCRA permitting requirements (some or all CEP feeds and process residuals may also be excluded from regulation as hazardous wastes).

Variance from otherwise applicable technology-based land disposal restrictions -- This may be required if the waste slate contains wastes subject to technology-based Best Demonstrated and Available Technology (BDAT) standards. Review and approval of such variance requests are coordinated by regional EPA offices but are the responsibility of EPA's Waste Treatment Branch in Washington, DC.

Clean Air Act (CAA) - The following may be of concern to Federal and State authorities involved with the CAA:

Intermittent flaring of gasses during CEP unit startup, shutdown and upset conditions probably can be authorized under exemptions in the state air permitting regulations for startup, shutdown and upset emissions and/or "smokeless flares." .

7.3. Design Philosophy

7.3.1. Design Tradeoff Philosophy

When performing tradeoff studies between alternative designs, selection of the best alternative shall be based on the following list of priorities:

1. Safety;
2. Environmental integrity;
3. Availability (reliability);
4. Maintainability;
5. Schedule;
6. Operating cost;
7. Capital cost.

7.3.2. Equipment

Sparing Philosophy: Spares carried in inventory shall be minimized based on the availability of replacement parts. Recommended consumable spares, such as

gaskets, filters and lubricants, shall be supplied in accordance with the manufacturer's suggested spares and as modified by operations.

Use of Standard Specifications: Standard Equipment Specifications (SESs) shall be used to the maximum extent practicable. They shall be used as a guide. When it makes sense to use alternative specifications, the standard specifications shall not impede process improvement.

An SES shall be used to help minimize the spare parts inventory for such items as motors, pumps, valves, gaskets, nuts, and bolts. SESs enhance the use of uniform operating procedures and standard operating instructions. SESs shall be used only for equipment that has demonstrated satisfactory operation at MMT field installations.

Input from operators using the equipment shall be considered prior to sending out bid documents so that potential design improvements can be included in the standard specifications.

7.4. Testing and Inspection

Shop Inspections: During the course of design, a field inspection plan will be developed to assure fabricated items meet design standards. A general test and inspection plan will be included with each competitive procurement to convey to the vendors the standards for which they will be accountable.

The inspection activities for materials, welding, and other fabrication practices will be accomplished by contracted personnel. Inspection reports will be reviewed by project personnel and issues resolved expeditiously.

Progress visit shall be made to the fabrication or erection site for all major items of equipment to verify work is performed in accordance with the design intent. A project representative may be temporarily located on site.

Shop Testing: As modules and equipment are completed in the fabricators' shops, MMT will conduct tests to assure the functionality of the equipment.

Certified performance curves are required for all pumps, fans and blowers to demonstrate capacity, pressure, power and efficiency. Variable speed units will have a series of curves that show the envelope of satisfactory operation.

Hydrostatic tests are required for all pressure vessels in accordance with applicable codes.

Field Inspection: As part of the entire inspection and testing program, site construction activities will be subjected to the same rigorous quality control. The

inspection plan will address such items as the taking and testing of concrete cylinders, the tying and installation of rebar, structural steel assembly, pipe welding, and the myriad of other activities necessary to construct a quality plant.

The test plan will be prepared, reviewed and approved by a MMT management group. The culmination of the Field Test Program is mechanical completion as defined in the Project Management Plan.

Systems Testing: This phase of testing will begin upon the mechanical completion of an entire system. A systems completion section of the project schedule will be developed to allow Operations to plan activities for the turnover. During the course of design and construction, Operations will develop comprehensive systems testing plans and will identify their preferred systems testing sequence. Construction will then focus their efforts to complete systems ins the requested order.

This work will consist of verifying that each system meets the necessary performance requirements established in the design documentation. At the start of systems testing, Operations will take control of the safety tagout process.

Integrated Testing: Upon satisfactory completion of all systems testing, the Integrated Test Plan will be initiated. During both integrated and systems testing, construction personnel must be available for correcting deficiencies or making modifications. Engineering support from key design personnel must also be available.

7.5. Modular Design

MMT desires that each logical equipment grouping be designed into a module, skid, or prefabricated unit which can easily be installed in the field.

The flow of materials through a CEP plant and through each module is assumed to be from left to right when facing the primary equipment area. The front of each module is generally taken to be facing the viewer. The following module design principles should be used for MMT facilities.

Piping entering and exiting a module should be located approximately 8 ft. above the floor or walkway and should be brought to the face plane of the module boundary. The designer of the discharge from a module will be responsible for the connection to the "receiving" module. A loose connector and pipe length, spanning the distance between modules, will be supplied for field adjustment and fitup.

All electrical and instrumentation connections shall be brought to a single location which is accessible from the front and back. At this point continuity checks, simulated operations, and data readouts should be available. Power connections

must be set up for direct connection by attaching conduit and pulling cable into a single panel. Remote I/Os will be utilized.

Access ladders, stairs, walkways, and hand rails will also be designed for each module and assembled in the fabricator's shop. They may be removed for shipment.

The module and all components contained in the module shall have a finished coat of paint applied before shipping to the plant site.

Modules containing toxic or hazardous materials shall have a built-in catch basin capable of containing the maximum potential spill. Spill detection shall also be included.

"Clean Design" principals such as those used in the food processing industry shall be used for the design of modules. The elimination of spaces where materials may accumulate and designing for easy "hose down" cleanup of spills is a facility requirement.

Modules will be tested to the maximum extent possible in the fabricator's shop. This should be taken into account during the design process. Each module will be shop tested. An inspection and quality control plan will be prepared prior to bidding the work or delivering the scope of work to preselected vendors.

Modules should be transportable down public roads on readily available trucking. Oversize loads requiring permitting or escorts are acceptable. Each module should be equipped with lifting lugs or marked locations for handling and erecting.

Modules shall include provisions for process drains. Hydraulics of the system shall be evaluated. If gravity flow is not feasible or practicable, then suitable pumping units shall be provided with the module for the process drains.

Modules shall contain provisions for process cleanouts and maintenance in addition to the spill control and cleanup requirements.

Modules should have noise control features included that meet or exceed OSHA requirements. Fans and blowers shall have absorptive type silencers or equivalent acceptable product that attenuates the most offensive frequencies based on the speed and other characteristics of the machine. Where silencers are not practicable, acoustic louvers and baffles shall be used. Such devices shall not adversely affect the proper cooling and functioning of the equipment.

These guidelines are considered the normal standards and deviations should be by written exception only.

7.6. Operating Philosophy

7.6.1. Safety

Personnel safety is practiced as the responsibility of the organization as well as the individual and takes precedence over operations, maintenance, and any other activity. The Safety philosophy will be based on the principles outlined in the OSHA 29 CFR Part 1910.119 regulation for "Process Safety Management of Highly Hazardous Chemicals", Code of Federal Regulations Title 10 Part 20 "Standards for Protection Against Radiation" , and all applicable state safety regulations. The principles will be followed because they are fundamentally sound practices for operating a CEP plant, and not because of possible legal compliance requirements. Sections of the regulation and some of their key components are listed below:

Employee participation - Team approach used in developing process safety management program and all plant personnel have access to process hazard analysis.

Process safety information - Complete information is compiled and readily available on: (1) hazards of highly hazardous chemicals in the process, (2) information pertaining to the technology of the process including consequences of deviation, and (3) information pertaining to the equipment in the process (materials of construction, design codes and standards).

Process Hazard Analysis - Initial process hazard analyses are conducted during the design phase, and follow-up analyses are performed at minimum 5 year intervals.

Operating procedures and practices- Detailed procedures are developed that cover initial startup, normal operations, temporary operations, emergency operations, established operating limits, and steps to correct deviations from operating limits. Procedures are updated to assure that they reflect current operating practices. Safe work practices and procedures are developed to cover lockout/tagout, confined space entry, opening process piping or equipment, and work authorization including radiological control measures and personal protection consistent with exposures as low as reasonably achievable (ALARA).

Training - All employees involved in operating a process shall receive documented training on an overview of the process and the process operating procedures. The employees will also receive documented refresher training on a minimum of every 3 years.

Contractors - Contractors will be informed of all hazards related to the contractors work and the process, and will follow all plant safety practices and procedures. Contract employers assure that each contract employee is trained in the process hazards and safe work practices necessary to perform their job.

Incident investigation - All incidents that result in, or could have resulted in a catastrophic release of highly hazardous chemicals will be investigated by an appropriate team within 48 hours. Corrective actions from the report will be documented and implemented as soon as possible. The reports will be reviewed by all affected personnel whose job tasks are relevant to the findings, including contractors.

Emergency planning and response - An emergency action plan for the entire site will developed.

Compliance audits - The plant will conduct an internal audit every 3 years minimum.

Substance abuse- Policies, including testing, will be in place to ensure a drug and alcohol free work environment.

Statistics that may be tracked using SPC are: First aid reports, serious injuries, near-miss incidents, and fires. After sufficient data is collected, normal or "in control" performance parameters are established (Obviously with safety statistics zeros are targets for performance). After normal safety performance parameters are established, system changes such as levels of training, % overtime hours worked, and employee turnover rate can be evaluated as to their true impact on safety performance.

7.6.2. Environmental Compliance / Community Relations

- The "Regulator is a customer" philosophy will be practiced.
- Site personnel trained to have a thorough understanding of environmental regulations.
- Process control system will be configured so that waste injection not allowed if process variables are beyond compliance limits.
- Process hazards analyses review recommendations will mitigate environmental impacts of equipment failures, process upset conditions, and spills.
- All stored materials will be properly labeled.
- Community relations such as noise levels, visibility, and emergency response issues will be addressed.
- Statistics that may be tracked using SPC are: Stack emissions *(lb. CO emitted per lb. of waste)*, number of "out of compliance" reports.

7.7. Maintenance Philosophy

Routine Maintenance: The maintenance principle to be followed throughout the course of design will be to minimize or eliminate any routine maintenance. Toward that objective, the following guidelines are offered:

Failure detection equipment shall be provided for components subject to excessive wear, where applicable.

The plant shall be designed to utilize commonalty of design and equipment.

Equipment and component handling features shall be provided to facilitate removal and replacement.

All equipment and modules shall be designed to facilitate easy access for maintenance or replacement of components.

Specialized equipment necessary to perform maintenance functions shall be provided as part of the equipment or module package.

The facility shall include over-sized doors where required for equipment or module installation and removal.

Sufficient permanent blinds and adequate and accessible equipment test features shall be provided.

Equipment and modules shall be designed to allow routine maintenance to be completed within two hours and to permit the removal and replacement of equipment within six hours.

Contracted: The CEP vessel and other key components will require major maintenance periodically. When major shutdowns are planned, such as replacing the refractory, the work will be subcontracted to firms specializing in that type of work. The period between relinings will be determined during the first year of operation. The selected firm would also be a candidate for other MMT plants and they would also be considered for long term relationships in accordance with the TQM approach.

7.8. Radiation Management

7.8.1. Performance Objectives

Radiation exposures of the work force, the public, and the environment will be maintained well below applicable regulatory limits and generally accepted radiochemical management guidelines, consistent with the As-Low-As-Reasonably-Achievable (ALARA) principal.

7.8.2. Radiological Control Leadership

Management will emphasize the need for high standards for radiological control through direct communication, instruction, and inspection of the work site. The authority and responsibility to establish a comprehensive and effective radiological control program will be assigned to line managers and their subordinates. A performance indicator program for measuring and trending the effectiveness of the radiological control program against predetermined goals will be established and maintained. Workers and their supervisors will be held accountable for radiological control performance.

7.8.3. Radiological Performance Goals

The ALARA process of reducing radiation exposures is a basic tenet of the radiological control program. The senior site executive will establish, approve, and maintain a radiological performance goals program. The goals program will encourage operations with smaller contaminated areas and radioactive waste minimization to reduce the radiological impact of operations.

7.8.4. Administrative Control Levels and Dose Limits

The radiation control objective is to maintain personnel radiation exposure well below the regulatory dose limits given in Table 7.2. The Administrative Control Level for radiation workers will be 2.0 rem per year per person. The annual facility Administrative Control Level will be 0.5 rem or less. Visitors will be limited to an annual radiation dose of 0.1 rem.

7.8.5. Contamination Control and Control Levels

Control of radioactive contamination will be achieved by using engineering controls and worker performance to contain contamination at the source, minimize work areas of contamination, and promptly decontaminate areas that become contaminated. Personnel will not be exposed unnecessarily to airborne radioactivity. Any work area containing equipment or work surfaces with surface contamination in excess of Table 7.3 values shall be posted and managed as a Regulated Area (<10x Table 7.3 values) or Contamination Area (>10x Table 7.3 values). Radiological posting will be used to alert personnel to the presence of radiation and radioactive materials. Personnel shall not enter a radiological area unless required by their job assignment and they have been trained in radiological control practices. Untrained visitors and new (untrained) employees shall be escorted in radiological areas at all times. Personnel exiting contamination areas will frisk for contamination.

7.8.6. Radiological Work Planning

Technical requirements for the conduct of work, including construction, modification, operations, maintenance, and decommissioning, will incorporate radiological criteria to ensure safety and maintain radiation exposures ALARA. The

design and planning processes will incorporate radiological considerations in the early planning stages. Procedures, work packages, and job plans will be used to control hands-on work with radioactive materials. Engineering controls, including containment of radioactive material at the source as practicable, will be the primary method of minimizing airborne radioactivity and internal exposure to workers. Administrative controls, including access restrictions and the use of specific work practices designed to minimize airborne contamination, will be used as the secondary method to minimize worker internal exposure. Use of respiratory protection will also be used as appropriate but only for special situations or procedures where engineered containment is not practical.

7.8.7. External and Internal Dosimetry

Personal dosimetry will be required for personnel who are expected to receive an annual external whole body dose greater than 100 mrem. Dosimeters will be issued only to personnel formally trained in their use. Personnel who enter radiological work areas will also participate in a bioassay program.

7.8.8. Radiological Monitoring and Surveys

Radiological monitoring of radiation exposure levels, contamination and airborne radioactivity will be conducted to characterize workplace conditions and to identify areas requiring decontamination or radiological posting. Area radiation monitors will be installed in frequently occupied locations with the potential for unexpected increases in dose rates and in remote locations where there is a need for local indication of dose rates prior to personnel entering remote locations. Air monitoring equipment will be used in situations where airborne radioactivity levels can fluctuate and early detection of airborne radioactivity could prevent or minimize inhalation of radioactivity.

7.8.9. Training and Qualification

Radiological workers will have sufficient performance-based training to work safely in and around radiological areas and to maintain their individual radiation exposure and the radiation exposure of others ALARA. Standardized core courses and training materials will be used. Training will address both normal and abnormal situations in radiological control. Separate radiological control training will be required for tour groups and visiting dignitaries, scientists and specialists commensurate with the areas they are to enter.

7.8.10. Radiological Records

A radiological records management program will be established to ensure that audible records and reports are controlled through the stages of creation, distribution, use, arrangement, storage, retrieval, and disposition.

7.9. Design Requirements

Engineered controls (e.g., equipment layouts, confinement, ventilation, shielding, and remote handling) with design emphasis on containment of radioactive material at the source, as practicable, shall be the primary method of minimizing airborne radioactivity and internal exposure to the workers. The design of process equipment shall address the health hazards represented by all hazardous materials in enclosures, general work areas, and non-contaminated areas. Administrative controls, including access restrictions and the use of specific work practices designed to minimize airborne contamination, will be used as a secondary methodology to minimize worker exposure.

The design of process equipment and containment systems shall emphasize specific features that protect the public and facility personnel from hazards associated with the use of radioactive and other hazardous materials as a result of normal operations, anticipated operational occurrences, and design basis accident (DBA) conditions, including the effects of natural phenomena pertinent to the site, and maintain these effects ALARA.

7.9.1. Building Layout

Radiological controlled-access and uncontrolled-access work and support areas will be established within each facility for better management of surface and airborne contamination and radiation sources. Building layouts that physically separate as well as restrict the bulk movement of radioactive materials relative to non-radiological functions and the general plant population will be emphasized. Casual or secondary exposures of personnel to contamination and significant radiation sources will be minimized with the establishment of radiological buffer zones. The building layout will also minimize potential exposure pathways to maintenance and other emergency personnel working under design basis abnormal or emergency situations. Personnel monitoring and protection equipment requirements will be established according to the particular radiological risk of each designated area.

Controlled-access areas will be established where workers can potentially encounter contamination or receive dose equivalents that are higher than those normally received by non-radiation workers. Uncontrolled access areas including administrative offices and non-radiological support shops and laboratories, will be maintained below contamination thresholds.

Limited access radiological buffer zones such as corridors that are adjacent to, or connect with, areas that contain radioactive materials will be established to better ensure isolation of radiological control areas from radiological clean areas.

Radiological controlled-access areas will be subdivided into contamination control and radiation management areas depending on the type and level of radioactivity

and potential for worker exposure. Contamination control areas with small inventories of radioactive materials with low surface contamination and low dose-rate potential will be defined and managed as Regulated Areas.

Radiological control areas with sufficient radionuclide inventory to yield potential worker dose rates in excess of 5 mrem/hr will be classified and managed as Radiation Areas. Examples of process operation areas are glove box and hot-cell operating areas. Any controlled areas where a worker can receive a dose equivalent of 100 mrem or greater in 1 hour at 30 centimeters from the radiation source or from any surface through which the radiation penetrates will be defined and managed as a High Radiation Area. Occupancy in these areas is predominantly for process monitoring or the adjustment of operations occurring in areas of high hazard. Examples of this type of area are hot-cell service and maintenance areas, and transfer areas where highly dispersible materials of high-dose-rate are entered into the process system or hot cell.

Engineering controls, personnel protection requirements, monitoring, and work procedures governing operational and maintenance activities inside Contamination and Radiation Control Areas will be commensurate with the level of risk to workers, visitors, and the environment.

Any controlled area where airborne radioactive material concentrations are greater than 10% of the derived air concentration (DAC) will be posted and managed as an Airborne Radioactivity Area. Areas with potential for significant concentration of airborne radioactive materials will be provided with physical barriers to prevent the inadvertent entry of workers who are not wearing respiratory protection.

Change rooms will be provided for changing into and from protective clothing. These areas will be adjacent to shower facilities. Change rooms will be designed to ensure that clean clothing (e.g., personal clothing) and protective clothing are segregated. The design will ensure that storage of contaminated protective clothing will control contamination so that it does not spread beyond the storage container. The change room exhaust air shall be HEPA-filtered if dispersible radionuclides are handled in the process areas it serves.

7.9.2. Confinement Systems

Confinement capabilities, including confinement barriers and associated ventilation systems, will be designed to maintain a controlled airflow pattern from the environment into the confinement building, and then from non-contaminated areas of the building to potentially contaminated areas, and then to normally contaminated areas.

The number and arrangement of confinement barriers and their required design features and characteristics will be determined on a case-by-case basis according to

the particular hazards and risks of the process. Typical factors that affect confinement system design are the type, quantity, form, and conditions for dispersing the radioactive material, including the type and severity of design basis accidents. Alternative process and facility designs may reduce the potential hazards and the requirements for confinement system design. Engineering evaluations, trade-offs, and experience shall be used to develop a practical design that achieves confinement system objectives. To the extent practical, the ALARA concept shall be applied to the design of all confinement systems to minimize exposures to radioactive materials. Design of confinement systems shall provide adequate means for decontamination of the areas prior to entry or breaching for maintenance and repair purposes.

In general, the primary confinement system consists of the process enclosures and their ventilation system. In those cases where the process requires the use of corrosive or noxious materials, the process system shall be totally enclosed (i.e., pipes and vessels) and provided with its own ventilation and off-gas cleanup system. In such cases, the process system and its associated purge and off-gas system shall be treated as the primary confinement system. Some portions of the primary confinement may not form a complete physical enclosure. For these, the primary confinement function shall be ensured by adequate air flow and appropriate process equipment design. Special design features shall be considered to ensure safe introduction and removal of materials from process confinements.

The secondary confinement system consists of the barriers that enclose the areas that house the primary confinement and the system that ventilates those areas. The tertiary or final confinement system is generally the building structure and its ventilation system.

The secondary confinement barriers shall be designed and located to allow access to all sides of enclosed equipment to facilitate equipment maintenance, inspection, installation, and removal. As required, access panels shall be provided to allow operation and observation of equipment inside an enclosed area by personnel outside the enclosure. The secondary confinement areas shall be equipped with sensors to detect releases of process gases/vapors from the primary confinement boundary and provide appropriate alarms. Penetrations of the secondary confinement barriers shall be minimized. To the extent practical, all equipment components not functionally required to operate adjacent to the primary process shall be located outside the secondary confinement. The design of equipment that must be located within the secondary confinement area shall, to the extent practical, allow for in-place maintenance and/or replacement. Penetration of the secondary confinement barriers shall have positive seals to prevent the migration of contamination out of the confinement area if there is a failure of the process system or primary confinement.

Each secondary confinement area shall be supplied with ventilation air from the building ventilation system. The area shall be provided with exhaust ventilation with sufficient capacity to ensure an adequately controlled ventilation flow as required in the event of a credible breach in the secondary confinement barrier. Pressure in the secondary system shall be negative with respect to the building ventilation system.

Special features (e.g., air locks, enclosed vestibules) shall be considered for access through confinement barriers to minimize the impact of facility access requirements on the ventilation system and to prevent the release of radioactive airborne materials. Double-walled pipes or pipes within a secondary confinement structure encasement shall be used in all areas where the primary pipe leaves the facility.

All process operations that involve oxide powder or can generate powder or dust shall be provided with special containment to prevent contamination spread. Facility design shall, in particular, preclude the handling of uranium oxides in large open rooms. Discrete process work that could subject workers to possible inhalation exposures shall be performed in process confinement enclosures by using glove boxes, walk-in hoods, and similar environmental isolation devices. When glove boxes are used, their design and construction shall allow replacement of parts (e.g., gloves) and/or relocation of the box(es) within the facility or system(s) with a minimum of contamination spread.

7.9.3. Ventilation

The average concentration of airborne radioactive materials within radiation areas, at all locations normally accessible to personnel, will be kept ALARA. Primary and secondary ventilation systems are essential design features for controlling airborne radiation and minimizing internal radiation doses in occupied areas under routine operation as well as abnormal conditions or accidents that generate airborne radioactive materials outside normal containment. A gradient will be established on a facility and room basis so that the lowest pressure and exhaust collection points are located in areas with potentially dispersible materials. Isolation areas will operate under the least pressure (relative to the outside atmosphere). The required pressure differential between isolation areas and adjacent areas is 0.1 to 0.5 inches of water gauge (WG). The exhaust volume rate in an isolation area should be at least 10% of the actual room air volume per minute.

Single-stage HEPA filtration is required in areas where air contamination from particulates is not expected except during an accident. Multistage HEPA filtration is required for facilities that contain radioactive materials in a dispersible form and in facilities, areas, or containment boundaries that contain unsealed, highly radiotoxic material. The design of the ventilation system will allow filters to be changed easily and with a minimum potential for the release of radioactivity and worker exposure.

The design will also provide the capability for in-place testing of the filtration system. The design should allow for continuous particulate sampling before the first testable stage and after the last stage, to provide direct evidence of filter performance.

Room air may be recirculated if adequate filtration and monitoring are provided. However, recirculation from an area of higher contamination to an area of lower contamination is not allowed. Air sampling and monitoring will be provided in all work areas for the detection and measurement of airborne radioactive material.

7.9.4. Shielding

Remote shielded operation (i.e., with remote handling equipment such as remote manipulators) will be considered where it is anticipated that exposures to hands and forearms would otherwise approach the dose guidance in Table 7.2 or where contaminated puncture wounds could occur.

Shielding will be designed with the objective of limiting the total effective dose equivalent to less than 1 rem per year to workers based on their predicted exposure time in the normally occupied area. Within this design basis, personnel exposures will be maintained ALARA. In most cases, the confinement barrier or process equipment provides the necessary shielding. Straight-line penetration of shield walls will be avoided to prevent radiation streaming.

7.9.5. Waste Management

Wastes may include both radioactive and non-radioactive materials and may be in the form of liquid or airborne effluents, or solids. Operations will minimize the production of waste at the sources and minimize the mixing of radioactive and non-radioactive waste materials. In particular, clean materials such as incoming dunnage will be excluded from radiological control areas. Facilities will provide equipment and systems to handle waste safely and effectively. Waste handling areas will comply with the standards of confinement and ventilation requirements commensurate with the potential for spreading contamination by the waste packages/forms handled.

Laboratory or operating areas will not be prime areas for radioactively contaminated bulk waste storage. Instead, locations for the temporary storage of radioactive wastes will be designed into the building plan for each laboratory or individual radiation area. These areas will be located so that wastes being removed from the process will not have to be transported along major personnel traffic routes or through uncontrolled-assess areas. Fire suppression systems will be install in all waste management areas where combustibles are accumulated or stored.

Liquid and gaseous contaminated waste transported in pipes and ducts will be isolated from uncontrolled areas in the facility. Further, special design attention will be given to spill control.

Table 7.2
Maximum Dose Limits for Radiological Work

Type of Exposure		Annual Limit
Radiological Worker:	Whole Body (internal + external)	5 rem
Radiological Worker:	Lens of Eye	15 rem
Radiological Worker:	Extremity (hands and arms below the elbow; feet and legs below the knees)	50 rem
Radiological Worker:	Any organ or tissue (other than the lens of the eye) and skin	50 rem
Declared Pregnant Worker:	Embryo/Fetus	0.5 rem
Visitors and Public:	Whole Body (internal + external)	0.1 rem

NOTES:

Exposures shall be well below the limits in this table and maintained ALARA.

Internal dose to the whole body shall be calculated as effective dose equivalent. The committed effective dose equivalent is the resulting dose committed to the whole body from internally deposited radionuclides over a 50-year period after intake.

Background, therapeutic and diagnostic medical exposures shall not be included in either personnel radiation does records or assessment of dose against the Table limits.

Table 7.3
Maximum Allowable Surface Contamination in a Non-Radiological Area

Radionuclide	Removable dpm/ 100 cm^2	Total (fixed + removable) dpm/100 cm^2
U-natural, U-235, U-238 and associated decay products	1,000 α	5,000 α
Transuranics, Ra-226, Ra-228, Th-230, TH-228, Pa-231, Ac-227, I-125, I-129	20 α	500 α
Th-natural, Th-232, Sr-90, Ra-223, Ra-224, U-232, I-126, I-131, I-133	200 α	1,000 α
Beta-gamma emitters (nuclides with decay modes other than alpha) except Sr-90 and others above	1,000 β/ϒ	5,000 β/ϒ
Tritium organic compounds, surface contamination by HT, HTO, and metal tritide aerosols	10,000 α	10,000 α

NOTES:

The values in this table apply to radioactive contamination deposited on, but not incorporated into the interior of the contaminated item. Where contaminated by both α and β/ϒ nuclides, the limits established for the α and β/ϒ nuclides apply independently.

The amount of removable radioactive material should be determined by swiping the area with dry filter or absorbent paper while applying moderate pressure and then assessing the amount of radioactive material on the swipe.

The levels may be averaged over 1 square meter provided the maximum activity in any area of 100 cm^2 is less than three times the table value.

7.9.6. Codes And Standards

7.9.6.1. Structural

AISC Manual of Steel Construction, 8th ed.

AISC Code of Standard Practice for Steel Buildings and Bridges

7.9.6.2. Architectural

MBMA	Metal Bldg. Systems Manual
SMACNA	Industrial Duct Construction
SSPC	Paint Systems & Specs.
UBC	Uniform Building Code
UPC	Uniform Plumbing Code

7.9.6.3. Piping

ANSI B31.3	Chem. Plant and Petroleum Refinery Piping
API 526	Flanged Steel Safety Relief Valves
API 600	Steel Gate Valves
API 605	Large Diameter Carbon Steel Flanges
API 609	Butterfly Valves, Lug Type and Wafer Type

7.9.6.4. Fire and Safety

Factory Mutual Standards

NFPA 13	Installation of Sprinkler Systems
NFPA 24	Installation of Private Fire Service Mains
NFPA 30	Flammable and Combustible Liquids Code
OSHA 1910	Occupational Safety & Health Administration
UFC	Uniform Fire Code
UL	Building Materials Directory

7.9.6.5. Equipment

ANSI B30.17	Overhead and Gantry Cranes
API 610	Centrifugal Pumps For General Refinery

	Service
API 660	Shell and Tube Heat Exchangers For General Refinery Service
ARI 410	Forced-Circulation Air Cooling & Air Heating Coils
ARI 441	Room Fan Coil Air Conditioners
ASHRAE Applications Handbook	
ASME S2 Part A	Matl. Specs, Ferrous Materials
ASME S2 Part B	Matl. Specs, Nonferrous
ASME S8 Div 2	Pressure Vessels
ASME S9	Welding & Brazing Qualifications
ASTM	Matl. Specs
AWS D1.1	Structural Welding Code
AWS D10.9	Qualification of Welding Procedures and Welding For Piping & Tubing
EJMA	Expansion Joint Mfg. Association
IES-RP-CC-001	HEPA Filters
NEMA MG1	Motors & Generators
TEMA	Tubular Exchanger Manufacturers. Association
UMC	Uniform Mechanical Code

7.9.6.6. Electrical

IEEE	Electrical Standards

NEMA 210	Secondary Unit Substations
NEMA 250	Enclosures for Electrical Equipment
NEMA AB1	Molded Case Circuit Breakers
NEMAFB11	Plugs, Receptacles & Connectors For Hazardous Locations
NEMA SG5	Power Switch Gear Assemblies
NFPA 70	National Electric Code
NFPA 50	Bulk Oxygen Systems
NFPA 110	Emergency & Standby Power Systems
NFPA 75	Protection of Electronic Computer Equipment

7.9.6.7. Instrumentation

ISA S5.1	Instrument Symbols/Identification
NEMA ICS 1	General Standards For Industrial Control & Systems
NEMA ICS 2	Stds For Industrial Control Devices, Controllers & Assemblies

7.10. Process System Requirements And Description

7.10.1. Area 100 Feed Prep

The Feed Preparation area is comprised of equipment needed to off-load and handle incoming containers, remove the contents safely, and condition the feed for slurry or top injection into the Catalytic Processing Unit (CPU). The feed preparation operations are performed within the building and have emission control systems. Each step of the feed preparation operation will be engineered to isolate and protect the operating staff in accordance with accepted standards that meet or exceed all other health and safety requirements.

7.10.1.1. Material Receiving

The facility receives wastes in 55 gallon drums or other containers. Four drums at a time are unloaded from trucks on pallets using a propane-fueled fork truck. The drums are weighed, and various administrative functions are performed in the adjacent area. If necessary, the drums are staged on RCRA spill pallets prior to preparation as Q-CEP™ feed. The propane-fueled fork truck handles the drums, other containers with clean exteriors, and uncontaminated materials entering the facility in clean areas.

7.10.1.2. Drum Sampling

Drums for a Q-CEP™ run are transported to the Feed Preparation Room. An electric fork truck transports the drums, one drum at a time, within the Feed Preparation Room. Waste sampling occurs in the enclosed and ventilated confinement area. A single drum is placed on the roller conveyor at the entrance to the confinement area. A sliding door in manually opened and the drum is then pushed inside the confinement area. An air sweep through the open door ensures that air-borne dusts or fumes are confined within the structure.

Employees wearing appropriate protective equipment enter the confinement structure via a separate personnel door. Protective equipment typically includes booties, overalls or lab coat, gloves, and respirator. Inside the confinement area, the drum lid is removed, the contents are visually inspected, and a representative sample is obtained. The drum lid is then replaced, the drum is removed from the confinement area for staging within the Feed Preparation Room. Care is taken to prevent contamination of the drum exterior. If necessary, the drum is wiped down to prevent contamination spread within the Feed Preparation Room.

7.10.1.3. Drum Emptying And Waste Screening

When the sample analysis is complete, and the facility is prepared to process the waste, individual drums are moved back to the confinement area. The drums enter the confinement area via the roller conveyor and sliding door previously used for drum sampling. The drum lid is removed at the drum emptying station. If free liquid is present, a spout is placed on the drum to prevent liquid from running down the side of the drum when tilted. The drum is clamped into place, and the drum is first elevated vertically and then tilted. The free liquid drains out of the drum and then through the screen. When the free liquid is drained, the drum is straightened and then lowered back to its original position. The spout is removed and the drum is again elevated and tipped so that the waste falls out and onto the screen. If necessary, tools are provided for removing the waste from the drum. When the drum is empty, it is decontaminated with recycled rinse water, evaporated rinse water, or steam. A spray nozzle provides 10 gpm of rinse water at 60 psig for rinsing. The drum is returned to an upright position and lowered back to

the roller conveyor. The drum is swiped prior to removal from the confinement area. The drum may be staged for reuse as the ceramic disposal container or for disposal via the Q-CEP™ process. Disposal requires drum shredding for top feed through a lance. Drums containing liquids are pumped directly into one of the Q-CEP™ Feed Tanks.

A number of process activities, such as drum sampling, emptying, screening, drying, and milling occur in the same confinement structure. As its name implies, the confinement structure provides confinement of the wastes and capture of any airborne effluents. The confinement structure also includes a spill pan and a collection sump for equipment washdown or process liquids or solids inadvertently released from equipment. The walls of the confinement structure are sealed and are made of Plexiglas for viewing operations occurring inside the structure. Air sweep through openings ensures that air-borne dusts or fumes are confined within the structure. The exhaust air from the structure is subject to carbon bed filtration and HEPA filtration (in the HVAC system) for removal of dust, organic, or mercury that become airborne during waste handling operations. This ventilation discharges directly into the facility stack after control.

The wastes are emptied from the drum onto the Debris Screen. Debris that is larger than 1/2" is retained on the screen for rinsing and manual removal. Recycled rinse water and evaporated rinse water are provided for the rinsing. The debris is staged in 55 gallon drums for CPU top feed in a subsequent run. Tools are provided for manually pushing the waste through the screen, if necessary. These tools, those for emptying the drums, and the samplers may also be rinsed on the screen. Space is also provided for a future sorting table and separate 55 gallon drums for inorganic debris, scrap metal, organic debris, and reject. Debris from the recycled sludge in the effluent treatment coalescing separator is also removed on the debris screen.

7.10.1.4. Moisture Removal

Moisture is then removed from the screened waste. Moisture removal includes vacuum filtration and drying to reduce the moisture content to a nominal 10%.

The head of the filter is removed during the drum emptying and screening operations. The screen is placed on the open filter housing, allowing access to the filter cress section. Waste from the screen descends into the filter housing and onto the filter media. The screen is physically removed from the filter housing once the drum is empty, the drum is clean, and the waste and debris removed from the screen. The top head of the filter is then replaced on the housing. The top head of the filter contains an agitator that can break up or smooth the waste, aiding filtration and drying.

A vacuum pump pulls a vacuum below the filter media, which draws free moisture from the waste and through the filter media for liquid collection. The 150 psig steam

enters the filter jacket, hollow support plate and hollow agitator to provide heat for drying. Moisture evaporated during the drying operation is condensed in the filter condenser for collection in the Effluent Treatment System. The discharge from the vacuum pump is directed to the thermal oxidizer for VOC control.

7.10.1.5. Size Reduction

When the waste has been adequately dried, the filter chute opens to discharge the waste into the ball mill feed hopper. Fuel oil joins with the dried waste in the feed hopper. When the ball mill is ready to receive the waste/fuel oil mixture, the feed passes to the Ball Mill where it is ground to 150 microns and smaller for tuyere feed to the CPU. The tuyere is a triple concentric tube through which the feed and coreactant such as oxygen, nitrogen and natural gas are fed. The ball mill is operated on a batch basis to coincide with the drum emptying and filtration/drying. It is anticipated that the feed will be mixed with fuel oil to improve the milling characteristics. Due to the possible presence of flammable materials in the waste feed, the ball mill is purged with nitrogen prior to filling it for each batch. Precautions must be taken to prevent an oxygen deficiency inside the confinement structure. CPU cofeeds, which can include pulverized lime, coke, and fluxing agents, are added to the feed to adjust reactor chemistry and ceramic characteristics. These cofeeds can be added to the ball mill for size reduction in the ball mill or screening in the tuyere feed screen prior to addition to the CEP feed tanks.

A diaphragm pump transfers the waste from the ball mill to the Tuyere Feed Screen, where oversized particulates are removed from the tuyere feed. The feed screen vibrates to improve the slurry processability. The uppermost screen retains any debris larger than 1/8" that has passed through the 1/2" debris screen. Any material collected on this screen is manually removed. The lower screen removes particles larger than 100 microns. These particles, still slurried in fuel oil, exit the screen and return to the ball mill feed hopper for additional size reduction. The slurried particles smaller than 100 microns pass through the screen and gravity flow into one of the CEP Feed Tanks.

7.10.1.6. CEP Feed Tanks.

The undersized materials passing through the feed screen then flow to one of two CEP feed tanks. The feed for a single Q-CEP™ run is collected in one of the feed tanks. Cofeeds may be added and samples are taken.

Cofeeds, which are added to the CPU feed to adjust reactor chemistry and ceramic characteristics, may be added manually to the feed tanks. Cofeeds may also be added manually to the ball mill for size reduction and then screening prior to addition to the feed tanks. A local hood provides ventilation for dust control during bag dumping, and a lock hopper provides contamination control. The hood ventilates through a HEPA filter and discharges to the Facility stack.

Materials recycled to the CPU reactor also join with the feed in the CEP feed tanks. For example, oil-slurried solids from the ceramic filtering the Gas Handling Train are added to the CEP feed tanks. Recovered oil from the coalescing separator and the evaporator in effluent treatment are also added to the CEP feed tanks.

A grinder pump circulates the Q-CEP™ feed through the tank to circulate the tank and break up any agglomerated solids. The piping and valving is designed to allow for independent circulation of each feed tank. Grinder pump operation requires indication of proper valve positioning to ensure that the grinder pump is not operated deadheaded. The feed is sampled at the pump discharge for analysis of feed composition and applicable handling properties.

When the feed has been appropriately adjusted, it is tested in the tuyere test stand to ensure that its particle size and thermal stability are suitable for CPU tuyere injection. A slip stream from the grinder pump feeds the Injection Pump suction. A slip stream from the injection pump feeds the test stand or tuyere. A filter prevents oversized materials from entering the test stand or the tuyere itself. The feed from the test stand returns to the feed tanks.

Fugitive emissions were estimated from the Grinder Pump, Injection Pump, Feed Tanks, and associated valves and flanges. The fugitive emissions are collected via the Feed Preparation Room's ventilation system and controlled with activated carbon and HEPA filtration prior to discharge to the facility's stack.

7.10.1.7. Bulk Feeds

The functionality specified for the units includes Q-CEP™ top feed for inorganic debris, scrap metal, and organic debris. As such, a Jaw Crusher and Shredder provide the size reduction required for top feeding these materials.

7.10.2. Area 200 Reactor Systems

7.10.2.1. Ceramic & Metal Tapping System

The purpose of this system is to discharge ceramic or metal from the CPU as it is generated during processing of mixed waste from the DOE. Much of the waste is expected to have a very high inorganic content which, with appropriate additives, will become the final form for disposal as radioactive waste. This material must be checked for proper chemical composition before being discharged from the reactor. Initial runs will set the parameters for the final composition of waste and additives.

7.10.2.1.1. System description

The CPU is designed to rotate for deinventory of the metal upon completion of a campaign. The ceramic tapping system is designed to take advantage of this feature by tipping about 5^0. Rotating the vessel achieves three key objectives:

- Allows the ceramic lined discharge pipe to pass through the isolation valve and mate with a similar pipe leading into the tapping container. This eliminates the need for a valve to interrupt the flow of ceramic or to risk ceramic or metal solidification on the interior valve surfaces; potentially damaging the valve seals and making pressurized operations difficult.

- Provides an opportunity to chemically tailor the ceramic before discharging by introducing additives through the bulk feed port.

- Eliminates the need to start and stop feed during a run.

The system is comprised of the following major components:

- A discharge nozzle lined with ceramic reaching to just above the isolation valve.

- A bellows.

- An isolation valve operable at elevated temperatures.

- A quick disconnect (bayonet type, lever operated) device to disconnect the tapping system from the vessel when rotating.

- A pressure tapping vessel housing the ceramic container (55 gallon drum anticipated) with vents drains, and purge connections.

- A cooling water system comprised of multiple spray heads to keep the drum surface cool during tapping operations.

- An off gas education system to preheat the tapping nozzle and reinject the gases into the Gas Handling Train.

7.10.2.2. Inst. & Control: General Design Requirements

7.10.2.2.1. Instrument Identification

All instruments, including hand valves, will be assigned unique alpha-numeric tag names. Generally accepted industry standards will be followed in the assignment of tag names. Tag names will be limited to eight (8) characters. An instrument database will be created and maintained throughout the life of the project.

Engineering flow diagrams will contain a legend defining the method of assignment. All components necessary to understand system function will be assigned tag names. Engineering loop diagrams will show all hardwired instruments.

Stainless steel engraved or stamped identification tags will be attached to all non-panel field instruments. Identification tags will be supplied by the manufacturer with the instrument. Front and rear panel instruments will have nameplates of laminated phenolic plastic with engraved lettering.

7.10.2.2.2. Calibration

Certified factory calibration data sheets will be provided with all instruments and will be made a permanent part of the instrument record.

Subsystem module vendors will perform an incoming inspection and functional test of all instruments and record the results as part of the instrument record.

Loose instruments installed at the plant site will be subjected to incoming inspection and functional test and the results will be recorded as part of the instrument record.

All instruments will be provided with a calibration sticker.

Calibration interval requirements will be made a part of the instrument database.

7.10.2.2.3. Control and Transmission Signal Ranges

The operating signal range for pneumatic control and transmission systems will be 3 to 15 PSIG.

The operating range for analog control and transmission signals will be 4 to 20 milliamps DC.

Dry contact discrete signals will be 120 VAC, 60 Hz nominal.

7.10.2.2.4. Instrument Air System

The source of instrument air should be independent of other users and should be essentially oil free. Pressure should be 80 PSIG minimum with a dew point at least 10 °F below minimum ambient temperature.

Local instruments will be supplied with 20 PSIG instrument air from a combination filter-dripwell regulator with integral relief valve. Line pressure air supplies will include filters.

7.10.2.2.5. Instrument Purges

Nitrogen purges to instruments which enter the process gas stream will be taken from a separate purge gas header for the purpose of measuring purge gas flow to the process gas.

7.10.2.2.6. Documentation Requirements

Project specific documentation will be prepared in accordance with the engineer's standard procedures using the engineer's standard drawing formats, forms, and specifications. This includes as a minimum the following project specific drawings, diagrams, forms, and lists:

- Instrument Panel Specifications;
- Instrument Installation Materials Specifications;
- Instrument Requisitions;
- Calculations;
- Logic Flow Diagrams;
- Loop Diagrams;
- Panel, Console, and Rack Drawings;
- Arrangement Drawings;
- Tubing Schedules;
- Installation Details;
- Elementary Diagrams;
- Electrical Area Classification Plan;
- Instrument Index Database;
- Graphic Display Drawings;
- Annotated software Listings;
- Standard Manufacturer's Manuals and Data Sheets;
- Recommended Startup Spares;

- Recommended Operating Spares.

7.10.3. Area 300 Gas Handling Train

7.10.3.1. Overview

The purpose of the Gas Handling Train (GHT) is to remove contaminants and particulates from the gas effluent stream exiting the reactor system. This includes the removal of volatile heavy metals such as mercury, any radioactive components, and other particulates such as entrained dust. Both wet and dry operations are employed to accomplish this goal. The sub-systems include a gas quench system, venturi scrubbers, ceramic filtration, water wash system, hydrocyclone, carbon bed adsorption, HEPA filtration, and caustic scrubbing. The clean gas stream that is predominantly carbon monoxide (CO) and hydrogen (H_2) is thermally oxidized to produce carbon dioxide (CO_2) and water (H_2O).

The gas handling train is designed to provide both primary and secondary systems for removal and recovery of contaminants and to produce a clean gas stream for discharge to the atmosphere.

7.10.3.2. Gas Quench

The gas stream exiting the central processing unit (CPU) feeds directly to the Gas Quench exchanger. It is cooled to allow for processing through the GHT. The gas quench exchanger is an MMT design using a jacket with cooling water on the outer side of the process pipe to lower the process stream temperature. In addition, evaporative cooling is utilized by allowing deionized water to enter the gas stream through a porous metal pipe located inside the exchanger. The amount of deionized water to be injected into the gas stream is controlled by monitoring the exchanger outlet temperature.

The materials of construction for the gas quench exchanger are critical and must allow for high temperatures and possibly corrosive elements in the gas stream such as HCl and H_2S. The temperature of the gas stream is maintained well above the dew point of the gas.

7.10.3.3. Ceramic Filtration

The cooled gases from the quench exchanger enter the Ceramic Filter where suspended particulates are removed. The particulates collected are accumulated in the Ceramic Filter Collector and are removed from the system and placed in drums.

The differential pressure across the ceramic filter is monitored and a controller is utilized to provide a pulse of nitrogen to blow the filter clean periodically. Also, a timer to control the cycle time for cleaning the filter will be used. A bypass will be

provided around the ceramic filter to be used in the event the filter becomes plugged during an operation. The quench gas will then feed directly to the venturi scrubber system.

7.10.3.4. Venturi Scrubber System

The gas entering the liquid Venturi Scrubber system passes through a duct that has a venturi-shaped throat section. A coarse caustic spray is injected into the throat of the venturi where the liquid droplets collide with the particles in the gas stream. The gas-liquid mixture is then separated in the Gas Quench Accumulator. The separation of the liquid from the gas occurs due to the velocity change upon entrance into the accumulator, the heavier liquid settles with the particulates. The gas stream exits to the High Efficiency Fume Scrubber which further removes particulates that will be recovered in the Wash Tower.

The venturi scrubbing system acts as the primary removal point from the gas stream for heavy volatile metals such as mercury, cesium, and solid particulates. The removal of the heavy metals and particulates from the GHT is accomplished by the Wash Tower System via a Hydrocyclone. The Venturi Scrubber and Wash Tower Systems are equipped with a bypass so that certain process gas streams may be sent directly to the Gas Cooler.

7.10.3.5. Wash Tower System

The wash tower system is designed to further remove particulates from the gas streams and recover the condensed mercury, cesium in the form of cesium hydroxide, and any entrained radionuclides.

The saturated gas stream enters the Wash Tower at which point the entrained liquid falls to the bottom of the tower and the contaminated gas stream rises to the bubble cap trays. The gas rises upward until contact is made with the bubble caps and the gas is diverted downward and discharged as small bubbles from the slots at the base of the caps. As the gas continues upward, the same water-gas contact occurs until the clean gas emerges from the top. The contaminant rich liquid flows to the bottom of the tower.

The bottom of the tower acts as the settling point for elemental mercury where it is withdrawn from the system. The liquid from the wash tower bottom is pumped and cooled by the Wash Tower Loop Cooler, and a slip stream goes to the Hydrocyclone. The Hydrocyclone concentrates the contaminants and the effluent removed is stored for later use as feed to the CPU. The clean liquid stream exiting the Hydrocyclone is filtered and passed through the Cesium Trap prior to mixing with the makeup caustic stream and being fed to the top of the wash tower.

A liquid stream is recycled back to the Liquid Venturi Scrubber and to the High Efficiency Fume Scrubber from the Wash Tower Circulation Pump.

7.10.3.6. Carbon Bed Adsorption

The overhead gas stream from the Ceramic Filter enters the Gas Cooler if the Venturi Scrubbing system is bypassed, to cool the gas stream and lower the dew point subsequent to entering the carbon bed adsorbers. A bypass will be provided around the Gas Cooler in the event the Venturi Scrubber and Wash Tower Systems are in service and cooling is not required, allowing for flexibility in the system operation.

The carbon within the carbon bed is impregnated with sulfur to further aid in the removal of mercury from the gas stream. Two carbon beds are utilized in series to ensure contaminant removal from the system in the event filter break through occurs. The Carbon Bed System is a secondary removal system for mercury.

7.10.3.7. HEPA Filtration

Gas from the carbon beds feeds directly to the HEPA filter. The HEPA filter is designed to extract any radionuclides and remaining particulates from the gas stream. The HEPA system is considered a secondary removal sub-system for radionuclide contaminants.

7.10.3.8. Vent Scrubber System

The Vent Scrubber System is designed for operation during relief service from the reactor system, normal gas flow from the reactor, and processing of gas from vents on the Ceramic Filter Collector and feed handling tanks. The system will remove H_2S and other acids from the gas stream by employing counter-current gas liquid extraction in a packed tower. The gas is contacted in the packed section by the caustic liquid flowing down from the top distributor. The liquid is pumped from the bottom of the tower by a Caustic Scrubber Circulation Pump.

The liquid level in the tower is controlled by allowing a small stream of caustic to be removed from the system when the liquid level is high. At low level, a valve opens allowing plant water to feed into the Thermal Oxidizer Seal Pot, which allows overflow to the vent scrubber tower. Caustic addition to the system is directly to the bottom liquid section of the tower. Clean gas exits the tower at the top and flows to the thermal oxidizer system. Spent caustic removed from the system is treated and discharged or sent to the CPU.

7.10.4. Area 500 Effluent Treatment

7.10.4.1. Thermal Oxidizer

Gas from the vent scrubber system flows to the Thermal Oxidizer Seal Pot and bubbles through the liquid seal and directly to the Thermal Oxidizer. The thermal oxidizer converts the CO and H_2 to CO_2 and H_2O. The Thermal Oxidizer control system regulates the natural gas feed to the burners and the flow of the combustion air to optimize the CO_2 and H_2O formation. Exit gas analysis from the stack guarantees performance of the thermal oxidizer.

7.10.4.2. Aqueous Effluent Treatment

Aqueous effluent treatment system includes the Oil/Water/Sludge Coalescing Separator, the Rinse Water Collection Tank, the Effluent Filter, the Effluent Adsorber, the Effluent Evaporator, Condenser, Condensate Collection Tank, Sludge/Oil Collection Pot and Transfer Pumps. The aqueous effluents are first collected for treatment. The filtrate from the Filter contains the free water removed from the waste. It also contains rinse water from rinsing the drums at the drum emptying station and from rinsing debris on the feed screen. Contaminated materials resulting from spills and equipment washdown are first collected in spill pans and collection sumps for transfer to the effluent treatment system. Collection sumps are provided in the feed preparation room. Washdown water from potentially contaminated areas, such as the feed preparation room, contaminated maintenance, the CEP and Gas Handling room, and the laboratory, are also collected for effluent processing. If desired, the caustic purge from the Gas Handling Train can also be collected for treatment. To facilitate the drainage of all aqueous effluents, the Coalescing Separator, the Rinse Water Collection Tank, the Sludge/Oil Collection Pot and associated Pumps will be located in the basement of the plant.

The aqueous effluents are first collected in the Oil/Water/Sludge Coalescing Separator for removal of oil, sludge and solids. The oil coalesces and is decanted into a chamber where it gravity flows to the Sludge/Oil Collection Pot. The sludge and solids are separated and settled into the collection hopper and gravity flow to the collection pot. The effluent water gravity flows from the Coalescer to the Rinse Water Collection Tank, where the pH can be adjusted as required. The Coalescer is sized to accommodate rinse water and other aqueous effluents. The Coalescer vents to the Thermal Oxidizer for VOC control. The Rinse Water Collection Tank provides surge capacity for the rinsing operations in the feed preparation area and feed to the Evaporator System, using Rinse Water Circulation Pump. A small and controlled amount of rinse water could be sent to the CEP Reactor via Feed Tanks. The Effluent Filter and the Effluent Adsorber will ensure that the effluent water is free of sludge, solids and other dissolved hydrocarbons or organic chlorides. The Effluent Adsorber is by-passed if the effluent water is recycled as rinse water in the feed preparation area. The system also includes a provision for future installation of a Mercury Carbon Adsorber, if necessary. The excess water is pumped to the

Effluent Evaporator, steam is used as a heating medium. The vapor from the Evaporator is either sent to the Thermal Oxidizer for VOC control or condensed in the Effluent Condenser and gravity flows to the Condensate Collection Tank. Offgas is routed to the thermal oxidizer for VOC Control. The sludge and solids collected at the bottom of the Evaporator is drained to the Collection Pot. The sludge, oil and solids in the Collection Pot are pumped to the Ball Mill in the feed preparation area for processing. The condensate is recycled) as rinse water in feed preparation or, if the water is free of organic chlorides, as make up water for the Gas-Liquid Separator and Gas Scrubber in the Gas Handling Train.

7.10.4.3. HVAC Design Requirements

7.10.4.3.1. General

The ventilation system for radiologically contaminated areas shall be designed to provide proper environmental condition for health, safety and comfort of personnel. The contaminated areas shall be designed to provide a continuous air flow pattern from the outside environment into the building and then from areas of lower potential for contamination to areas of higher potential for contamination.

The radiological ventilation system will serve the areas that have potential for radioactive contamination which are: the insides of the glove boxes, fume hoods, canopy hoods, equipment enclosures and the Reactor area.

The non-radiological ventilation system will serve the areas or rooms where the glove boxes, hoods and enclosures are located and have very low potential of contamination.

7.10.4.3.2. Confinement Ventilation Requirements

The confinement ventilation system shall be designed to provide confinement of radioactive and hazardous materials within the area as close to the point of origin as practicable and to prevent or minimize the spread of contaminants within the facility as well as to the environment.

The radiological confinement areas or zones shall be provided with continuous airflow and air changes to maintain the desired environmental conditions and proper pressure differentials between radiological confinement areas.

The confinement ventilation system shall remain functional for all normal operations and anticipated operational occurrences.

The glovebox or other enclosure's exhaust system shall be sized to ensure inward air nominal velocity of 125 fpm through any credible breach in the enclosure.

Ductwork handling potentially contaminated exhaust air shall be of welded construction and shall have smooth interior finish to prevent the accumulation of contaminated particulates.

The confinement exhaust system shall discharge to an elevated stack and shall be monitored to ensure that the radiological limits on site doses and the off site doses are not exceeded. Stack location and height shall also consider intakes of the facility it serves and adjacent facilities to preclude cross contamination.

The confinement exhaust system shall be provided with the required number of stages of HEPA filters as determined by a contamination safety analysis.

7.10.4.3.3. Design Basis

Pressure Differentials

Pressure differentials between confinement areas of different degree of contamination shall be maintained at a minimum of 0.1 in-WG.

Gloveboxes shall be maintained at a negative pressure between 0.3 to 1.0 in-WG differential with the surrounding area.

Ventilation Air Changes

Air changes for the radiological areas shall be 4 air changes per hour. Glovebox shall be designed for 40 air changes per hour.

HEPA Filtration: One stage of final HEPA filter supplemented with local HEPA filters at the source will be provided. A bag-in/bag-out type of filter plenum shall be used for better contamination control. Filter arrangement shall allow replacement of filter units without shutting down the ventilation system.

7.10.4.3.4. System Description

Radiological Ventilation System

The radiologically contaminated areas (Reactor area and Feed Preparation area) shall be each served by a new packaged roof-top A/C unit located on the roof. The air supply system shall contain cooling coils, gas-fired furnace, filters, supply air fan and backflow prevention device. The supply air system shall provide a continuous once-through exhaust airflow.

The exhaust air for this system shall be through direct connection to the rooms, fume hoods and containment enclosures. A confinement enclosure or equivalent localized exhaust hood shall be provided to process components that have the potential of releasing radioactive contamination. The fume hood exhaust shall be provided with

local HEPA filters and booster exhaust fan before connecting to the exhaust header. The exhaust system shall be provided with dedicated ductwork, single-stage HEPA filtration with pre-filter, and exhaust fans. For reliability, redundancy of fans and filters shall be provided. The final exhaust shall be discharged to the environment through a monitored exhaust stack. The stack height shall be a minimum of 10 feet above the roof.

Non-radiological Ventilation System

The non-radiological areas shall obtain makeup air from the surrounding area. The makeup air system shall be provided with a proper backflow device to prevent backflow of potentially contaminated air to the surrounding areas.

The exhaust system shall be provided with dedicated ductwork and exhaust fans. The exhaust fan discharge shall be at least 10 feet above the roof level.

Hydronic Systems

The cooling requirement for the HVAC system and the Process cooling water system shall be provided by a central chilled-water system. A heat exchanger shall be provided to branch out from the main chilled water system to serve either the HVAC system or the process cooling water system. The equipment for the chilled water system shall be sized for three 50% capacity with one unit for stand-by. The chilled water system shall be mixed with required amount of glycol for anti-freeze protection.

7.10.4.4. Fire Protection

In areas where the use of water does not pose a hazard, fire protection shall be designed and installed in accordance with NFP Codes 13. In other areas where sprinklers pose a hazard, other means of controlling fire damage, such as inert gas, liquid nitrogen, isolation, or rapid drowning, shall be employed. The following criteria shall also be addressed:

Containment for maximum sprinkler flow of a system for 15 minutes minimum shall be provided for hazardous material process areas.

The design of fire protection systems shall be approved by Factory Mutual.

Fire hydrants and hose houses shall be provided as required.

The process control room and the office shall have a wet pipe sprinkler system and smoke detection.

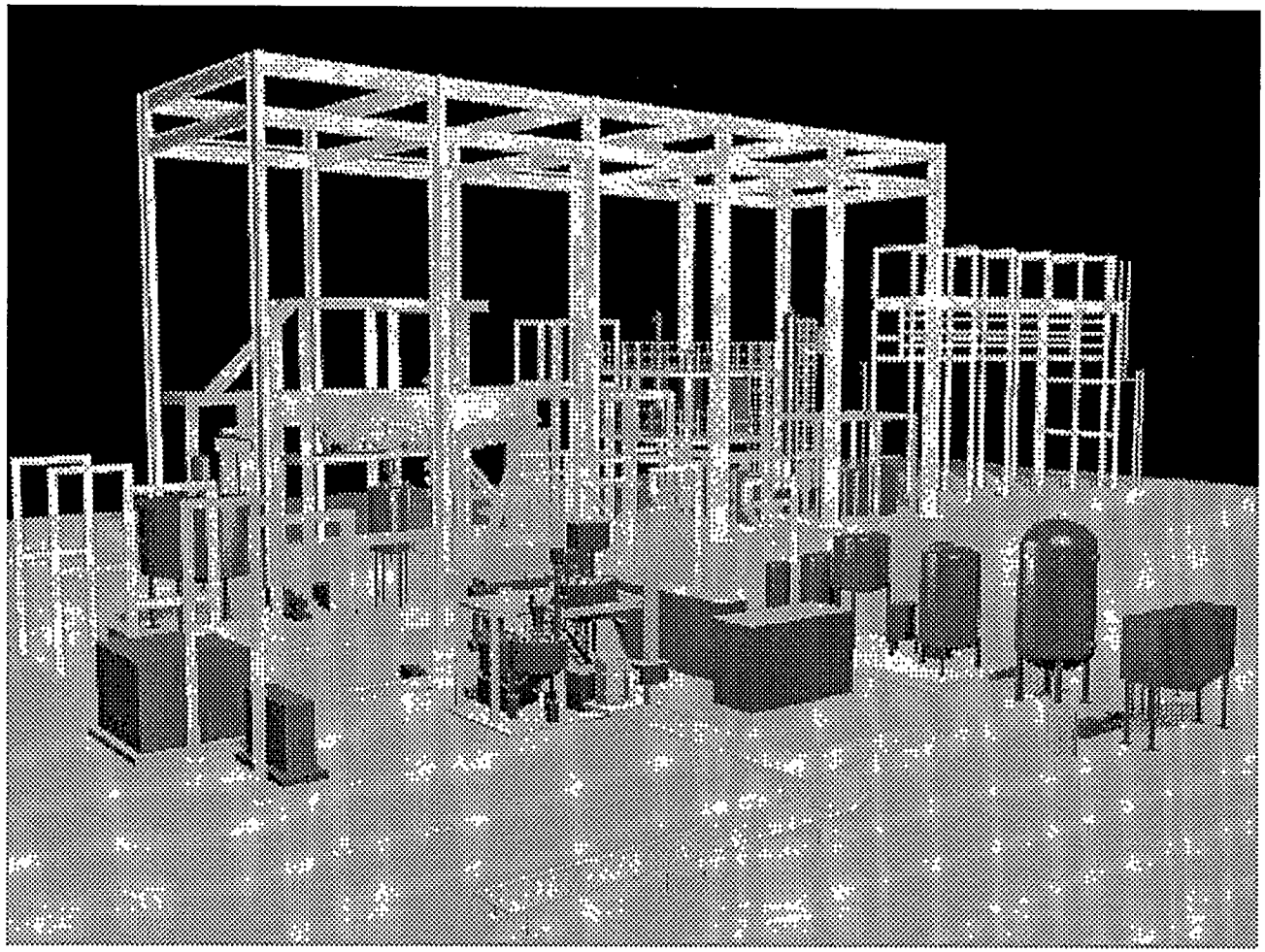

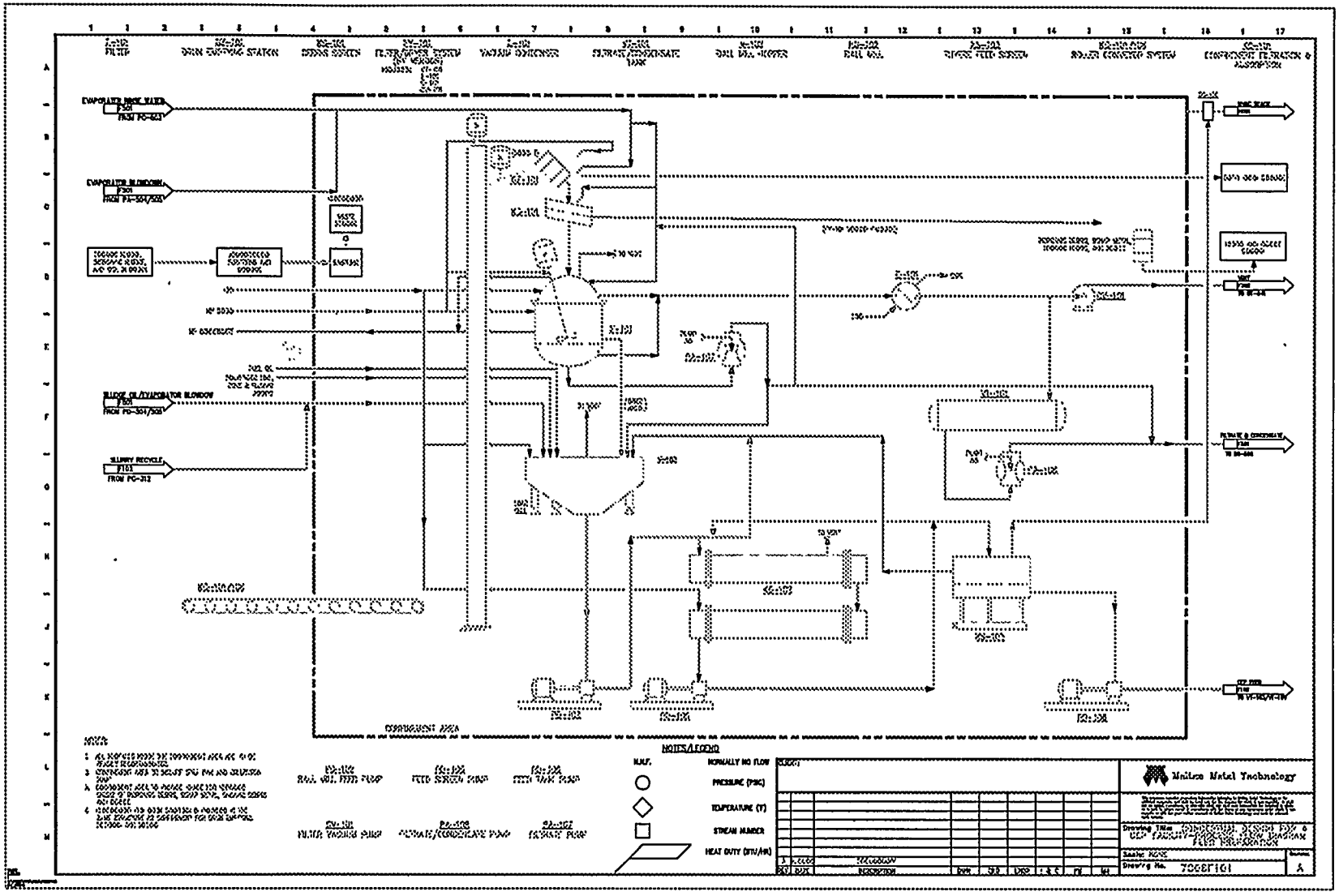

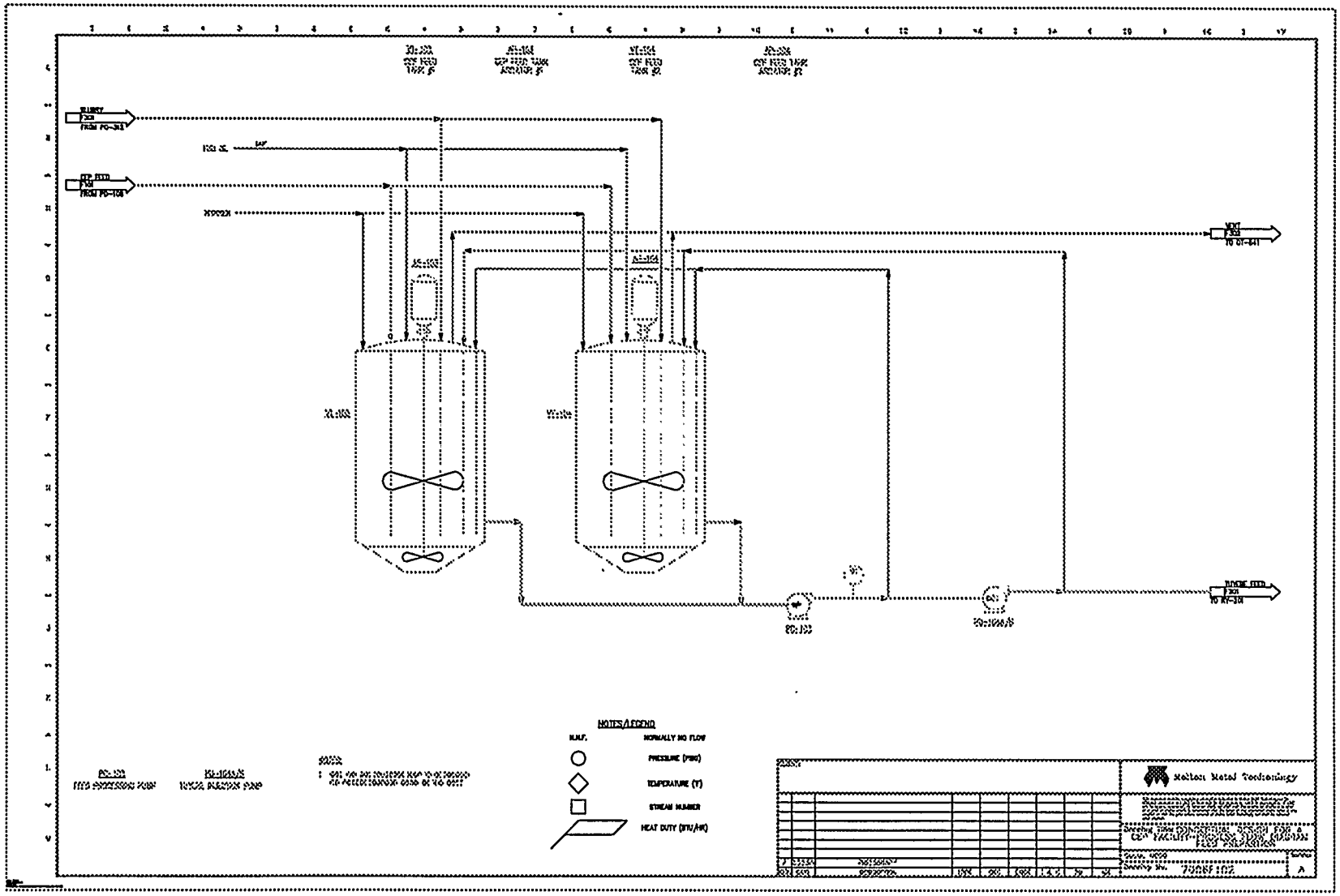
NOTES/LEGEND
N.N.F. NORMALLY NO FLOW
PRESSURE (PSIG)
TEMPERATURE (T)
STREAM NUMBER
HEAT DUTY (BTU/HR)
Molten Metal Technology

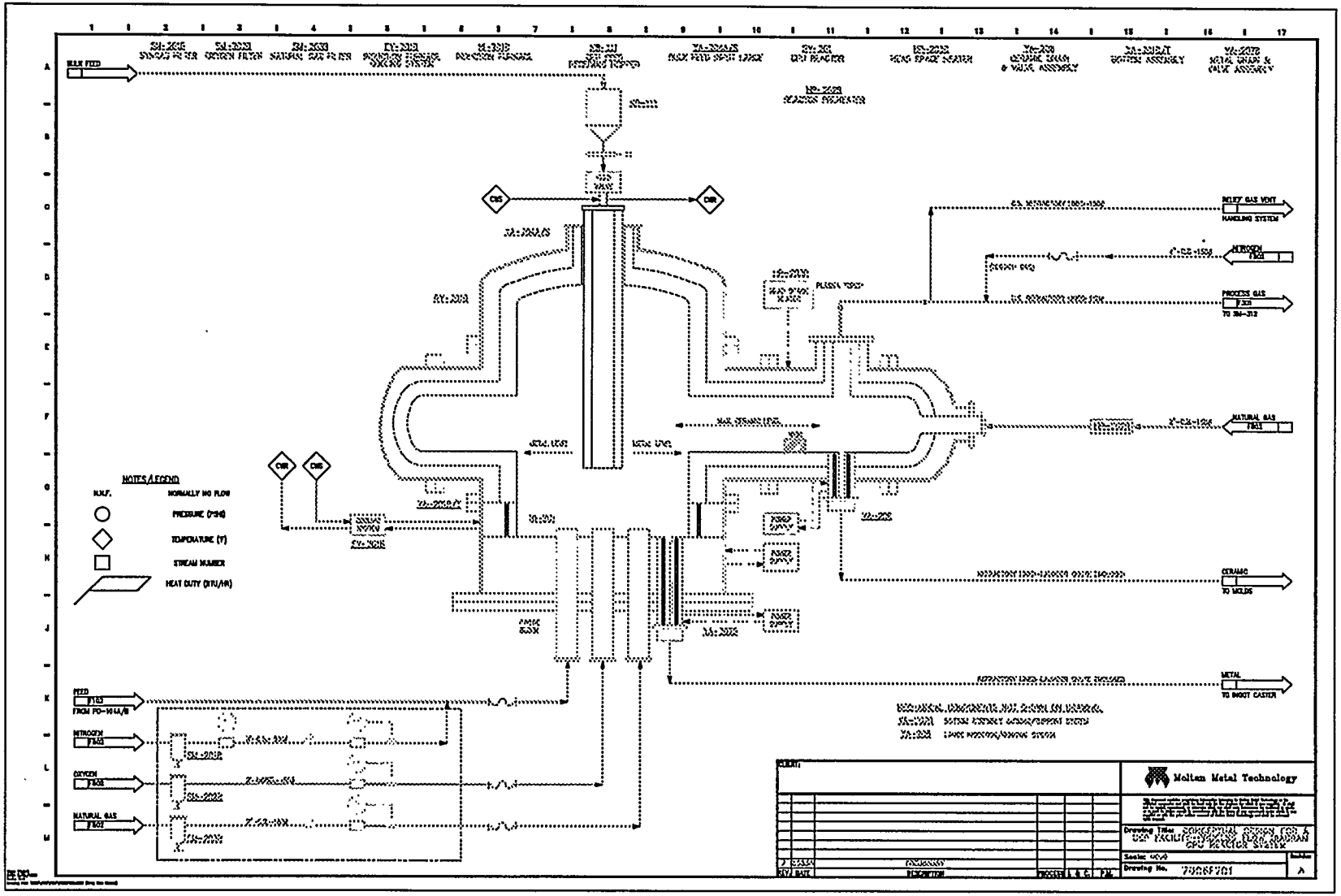
NOTES/LEGEND
N.N.F. NORMALLY NO FLOW
PRESSURE (?PSI)
TEMPERATURE (T)
STREAM NUMBER
HEAT DUTY (BTU/HR)
Molten Metal Technology

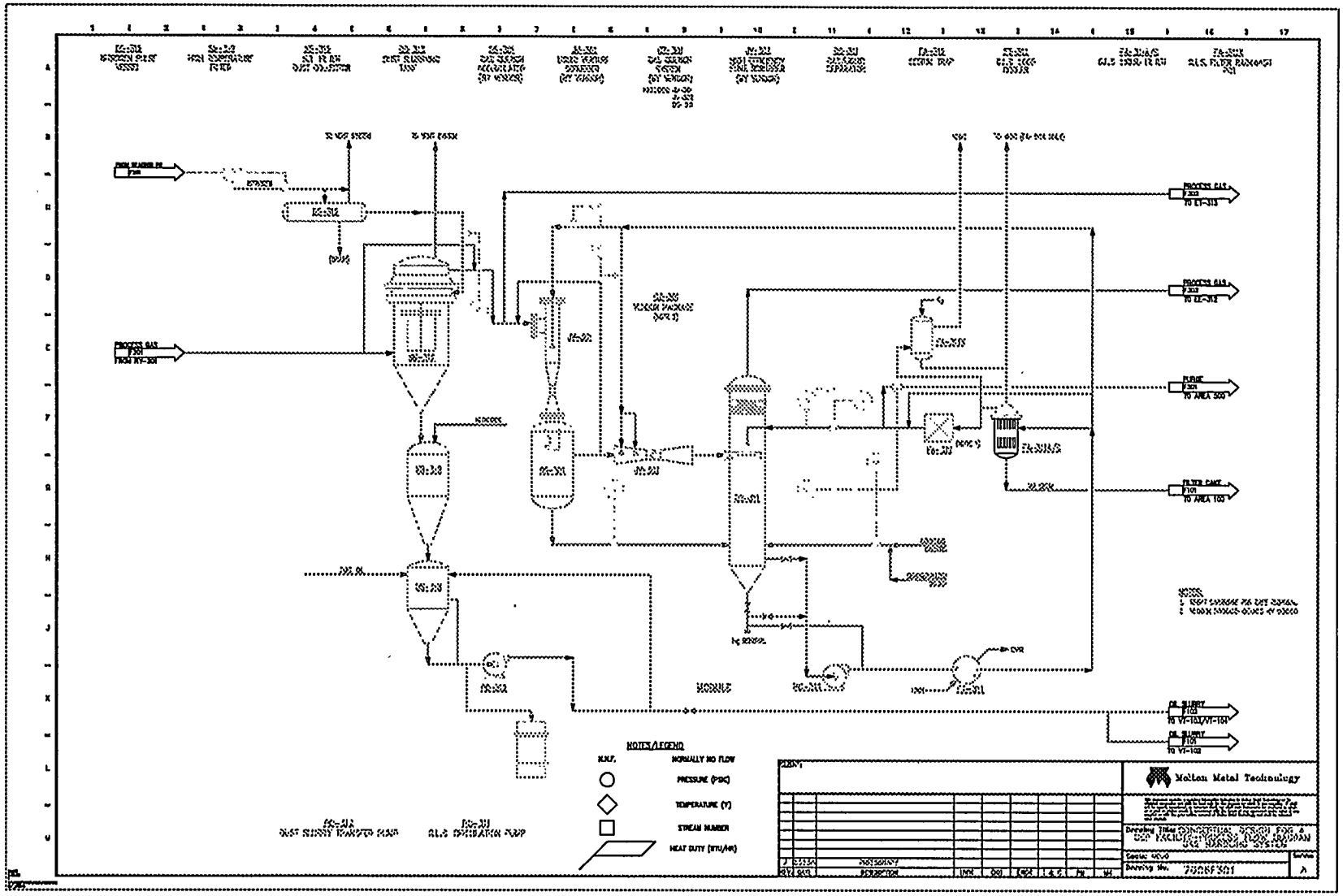
NOTES/LEGEND
N.N.F. NORMALLY NO FLOW
PRESSURE (PSIG)
TEMPERATURE (°F)
STREAM NUMBER
HEAT DUTY (BTU/HR)
Molten Metal Technology

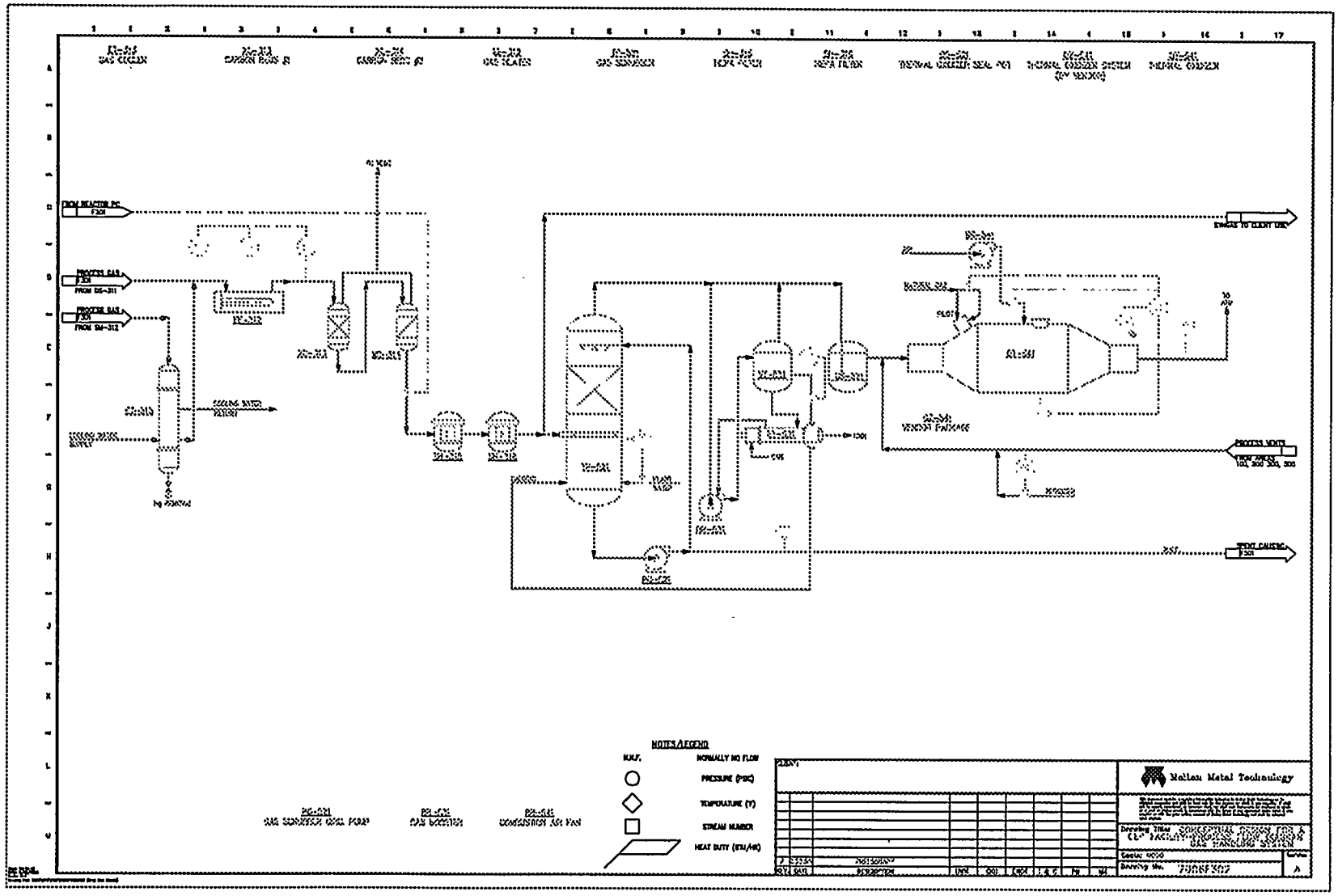
NOTES/LEGEND
NORMALLY NO FLOW
PRESSURE (PSIG)
TEMPERATURE (T)
STREAM NUMBER
HEAT DUTY (BTU/HR)
Molten Metal Technology